

การย่อยสลายไคยูรอนด้วยแสงบนไทเทเนียและซิงค์ออกไซด์



นางสาววรรณนิภา ประดิษฐการ

ศูนย์วิทยทรัพยากร จุฬาลงกรณ์มหาวิทยาลัย

วิทยานิพนธ์นี้เป็นส่วนหนึ่งของการศึกษาตามหลักสูตรปริญญาวิศวกรรมศาสตรมหาบัณฑิต

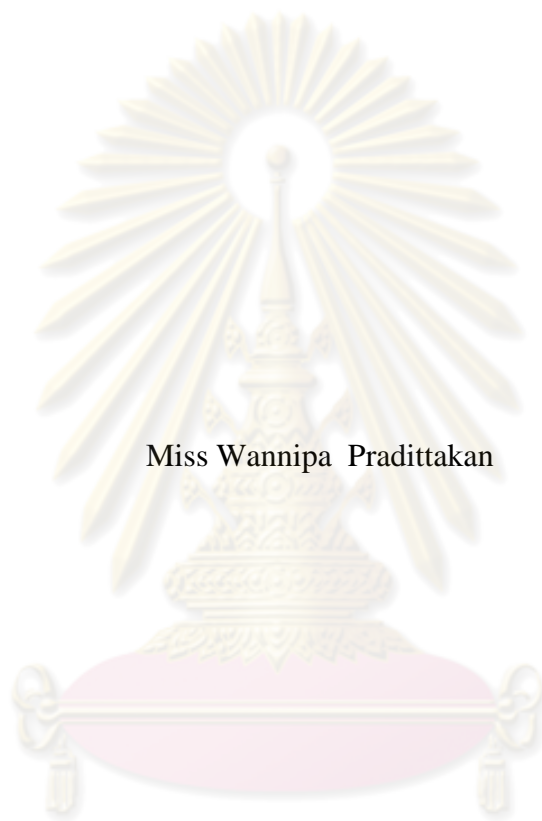
สาขาวิชาวิศวกรรมเคมี ภาควิชาวิศวกรรมเคมี

คณะวิศวกรรมศาสตร์ จุฬาลงกรณ์มหาวิทยาลัย

ปีการศึกษา 2553

ลิขสิทธิ์ของจุฬาลงกรณ์มหาวิทยาลัย

PHOTODEGRADATION OF DIURON ON TITANIA AND ZINC OXIDE



Miss Wannipa Pradittakan

ศูนย์วิทยทรัพยากร
จุฬาลงกรณ์มหาวิทยาลัย

A Thesis Submitted in Partial Fulfillment of the Requirements
for the Degree of Master of Engineering Program in Chemical Engineering

Department of Chemical Engineering

Faculty of Engineering

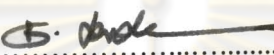
Chulalongkorn University

Academic Year 2010

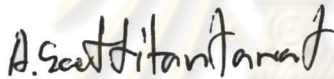
Copyright of Chulalongkorn University


Thesis Title PHOTODEGRADATION OF DIURON ON TITANIA AND
ZINC OXIDE
By Miss Wannipa Pradittakan
Field of study Chemical Engineering
Thesis Advisor Assistant Professor Varong Pavarajarn, Ph.D.

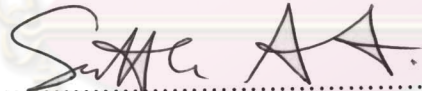
Accepted by the Faculty of Engineering, Chulalongkorn University in Partial
Fulfillment of the Requirements for the Master's Degree


.....Dean of the Faculty of Engineering
(Associate Professor Boonsom Lerdhirunwong, Dr.Ing.)

THESIS COMMITTEE

.....Chairman
(Apinan Sootitantawat, D.Eng.)

.....Thesis Advisor
(Assistant Professor Varong Pavarajarn, Ph.D.)

.....Examiner
(Professor Suttichai Assabumrungrat, Ph.D.)

.....External Examiner
(Kajornsak Faungnawakij, D.Eng.)

คณะวิศวกรรมศาสตร์
จุฬาลงกรณ์มหาวิทยาลัย

วรรณิกา ประดิษฐการ: การย่อยสลายไดยูรอนด้วยแสงบนไทเทเนียมและซิงค์ออกไซด์
(PHOTODEGRADATION OF DIURON ON TITANIUM DIOXIDE AND ZINC
OXIDE) อ.ที่ปรึกษาวิทยานิพนธ์หลัก: ผศ.ดร.วรงค์ ปวรจารย์, 176 หน้า.

การย่อยสลายไดยูรอนด้วยแสงได้ถูกศึกษาโดยใช้ซิงค์ออกไซด์และไทเทเนียมไดออกไซด์เป็นตัวเร่งปฏิกิริยา โดยตัวเร่งปฏิกิริยาได้ถูกสังเคราะห์ด้วยวิธีการโซล-เจล และเติมแอมโมเนียลงไป ปริมาณ 0% 7% และ 28% โดยมวล ตัวเร่งปฏิกิริยาที่ได้ถูกวิเคราะห์สมบัติด้วยหลายเทคนิค จากนั้นทำการศึกษาการย่อยสลายไดยูรอนที่ความเข้มข้น 10 ppm ในเครื่องปฏิกรณ์แบบกะและเก็บตัวอย่างสารละลายไปวัดความเข้มข้นของไดยูรอนที่เปลี่ยนไปด้วยเครื่องโครมาโทกราฟีชนิดของเหลวเป็นระยะๆ การลดลงของปริมาณสารอินทรีย์รวมทั้งละลายอยู่ในน้ำนั้นเป็นผลของการย่อยสลายไดยูรอนซึ่งพบว่า ความว่องไวของตัวเร่งปฏิกิริยาเพิ่มขึ้นเมื่อปริมาณแอมโมเนียเพิ่มขึ้น ซิงค์ออกไซด์มีประสิทธิภาพในการย่อยสลายและกำจัดไดยูรอนได้ดีกว่าไทเทเนียมไดออกไซด์ แม้ว่าซิงค์ออกไซด์จะมีพื้นที่ผิวน้อยกว่าก็ตาม ซิงค์ออกไซด์สามารถย่อยสลายไดยูรอนได้ 98% ภายใน 6 ชั่วโมง ในขณะที่ไทเทเนียมไดออกไซด์ทำการย่อยสลายไดยูรอนได้เพียง 45% นอกจากนี้การย่อยสลายไดยูรอนยังทำให้เกิดสารตัวกลางของการเกิดปฏิกิริยาซึ่งสามารถระบุถึงสารตัวกลางที่เกิดขึ้นได้โดยใช้เครื่องโครมาโทกราฟีชนิดของเหลวกับแมสสเปกโตรมิเตอร์ การย่อยสลายไดยูรอนจะเกิดสารตัวกลางต่างชนิดกัน โดยขึ้นอยู่กับค่าความเป็นกรดเบสของสารละลาย ความยาวคลื่นของแสงเหนือม่วงที่ใช้และชนิดของตัวเร่งปฏิกิริยา สารตัวกลางที่เกิดจากปฏิกิริยานั้นเกิดจากการเข้าทำปฏิกิริยาของอนุมูลไฮดรอกซีที่ตำแหน่งต่างๆ ของไดยูรอน

ภาควิชา.....วิศวกรรมเคมี.....ลายมือชื่อนิสิต.....วรรณิกา ประดิษฐการ.....
สาขาวิชา.....วิศวกรรมเคมี.....ลายมือชื่อ.ที่ปรึกษาวิทยานิพนธ์หลัก.....
ปีการศึกษา...2553

5270478421: MAJOR CHEMICAL ENGINEERING

KEYWORDS: DIURON/ZINC OXIDE/TITANIUM DIOXIDE/PHOTOCATALYTIC
DEGRADATION/INTERMEDIATE

WANNIPA PRADITTAKAN: PHOTODEGRADATION OF DIURON ON TITANIA
AND ZINC OXIDE. ADVISOR: ASST. PROF. VARONG PAVARAJARN, Ph.D., 176
pp.

Photocatalytic degradation of diuron was investigated in the presence of zinc oxide and titanium dioxide as photocatalysts. The photocatalysts were synthesized via sol-gel method with an addition of ammonia at the content of 0%, 7%, and 28% by mass. The powder obtained was characterized by various techniques. The photocatalytic degradation of 10 ppm diuron aqueous solution was conducted in a batch photo-reactor. The solution was periodically sampled to monitor the concentration of diuron via HPLC. The decrease of total organic carbon as a result of mineralization of diuron was also observed during the degradation process. It was found that the activity of photocatalysts increases when the ammonia content is increased. Zinc oxide shows higher performance in degradation and mineralization of diuron than titanium dioxide, regardless of much lower surface area. The degradation of diuron on zinc oxide is about 98% within 6 hours, while that achieved on titanium dioxide is only 45%. The degradation generates several intermediates. The intermediates species were identified by LC-MS. Degradation of diuron produces different degradation products depending on pH of the solution, wavelength of UV-radiation, and type of photocatalyst. Several degradation intermediates are generated by reactions of hydroxyl radical attacking to several sites of diuron structure during the photocatalytic degradation process.

ศูนย์วิทยทรัพยากร
จุฬาลงกรณ์มหาวิทยาลัย

Department Chemical Engineering Student's Signature: วราณิภา ปะติตตะกัน
Field of study Chemical Engineering Advisor's Signature: Varong Pavrajarn
Academic Year: 2010

ACKNOWLEDGEMENTS

The author would like to express her gratitude to her advisor, Assistant Professor Dr. Varong Pavarajarn, for his extensive guidance, patience, support, and encouragement throughout the research.

I would also be grateful to thank to Dr. Apinan Sootitawat as the chairman, Professor Dr. Sutthichai Assabumrungrat, and Dr. Kajornsak Faungnawakij, members of the thesis committee for their kind cooperation, comment, and discussions.

I would like to thank the National Research Council of Thailand for financial support.

I would also like to thank all my friends and all members of the Center of Excellence in Particle Technology who always provide the encouragement and cooperate along the research study.

Finally, I would like to dedicate this thesis to my parents and my families, who have always been the source of her support and encouragement.



ศูนย์วิทยทรัพยากร
จุฬาลงกรณ์มหาวิทยาลัย

CONTENTS

	Page
ABSTRACT (THAI).....	iv
ABSTRACT (ENGLISH).....	v
ACKNOWLEDGEMENTS.....	vi
CONTENTS.....	vii
LIST OF TABLES.....	x
LIST OF FIGURES.....	xii
CHAPTER	
I INTRODUCTION.....	1
II THEORY AND LITERATURE REVIEWS	3
2.1 Photocatalysts.....	3
2.1.1 Physical and chemical properties of titania.....	3
2.1.2 Physical and chemical properties of zinc oxide.....	5
2.1.3 Photocatalyst synthesis.....	8
2.2 Diuron.....	9
2.3 Photocatalytic Degradation.....	10
2.4 Photocatalytic Degradation of Diuron.....	13
2.4.1 The kinetic of photodegradation of diuron.....	13
2.4.2 Diuron degradation products.....	15
III EXPERIMENTAL	20
3.1 Preparation of TiO ₂ and ZnO.....	20
3.1.1 Synthesis of titania particles.....	20
3.1.2 Synthesis of zinc oxide particles.....	20
3.1.3 Characterizations of photocatalysts.....	21
3.2 Adsorption Studies.....	22
3.3 Photocatalytic Degradation Procedure.....	22

	Page
IV RESULTS AND DISCUSSION	24
4.1 Properties of Synthesized Photocatalysts.....	24
4.1.1 Synthesized zinc oxide.....	24
4.1.2 Synthesized titania.....	28
4.2 Adsorption of Diuron onto the Catalysts.....	33
4.2.1 Adsorption isotherm.....	33
4.2.2 FTIR studies.....	37
4.3 Photodegradation of Diuron.....	39
4.3.1 Photodegradation of diuron on zinc oxide.....	40
4.3.2 Photodegradation of diuron on titania.....	44
4.4 Intermediate Products of the Photodegradation.....	48
4.4.1 Photodegradation on zinc oxide.....	48
4.4.1.1 Effect of pH of diuron solution.....	48
4.4.1.2 Effect of UV light.....	60
4.4.2 Photodegradation on titanium dioxide.....	69
4.4.2.1 Effect of pH of diuron solution.....	69
4.4.2.2 Effect of UV light.....	77
4.4.3 Effect of type of photocatalysts.....	85
V CONCLUSIONS	91
5.1 Conclusions.....	91
5.2 Recommendations.....	91
REFERENCES.....	93
APPENDICES.....	100
APPENDIX A NMR STUDIES.....	101
APPENDIX B DIURON CALIBRATION CURVE.....	104
APPENDIX C LC/MS MASS SPECTRUM.....	105
APPENDIX D LC/MS/MS MASS SPECTRUM.....	140

	Page
APPENDIX E ADSORPTION OF FILTER TEST.....	143
APPENDIX F TOXICITY OF SOME INTERMEDIATES.....	144
VITA	150



ศูนย์วิทยทรัพยากร
จุฬาลงกรณ์มหาวิทยาลัย

LIST OF TABLES

Table	Page
2.1 Crystallographic characteristic of anatase, brookite and rutile.....	4
2.2 Physical and chemical properties of zinc oxide.....	6
2.3 Physicochemical properties of diuron.....	10
4.1 Crystallite size and surface area of the synthesized zinc oxide.....	25
4.2 Crystallite size and surface area of synthesized titania.....	29
4.3 Constants of Langmuir and Freundlich isotherm model for adsorption of diuron on synthesized ZnO and synthesized TiO ₂	36
4.4 The apparent rate constant (k_{app}), reaction rate constants (k_r), and the adsorption constant (K) for the photocatalytic degradation of diuron using zinc oxide at various mass fraction of ammonia.....	43
4.5 The apparent rate constant (k_{app}), reaction rate constants (k_r), and the adsorption constant (K) for the photocatalytic degradation of diuron using titania at various mass fraction of ammonia.....	46
4.6 The apparent rate constant (k_{app}), reaction rate constants (k_r), and the adsorption constant (K) for the photocatalytic degradation of diuron using zinc oxide at various pH of solution.....	50
4.7 Possible intermediates generated from photodegradation of diuron on zinc oxide at pH of solution were adjusted at 3, 7, and 10.....	54
4.8 The apparent rate constant (k_{app}), reaction rate constants (k_r), and the adsorption constant (K) for the photocatalytic degradation of diuron using zinc oxide at at different UV lamp.....	62
4.9 Possible intermediates generated from photodegradation of diuron on zinc oxide at different UV-lamp.....	64
4.10 The apparent rate constant (k_{app}), reaction rate constants (k_r), and the adsorption constant (K) for the photocatalytic degradation of diuron using zinc oxide at at various pH of solution.	70

Table	Page
4.11 Possible intermediates generated from photodegradation of diuron on titanium dioxide at pH of solution were adjusted at 3, 7, and 10.....	73
4.12 The apparent rate constant (k_{app}), reaction rate constants (k_r), and the adsorption constant (K) for the photocatalytic degradation of diuron using titania at different UV lamp.....	79
4.13 Possible intermediates generated from photodegradation of diuron on titanium dioxide at different UV-lamp.....	81
4.14 Possible intermediates generated from photodegradation of diuron on zinc oxide and titania.....	85
D.1 Mass spectral data for photocatalytic degradation of diuron as analyzed by LC/MS/MS.....	142



ศูนย์วิทยทรัพยากร
 จุฬาลงกรณ์มหาวิทยาลัย

LIST OF FIGURES

Figure	Page
2.1	Crystal structure of TiO ₂ ; (a) Rutile, (b) Anatase, (c) Brookite.....5
2.2	Stick and ball representation of zinc oxide crystal structures: (a) cubic rocksalt, (b) cubic zinc blende, and (c) hexagonal wurtzite. The shaded gray and black spheres denote Zn and O atoms, respectively.....7
2.3	Proposed degradation mechanism of diuron by the photocatalytic system.....16
2.4	Degradation pathways of diuron by the TiO ₂ as photocatalyst.....18
2.5	Degradation pathways of diuron by catalytic wet air oxidation.....19
3.1	Diagram of the equipment setup for the photocatalytic degradation.....23
4.1	XRD patterns of the zinc oxide powder synthesized with the addition of ammonia in the amount of 0%, 7%, and 28% by weight of the solution. All products were calcined at 500°C for 2 hours.....25
4.2	Adsorption/desorption isotherm of zinc oxide powder synthesized with the addition of ammonia in the amount of 0%, 7%, and 28% by weight of the solution. All products were calcined at 500°C for 2 hours.....26
4.3	SEM micrographs of the zinc oxide powder synthesized with the use of ammonia at various content: (a) 0% NH ₃ , (b) 7% NH ₃ , and (c) 28%NH ₃ after calcined at 500°C for 2 hours.....27
4.4	TG/DTA curves of the synthesized zinc oxide powder after calcined at 500 °C for 2 hours (heating rate of 10°C/min) without ammonia content.....28
4.5	XRD patterns of the titania powder synthesized by treated with ammonia solution at the mass fraction of 0%, 7%, and 28% for 2 hours followed by calcination at 500°C for 2 hours.....29
4.6	Adsorption/desorption isotherm of titanium dioxide powder synthesized with the addition of ammonia in the amount of 0%, 7%, and 28% by weight of the solution. All products were calcined at 500°C for 2 hours.....30

Figure	Page
4.7 SEM micrographs of the synthesized TiO ₂ powders synthesized with the use of ammonia at various content: (a) 0% NH ₃ , (b) 7% NH ₃ , and (c) 28% NH ₃ after calcined at 500°C for 2 hours.....	31
4.8 TG/DTA curves of the synthesized titaniumdioxide powder after calcined at 500 °C for 2 hours (heating rate of 10°C/min) without ammonia content.....	32
4.9 Adsorption of diuron on ZnO at room temperature (27-30°C) The initial diuron concentration was 1, 5, 10, 15, and 20 ppm, respectively.....	33
4.10 Adsorption of diuron on TiO ₂ at room temperature (27-30°C) The initial diuron concentration was 1, 5, 10, 15, and 20 ppm, respectively.....	34
4.11 Adsorption isotherm of diuron onto synthesized ZnO, synthesized TiO ₂ , commercial ZnO, and commercial TiO ₂ at room temperature (27-30°C).....	34
4.12 Langmuir isotherm for adsorption of diuron on synthesized ZnO and synthesized TiO ₂	35
4.13 Freundlich isotherm for adsorption of diuron on synthesized ZnO and synthesized TiO ₂	36
4.14 FTIR spectrum obtained from (a) diuron solution in methanol, (b) diuron solution in methanol mixed with ZnO for 180 min.....	38
4.15 FTIR spectrum obtained from (a) diuron solution in methanol, (b) diuron solution in methanol mixed with TiO ₂ for 180 min.....	39
4.16 Concentration of diuron with respect to the initial diuron concentration (C/C ₀) during the photocatalytic degradation on zinc oxide at various mass fraction of ammonia: 0% NH ₃ , 7% NH ₃ , 28% NH ₃ , and without catalyst. The reaction was conducted using 1 mg of zinc oxide per 10 ml of solution and using the initial concentration of diuron is 10 ppm.....	41
4.17 First –order linear transforms of the photocatalytic degradation on zinc oxide at various mass fraction of ammonia: 0% NH ₃ , 7% NH ₃ , and 28% NH ₃ . The reaction was conducted using 1 mg of zinc oxide per 10 ml of solution and using the initial concentration of diuron is 10 ppm.....	42

Figure	Page
4.18 Total organic carbon (TOC) with respect to the initial TOC of diuron solution (TOC/TOC_0) during the photocatalytic degradation on zinc oxide at various mass fraction of ammonia: 0% NH_3 , 7% NH_3 , and 28% NH_3 . The reaction was conducted using 1 mg of zinc oxide per 10 ml of solution and using the initial concentration of diuron is 10 ppm.....	44
4.19 Concentration of diuron with respect to the initial diuron concentration (C/C_0) during the photocatalytic degradation on titania at various mass fraction of ammonia: 0% NH_3 , 7% NH_3 , 28% NH_3 , and without catalyst. The reaction was conducted using 1 mg of titania per 10 ml of solution and using the initial concentration of diuron is 10 ppm.....	45
4.20 First-order linear transforms of the photocatalytic degradation on titania at various mass fraction of ammonia: 0% NH_3 , 7% NH_3 , and 28% NH_3 . The reaction was conducted using 1 mg of zinc oxide per 10 ml of solution and using the initial concentration of diuron is 10 ppm.....	45
4.21 Total organic carbon (TOC) with respect to the initial TOC of diuron solution (TOC/TOC_0) during the photocatalytic degradation on titania at various mass fraction of ammonia: 0% NH_3 , 7% NH_3 , and 28% NH_3 . The reaction was conducted using 1 mg of zinc oxide per 10 ml of solution and using the initial concentration of diuron is 10 ppm.....	47
4.22 Effect of pH of the solution on photodegradation efficiency of diuron. The pH is adjusted at pH 3, pH 7, and pH 10.....	49
4.23 First-order linear transforms of the photodegradation efficiency of diuron at various pH values. The pH is adjusted at pH 3, pH7, and pH 10.....	49
4.24 HPLC peak height of intermediates generated during photocatalytic degradation on diuron on zinc oxide and the initial pH of 3.....	52
4.25 HPLC peak height of intermediates generated during photocatalytic degradation on diuron on zinc oxide and the initial pH of 7.....	52
4.26 HPLC peak height of intermediates generated during photocatalytic degradation on diuron on zinc oxide and the initial pH of 10.....	53
4.27 Dechlorination reaction.....	58

Figure	Page
4.28 Hydroxylation reaction.....	59
4.29 Decarboxylation reaction.....	59
4.30 The effect of UV-lamp, i.e. UV-A, UV-C on the photolysis of diuron.....	60
4.31 The effect of UV-lamp, i.e. UV-A, UV-C on the degradation of diuron using zinc oxide as catalyst.....	61
4.32 First order linear transforms of the photodegradation efficiency of diuron, UV-A, UV-C on the degradation of diuron using zinc oxide as catalyst.....	61
4.33 HPLC peak height of intermediates generated during photocatalytic degradation on diuron on zinc oxide using UV-A as light source.....	62
4.34 HPLC peak height of intermediates generated during photocatalytic degradation on diuron on zinc oxide using UV-C as light source.....	63
4.35 Effect of pH of the solution on photodegradation efficiency of diuron on titania. The pH is adjusted at pH 3, pH7, and pH 10.....	69
4.36 First order linear transforms of the photodegradation efficiency of diuron on titania at various pH values. The pH is adjusted at pH 3, pH 7, and pH 10.....	70
4.37 HPLC peak height of intermediates generated during photocatalytic degradation on diuron on TiO ₂ and the initial pH of solution 3.....	71
4.38 HPLC peak height of intermediates generated during photocatalytic degradation on diuron on TiO ₂ and the initial pH of solution 7.....	72
4.39 HPLC peak height of intermediates generated during photocatalytic degradation on diuron on TiO ₂ and the initial pH of solution 10.....	72
4.40 The effect of UV-lamp UV-A, UV-C on the degradation of diuron using titania as catalyst.....	78
4.41 First order linear transforms of the photodegradation efficiency of diuron, UV-A, UV-C on the degradation of diuron using titania as catalyst.....	78
4.42 HPLC peak height of intermediates generated during photocatalytic degradation on diuron on TiO ₂ using UV-A as light source.....	80
4.43 HPLC peak height of intermediates generated during photocatalytic degradation on diuron on titanium dioxide using UV-C as light source.....	80

Figure	Page
A.1 ¹³ C NMR spectra from diuron solution in methanol (CD ₃ OD) diuron solution in methanol (CD ₃ OD) with TiO ₂ , and diuron solution in methanol (CD ₃ OD) with ZnO in the chemical shift from (a) 0-80 ppm and (b) 110-240 ppm.....	102
A.2 Chemical structure of diuron.....	102
A.3 ¹ H NMR spectra from diuron solution in methanol (CD ₃ OD) diuron solution in methanol (CD ₃ OD) with TiO ₂ , and diuron solution in methanol (CD ₃ OD) with ZnO in the chemical shift from (a) 2.5-3.5 ppm, (b) 3.5-6.5 ppm, and (c) 7.2-7.8 ppm. (CD ₃ OD).....	103
B.1 The calibration curve of diuron.....	104
C.1 Chromatogram of diuron solution photodegradation at pH3 obtained from UV detector and mass detector are displayed in (a). Mass spectrums were obtained using fragmentator of 120 V at various retention time as shown in (a)-(p).....	105
C.2 Chromatogram of diuron solution photodegradation at pH7 obtained from UV detector and mass detector are displayed in (a). Mass spectrums were obtained using fragmentator of 120 V at various retention time as shown in (a)-(q).....	109
C.3 Chromatogram of diuron solution photodegradation at pH10 obtained from UV detector and mass detector are displayed in (a). Mass spectrums were obtained using fragmentator of 120 V at various retention time as shown in (a)-(n).....	114
C.4 Chromatogram of diuron solution photodegradation by UV-C obtained from UV detevtor and mass detector are displayed in (a). Mass spectrums were obtained using fragmentator of 120 V at various retention time as shown in (a)-(n).....	118
C.5 Chromatogram of diuron solution photodegradation at pH3 obtained from UV detector and mass detector are displayed in (a). Mass spectrums were obtained using fragmentator of 120 V at various retention time as shown in (a)-(p).....	122
C.6 Chromatogram of diuron solution photodegradation at pH7 obtained from UV detector and mass detector are displayed in (a). Mass spectrums were obtained using fragmentator of 120 V at various retention time as shown in (a)-(r).....	127

Figure	Page
C.7 Chromatogram of diuron solution photodegradation at pH10 obtained from UV detector and mass detector are displayed in (a). Mass spectrums were obtained using fragmentator of 120 V at various retention time as shown in (a)-(n).....	132
C.8 Chromatogram of diuron solution photodegradation by UV-C obtained from UV detevtor and mass detector are displayed in (a). Mass spectrums were obtained using fragmentator of 120 V at various retention time as shown in (a)-(r).....	136
D.1 Chromatogram of diuron solution photodegradation (set mass ~ 213) obtained from LC/MS/MS displayed in (a) (f).....	140
E.1 Adsorption of diuron on filter.....	143



ศูนย์วิทยทรัพยากร
จุฬาลงกรณ์มหาวิทยาลัย

CHAPTER I

INTRODUCTION

Chemicals used in agriculture have posed environmental problems in the present [1]. The chemicals can contaminate soil and underground water [2]. The most chemicals used in agriculture are pesticides and herbicides. Diuron is one of the most commonly used herbicides in Thailand. Diuron is also classified as a harmful chemical [1]. It has effect for human health and the equilibrium of ecosystems. Although diuron can be naturally degraded in the environment via biological or photochemical degradation [3], the degradation rate is slow. Diuron can also be degraded by photocatalytic degradation process [2]. The photodegradation of diuron has often been reported on oxide semiconductor photocatalysts. Among various oxide semiconductors, titanium dioxide (titania) and zinc oxide have been investigated and reported as one of the most suitable catalyst in widespread environmental applications. They are effective for the decomposition of environmental pollutant via photocatalysis reaction. They have good physical and chemical properties, such as strong oxidizing power [4, 5] and high photocatalytic activity [4, 6]. In addition, they are non-toxic and available at low price. Both zinc oxide and titania have similar electronic properties [7]. They have the same band gap energy of 3.2 eV. Yet, the effectiveness in photocatalytic degradation of zinc oxide and titania is different [6, 8].

Titania and zinc oxide can be prepared by several ways. One of the popular techniques is sol-gel method because of its low cost, reliability, reproducibility, simplicity and relative mild conditions of synthesis [9]. Sol-gel process is a route generally applied to prepare nanomaterial with notable advantages of high purity and good microstructure [5]. In this work, photocatalysts are synthesized via the sol-gel process.

The chemistry of the photodegradation processes is complex. Careful analytical monitoring using different techniques is essential in order to control all transformation steps, to identify harmful intermediates and to understand and interpret the reaction mechanism. The assessment of pollutant disappearance in the early steps is not sufficient to ensure the absence of residual products. The heterogeneous photocatalytic treatment may give rise to a variety of organic intermediates which can themselves be toxic, and in some cases, more persistent than the original substrate [10]. Therefore, it is an interest of this research to identify the formation of intermediates during the photodegradation of diuron.

The objective of this research is to investigate the photocatalytic degradation and the formation of intermediates during the photodegradation of diuron solution, using zinc oxide and titanium dioxide as catalyst.

The present thesis is arranged as follows:

Chapter I is the introduction of this work. Chapter II describes basic theory about diuron such as chemical and physical of diuron. Photocatalytic reaction, physical and chemical properties of zinc oxide and titanium dioxide, photocatalytic degradation of diuron are also described. Furthermore, literature reviews of the previous works related to this research are presented in this chapter as well. Chapter III shows experimental systems and procedures for the photocatalytic degradation and identifies the intermediates products. Chapter IV presents the experimental results and discussion. In the last chapter, the overall conclusions of this research.



ศูนย์วิทยทรัพยากร
จุฬาลงกรณ์มหาวิทยาลัย

CHAPTER II

THEORY AND LITERATURE REVIEWS

2.1 Photocatalysts

Various types of photocatalyst have been investigated as a potential catalyst to degrade organic matters. Titania and zinc oxide, which are inexpensive and non-toxic, becomes attractive for this research.

2.1.1 Physical and chemical properties of titania

Titanium dioxide is known as titanium (IV) oxide or titania, has great potential for many industrial applications. Titania has been used in many fields of application such as catalyst, catalyst support, electronics, cosmetic pigment and filter coating. In recent years, main attention has been devoted to its photocatalytic activity and photoinduced superhydrophilicity. Since titania has relatively wide band gap (3.2 eV), charge carriers, i.e. electrons and holes, are produced when titania is excited. Consequently, highly reactive radicals are generated and oxidation-reduction reaction of species adsorbed on the surface of titania can occur. The use of titania in the photocatalytic degradation of organic pollutants has attracted much attention as a promising method of depolluting contaminated waters and soils [11].

Titania occurs in nature as well-known minerals rutile, anatase and brookite, and additionally as two high pressure forms, a monoclinic baddeleyite-like form and an orthorhombic α - PbO_2 -like form. The most common form is rutile, which is also the most stable form. Anatase and brookite can both convert to rutile upon heating. Anatase is a metastable phase, which tends to be more stable at low temperature. For brookite, it is formed under hydrothermal conditions and usually found only in mineral. Brookite has been produced by heating amorphous titania, which is prepared from the reaction between alkyl titanates with sodium or potassium hydroxide in an autoclave at 200 to 600°C. Although titania is known to have three natural polymorphs, only anatase is generally accepted to have significant photocatalytic activity [6].

The crystallographic characteristic of these varieties are shown in Table 2.1. Although anatase and rutile are both tetragonal, they are not isomorphous as shown in Figure 2.1. Anatase usually occurs in near-regular octahedral form, while rutile forms slender prismatic crystals that are frequently twinned. Nevertheless, both anatase and rutile are anisotropic of which physical properties vary according to direction relative to the crystal axes. However, in most applications using these substances, the distinction between crystallographic directions is lost because of the random orientation from large number of small particles or grains in the particle.

Table 2.1 Crystallographic characteristic of anatase, brookite and rutile.

Properties	Anatase	Brookite	Rutile
Crystal Structure	Tetragonal	Orthorhombic	Tetragonal
Optical	Uniaxial	Biaxial	Uniaxial
Density, g/cm ³	3.9	4.0	4.23
Lattice parameter, nm			
<i>a</i>	0.3758	0.9166	0.4584
<i>b</i>		0.5436	
<i>c</i>	0.9514	0.5135	2.953

Three allotropic forms of titania have been prepared artificially, but only rutile has been obtained in the form of transparent large single crystal. The transformation from anatase to rutile is accompanied by evolution of ca. 12.6 kJ/mol (3.01 kcal/mol). The rate of phase transformation is greatly affected by temperature and by presence of other substances which may either catalyze or inhibit the transformation. The lowest temperature at which the conversion from anatase to rutile takes place at a measurable rate is approximately 500-550°C [12]. The change is not reversible and it has been shown that ΔG for the transformation from anatase to rutile is always negative.

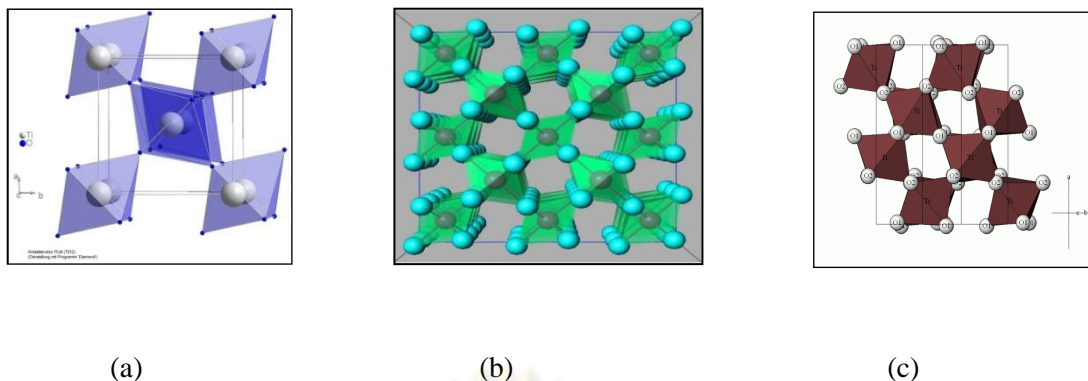


Figure 2.1 Crystal structure of TiO_2 ; (a) Rutile, (b) Anatase, (c) Brookite.

2.1.2 Physical and chemical properties of zinc oxide

Zinc oxide is an inorganic compound with the formula ZnO . Zinc oxide is a white or yellowish powder. It occurs in nature as the mineral zincite. It is nearly insoluble in water or alcohol, but it is soluble in acids and alkalis. Zinc oxide particles may be spherical, acicular or nodular depending on the manufacturing process. The particle shape is important for maximizing physical properties. Zinc oxide absorbs all UV light radiation at wavelength below 360 nm. Zinc oxide has received considerable attention because of its unique optical, semiconducting, piezoelectric, and magnetic properties. ZnO nanostructures exhibit interesting properties including high catalytic efficiency and strong adsorption ability. ZnO is able to degrade a wide range of recalcitrant organic and inorganic pollutants due to its ability to generate highly oxidizing and reducing species. It could be photo-excited by absorbing light of suitable wavelength to generate two types of electronic carriers, i.e. electrons (e^- ; the reducing species) and holes (h^+ ; the oxidizing species).

Zinc oxide is an n-type semiconductor with a band gap of 3.20 eV and the free excitation energy of 60 meV, which makes it very high potential for room temperature light emission. This also gives zinc oxide strong resistance to high temperature electronic degradation during operation. Therefore, it is attractive for many opto-electronic applications in the range of blue and violet light as well as UV devices for wide range of technological applications. Zinc oxide also exhibits dual semiconducting and piezoelectric properties. A summary of the physical and chemical properties of zinc oxide are given in Table 2.2.

Table 2.2 Physical and chemical properties of zinc oxide.

Molecular formula	ZnO
Molecular weight	81.38 g/mole
Crystal structure	Hexagonal wurtzite Cubic zincblende Cubic rocksalt (The hexagonal wurtzite structure is most stable at ambient conditions and thus most common.)
Lattice parameters of hexagonal wurtzite at 300 K	
<i>a</i>	0.32495 nm
<i>c</i>	0.52069 nm
<i>c/a</i>	1.602 (ideal hexagonal structure is 1.633)
Density	5.606 g/cm ³
Melting point	1970 – 1975 °C (decomposes)
Energy gap	3.2 eV, direct
Excitation binding energy	60 meV
Appearance	White solid
Synonyms	Zinc white; Zinc flowers; Calamine; C.I. pigment white 4
Solubility	Insoluble in water and alcohols. Soluble in acids and bases.
Physicochemical stability	Stable under normal conditions of handling and storage.

Zinc oxide is a II-VI compound semiconductor of which the ionicity resides at the borderline between covalent and ionic semiconductor. The crystal structures shared by zinc oxide are wurtzite, zinc blende, and rocksalt, as schematically shown in Figure 2.2. At ambient conditions, the thermodynamically stable phase is wurtzite. The zinc-blende structure can be formed only by the growth of ZnO on cubic substrate. The rocksalt structure may be obtained at relatively high pressure.

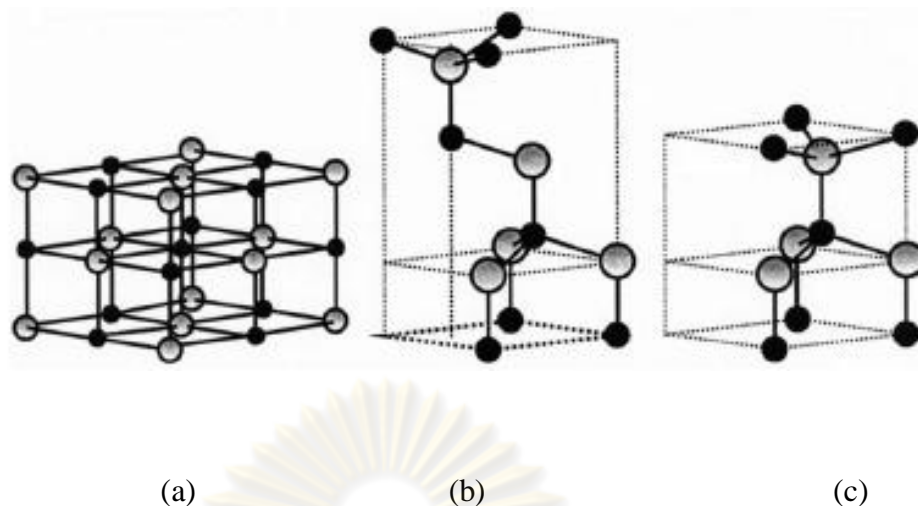


Figure 2.2 Stick and ball representation of zinc oxide crystal structures: (a) cubic rocksalt, (b) cubic zinc blende, and (c) hexagonal wurtzite. The shaded gray and black spheres denote Zn and O atoms, respectively.

Zinc oxide occurs in nature as mineral. Zinc oxide is prepared in industrial scale by vaporizing zinc metal and oxidizing the generated zinc vapor with preheated air. Zinc oxide has numerous industrial applications. It is a common white pigment in paints. It is used to make enamel, white printing ink, white glue, opaque glasses, and floor tiles. It is also used in cosmetics, pharmaceutical applications such as antiseptic and astringent, dental cements, batteries, electrical equipments, and piezoelectric devices. Other applications are the use as flame retardant, and UV absorber in plastics. Nevertheless, the current major application of zinc oxide is in the preparation of most zinc salts.

Gouvea et al. have reported that the activity of nanosized zinc oxide is higher than nanosized titania [13]. The smaller particle, the higher the photocatalytic activity and the coupling of titania with zinc oxide seems useful in order to achieve more efficient electron-hole pair separation under illumination and, consequently, a higher reaction rate. The increase in the lifetime of the photoproduced pairs, due to hole and electron transfer between the two coupled semiconductors, is produced in many cases as key factor for the improvement of the photoactivity [14].

2.1.3 Photocatalyst synthesis

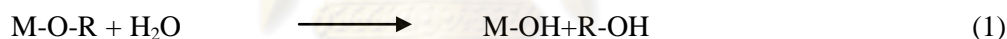
There are several methods that can be used to synthesize photocatalyst. In general, methods which have been reported for titania and zinc oxide are: sol-gel method [5, 15], hydrothermal or solvothermal method [16, 17], and precipitation method [18, 19]. Previous researches have revealed that different photocatalyst synthesis methods result in different surface properties, which consequently affect the interaction between catalyst surface and the compound to be degraded. One of the popular techniques is sol-gel method because of its low cost, reliability, and simplicity. Sol-gel process is a route generally applied to prepare nanomaterial with notable advantages of high purity and good microstructure. So this method was selected to prepare photocatalyst in this work.

Sol-gel technology is quite important for processing materials [20]. This method can be performed at relatively low temperature to prepare a solid. Sol is firstly prepared from suitable reactants in suitable liquid. Sol preparation can be either simply the dispersion of insoluble solids in liquid or addition of precursor which reacts with the solvent to form a colloidal product. A typical example of the former approach is the dispersion of oxides or hydroxides in water with the pH adjusted so that the solid particles remain in suspension rather than precipitate out. A typical example of the later approach is the addition of metal alkoxide to water. The alkoxides are hydrolyzed giving the oxide as a colloidal product. The sol is then either treated or simply left to form gel. To obtain a final product, the gel is heated. This heating serves several purposes. It removes the solvent, decomposes anions such as alkoxides or carbonates to give oxides, allows rearrangement of the structure of the solid and allows crystallization. For the synthesis of titania, the process starts with the mixing of titanium alkoxide with alcohol. Acidic aqueous solution is subsequently added to the mixture [21]. Su et al. revealed that, the titania particles in the initial sol were elliptical in shape. The crystal size of titania increased from 4 to 35 nm as the temperature of the calcination was increased to 700 °C. The specific surface area decreased from 122 to 11.5 m²g⁻¹ [15]. This technique can be adapted by adding urea to the sol, which can result in titania with higher specific surface area as well as larger pore size of titania nanoparticles. Urea showed a retarding effect on the transformation of titania from anatase to rutile [22]. In 2009, the composite of zinc oxide and titania were prepared by sol-gel process. The results indicated that the as-synthesized powder was consisted of anatase TiO₂, zincite ZnO, and Zn(OH)₂ phase. Upon the heating up to 220 °C all of Zn(OH)₂ phase was transformed into ZnO. Increasing calcination temperature up to 680 °C produced Zn₂TiO₄ and ZnTiO₃ solid solution in ZnO/TiO₂ system. With an increase in temperature, the amount of ZnTiO₃ phase decreased in way that it totally disappeared at 900 °C and transformed into Zn₂TiO₄. The specific

surface area of the samples after being calcined at 220, 420, and 800 °C were 51.24, 46.32, and 26.28 m²g⁻¹, respectively [19]. Increase in particle size and aggregation occurred after high temperature treatment. Tian et al. prepared N-doped titania/zinc oxide composite powder by sol-gel method whereas ammonia was used as a nitrogen source. The phase transformation of anatase to rutile was retarded via the ammonia treating process, leading to the presence of anatase phase in the composite. Crystallite size of the composite powder was about 15 nm [5]. The biggest advantage of N-doping, compared to undoped titania, is their lowered excitation energy [23]. N-doping is reported to be a good way for the preparation of TiO₂ photocatalysts with enhanced photocatalytic activity and modified the particle and crystallite size [24].

Sol-gel process is considered as one of the most promising alternative because it presents a number of advantages such as low sintering temperature, versatility of processing and homogeneity at molecular level [25]. However, the limit of this method is that strong reactivity of alkoxide toward water often results in uncontrolled precipitation. The parameters effect to rate reaction of sol-gel is solution pH, molar ratio of reactants, aging time and temperature. The reaction of sol-gel process follows Equation (1)-(3).

Hydrolysis:



Condensation:



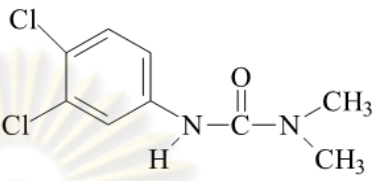
whereas, M is Metal and OR is Alkoxy group

2.2 Diuron

Diuron [3-(3,4-dichlorophenyl)-1,1-dimethylurea], is a long acting herbicide, belonging to the family of halogenophenylureas. It has been one of the most commonly used herbicides for more than 40 years. Diuron has been reported to be highly toxic for some non-target organisms. Diuron in agricultural may penetrate through soil slowly and contaminate groundwater. It may pose potential environment and health problems from runoff waters coming from agricultural land where diuron has been used extensively [26]. Therefore, diuron

was selected for investigation of the photocatalytic degradation in this research. There are some human health concerns about the toxicity of some impurities in the active constituent of diuron as well. Its properties are shown in Table 2.3.

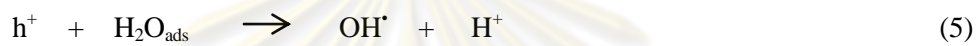
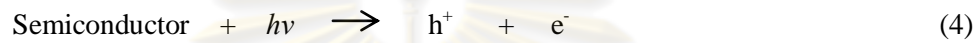
Table 2.3 Physicochemical properties of diuron.

Structure formula	
Molecular weight	233.10 g/mol
Molecular formula	C ₆ H ₁₀ Cl ₂ N ₂ O
Melting point	158 – 159°C
Vapor pressure	0.0041 Pa at 30°C
Appearance	White crystalline solid
Synonyms	Cekiuron; Crisuron; Dailon; Di-on; Krovar; Unidron; Vonduron; Xarmex; etc.
Solubility	42 ppm in water at 25°C
Toxicity	The concentrated material may cause irritation to eyes and mucous membrane, but a 50% -water paste is not irritating to the intact skin of mammal.
Half-life	372 days in soil [27]

2.3 Photocatalytic Degradation

Photocatalytic process is a technology for oxidation/degradation of organic contaminants in environmental control. It can use sunlight, which is available in abundance, as the energy source to initiate the photodecomposition of pollutants. The end products of this treatment process are usually harmless compounds such as carbon dioxide, water and inorganic ions such as chloride and nitrate. It has been widely used as an alternative physical-chemical process for the elimination of toxic and hazardous organic substances in wastewater, drinking water, and air. In this process, a semi-conductor activated by ultra-violet (UV) radiation is used as a catalyst to destroy organic contaminants.

The photocatalysis can be defined as the acceleration of a photoreaction by the presence of a semiconductor catalyst that can be activated by the absorption of light of energy greater than its band gap. Since the contaminants are present in the aqueous phase, while the semiconductor is solid, this process can be called heterogeneous photocatalysis process. The generations of electron-hole pairs are represented in Eq. (4). The photo-generated holes and electrons give rise to oxidation and reduction processes, respectively. In an aqueous solution, water molecules adsorb onto surface of the catalyst. They are oxidized giving rise to OH[•] radicals. As the process is usually carried out in aerobic conditions, the species to be reduced is oxygen, generating the superoxide radical as following Eq. (5) to (7). Organic pollutants adsorb onto the surface of the catalyst are subsequently oxidized by OH[•] radicals.



Support of the OH[•] radical as the main reactive oxidant derives from the observation that intermediates detected during the photocatalytic degradation of halogenated aromatic compounds are typically hydroxyl structures, as those found when similar aromatics react with a known source of OH[•] radicals. The hydroxyl radical has a very short half-life of approximately 10⁻⁹ seconds and a high reactivity [28].

The mechanism of the photocatalytic degradation of aqueous organic compound on anatase titania can be expressed by a series of advanced oxidation process as following [28].

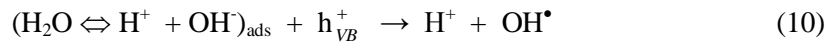
- 1) Absorption of efficient photons ($h\nu \geq E_G = 3.2 \text{ eV}$) by titania



- 2) Oxygen ionosorption (first step of oxygen reduction)



- 3) Neutralization of OH⁻ groups by photoexcited holes



4) Neutralization of $\text{O}_2^{\bullet-}$ by protons



5) Transient hydrogen peroxide formation



6) Decomposition of H_2O_2 and second reduction of oxygen



7) Oxidation of the organic reactant via successive attack by OH^\bullet radical



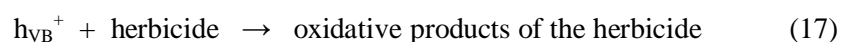
8) Direct oxidation by reaction with holes



The mechanisms of photocatalytic degradation of matter on nanosized ZnO powder can be expressed by applying the research of N. Daneshvar [29]. The photocatalytic degradation of organic matter in the solution is initiated by photoexcitation of the semiconductor, followed by the formation of electron-hole pairs on the surface of the catalyst (Eq.16).



The high oxidative potential of the hole (h_{VB}^+) in the catalyst permits the direct oxidation of herbicide into the reactive intermediates (Eq.17).

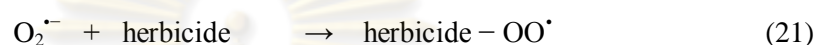
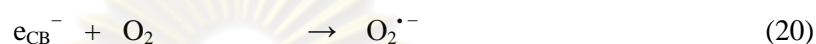


Very reactive hydroxyl radicals can also be formed either by the decomposition of water (Eq.18) or by the reaction of the hole with OH^- (Eq.19).



The hydroxyl radical is an extremely strong, non-selective oxidant that brings about the degradation of organic chemicals as well [30, 31].

Electron in the conduction band (e_{CB}^-) on the catalyst surface can reduce molecular oxygen to superoxide anion (Eq.20). This radical, in the presence of organic scavengers, may form organic peroxides (Eq.21) or hydrogen peroxide (Eq.22). Electrons in the conduction band are also responsible for the production of hydroxyl radicals, which have been indicated as the primary cause of organic matter mineralization (Eq.23) [10, 30]



Photodegradation is heterogeneous reaction. The reaction is surface reaction since the reaction occurs when the organic matter adsorbs onto the catalyst surface. The reaction is heterogeneous catalytic reaction with the step of reaction as followed: diffusion of reactants, adsorption, surface diffusion, reaction, desorption, and diffusion of products.

2.4 Photocatalytic Degradation of Diuron

Advanced Oxidation Process (AOPs) are alternative and very useful for the degradation of non-biodegradable organic pollutants. They are much more efficient than conventional techniques such as precipitation, flocculation, and adsorption. The chemical processing by AOPs could lead to the complete mineralization of pollutants. AOPs are based on the generation of the hydroxyl radicals and use them as primary oxidant for the degradation of organic pollutants.

2.4.1 The kinetic of photodegradation of diuron

Several papers on photocatalytic processes have been presented in the recent years [1, 6, 10, 18, 26, 29, 32-36]. The degradation rate of diuron depending on parameters influencing the oxidation such as pH value, light intensity, and concentration of photocatalyst. According to these papers, the photocatalytic processes are able to degrade non-biodegradable organic pollutants. They have also found that the kinetic model suitable for, the photocatalytic

reaction is the Langmuir – Hinshelwood model, in which the substrates must adsorb on the catalyst surface sites for bond breaking or bond formation. The adsorption of substrates and the availability of sites are important parameters in photocatalytic reactions. The rate of substrate conversion is proportional to the available active sites. As the reaction proceeds, the amount of substrate adsorbed on the catalysts surface will decrease until the substrate is completely converted. In general, kinetic models are often formulated to describe photocatalytic reactions with respect to the initial substrate concentrations. For the Langmuir – Hinshelwood kinetic model, it is assumed that the reaction occurs on the surface and the reaction rate (r) is proportional to the fraction of surface coverage by the substrate (θ):

$$r = -\frac{dC}{dt} = k_r\theta = k_r \frac{KC}{1 + KC} \quad (24)$$

where k_r is the reaction rate constant, K is the adsorption constant and C is the substrate concentration at any time t . When the solution is highly diluted, the term KC can be neglected. Previously several researchers approximated Langmuir-Hinshelwood kinetics to first order by assuming the term $KC \ll 1$ [37, 38]. Thus the Langmuir-Hinshelwood kinetic expression can be written as equation (25). The constants k_r and K can be calculated from the corresponding integrated expression in equation (26).

$$r = -\frac{dC}{dt} = k_r KC \quad (25)$$

$$\ln \frac{C_0}{C} + K(C_0 - C) = k_r Kt \quad (26)$$

The L-H model includes adsorption and reaction data. Moreover, the results of some papers indicated that the photocatalytic process is very efficient because it often achieves a complete mineralization of organics. Bamba et al. have investigated the photodegradation of diuron from aqueous solution by UV irradiation in the presence of commercial TiO_2 (P25 and PC500). The results of kinetic study showed that kinetic model for diuron photocatalytic degradation follows the Langmuir – Hinshelwood model. At concentration of diuron 10 ppm the pseudo – first order Langmuir – Hinshelwood rate coefficient were 1.787 and 0.576 ppm/min and the constant of adsorption equilibrium of Langmuir – Hinshelwood were 0.801 and 0.451 ppm^{-1} for the use of TiO_2 – P25 and TiO_2 PC500 respectively [35]. The kinetic rate constant of photodegradation of diuron depend on initial diuron concentration, catalyst loading, pH, and temperature [35, 39, 40]. High catalyst loading produces great number of

OH radicals and accelerates the reaction. In addition, it is media to the adsorbed diuron. Amount of catalyst loading and particle size of catalyst affect on photodegradation rate such that the degradation is increased when the catalyst loading is increased.

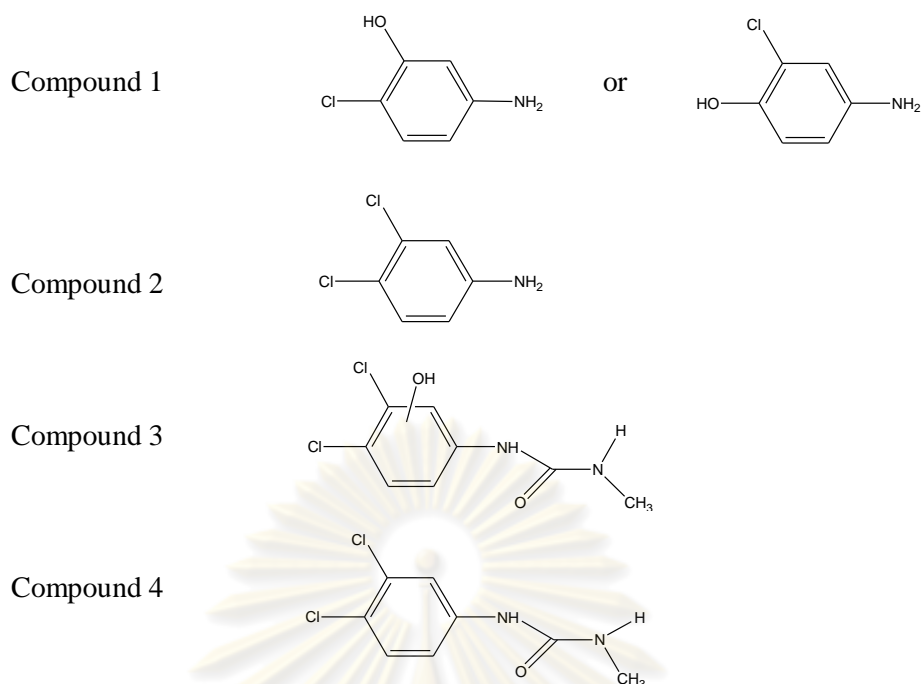
2.4.2 Diuron degradation products

The disappearance of the initial compound is not sufficient to demonstrate the effectiveness of the photocatalytic process because the intermediate compounds formed during the reaction could be even more toxic and resilient towards degradation than the parent compound. It is hence of interest not only to monitor the degradation of the parent compound but also to identify the intermediate compounds formed. In general, the oxidation of straight-chained hydrocarbon is relatively easy, while dearomatisation of aromatic compounds has been found to be harder, taking longer time and involves the formation of many intermediate compounds before mineralization is achieved.

The degree of degradation of diuron was obviously affected by photocatalyst amount, initial concentration of diuron, pH of solution, and temperature [18, 35]. For the photocatalytic degradation of the diuron contaminants, which has been investigated in the past, Klongdee et al. studied the degradation of diuron in aqueous solution by photocatalyzed oxidation, using synthesized titania as catalyst. Titania was synthesized by the thermal decomposition method. The results indicated that the conversions achieved from the prepared titania were about 70-80% within 6 hours, using standard UV lamps, while about 99% conversion was achieved under solar irradiation. The enhanced photocatalytic activity was the result from higher crystallinity of the synthesized titania. The presence of oxygen as an electron scavenger in the system was required for the reaction to progress [6]. However, the degradation rate of diuron depending on parameters influencing the oxidation such as pH value, light intensity, and concentration of photocatalyst [2]. The mineralization reaction (first order reaction) can be estimated as follows [1] :



The organic intermediates formed during the degradation of diuron could be classified into two categories. One is the non-chlorinated intermediates, another is the chlorinated and nitrated intermediates [2]. Most detected degradation products are constituted by diuron de-methyl derivatives, such as DCPMU [3-(3,4-dichlorophenyl)-1-methylurea], DCPU [3-(3,4-dichlorophenylurea)], and 3,4-DCA (3,4-dichloroaniline) [41] The structures of the photoproducts are represented as follows: [1]



The product compound number 1, 2, and 4 were identified as the compounds resulting from the elimination of alkyl groups from diuron. The product compound number 3 was found to be the product in which hydroxyl group was added to benzene ring of diuron. Therefore the possible degradation pathway for diuron based on the intermediate products was proposed in Figure 2.3 [1].

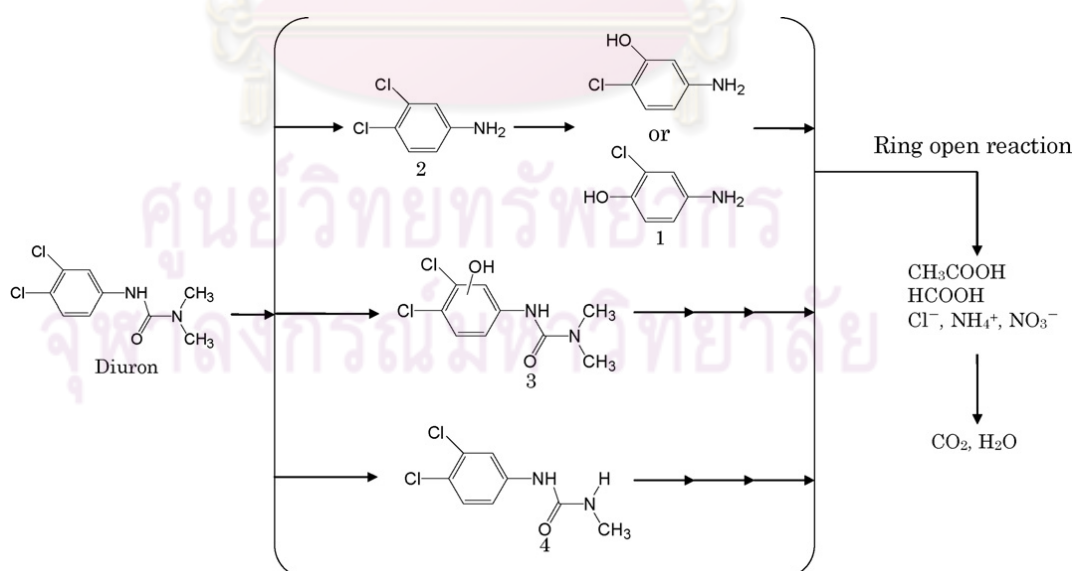
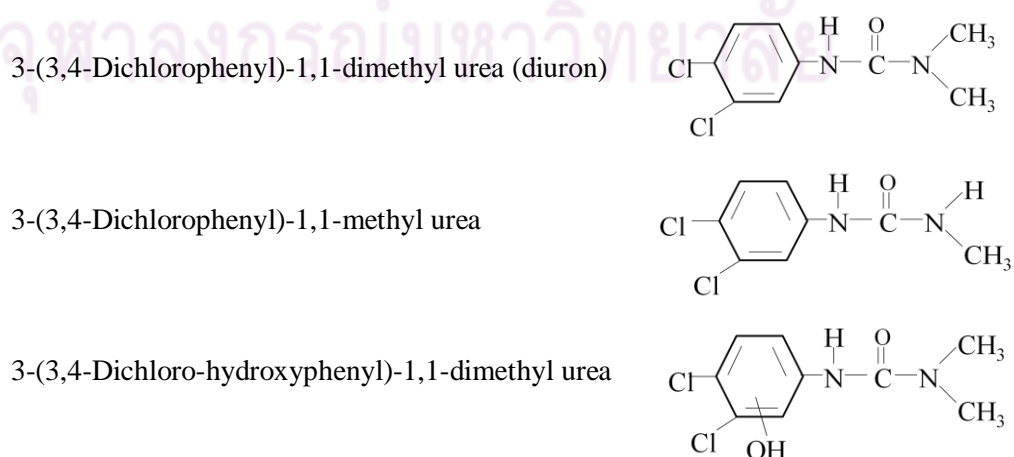
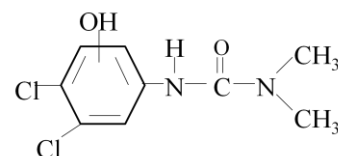


Figure 2.3 Proposed degradation mechanism of diuron by the photocatalytic system [1].

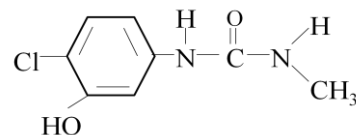
The previous researches have reported that different conditions of degradation produce different intermediate products. For instance, Carrier et al. investigated intermediate products of photocatalytic degradation using titania as photocatalyst. The possible degradation pathway for diuron was proposed in Figure 2.4. The reported steps of degradation included dehalogenation of the aromatic ring, hydroxylation of the aromatic ring and of the side chain, and demethylation [42]. Then they investigated the removal of diuron and thermal degradation products under catalytic wet air oxidation condition, using Ru/TiO₂ as catalyst at 140 °C and 180 °C. During the thermal degradation of diuron, three main intermediate compounds were formed, namely 3,4-dichloroaniline (DCA), dimethylamine (DMA), and 3-(3,4-dichlorophenyl)-1,1-methylurea. Degradation pathways of diuron by the catalytic wet air oxidation based on the identified intermediate products of the reaction, was proposed in Figure 2.5. The first step was a thermal degradation of diuron into DCA and DMA. The next step was a series of oxidation process of DCA that rapidly eliminated chlorine, opened the aromatic ring to yield small organics acids and led to inorganic species. Nitrogen in DCA was mainly transformed into NH₄⁺. The carboxylic acids formed (oxalic acid and acetic acid) reacted with DCA to form traces of 3,4-dichlorophenylamide and 3,4-dichlorophenylacetamide. DMA was more resistant and high temperature of the reaction was necessary. At 180 °C, DMA was converted into methylamine (MA), ammonium ions and nitrates. The higher temperature favoured the formation of nitrates [43]. Oturan et al. identified five kinds of intermediate products from electrochemical advanced oxidation method called “electro-Fenton process”. Several aromatic by-products, mainly formed by oxidation of the N-terminal group, accompanied by hydroxylation of the aromatic cycle and/or side methyl group, and aromatic dehalogenation were identified. Further steps involved the oxidative opening of the aromatic ring, leading to carboxylic acids and inorganic ions. Identification of the diuron degradation products was conducted by LC-MS and the results are represented as follow: [44]



3-(Trihydroxyphenyl)-1,1-dimethyl urea



3-(3-Hydroxy-4-chlorophenyl)-1,1-methyl urea



3-(3-Hydroxy-4-chlorophenyl)-1,1-dimethyl urea

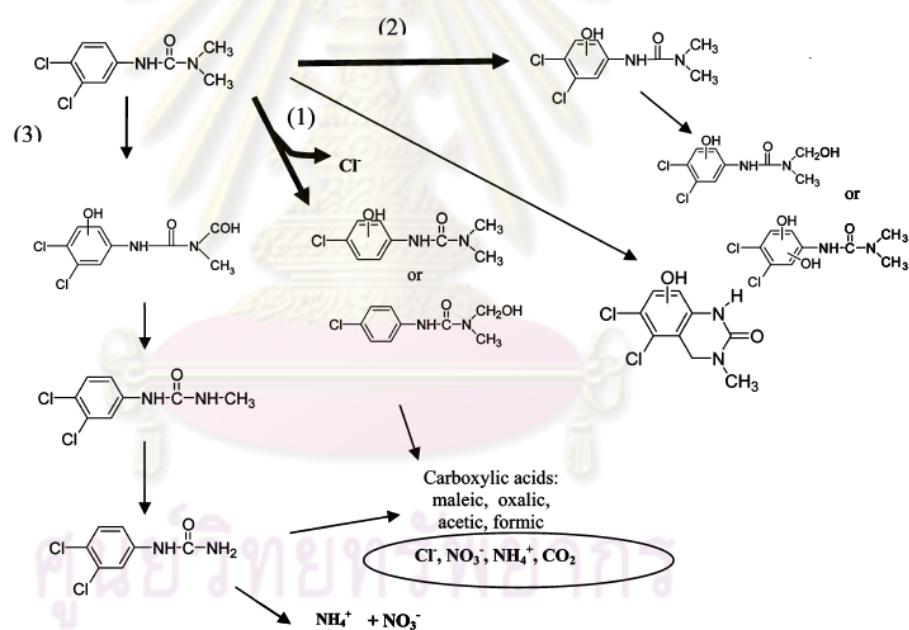
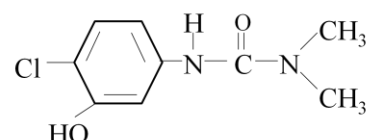


Figure 2.4 Degradation pathways of diuron by the TiO_2 as photocatalyst [42].

CHAPTER III

EXPERIMENTAL

3.1 Preparation of TiO₂ and ZnO

3.1.1 Synthesis of titania particles

Titania (TiO₂) was prepared by sol-gel method, according to the method proposed by Tian et al [5]. Tetrabutyltitanate (TBT, 97%, Fluka) was used as the starting material. First, 5 ml of TBT was dissolved in 20 ml ethanol and stirred for 30 minutes to get the precursor solution. Then, a mixture of 0.26 ml distilled water, 3.4 ml glacial acetic acid, 0.18 ml hydrochloric acid and 5 ml ethanol were added to the precursor solution under vigorous stirring. After stirring about 1 hour, the solution became transparent yellow. Now, titania sol was obtained. The titania sol was gelled at room temperature about 24 hours and dried at 80°C for 12 hours in an oven. Then, ammonia solution with mass fractions of 0%, 7% or 28% was dropped into the gel and left for 24 hours at room temperature. After that, the obtained product was calcined at 500°C for 2 hours in a box furnace with the heating rate of 1°C/min.

3.1.2 Synthesis of zinc oxide particles

Zinc oxide (ZnO) was prepared according to the method proposed by Tian et al. [5] as well. Zinc acetate (99.5%, UNIVAR) was used as a precursor to prepare ZnO sol. At first, 3.29 g of zinc acetate was dissolved in 20 ml ethanol and stirred for 5 min at 50°C to get the precursor solution. A mixture of 0.26 ml distilled water, 1.58 ml diethanolamine (98.5%, UNILAB), 0.18 ml hydrochloric acid, and 5 ml ethanol was dropped into the precursor solution under vigorous stirring. After stirring for 2 hours, a transparent ZnO sol was obtained. The ZnO sol was gelled at room temperature about 24 hours and dried at 80°C for 24 hours in an oven. Then, ammonia solution with mass fraction of 0%, 7% or 28% was dropped into the gel and left to rest for 24 hours at room temperature. After that, the obtained product was calcined at temperature in the range of 500°C for 2 hours in a box furnace with heating rate of 1°C/min.

3.1.3 Characterizations of photocatalysts

Synthesized photocatalysts were characterized by various techniques.

Phase composition of the powder was determined by X-ray diffraction (XRD) by a Siemens D5000 X-ray diffractometer using Ni-filtered CuK α radiation. The measurements were carried out in the 2θ range of 20-80 degree at the scan step of 0.04 degree. The crystallite size calculated from the half-height width of the diffraction peak of XRD pattern using the Debye - Scherer equation.

$$D = \frac{0.9\lambda}{\beta \cos\theta} \quad (27)$$

where D is crystal size, λ is wavelength of X-ray, β is full width at half maximum, θ is diffraction angle.

The particle morphology was investigated by Scanning Electron Microscopy (SEM) model JSM-6400 at Scientific and Technological Research Equipment Centre Foundation, Chulalongkorn University.

The surface area, pore volume and pore size were measured by Belsorp-Mini II adsorption analyzer using nitrogen as the adsorbate at the Center of Excellence on Particle Technology, Chulalongkorn University. The operating conditions are as follows:

Sample weight	~ 0.1- 0.2 g
Degas temperature	200°C
Vacuum pressure	< 10 mmHg

The thermal behavior was analyzed by Thermo-gravimetric analyzer (TGA) Model NETZSCH STA 409. The operating conditions are heating rate of 10°C/min from room temperature to 1000°C in air.

Finally, The ultraviolet–visible reflectance of all samples was analyzed by a UV – vis spectroscopy (Lambda 650, Perkin Elmer, USA).

3.2 Adsorption Studies

All adsorption equilibrium experiments of diuron on the TiO₂ and ZnO surface were carried out in 250 ml pyrex reactor under strong stirring and in the absence of light. Studies were conducted with suspensions prepared by mixing 550 ml of solution of diuron in various initial concentrations (1-20 ppm) and photocatalyst concentration of 1 mg/10 ml diuron solution at room temperature (27-30°C) for 3 hours. Changes of diuron concentration were measured by (HPLC), model Class VP (Shimadzu) and C18 column (Phenomenex Luna 5 µm particle size, 250×4.6 mm). The mobile phase was consisted of 70% acetonitrile and 30% deionization water with flow rate of 1.5 ml/min. Function groups of diuron solution after adsorbed by catalyst were identified by using Fourier Transform Infrared Spectrophotometer (FT-IR) Model Spectrum One (Perkin Elmer). Infrared spectra were recorded between wavenumber of 400 and 4000 cm⁻¹. The changing in the structure of diuron after adsorbed by catalyst was identified by using Fourier Transform Nuclear Magnetic Resonance (NMR, ¹³C: 125.777MHz, ¹H: 500.157 MHz) Model INOVA (Varia). In all experimentals, CD₃OD were used as solvent.

3.3 Photocatalytic Degradation Procedure

The photocatalytic activities of the synthesized photocatalysts were determined from the photodegradation of diuron (99.5%,N-(3,4-dichlorophenyl)-N,N-dimethyl urea) under UV irradiation. The photodegradation was conducted in a 600 ml pyrex reactor (the set up of the reaction system is shown in Figure 3.1), in which 550 ml of diuron solution (with predetermined concentration) and photocatalysts were added. The content of the photocatalyst was kept at 1 mg of the catalyst per 10 ml of the solution (initial diuron concentration 10 ppm). The mixture was kept in dark for 30 min to allow the complete adsorption of diuron on the surface of catalysts, prior to the reaction. After that, the solution was irradiated with six UV-A lamps (Phillips TLC 15w/05). During irradiation, agitation was maintained by a magnetic stirrer to keep the catalyst uniformly dispersed within the solution. The suspension was periodically sampled to monitor the concentration of diuron via a reverse-phase liquid chromatography (HPLC), model Class VP (Shimadzu) and C18 column (Phenomenex Luna 5 µm particle size, 250×4.6 mm). The mobile phase was consisted of 70% acetonitrile and 30% deionization water with flow rate of 1.5 ml/min. The organic matter within the sample was measured by Total Organic Carbon (TOC) analyzer model TOC-V_{CPH} (carrier gas flow rate 150 ml/min, 680°C catalytically-aided combustion oxidation/non-dispersive infrared detection). Identification of the reaction intermediates formed during the photocatalytic

degradation of diuron was done by LC-MS analysis (LC/MSD SL, Agilent technologies) with UV detector and MS detector (Single Quadrupole, Model G1956B, Agilent technologies). For the LC-MS analysis, column was Phenomenex Luna, 3 μm particle size, 150 \times 2 mm, while the mobile phase was 70% acetonitrile mixed with 30% water. The mass spectral data were obtained in both negative and positive ion mode, using fragmentor potential of 120 V.

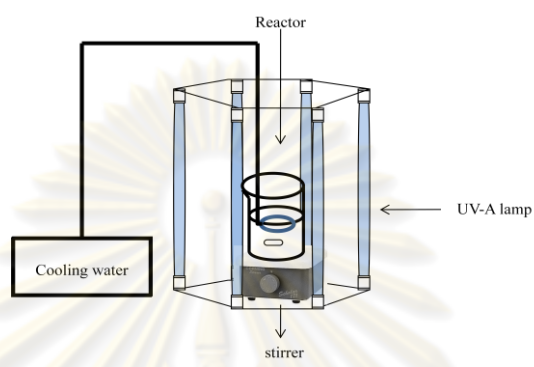


Figure 3.1 Diagram of the equipment setup for the photocatalytic degradation.

ศูนย์วิทยทรัพยากร
จุฬาลงกรณ์มหาวิทยาลัย

CHAPTER IV

RESULTS AND DISCUSSION

Photocatalytic degradation can be applied to remove many organic compounds from wastewater. In this study, titania and zinc oxide were used as photocatalyst to eliminate diuron from water. The photocatalysts were prepared by sol-gel method. Physical properties of the synthesized photocatalysts were investigated by many techniques. Then, they were compared in the photocatalytic degradation of diuron.

4.1 Properties of Synthesized Photocatalysts

4.1.1 Synthesized zinc oxide

In this research, zinc oxide was synthesized by sol-gel method and subsequently calcined at 500°C for 2 hours. Ammonia was also added during sol-gel process. The content of ammonia investigated was 0%, 7% and 28% by mass, respectively. Characterization techniques such as XRD, SEM, BET and TGA were used to investigate physical properties of the synthesized zinc oxide.

Phase composition of the zinc oxide powder was identified through XRD. XRD patterns of the zinc oxide synthesized in all conditions are shown in Figure 4.1. All of the diffraction peaks could be indexed as zinc oxide in wurzite structure. The crystallite sizes of zinc oxide calculated from the Scherer equation are shown in Table 4.1. No diffraction peaks corresponding to other phases are detected, even when high content of ammonia was added to the gel.

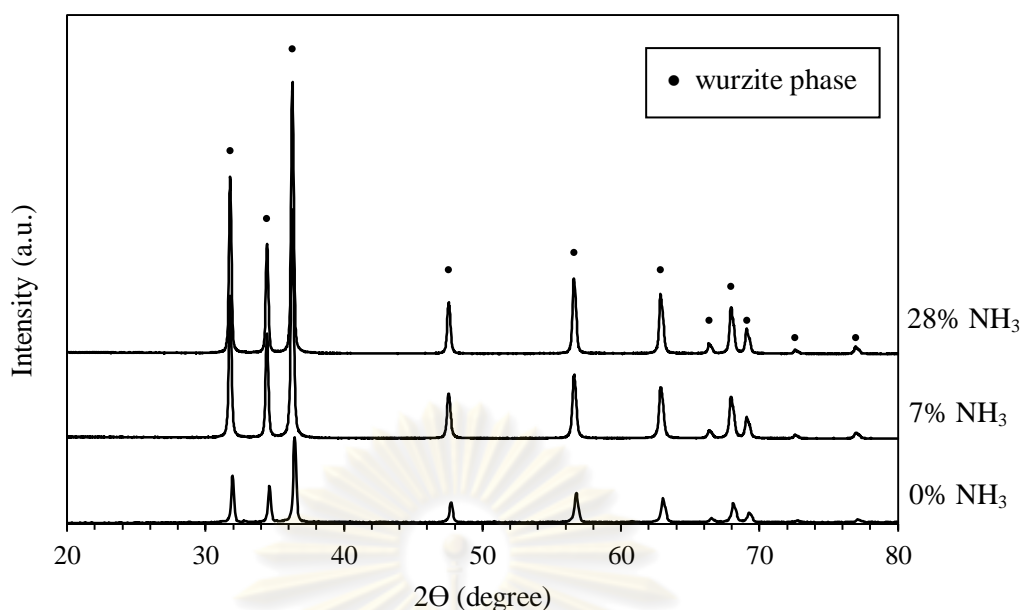


Figure 4.1 XRD patterns of the zinc oxide powder synthesized with the addition of ammonia in the amount of 0%, 7%, and 28% by weight of the solution. All products were calcined at 500°C for 2 hours.

Table 4.1 Crystallite size and surface area of the synthesized zinc oxide.

Condition of ammonia added in the solution	Crystallite size, (nm)	Specific surface area, S_{BET} , (m^2/g)	Average pore diameter (nm)	Band gap (eV)
0%	104	4	5	3.16
7%	106	8	11	3.14
28%	116	6	11	3.12

The specific surface areas of zinc oxide measured by nitrogen adsorption (S_{BET}) are also shown in Table 4.1. All samples showed Type - II adsorption/desorption isotherm which indicated the non - porous in the catalyst as shown in Figure 4.2. As the mass fraction of ammonia was increased from 0% to 7%, the specific surface area of the ZnO powder increased from 4 to 8 m^2/g while the further increase of ammonia content 28% the resulted in the decrease surface area to 6 m^2/g . However, the specific surface areas of zinc oxide are similar, so that the ammonia content did not affect to the specific surface area of zinc oxide.

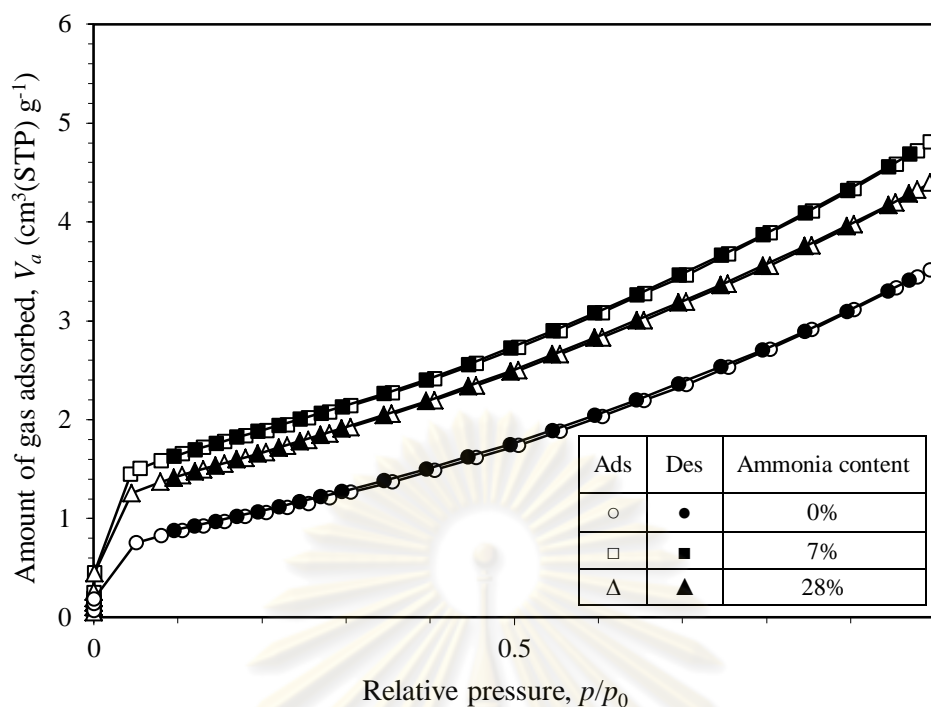


Figure 4.2 Adsorption/desorption isotherm of zinc oxide powder synthesized with the addition of ammonia in the amount of 0%, 7%, and 28% by weight of the solution. All products were calcined at 500°C for 2 hours.

Figure 4.3 shows SEM images of the synthesized ZnO powders ammonia treated with various mass fraction of ammonia solution after calcined at 500°C for 2 hours. The ZnO powders synthesized without ammonia as shown in Figure 4.3(a) were agglomerated with average particle size 175 nm. The increasing ammonia content led to the decrease in particle size as shown in Figure 4.3(b). The average particle size in the powder was 138 nm. The particles were uniform. As Figure 4.3(c) the particles were agglomerated with average size diameter 175 nm.

จุฬาลงกรณ์มหาวิทยาลัย

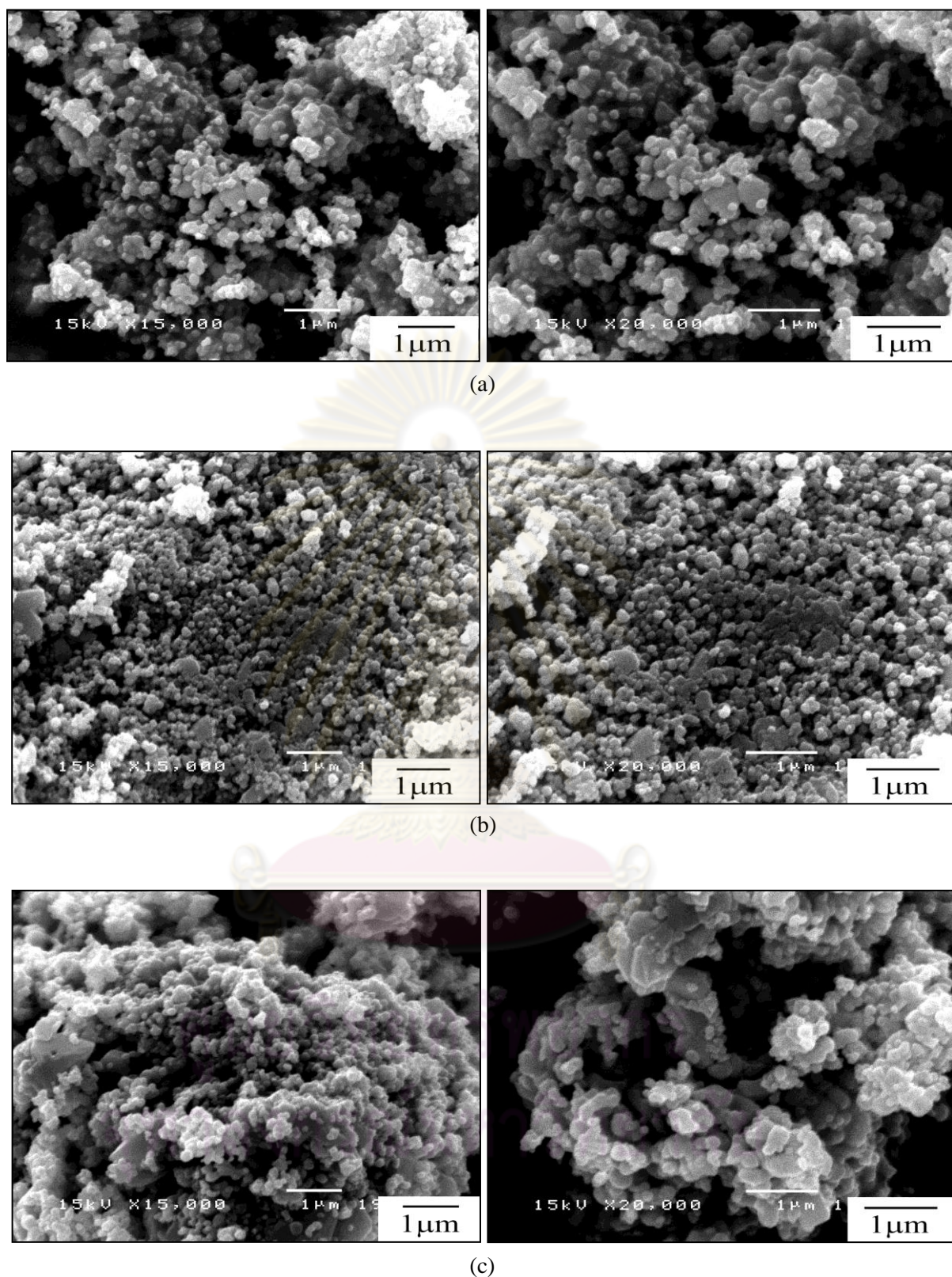


Figure 4.3 SEM micrographs of the zinc oxide powder synthesized with the use of ammonia at various content: (a) 0% NH₃ (b) 7% NH₃ and (c) 28% NH₃, after calcined at 500°C for 2 hours.

TG/DTA results for the ZnO powder, after calcined at 500°C for 2 hours (heating rate of 10°C/min), heated from 0-1000°C in flowing air are shown in Figure 4.4. It is clearly seen that the TGA curve indicates no weight loss while neither exothermic nor endothermic peaks are found in the DTA curve. This suggests that calcinations temperature of 500°C is enough for complete combustion of organic. The results confirm that the synthesized ZnO had no residual organics compound within the powder.

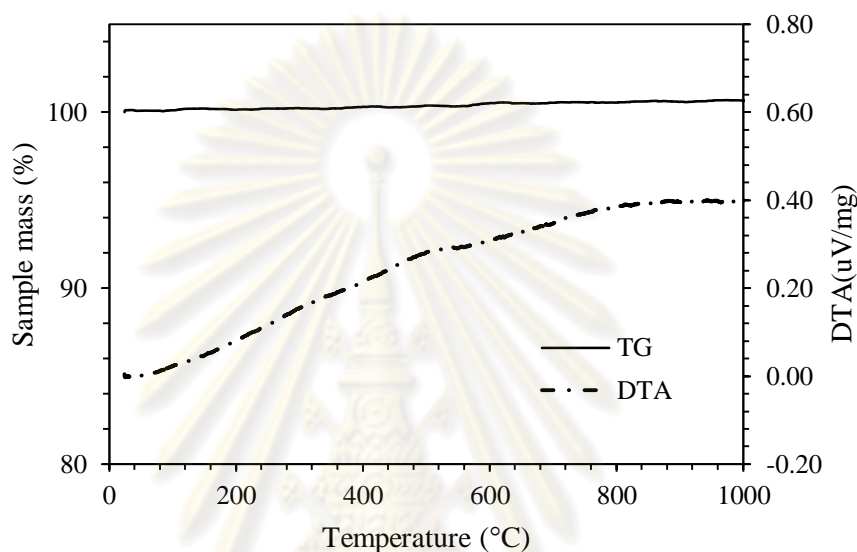


Figure 4.4 TG/DTA curves of the synthesized zinc oxide powder after calcined at 500 °C for 2 hours (heating rate of 10°C/min) without ammonia content.

4.1.2 Synthesized titania

Titania was synthesized by the sol-gel method. During the synthesis, the titania powder was treated with ammonia solution at mass fraction of 0%, 7%, and 28% for 24 hours followed by calcination at 500°C for 2 hours. The phase composition of titania powder after calcination was identified by XRD. XRD patterns of the titania are shown in Figure 4.5. It is confirmed that the product obtained is titania in anatase phase without contamination of rutile phases or other phases relating to nitrogen. The average crystallite size, calculated by the Scherrer equation based on the anatase (101) diffraction peak are shown in the Table 4.2.

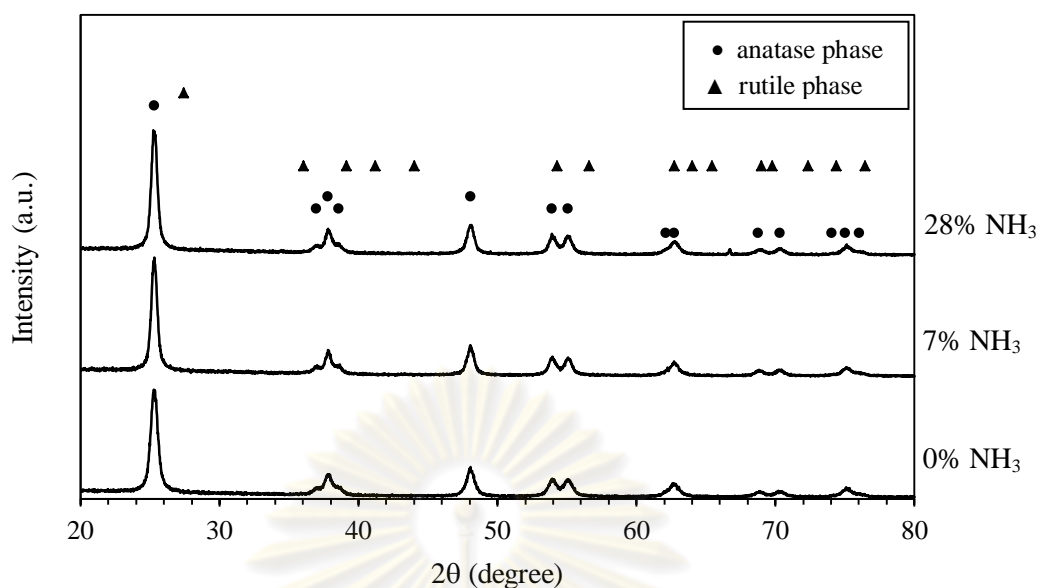


Figure 4.5 XRD patterns of the titania powder synthesized by treated with ammonia solution at the mass fraction of 0%, 7%, and 28% for 2 hours followed by calcination at 500°C for 2 hours.

Table 4.2 Crystallite size and surface area of synthesized titania.

Condition of ammonia added in the solution	Crystallite size, (nm)	Specific surface area, S_{BET} , (m^2/g)	Average pore diameter (nm)	Band gap (eV)
0%	14	36	5	3.30
7%	17	45	4	3.27
28%	16	52	4	3.25

The analysis of the catalyst surface via nitrogen adsorption revealed type IV adsorption/desorption isotherm with a hysteresis loop for the synthesized titania, which indicated the presence of mesopores in the catalyst as shown in Figure 4.6. The calculated specific surface areas based on BET model are also shown in Table 4.2. As the ammonia content was increased from 0% to 28%, the surface area of TiO_2 powder increased from 36 to 52 m^2/g . The results were in good agreement with SEM images.

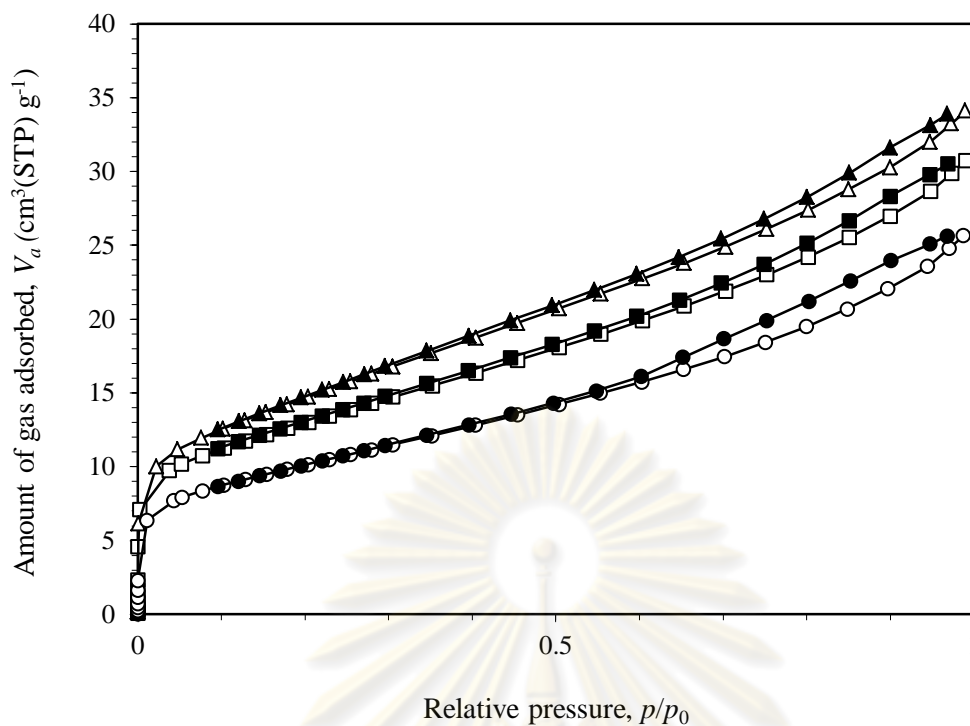
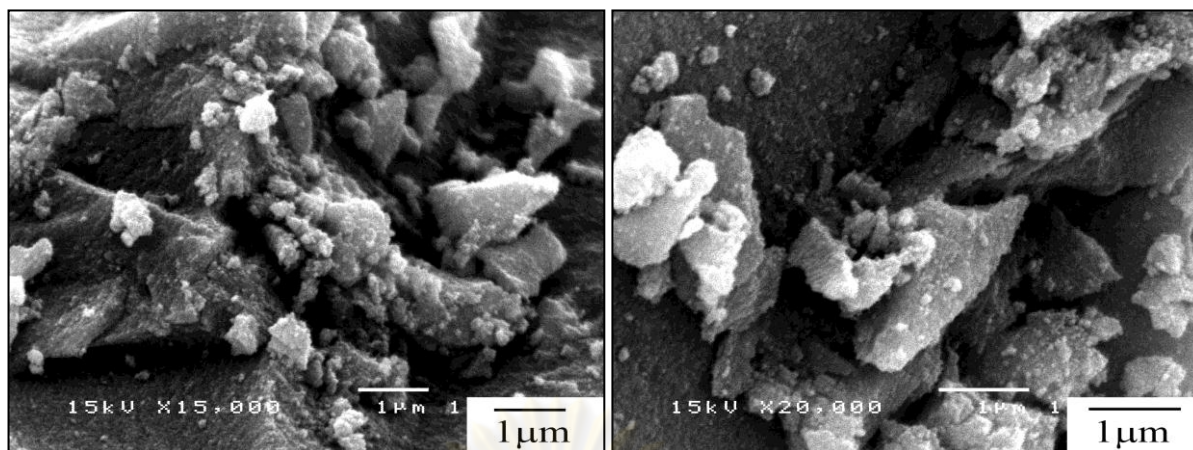
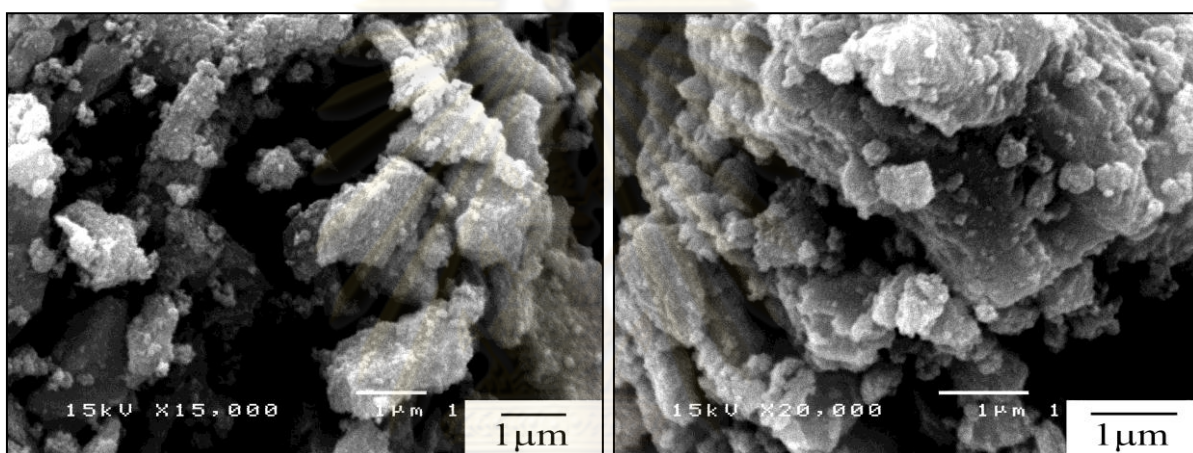


Figure 4.6 Adsorption/desorption isotherm of titanium dioxide powder synthesized with the addition of ammonia in the amount of 0%, 7%, and 28% by weight of the solution. All products were calcined at 500°C for 2 hours.

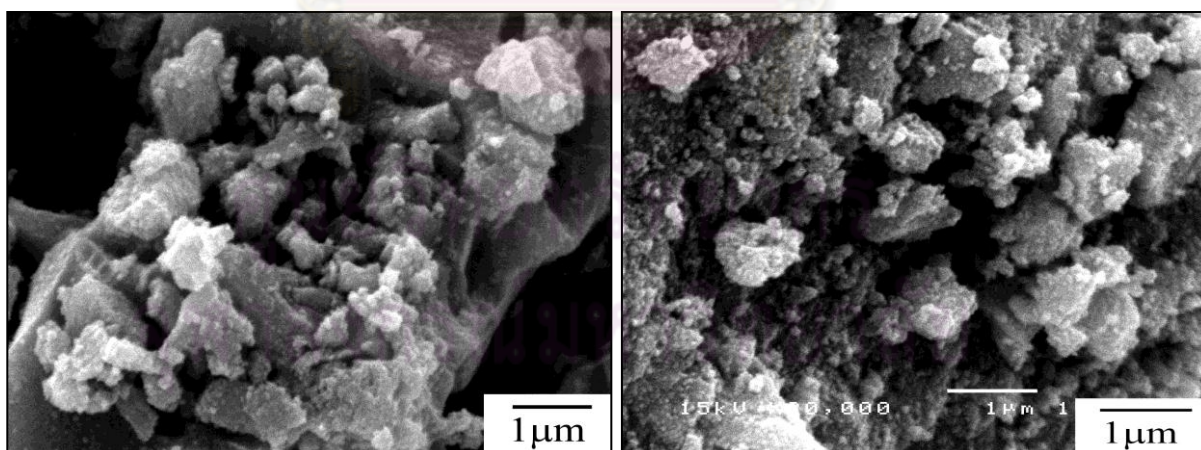
The synthesized TiO_2 powders are consisted of both large and small particles with a wide range of size distribution as shown in Figure 4.7. The powders are consisted of non-spherical particles that are high agglomerated. The aggregation could be due to the high viscosity of the sol, which reduces the dispersion of particles [33]. According to Figure 4.7, the surfaces of the TiO_2 powders become rougher when the content of ammonia used is increased. The particles are highly porous with high surface area which may have higher adsorption affinity towards diuron molecules filled in the pores and can play a role in enhancing the photocatalytic activity of titania particles.



(a)



(b)



(c)

Figure 4.7 SEM micrographs of the synthesized TiO₂ powders synthesized using ammonia at various contents: (a) 0% NH₃ (b) 7% NH₃ and (c) 28% NH₃, after calcined at 500 °C for 2 hours.

TG/DTA results for the TiO_2 powder, after calcined at 500°C for 2 hours (heating rate of $10^\circ\text{C}/\text{min}$), heated from 0 - 1000°C in flowing air are shown in Figure 4.8. The TGA curve indicates no weight loss, while the DTA curve shows no significant thermal event. The results confirm that TiO_2 powder had no residual organics compound within the powder.

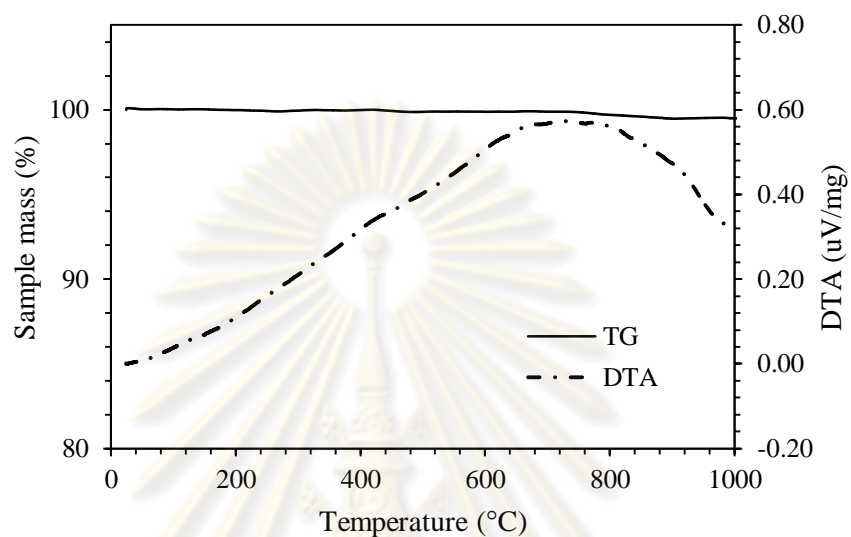


Figure 4.8 TG/DTA curves of the synthesized titanium dioxide powder after calcined at 500°C for 2 hours (heating rate of $10^\circ\text{C}/\text{min}$) without ammonia content.

ศูนย์วิทยทรัพยากร
จุฬาลงกรณ์มหาวิทยาลัย

4.2 Adsorption of Diuron onto the Catalysts

4.2.1 Adsorption isotherm

In this part, diuron was adsorbed onto the catalyst without illumination. Figure 4.9 and Figure 4.10 show the results of the adsorption of diuron onto zinc oxide and titanium dioxide as a function of time at room temperature (27-30°C). The initial concentration of diuron was varied from 1, 5, 10, 15, to 20 ppm respectively. The catalyst loading was 1 mg per 1 ml of the diuron solution. The results confirm that the adsorption takes place very fast, with the adsorption equilibrium occurring after 30 min at low concentration of 1, 5, and 10 ppm while, at the concentration of 15 and 20 ppm, the adsorption equilibrium is reached after 120 min. The amount of diuron adsorbed increased with increasing the concentration of diuron, especially at 20 ppm. Molecules of diuron have more chances to react with catalyst when concentration of diuron is increased. They were adsorbed on the surface of the catalyst better. It might be ascribed to increasing in the driving force of concentration gradient. Therefore the amount of diuron adsorbed increased. The sorption ability of a surface can be measured by the adsorption isotherm. The adsorption isotherm is characterized by the amount of diuron adsorbed per gram of catalysts (ZnO or TiO₂) at equilibrium. The adsorption isotherm of diuron on synthesized ZnO, synthesized TiO₂, commercial ZnO, and commercial TiO₂ at room temperature (27-30°C) are shown in Figure 4.11. The amount of diuron adsorbed at equilibrium increases with the concentration of diuron for all catalysts.

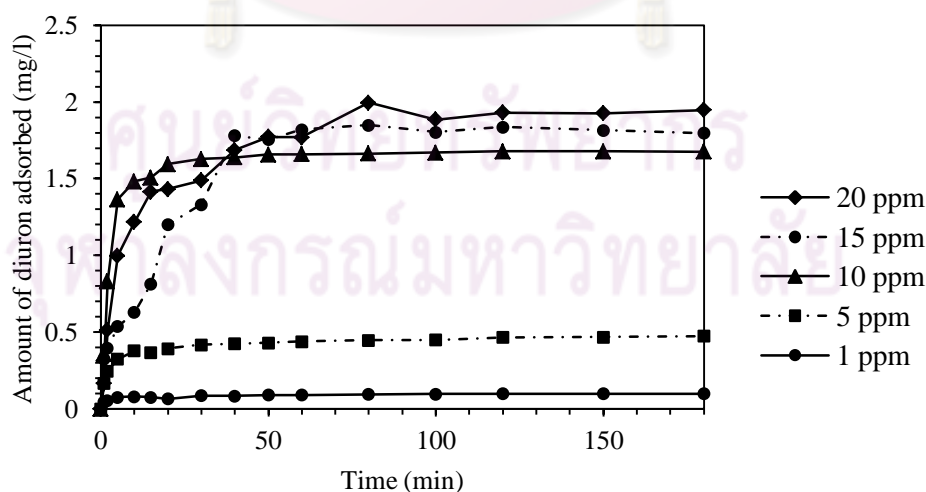


Figure 4.9 Adsorption of diuron on ZnO at room temperature (27-30°C). The initial diuron concentration was 1, 5, 10, 15, and 20 ppm, respectively.

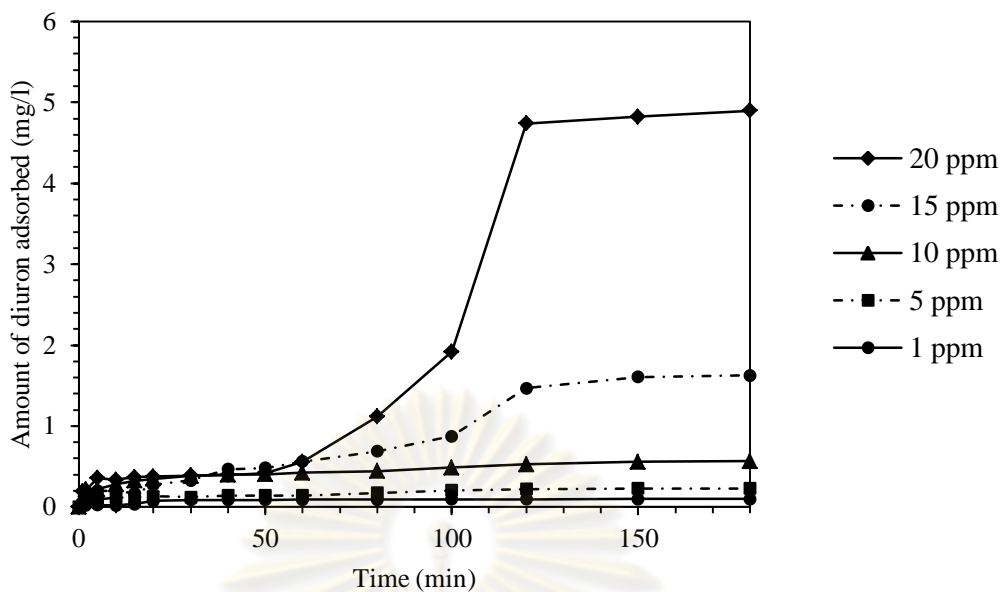


Figure 4.10 Adsorption of diuron on TiO_2 at room temperature ($27\text{-}30^\circ\text{C}$). The initial diuron concentration was 1, 5, 10, 15, and 20 ppm, respectively.

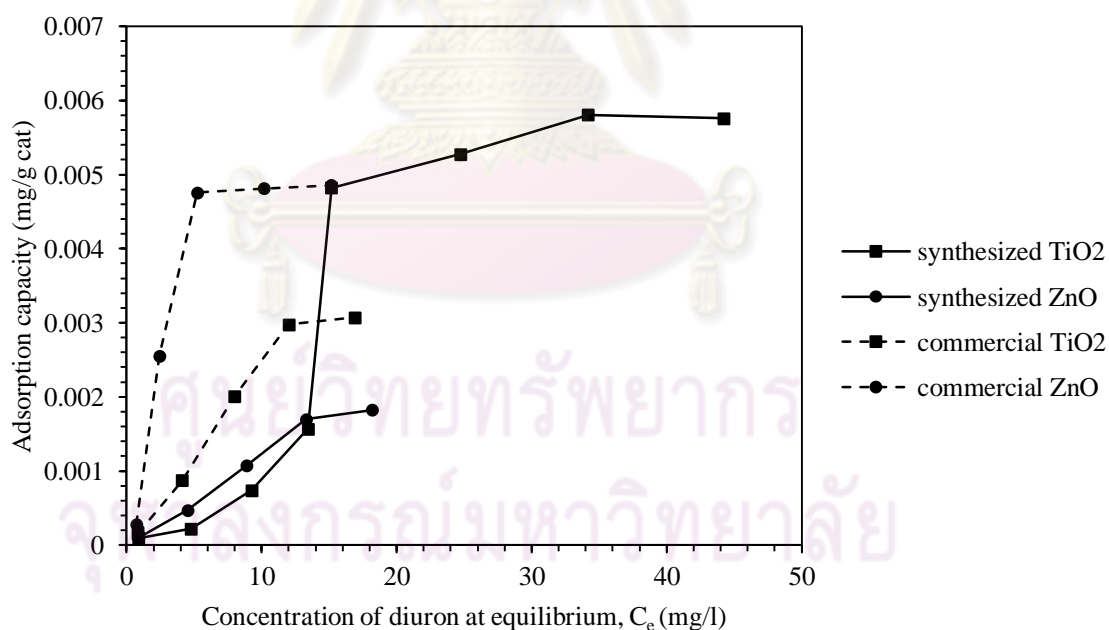


Figure 4.11 Adsorption isotherm of diuron onto synthesized ZnO , synthesized TiO_2 , commercial ZnO , and commercial TiO_2 at room temperature ($27\text{-}30^\circ\text{C}$).

Several models have been developed to define the adsorption isotherm. Among them, the isotherms according to Langmuir and Freundlich models have been often considered. According to the linearized form of the Langmuir isotherm model [36, 45, 46]:

$$\frac{1}{q_e} = \frac{1}{q_{\max}} + \frac{1}{bq_{\max}} \frac{1}{C_e} \quad (4.2)$$

where q_e is amount of adsorbate on adsorbent at equilibrium (mg/g), q_{\max} is maximum adsorption capacity (mg/g), C_e is equilibrium concentration (mg/l), and b is constant related to energy of the sorption system (l/mg). For Freundlich model, its linearized form of isotherm [36, 46, 47] is given by Equation 4.3 as follows:

$$\ln q_e = \ln K_f + \frac{1}{n} \ln C_e \quad (4.3)$$

where $\frac{1}{n}$ is adsorption intensity and K_f is Freundlich constant related to adsorption capacity (mg/g(mg/l)^{-1/n}). Figure 4.12 and Figure 4.13 show Langmuir isotherm and Freundlich isotherm for the adsorption of diuron on zinc oxide and titanium dioxide while the value of q_{\max} , b , K_f , n , and R^2 value obtained from the curves of Figure 4.12 and 4.13 are summarized in Table 4.3.

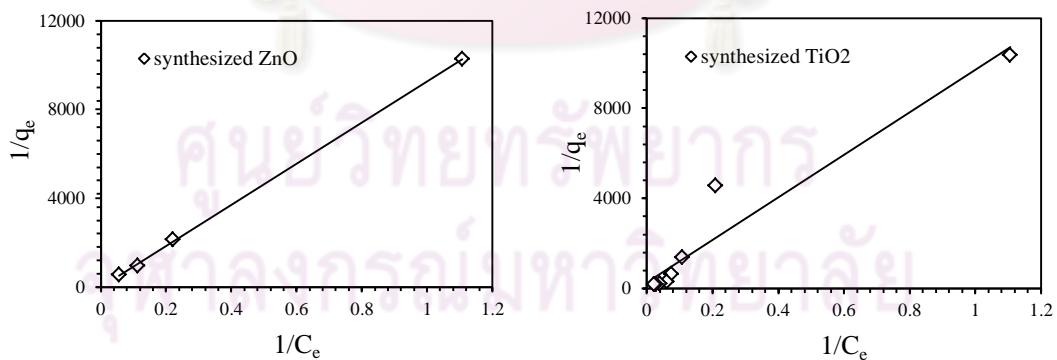


Figure 4.12 Langmuir isotherm for adsorption of diuron on synthesized ZnO and synthesized TiO₂.

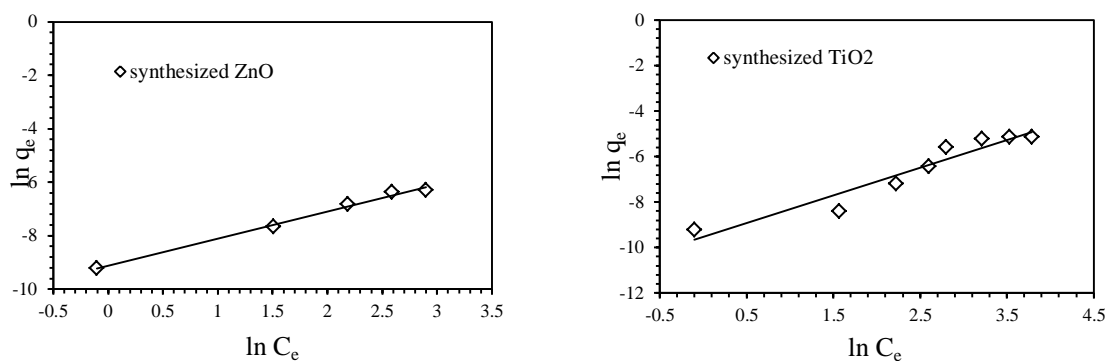


Figure 4.13 Freundlich isotherm for adsorption of diuron on synthesized ZnO and synthesized TiO₂.

Table 4.3 Constants of Langmuir and Freundlich isotherm model for adsorption of diuron on synthesized ZnO and synthesized TiO₂.

Model	Parameters	Values	
		synthesized ZnO	synthesized TiO ₂
Langmuir isotherm model	q_{max}	0.0030	0.0038
	b	0.0348	0.0277
	R^2	0.9974	0.9313
Freundlich isotherm model	K_f	10.8×10^{-5}	7.21×10^{-5}
	n	0.9819	0.8237
	R^2	0.9932	0.9194

Freundlich's parameter relates to the mean energy of adsorption. A very weak adsorbent/adsorbate interaction occurs at values of n lower than 1, while values higher than 1 suggest a strong adsorbent/adsorbate interaction. At value of n equal to 1 it is assumed that all sites are energetically similar [36, 39]. In our case, value of n lower than 1 for adsorption of diuron on TiO₂ indicated a weak diuron and catalyst interaction and value of n equal to 1 for adsorption of diuron on ZnO indicated all sites are energetically similar. This was confirmed by the values of Freundlich's constant, K_f , which also relates to the adsorption capacity.

For Langmuir's parameter, to examine the progression of adsorption dimensionless constant, separation factor r was calculated by following equation

$$r = \frac{1}{1 + bC_0} \quad (4.1)$$

Values $r > 1$ represents unfavorable adsorption condition, and values $0 < r < 1$ represents favorable adsorption conditions [45]. In this case, r value is between 0 and 1 (0.7418 and 0.7829 for synthesized ZnO and TiO₂, respectively), suggesting that the sorption is favorable for diuron on ZnO and TiO₂.

However, the experimental data were fitted well with Langmuir model as indicated by the high R² value.

4.2.2 FTIR studies

Figure 4.14 and 4.15 shows FTIR spectra obtained from diuron solution in methanol mixed with ZnO and TiO₂. The characteristic peaks of methanol were 1360, 1396 and 1050 cm⁻¹ corresponding to the O-H vibration [48, 49] and C-O stretching [50]. The characteristic peaks of diuron were 1655 cm⁻¹ corresponding to the N-H bending, at 1527, 1490 1396 cm⁻¹, and 899 cm⁻¹ corresponding to the C=C aromatic ring, C=C vibration, the benzene ring stretching, and meta benzene respectively, at 1027 and 810 cm⁻¹ corresponding to C-N stretching and C-Cl [48, 51]. A band shift of the C=C vibrations (1510 – 1470 cm⁻¹) towards lower wavenumber after interaction, would indicate an electrodonation reduction which add electron density to a system and tend to stabilize cations or electron poor system, to the ring as consequence of the molecule interaction with ZnO or TiO₂ surface.

According to Figure 4.14, absorption band of Zn-O stretching was around 430-550 cm⁻¹ [52] in curve (b). Considering the diuron-ZnO system only small band shifts are observed. This is the result from the fact that diuron adheres to the surface of zinc oxide only through Van der Waals, which is weak intermolecular interaction. Absorption bands of the C=C vibration and that of the C=C aromatic ring shift from 1490 and 1527 cm⁻¹ toward lower wavenumbers of 1485 and 1513 cm⁻¹, respectively, while the absorption band of C-Cl shift towards higher wavenumber (from 810 to 830 cm⁻¹).

In the diuron – TiO₂ system, only small band shifts are observed as well. In Figure 4.15, the broad band between 500 and 600 cm⁻¹ correspond to Ti-O band [53, 54]. The shifting in the absorption band of C=C aromatic ring (from 1527 to 1515 cm⁻¹) and C=C vibration (from 1490 to 1485 cm⁻¹) are similar to those observed in diuron – ZnO system, which also indicates an electrodonation reduction to the ring as consequence of the molecule

interaction with TiO_2 surface. Absorption band of CH_3 group was shift towards higher wavenumber (from 1037 to 1048 cm^{-1}).

However, the results indicated only small shift, it should be noted that, the adsorption of diuron on TiO_2 and ZnO are physisorption (Van der Waals and electrostatic forces). The structures have not change. This suggest, the reaction could not be occurs without UV irradiation.

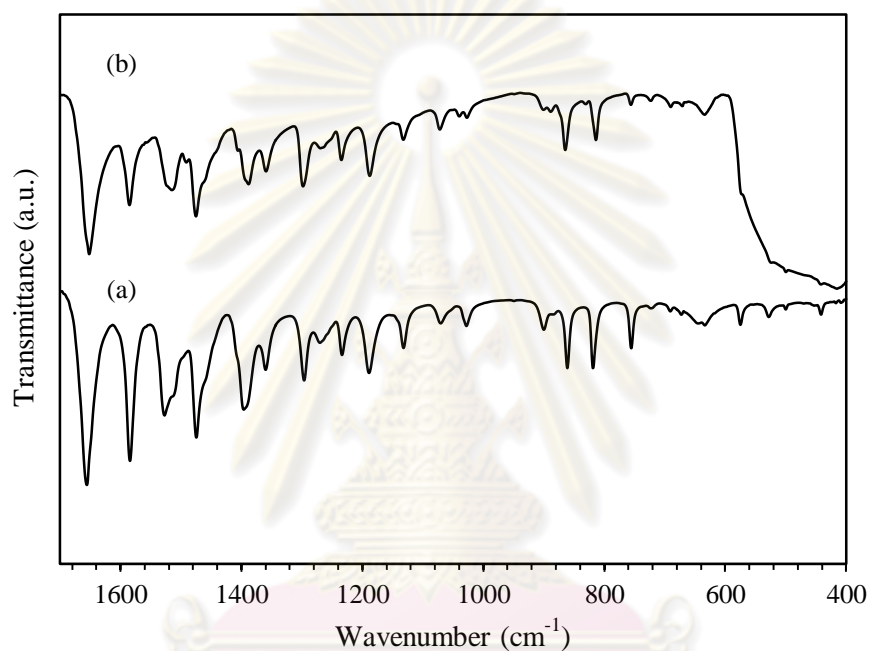


Figure 4.14 FTIR spectrum obtained from (a) diuron solution in methanol, (b) diuron solution in methanol mixed with ZnO for 180 min.

ศูนย์วิทยาศาสตร์
จุฬาลงกรณ์มหาวิทยาลัย

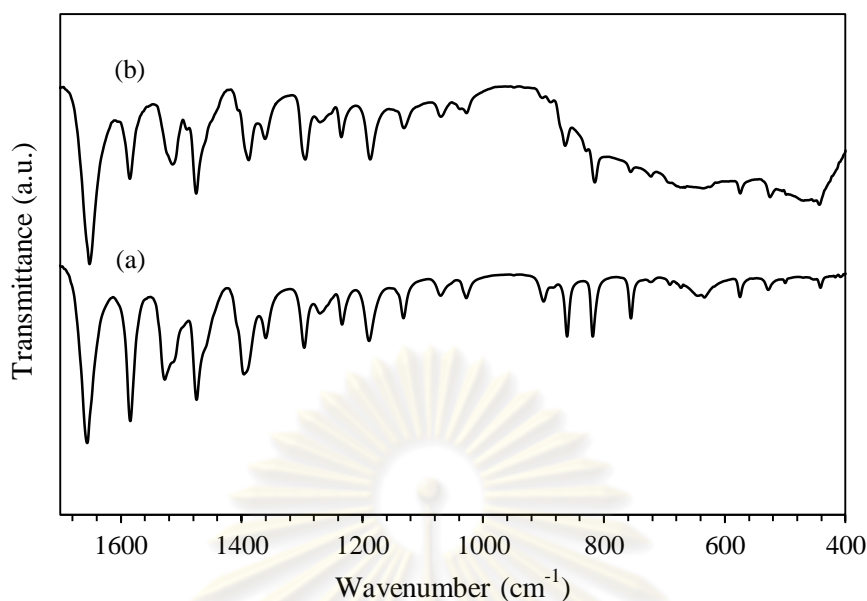


Figure 4.15 FTIR spectrum obtained from (a) diuron solution in methanol, (b) diuron solution in methanol mixed with TiO₂ for 180 min.

4.3 Photodegradation of Diuron

Conventionally, it has been reported that the photocatalytic system produces hydroxyl radical during the reaction. The radical is a strong oxidizing agent that reacts with diuron and causes its degradation [1]. Degradation of diuron can be expressed by the following reaction [55].



The complete mineralization expressed by the following equation [1, 55]:



In this work, the photodegradation of diuron aqueous solution was conducted in a pyrex reactor. The content of the photocatalyst was kept at 1 mg of the catalyst per 10 ml of the solution (initial diuron concentration of 10 ppm). The photodegradation of diuron solution using zinc oxide or titania as a catalyst was achieved within 6 hours of UV irradiation. The experiments under UV-light without catalyst, confirmed the absence of photolysis of diuron

as shown in Figure 4.16. Figure 4.16 describe the relative decrease in concentration of diuron as a function of irradiation time in the presence of catalysts, i.e. zinc oxide and titania are shown in Figure 4.19 It can be inferred that, there is no appreciable degradation when the aqueous solution is irradiated in the absence of titania or zinc oxide. The degradation of diuron is less than 5% after 6 hours of irradiation without the catalyst, which is similar to the result reported for self-degradation in the dark at room temperature indicating that hydrolysis of diuron can be neglected [56]. The enhanced degradation by the UV/photocatalyst suggests that both UV light and photocatalyst are required for efficient degradation of diuron.

4.3.1 Photodegradation of diuron on zinc oxide

Diuron is degraded in less than 360 minutes in the presence of zinc oxide. Concentration of diuron with respect to the initial diuron concentration (C/C_0) during the photocatalytic degradation on zinc oxide prepared using various mass fractions of ammonia is shown in Figure 4.16. The results reveal that the activity of zinc oxide increases when the higher amount of ammonia is used during preparation. The conversion obtained from zinc oxide powder ammonia-treated with NH_3 mass fraction of 28% is evidently the highest value, while in the case of zinc oxide without ammonia treatment the lowest conversion is achieved. Thus, the photocatalytic behavior of zinc oxide powder depends upon the ammonia treating process. It is found that diuron is degraded by about 92, 96, and 98%, when zinc oxide treated with ammonia at the fraction of 0, 7, and 28% is used, respectively.

According to many researchers, the photocatalytic degradation of organic pollutants is described by the pseudo-first order kinetics.

$$r = -\frac{dC}{dt} = k_{app}C \quad (4.4)$$

where r is the rate of diuron degradation, C is the concentration of diuron, t is the irradiation time, k_{app} is the apparent rate constant of a pseudo first order reaction [37, 57]. After integration, Equation 4.4 can be simplified to Equation 4.5 where C_0 is the initial concentration of diuron.

$$\ln\left(\frac{C_0}{C}\right) = k_{app}t \quad (4.5)$$

Kinetic studies were assessed by monitoring the change in diuron concentration at certain interval of time (C). The apparent first order rate constants (k_{app}) were determined by employing Equation 4.5 using the plot of $\ln(C_0 / C)$ versus irradiation time t as shown in Figure 4.17. The k_{app} was determined by calculating the slope of the line obtained. The resulting first order rate constant for each catalyst is shown in Table 4.3. The R^2 values are between 0.9878 and 0.9983. The degradation curve can be fitted reasonably well by an exponential decay curve suggesting the pseudo first order kinetics.

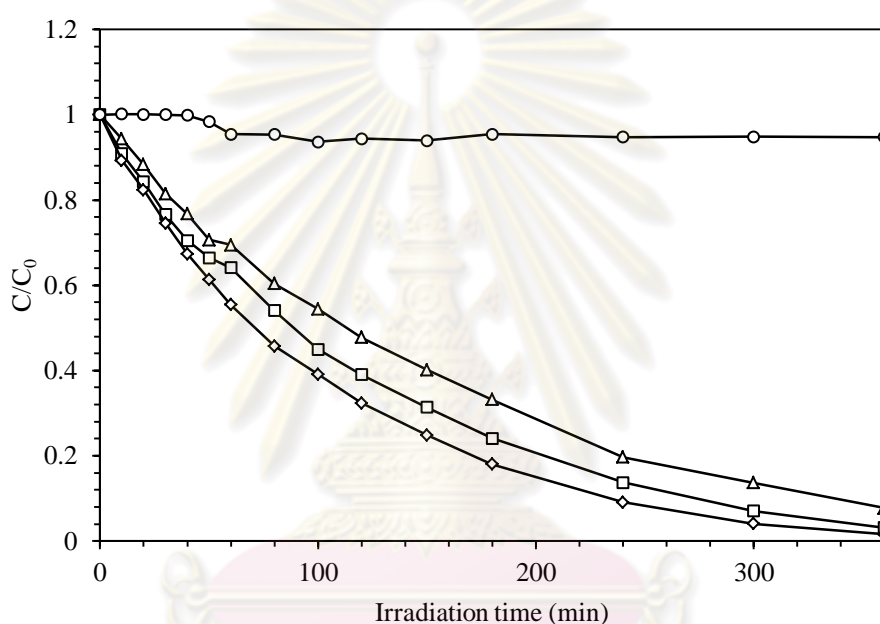


Figure 4.16 Concentration of diuron with respect to the initial diuron concentration (C/C_0) during the photocatalytic degradation on zinc oxide at various mass fraction of ammonia: \triangle : 0% NH_3 , \square : 7% NH_3 , \diamond : 28% NH_3 , and \circ : without catalyst. The reaction was conducted using 1 mg of zinc oxide per 10 ml of solution and using the initial concentration of diuron is 10 ppm.

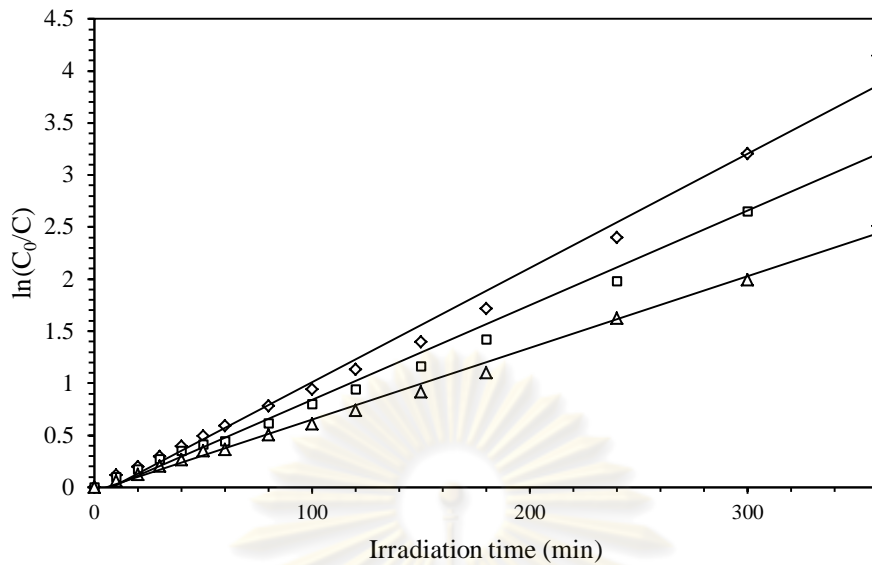


Figure 4.17 First –order linear transforms of the photocatalytic degradation on zinc oxide at various mass fraction of ammonia: \triangle : 0% NH_3 , \square : 7% NH_3 , and \diamond : 28% NH_3 . The reaction was conducted using 1 mg of zinc oxide per 10 ml of solution and using the initial concentration of diuron is 10 ppm.

The Langmuir-Hinshelwood (L-H) kinetics is the most commonly used kinetic expression to explain the kinetics of the heterogeneous catalytic processes.

$$r = -\frac{dC}{dt} = k_r \theta = \frac{k_r KC}{1 + KC} \quad (4.6)$$

where k_r is the true rate constant and K is the constant of adsorption equilibrium of Langmuir – Hinshelwood [37]. When the solution is highly diluted, the term KC can be neglected. Previously several researchers approximated the Langmuir-Hinshelwood kinetics to the first order by assuming the term $KC \ll 1$ [37, 38]. Thus the Langmuir-Hinshelwood kinetics expression can be written as Equation 4.7. The constants k_r and K can be calculated from the corresponding integrated expression in Equation 4.8.

$$r = -\frac{dC}{dt} = k_r KC \quad (4.7)$$

$$\ln\left(\frac{C_0}{C}\right) + K(C_0 - C) = k_r K t \quad (4.8)$$

The data shown in Figure 4.16 were fitted against the Langmuir – Hinshelwood kinetics model (Equation 4.8). The predicted k_r and K according to the Langmuir-Hinshelwood kinetics are shown in Table 4.4. The results show that describes a linear behavior and the R^2 values are comprised between 0.9968 and 0.9976. This clearly indicates that the photodegradation reaction of diuron follows the pseudo first order kinetics. Experimental data show that the photodegradation of diuron by using zinc oxide as the catalyst is consistent with the Langmuir-Hinshelwood model.

Table 4.4 The apparent rate constant (k_{app}), reaction rate constants (k_r), and the adsorption constant (K) for the photocatalytic degradation of diuron using zinc oxide at various mass fraction of ammonia.

%NH ₃	Pseudo first-order model		Langmuir-Hinshelwood model		
	k_{app} (min ⁻¹)	R ²	k_r (ppm/min)	K (min ⁻¹)	R ²
0%	0.0067	0.9935	0.1881	0.0439	0.9976
7%	0.0092	0.9983	0.1745	0.0656	0.9976
28%	0.0106	0.9878	0.2073	0.0634	0.9968

The decrease of TOC (Total Organic Carbon) as a result of mineralization of diuron was also observed during the degradation process. Figure 4.18 shows the depletion in TOC as a function of time on irradiation of an aqueous solution of diuron (10 ppm of diuron in the presence of zinc oxide 1 mg per 10 ml). It is found that, 49%, 40%, and 55% mineralization of diuron takes place after 360 min of irradiation by zinc oxide with ammonia mass fraction of 28%, 7%, and 0%, respectively. The plot between TOC vs. reaction time, indicates that organics intermediates are produced in the course of the photodegradation process. After the reaction time of 12 hours, it is found that the total organic carbon of the solution is lower than the detection limit of the TOC analyzer.

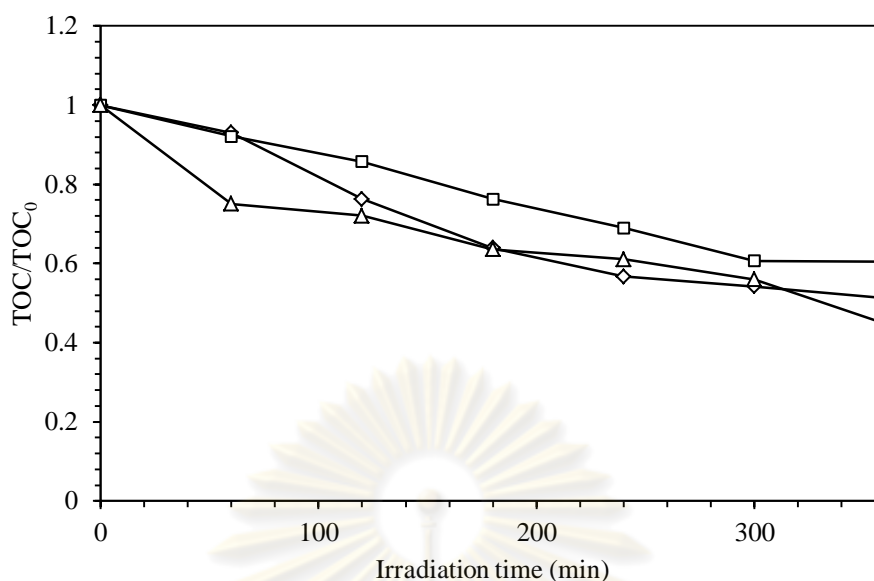


Figure 4.18 Total organic carbon (TOC) with respect to the initial TOC of diuron solution (TOC/TOC_0) during the photocatalytic degradation on zinc oxide at various mass fraction of ammonia: \triangle : 0% NH_3 , \square : 7% NH_3 , and \diamond : 28% NH_3 . The reaction was conducted using 1 mg of zinc oxide per 10 ml of solution and using the initial concentration of diuron is 10 ppm.

4.3.2 Photodegradation of diuron on titania

Figure 4.19 shows the disappearance of diuron by photocatalytic degradation using the synthesized titania as the catalyst, concentration of diuron with respect to the initial diuron concentration (C/C_0) during the photocatalytic degradation on titania at various mass fraction of ammonia. The results indicate that the activity of titania is increased when the ammonia mass fraction is increased. At ammonia mass fraction of 0, 7, and 28%, it is found that diuron is degraded by about 21, 33, and 45%, respectively. The transformed first order plots (Equation 4.5) are giving in Figure 4.20. The apparent rate constant can be determined from the slope of curve in Figure 4.20, obtained as shown in Table 4.5. It is observed that the first order kinetics does not provide good fit to the experimental data for all condition of ammonia mass fraction. The data shown in Figure 4.19 are fitted against the Langmuir – Hinshelwood kinetic model (Equation 4.8). The results are shown in Table 4.5. Experimental data show that the photodegradation of diuron on titania is inconsistent with the Langmuir-Hinshelwood model because R^2 value does not approach to 1.

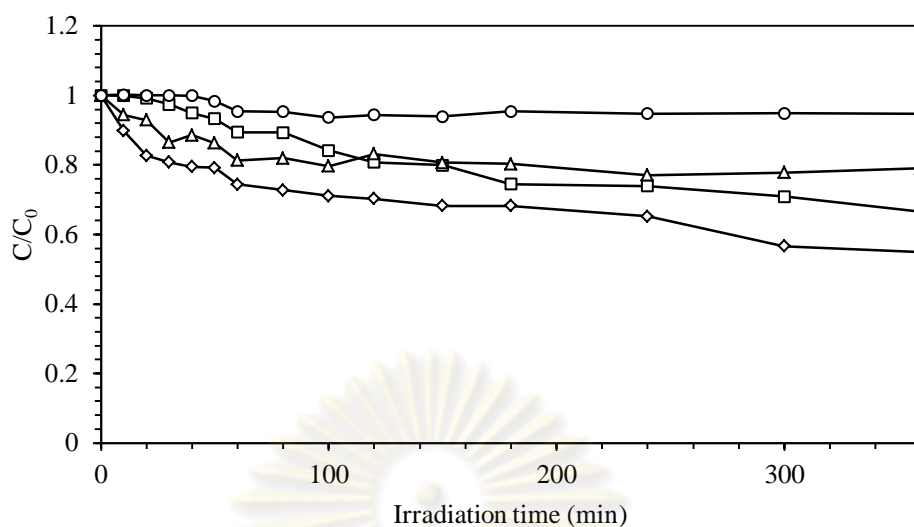


Figure 4.19 Concentration of diuron with respect to the initial diuron concentration (C/C_0) during the photocatalytic degradation on titania at various mass fraction of ammonia: \triangle : 0% NH_3 , \square : 7% NH_3 , \diamond : 28% NH_3 , and \circ : without catalyst. The reaction was conducted using 1 mg of titania per 10 ml of solution and using the initial concentration of diuron is 10 ppm.

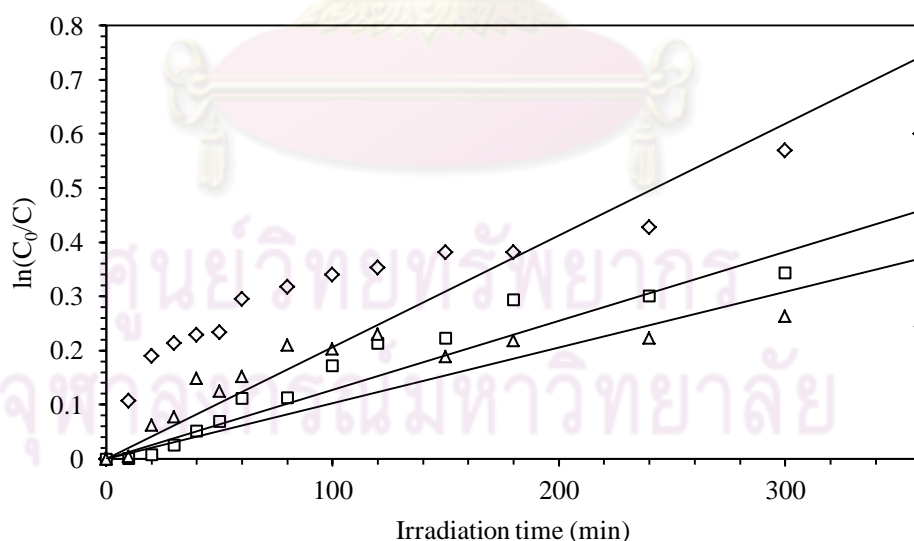


Figure 4.20 First-order linear transforms of the photocatalytic degradation of diuron on titania at various mass fraction of ammonia: \triangle : 0% NH_3 , \square : 7% NH_3 , and \diamond : 28% NH_3 . The reaction was conducted using 1 mg of titania per 10 ml of solution and using the initial concentration of diuron is 10 ppm.

Table 4.5 The apparent rate constant (k_{app}), reaction rate constants (k_r), and the adsorption constant (K) for the photocatalytic degradation of diuron using titania at various mass fraction of ammonia.

%NH ₃	Pseudo first-order model		Langmuir-Hinshelwood model		
	k_{app} (min ⁻¹)	R ²	k_r (ppm/min)	K (min ⁻¹)	R ²
0%	0.0010	0.7783	0.9992	0.0048	0.7716
7%	0.0013	0.7794	0.0001	0.0470	0.7405
28%	0.0021	0.8847	0.2689	0.0080	0.9178

Figure 4.21 shows the depletion in TOC (Total Organic Carbon) as a function of time on irradiation of an aqueous solution of diuron (10 ppm of diuron in the presence of titania 1 mg per 10 ml). It is found that, 19%, 7%, and 17% mineralization of diuron takes place after 360 min of irradiation by titania with ammonia mass fraction of 28%, 7%, and 0%, respectively. Variation of ammonia mass fraction in synthesized titania does not much affect the TOC removal. TOC values remain constant during illumination, which indicates that organics intermediates were produced during the photodegradation process. The plot between TOC vs. reaction time, indicates that organics intermediates are produced in the course of the photodegradation process. After the reaction time of 12 hours, it is found that the total organic carbon of the solution is lower than the detection limit of the TOC analyzer.

ศูนย์วิทยทรัพยากร
จุฬาลงกรณ์มหาวิทยาลัย

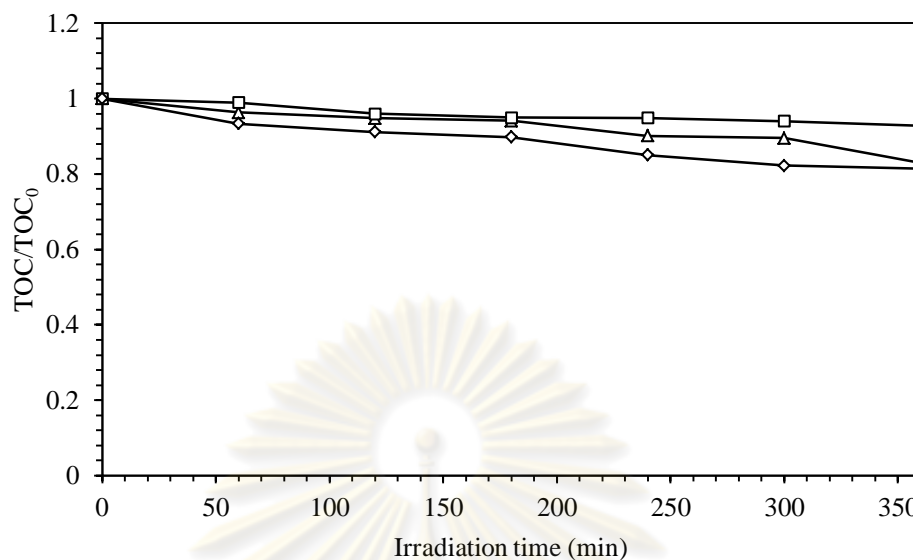


Figure 4.21 Total organic carbon (TOC) with respect to the initial TOC of diuron solution (TOC/TOC_0) during the photocatalytic degradation on titania at various mass fraction of ammonia: \triangle : 0% NH_3 , \square : 7% NH_3 , and \diamond : 28% NH_3 . The reaction was conducted using 1 mg of titanium dioxide per 10 ml of solution and using the initial concentration of diuron is 10 ppm.

Both zinc oxide and titania have been known to be capable of producing of radicals upon the exposure with UV light. However, comparison of the catalytic activities of zinc oxide and titania, in regard of the decrease in both diuron concentration and the total organic carbon in the solution, clearly indicates the difference in the degradation efficiency. It was found that the synthesized zinc oxide has higher performance in degrading and mineralization of diuron than titania, regardless of much lower surface area. Due to the amount of diuron adsorbed at equilibrium by zinc oxide rather than adsorbed by titania. The result of adsorption isotherm showed that the diuron concentration of 10 ppm, the amount of diuron adsorbed at equilibrium using zinc oxide as a catalyst larger than using titania as a catalyst.

4.4 Intermediate Products of the Photodegradation

During the photocatalytic reaction, radicals formed from the photocatalysts react with diuron to generate the intermediates. Structure of functional groups attaching to aromatic ring of diuron is mainly responsible for the structure of the intermediates formed. Diuron clearly offers two sites for the reaction, i.e. the aromatic ring and the aliphatic side chain [58].

4.4.1 Photodegradation on zinc oxide

4.4.1.1 Effect of pH of diuron solution

The effect of pH of the aqueous diuron solution on the photocatalytic degradation was studied. The pH value of the diuron solution was adjusted to the desired value in the range of 3 to 10 by using HCl or NaOH. For the study of this parameter, the amount of zinc oxide powder added into the solution was fixed at the ratio of 1 mg of zinc oxide to 10 ml of the solution. Intermediates were detected by HPLC, during the photocatalytic treatment. In Figure 4.22 - 4.23 and Table 4.6, the extent of photodegradation of diuron is reported for the reaction at pH 3, 7, and 10. The pH of the solution was adjusted before irradiation and it was not controlled during the course of the reaction. The results for the degradation are illustrated in Figure 4.22. The transform first order plots are given in Figure 4.23 whereas the apparent rate constants are shown in Table 4.5. The data shown in Figure 4.22 were fitted against the Langmuir-Hinshelwood kinetic model. The results are shown in Table 4.6.

Table 4.6 shows the apparent rate constant, calculated reaction rate constants and the calculated adsorption constant based on the Langmuir-Hinshelwood kinetic model of the photodegradation of diuron at various pH.

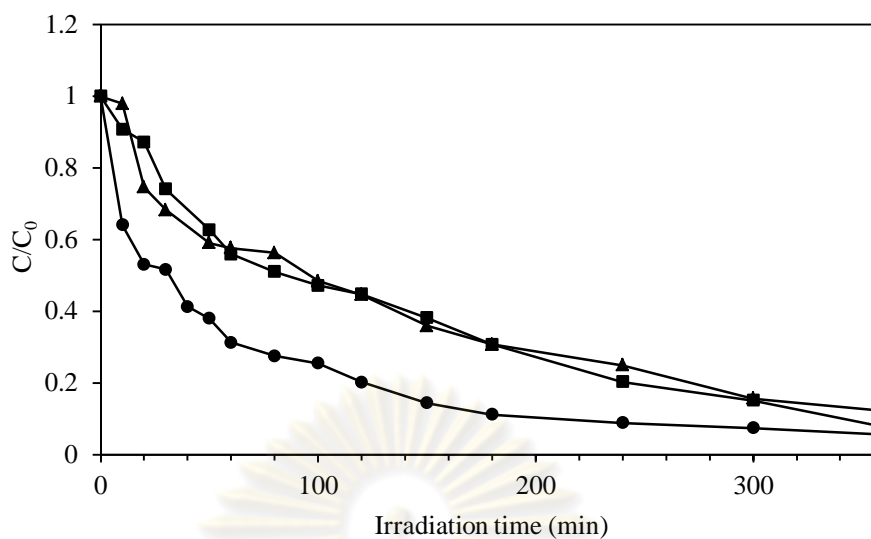


Figure 4.22 Effect of pH of the solution on photodegradation efficiency of diuron. The pH is adjusted at pH 3 (■), pH 7 (●), and pH 10 (▲).

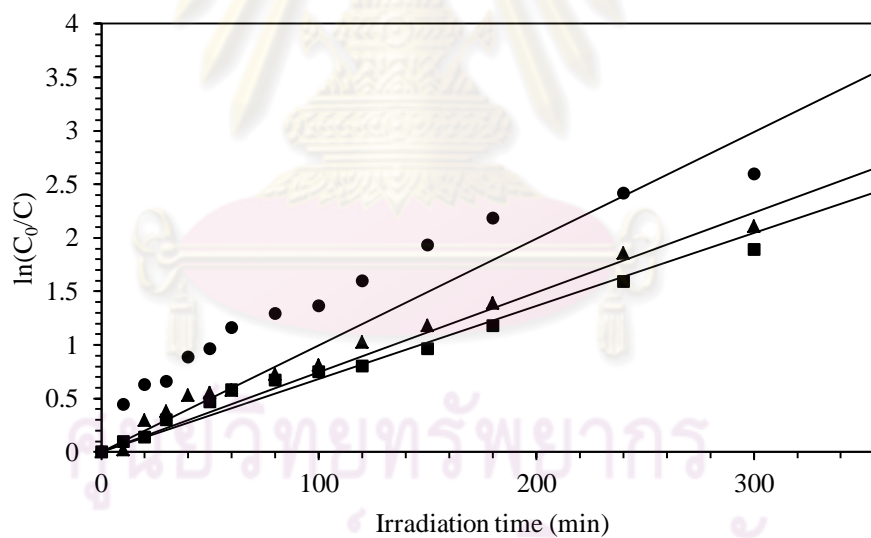
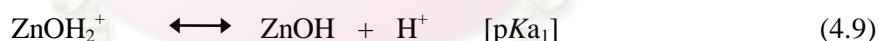


Figure 4.23 First order linear transforms of the photodegradation efficiency of diuron at various pH values. The pH is adjusted at pH 3 (■), pH 7 (●), and pH 10 (▲).

Table 4.6 The apparent rate constant (k_{app}), reaction rate constants (k_r), and the adsorption constant (K) for the photocatalytic degradation of diuron using zinc oxide at various pH of solution.

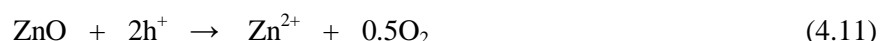
pH of solution	Pseudo first-order model		Langmuir-Hinshelwood model		
	k_{app} (min^{-1})	R^2	k_r (ppm/min)	K (min^{-1})	R^2
3	0.0068	0.9832	0.9999	0.0264	0.8246
7	0.0100	0.7281	0.9999	0.8097	0.8916
10	0.0074	0.9692	0.9995	0.1568	0.7612

The results indicate that the photodegradation of diuron is increased with increasing pH up to pH 7, beyond which the degradation decreases. At pH 3, 7, and 10 it was found that diuron is degraded by about 92, 94, and 91%, respectively. Generally, the effect of pH on organic degradation assisted by the semiconductor oxides has been related to the establishment of acid-base equilibria governing the surface chemistry of metal oxides in water, as shown in the following reactions.



The pH at which the surface of an oxide is uncharged is defined as the point of zero charge (pH_{pzc}). It has been reported that the point of zero charge for zinc oxide is about 9 [18]. The effect of pH on the photocatalytic performance can be explained in terms of electrostatic interaction between the catalyst surface and the target substrate. It is expected that this interaction affects the encounter probability between hydroxyl radical and diuron. The reaction would be enhanced or hindered depending on whether attractive or repulsive forces prevail, respectively. Diuron is negatively charged above its $\text{p}K_a$ (2.68), whereas catalysts are positively charged below $\text{pH} \sim 9$. Optimal conditions were found at $\text{p}K_a < \text{pH} < \text{pH}_{\text{pzc}}$ at which the positive charged zinc oxide and negative charged diuron should attract each other

[18, 29, 59]. Other concomitant effect can come into play. For example ZnO can undergo photocorrosion through self-oxidation.



In particular, ZnO powder exhibit tendency to dissolve with decreasing pH (Eq. 4.12) [18].



In a strongly alkaline environment, ZnO can undergo dissolution according to



Moreover, the possible formation of photocatalytically inert $\text{Zn}(\text{OH})_2$ surface layers upon UV irradiation (Eq. 4.14) has also to be considered in aqueous media [18].



Therefore, the reduction of photocatalytic activity of ZnO at exceedingly low and high pH values can originate from either acidic/photochemical corrosion of the catalyst from alkaline dissolution and/or surface passivation with $\text{Zn}(\text{OH})_2$.

The results regarding the intermediates formed are shown in Figure 4.24-4.26. The total number of intermediates are detected by HPLC from the reaction at pH 3, 7, and 10, are 8, 9, and 9 kinds of intermediates respectively. Concentrations of these intermediates are expected to be very low, since the intensities of the HPLC signals for the intermediates are much lower than that of diuron. It should be noted that, without identification of the intermediate, the standard calibration curve could not be constructed. Consequently, quantitative results of the intermediates were not obtained. Nevertheless, based on the intensity of the signal, it was found that the concentration of the intermediates also changes along the course of the photodegradation.

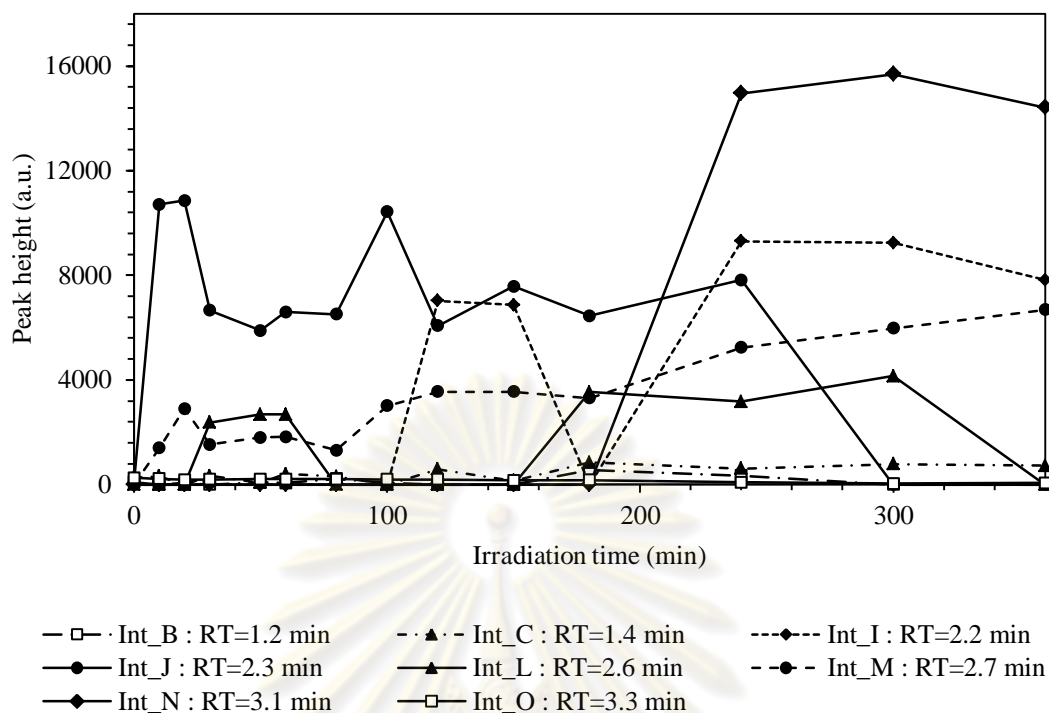


Figure 4.24 HPLC peak height of intermediates generated during photocatalytic degradation on diuron on zinc oxide and the initial pH of 3.

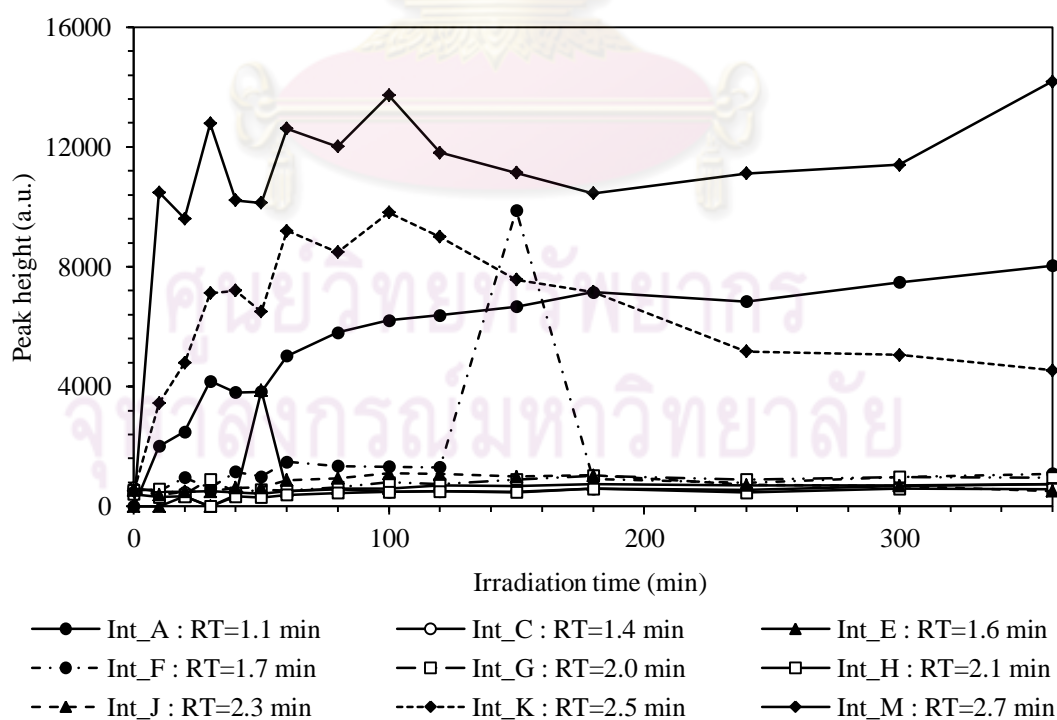


Figure 4.25 HPLC peak height of intermediates generated during photocatalytic degradation on diuron on zinc oxide and the initial pH of 7.

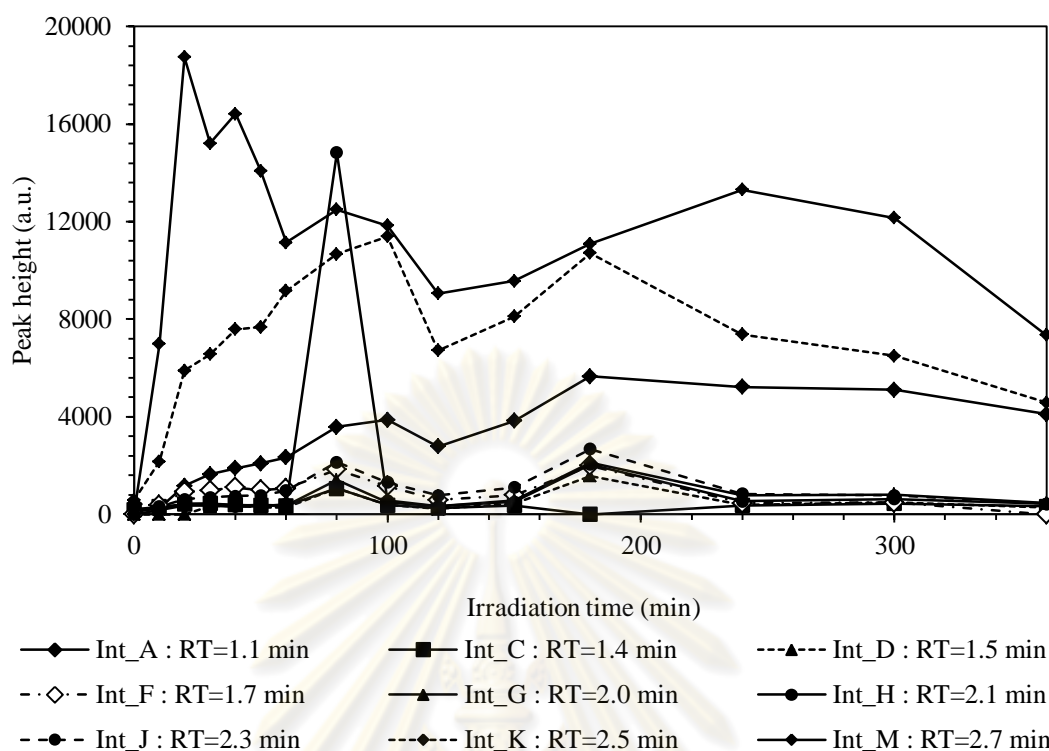


Figure 4.26 HPLC peak height of intermediates generated during photocatalytic degradation on diuron on zinc oxide and the initial pH of 10.

Concentration of most intermediate increase with irradiation time, although the data show some fluctuation. It can be observed that each unknown intermediates are presented at very low concentration. However these small molecules are not detectable by HPLC analysis. The effect of different pH of diuron solution using zinc oxide as catalyst and behavior of intermediates are also compared in Figure 4.24-4.26. It shows that most photodegradation intermediates are formed after 30 minutes of irradiation time. Several intermediates are formed within short time and the concentration of intermediates are high. Some intermediates remain stable at low concentration even after 6 hours of the reaction.

Comparison of the intermediates formed from the reaction at different pH, reveals common intermediates as well as different intermediates. The fact that different pH of the solution produces different combination of reaction intermediates might be the result of charge on the surface of catalyst. Attempts were made to identify the intermediate products through analysis using LC-MS.

Samples collected at different irradiation time were freeze dry for the purpose of concentrating the intermediates. These powders were resuspended in 70% acetonitrile per 30% water and injected into LC/MS. Diuron peak was observed as reported in literature at 231 m/z and 232 m/z in negative and positive detection mode respectively.

Two assumptions were made for the identification process. First, m/z values that were not observed in the mass spectrum of standard diuron were considered to belong to intermediates products derived from diuron. Second, peak of all m/z values reported were considered as pseudo molecular ion peak since at fragmentator voltage of 120 V was used for structural determination of intermediates.

Table 4.7 Possible intermediates generated from photodegradation of diuron on zinc oxide at pH of 3, 7, and 10.

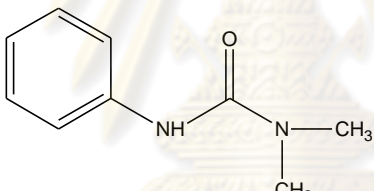
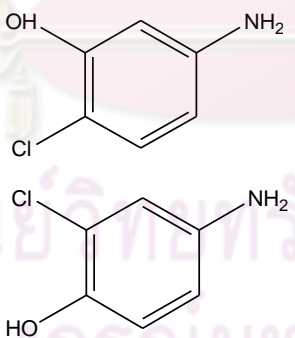
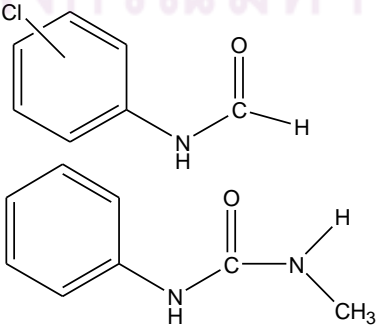
Compound	Propose structure	pH3	pH7	pH10
1 [60]		◆		
2		◆	◆	◆
3 [61]			◆	

Table 4.7 (continued)

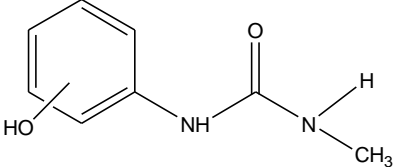
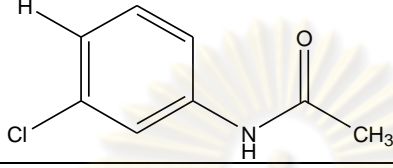
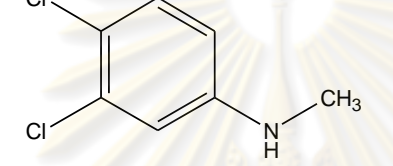
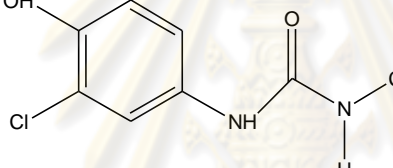
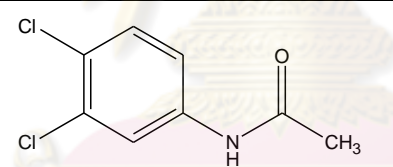
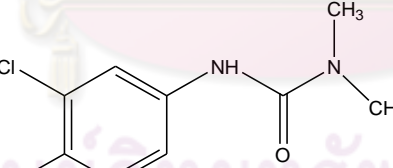
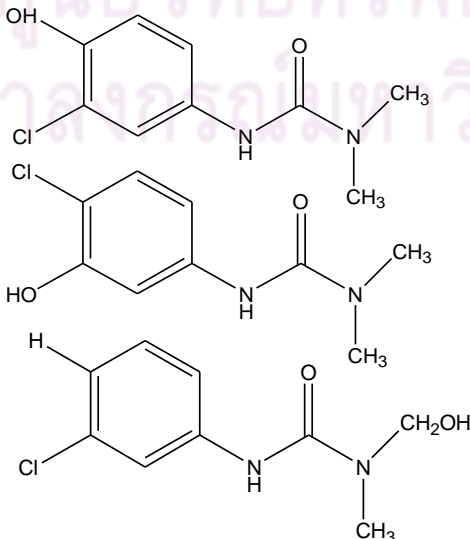
Compound	Propose structure	pH3	pH7	pH10
4 [44]		◆	◆	◆
5		◆	◆	
6		◆		
7 [62]		◆	◆	◆
8		◆	◆	
9 [63]				◆
10 [1, 60, 64]		◆	◆	◆

Table 4.7 (continued)

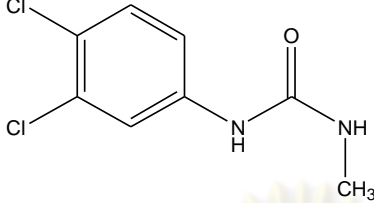
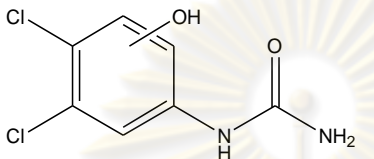
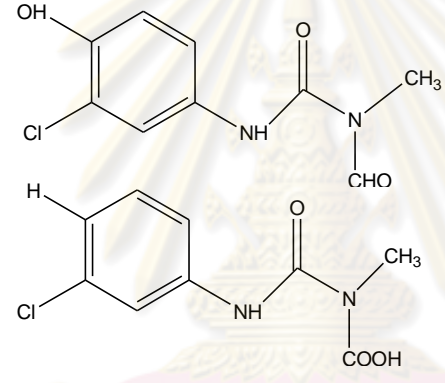
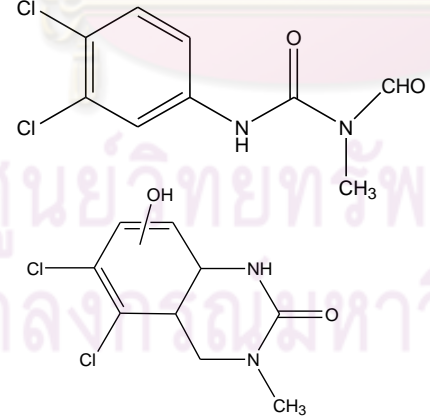
Compound	Propose structure	pH3	pH7	pH10
11 [42, 61, 64]		◆	◆	◆
12			◆	
13			◆	
14 [60, 62, 64, 65]		◆	◆	

Table 4.7 (continued)

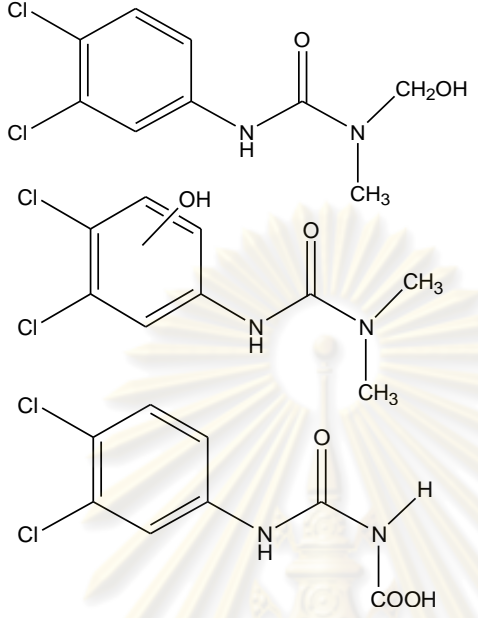
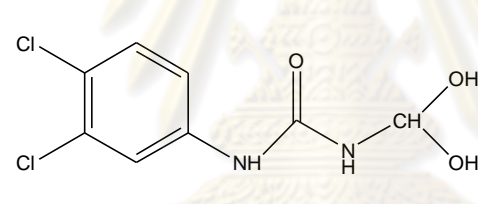
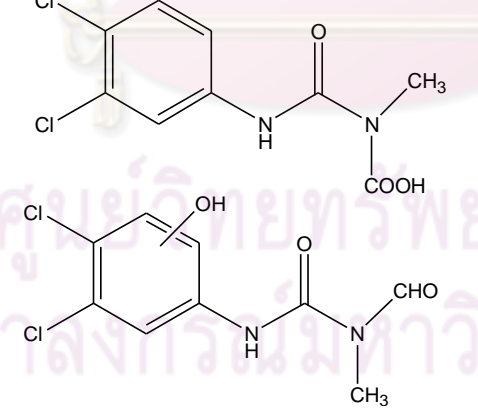
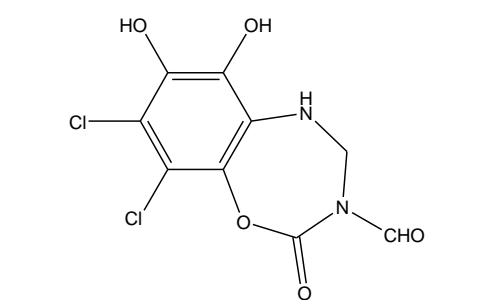
Compound	Propose structure	pH3	pH7	pH10
15 [42, 60, 66]		◆	◆	
16		◆		
17 [60, 64]		◆		◆
18		◆		

Table 4.7 shows representative of all intermediates appeared in LC/MS spectrum, which includes the structure of each unknown intermediates evaluated. Products were identified based on the molecular ion and mass spectrometric fragmentation peak. The results reveal that different pH of solution has different adsorption properties, which affect the reaction between diuron and the catalyst surface.

The addition of hydroxyl group onto the molecule, which supports the previous reports about the attack by hydroxyl radicals during the photocatalytic reaction, is also evidenced. The sites for hydroxyl radical to attack can be divided into two positions, i.e., the aromatic ring and the alkyl group. Although the detailed mechanisms of diuron degradation on zinc oxide and on titania are different, the main photocatalytic degradation pathways remained the same. They include hydroxylation of the aromatic ring and of the side chain (resulting in compound 4, 12, 15, and 17), dehalogenation or dechlorination of the aromatic ring (resulting in compound 1-5, 7, 10, and 13), demethylation (resulting in compound 12), and condensation (resulting in compound 14).

The sites for hydroxyl radical to attack can be divided into two regions, the aromatic ring and the alkyl group. When hydroxyl radical attacks the aromatic ring, it is more energetically favorable to attack carbon atom instead of chlorine atoms [42]. From the identified intermediates, a potential mechanism involving the reaction with the aromatic ring is shown as follows:

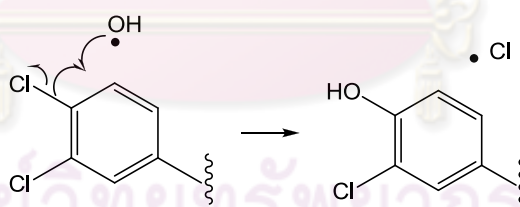


Figure 4.27 Dechlorination reaction.

Figure 4.27 can continue with the reaction with another hydroxyl radical and O_2 to add another hydroxyl group to the aromatic ring [67] as shown in Figure 4.28.

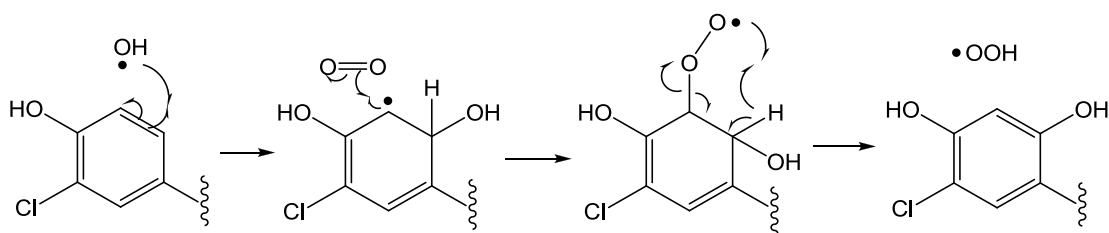


Figure 4.28 Hydroxylation reaction.

The attack of hydroxyl radical on the carbon of methyl group through hydrogen atom abstraction is energetically favorable [42]. The oxidation of methyl group yields an alcohol, and subsequently gets further oxidized to yield aldehyde and carboxylic acid, which then undergoes decarboxylation as shown in Figure 4.29.

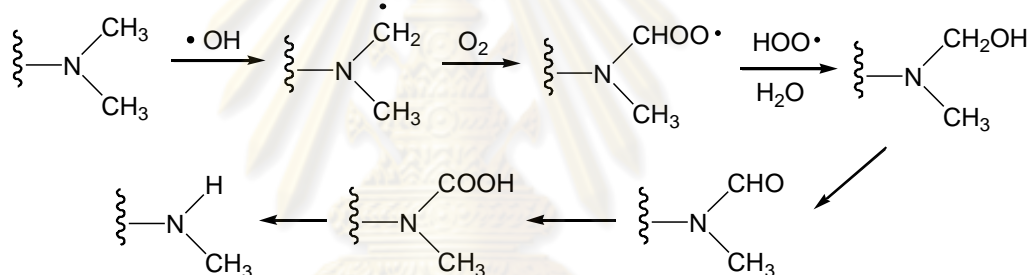


Figure 4.29 Decarboxylation reaction.

The analyzed of the first intermediate products suggest that substitution of chlorines and hydroxylation by hydroxyl radicals are the main degradation process of diuron before opening of the aromatic ring. Primary attack of diuron molecules by the hydroxyl radical is correlated with the frontier electron densities. So that primary position for hydroxyl radical attack are expected to be located on atoms with largest electron density [42].

4.4.1.2 Effect of UV Light

Photodegradation of diuron used zinc oxide as catalyst, for investigate the affect of UV-lamps to intermediate products. In this work, UV-lamps used were UV-A and UV-C. UV-A is a long wave (wave length ~ 360 nm), of which the energy is around 3.10 – 3.94 eV per photon. UV-C is a short wave (wave length ~ 254 nm), of which the energy is 4.43 – 4.40 eV per photon [68]. Both of UV-lamps were 1.5 Watt in power. In this process, the catalyst is activated by UV radiation. The photocatalysis can be defined as the acceleration of a photoreaction by the presence of a catalyst that can be activated by the absorption of light of energy greater than its band gap (3.2 eV for zinc oxide). From the research, it was found that the use of UV-A irradiation without catalyst, i.e. photolysis can degrade diuron by less than 5% even after 6 hours of irradiation. On the other hand, the photolysis by UV-C irradiation can degraded diuron up to 89% as shown in Figure 4.30. Thus intermediates generated from UV-C irradiation with catalyst might not be the effect from the catalyst.

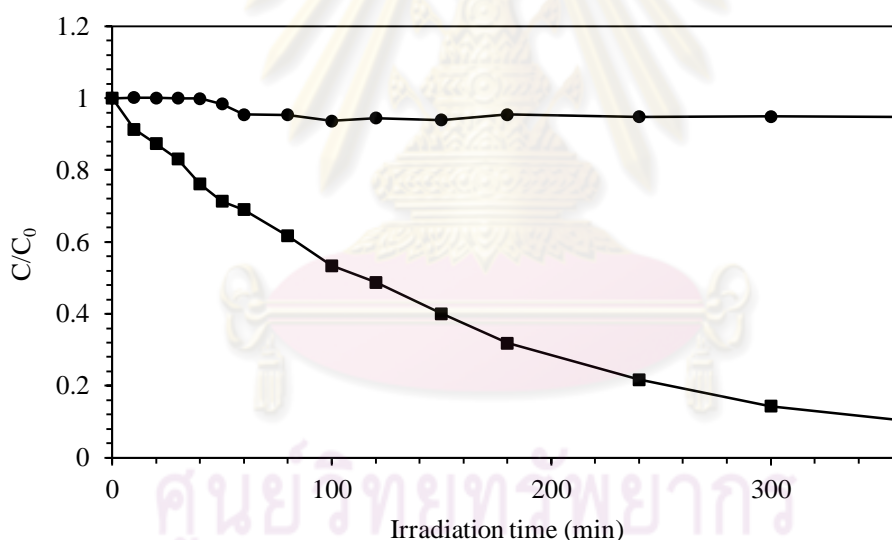


Figure 4.30 The effect of UV-lamp, i.e. (●) UV-A, (■) UV-C on the photolysis of diuron.

In Figure 4.31 shows the effect of UV-irradiation on degradation of diuron using zinc oxide as catalyst. The results reveal that diuron is degraded by 98% and 95% from the use of UV-A and UV-C respectively. The first orders plots are shown in Figure 4.32 and the apparent rate constant are shown in the Table 4.8. The reaction rate constant and the adsorption rate constant of diuron in the investigation of the effect of UV lamps based on the Langmuir-Hinshelwood model are shown in the Table 4.8.

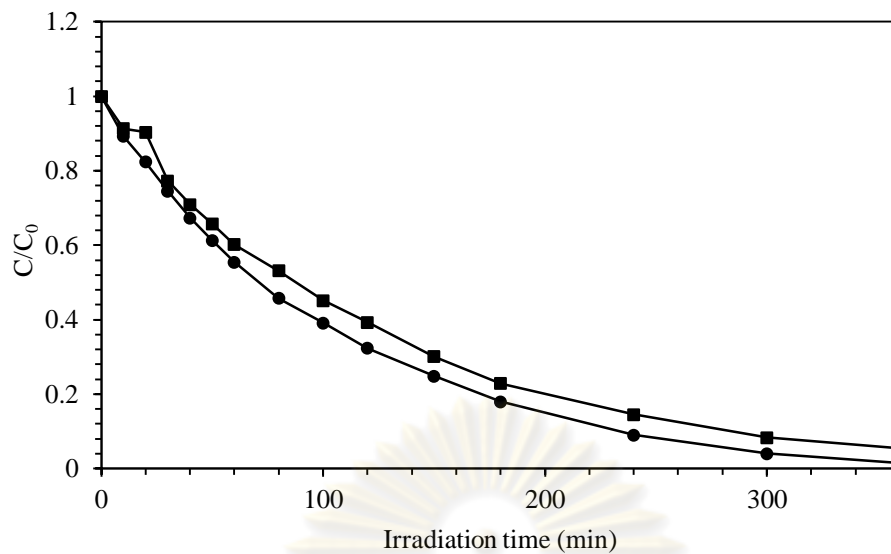


Figure 4.31 The effect of UV-lamp, i.e. (●) UV-A, (■) UV-C on the degradation of diuron using zinc oxide as catalyst.

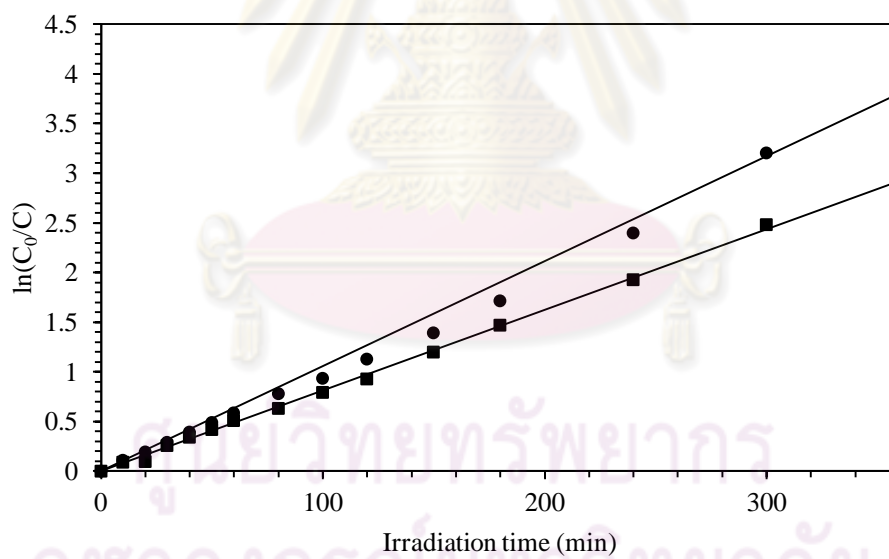


Figure 4.32 First order linear transforms of the photodegradation efficiency of diuron, (●) UV-A, (■) UV-C on the degradation of diuron using zinc oxide as catalyst.

Table 4.8 The apparent rate constant (k_{app}), reaction rate constants (k_r), and the adsorption constant (K) for the photocatalytic degradation of diuron using zinc oxide at different UV lamp.

Lamp	Pseudo first-order model		Langmuir-Hinshelwood model		
	k_{app} (min^{-1})	R^2	k_r (ppm/min)	K (min^{-1})	R^2
UV-A	0.0106	0.9878	0.2073	0.0634	0.9968
UV-C	0.0081	0.9991	2.6165	0.0031	0.9991

The results show the photodegradation of diuron follows the pseudo first order kinetics and consistent with the Langmuir – Hinshelwood model.

Figure 4.33 and 4.34 shows the intermediates generated during photocatalytic degradation of diuron on zinc oxide using different UV-lamps. It was found that 10 intermediates were detected by HPLC when UV-A lamps were used while the use of UV-C yielded only 3 kinds of intermediates.

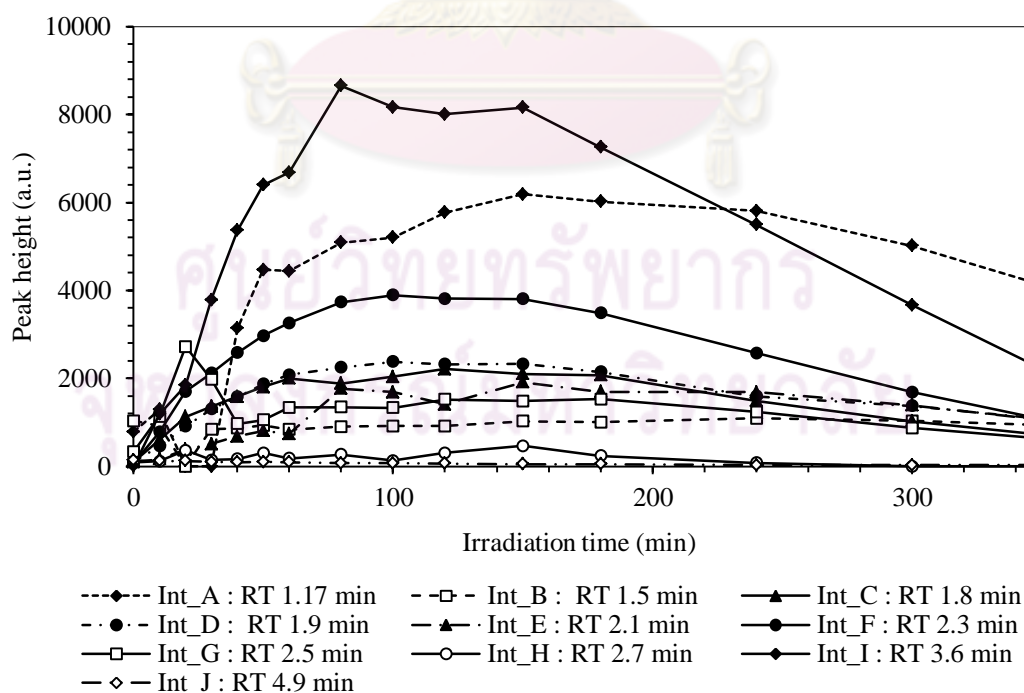


Figure 4.33 HPLC peak height of intermediates generated during photocatalytic degradation on diuron on zinc oxide using UV-A as light source.

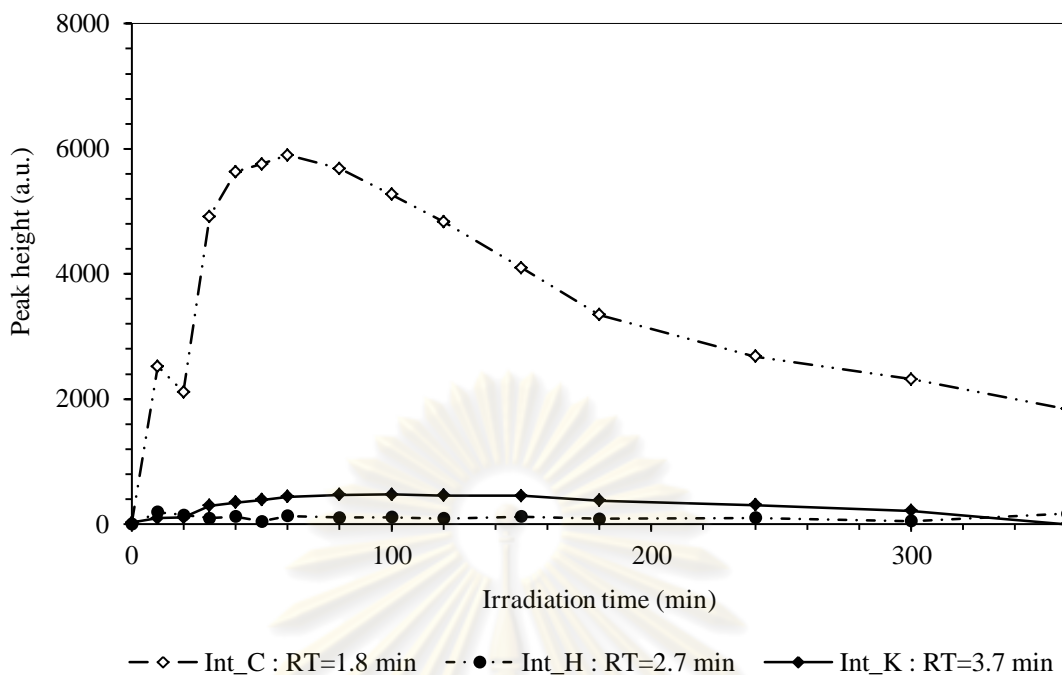


Figure 4.34 HPLC peak height of intermediates generated during photocatalytic degradation on diuron on zinc oxide using UV-C as light source.

It was found that the concentration of the intermediates also changes along the course of the photodegradation. The intermediates are generated and consumed within the short time. The UV-light affects the generation of intermediates. The use of UV-A, most intermediates are formed after 60 minutes of the irradiation time whereas the intermediates from UV-C are generated after 30 minutes. The structures of the intermediates product were identified by LC-MS as shown in Table 4.9. It was found that the result is contrary with HPLC analysis for the intermediates generates from UV-C. It can be suggested that each unknown intermediates are presented at very low concentration. However these small molecules are not detectable by HPLC analysis.

Table 4.9 Possible intermediates generated from photodegradation of diuron on zinc oxide using different kind of UV-lamp.

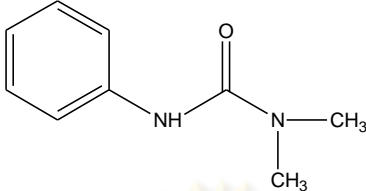
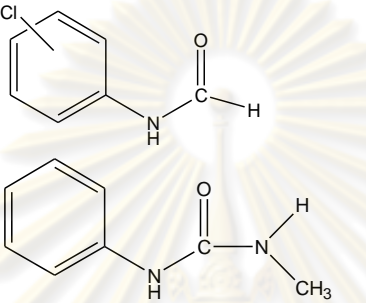
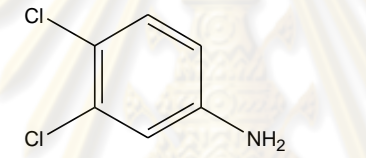
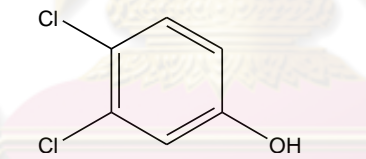
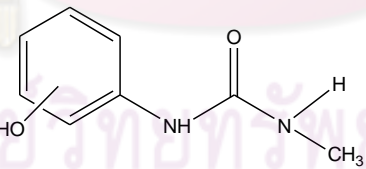
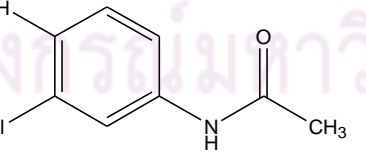
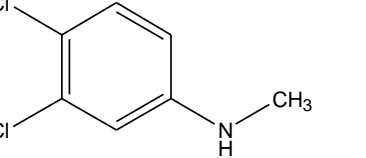
Compound	Propose structure	UV-A	UV-C
1 [60]			◆
2 [61]		◆	
3 [1, 60, 61, 65]		◆	
4		◆	
5 [44]			◆
6		◆	◆
7			◆

Table 4.9 (continued)

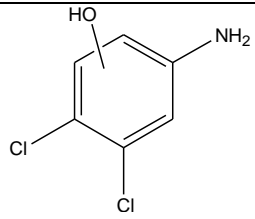
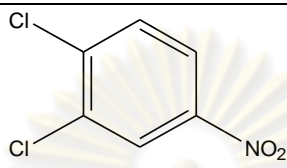
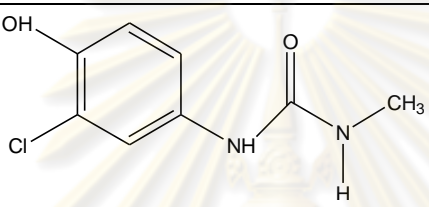
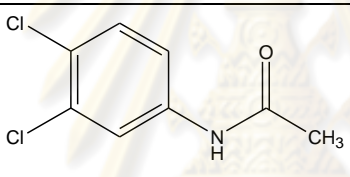
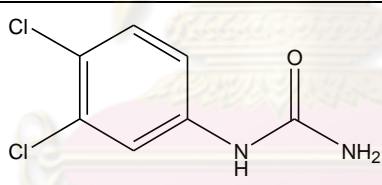
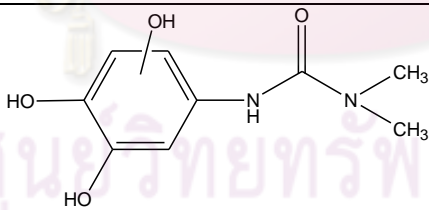
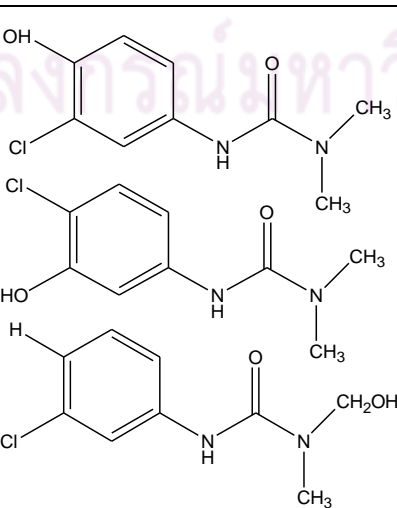
Compound	Propose structure	UV-A	UV-C
8 [62]			◆
9 [69]		◆	
10 [62]			◆
11		◆	◆
12 [70]		◆	◆
13 [66]			◆
14 [1, 60, 64]		◆	

Table 4.9 (continued).

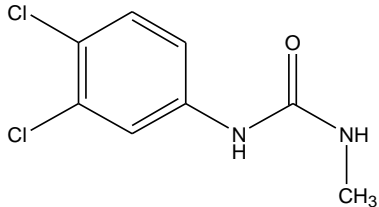
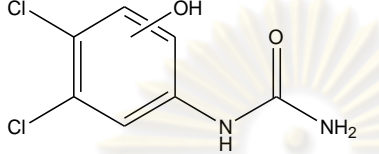
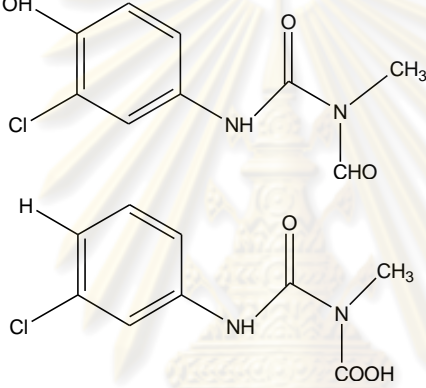
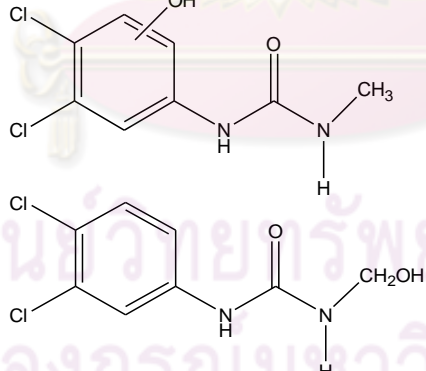
Compound	Proposed structure	UV-A	UV-C
15 [42, 61, 64]	 <p>Chemical structure of 2-(3,4-dichlorophenyl)acetamide N-methyl derivative. It consists of a benzene ring with chlorine atoms at the 3 and 4 positions, attached to a methylene group (-CH₂-), which is further attached to a carbonyl group (-C(=O)-) bonded to an N-methylamino group (-NH-CH₃).</p>	◆	◆
16	 <p>Chemical structure of 2-(3,4-dichlorophenyl)acetamide. It consists of a benzene ring with chlorine atoms at the 3 and 4 positions, attached to a methylene group (-CH₂-), which is further attached to a carbonyl group (-C(=O)-) bonded to an amino group (-NH₂).</p>	◆	
17	 <p>Chemical structures of 2-(3-chloro-4-hydroxyphenyl)acetamide N-methyl derivatives. The top structure is N-(3-chloro-4-hydroxyphenyl)acetamide N-methyl derivative, where the nitrogen is substituted with a methyl group (-CH₃) and a formyl group (-CHO). The bottom structure is N-(3-chloro-4-hydroxyphenyl)acetamide N-methyl derivative, where the nitrogen is substituted with a methyl group (-CH₃) and a carboxyl group (-COOH).</p>		◆
18 [70]	 <p>Chemical structures of 2-(3,4-dichlorophenyl)acetamide N-methyl derivatives. The top structure is N-(3,4-dichlorophenyl)acetamide N-methyl derivative, where the nitrogen is substituted with a methyl group (-CH₃) and a hydrogen atom (-H). The bottom structure is N-(3,4-dichlorophenyl)acetamide N-methyl derivative, where the nitrogen is substituted with a hydroxymethyl group (-CH₂OH) and a hydrogen atom (-H).</p>	◆	

Table 4.9 (continued).

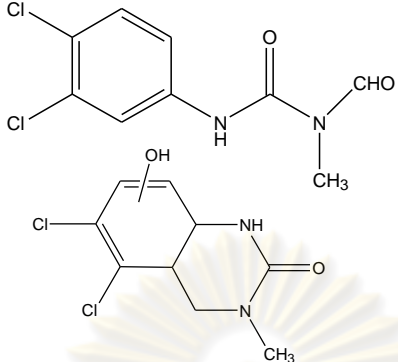
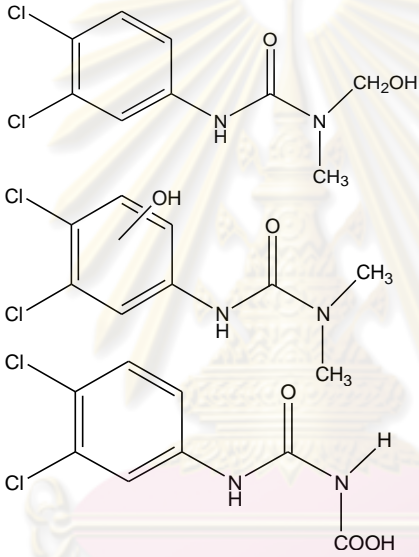
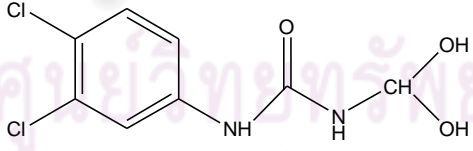
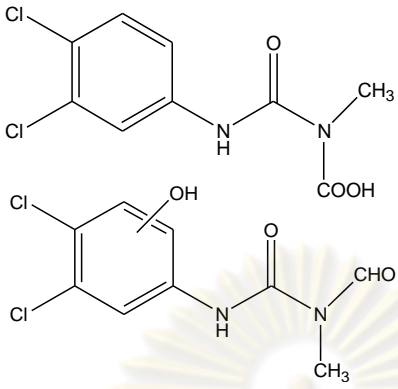
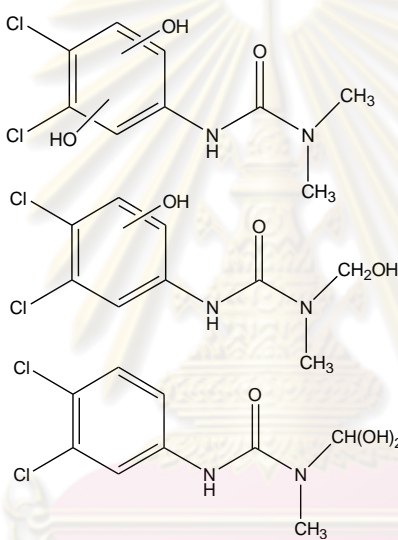
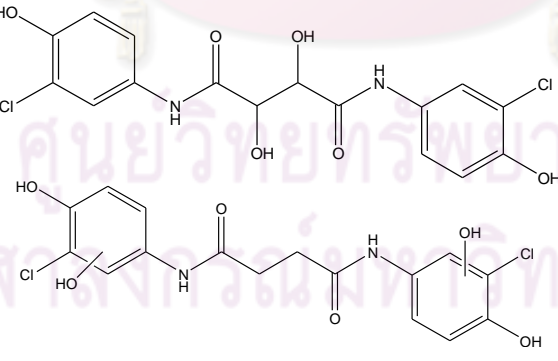
Compound	Proposed structure	UV-A	UV-C
19 [60, 62, 64, 65]		◆	◆
20 [60, 64, 65]		◆	◆
21			◆

Table 4.9 (continued).

Compound	Proposed structure	UV-A	UV-C
22 [42, 60]		◆	◆
23 [42, 62]		◆	
24		◆	

Several transformation products were detected. They correspond to the following reactions: the hydroxylation occurring on the aromatic ring (compounds 5, 8, 13, 16, 18, and 20), dechlorination (compounds 1, 2, 6, 10, 14, and 17), demethylation (compounds 2, 5, 10, 12, 15, and 19) and condensation (compound 19).

Diuron is degraded into smaller compounds during photodegradation process. At the same time, these radicals generated during photodegradation can form conjugates and resulted in a larger molecule. Larger molecules were observed in this experiment. For larger molecules, more complex combination of radicals and rearrangement can occur. More information is needed to determine the structure.

4.4.2 Photodegradation on titanium dioxide

4.4.2.1 Effect of pH of diuron solution

When titanium dioxide was employed as the catalyst, intermediates were also detected by HPLC during the photocatalytic treatment. Figure 4.35-4.36 and Table 4.9 shows the extent of photodegradation of diuron at pH 3, 7, and 10. The results for the degradation are illustrated in Figure 4.35. The first order transform plots are giving in Figure 4.36 whereas the apparent rate constants are shown in Table 4.9. The data shown in Figure 4.35 were fitted against the Langmuir-Hinshelwood kinetic model. The results are shown in Table 4.10, including the apparent rate constant, calculated reaction rate constants and the calculated adsorption constant based on the Langmuir-Hinshelwood kinetic model, of photodegradation of diuron at various pH.

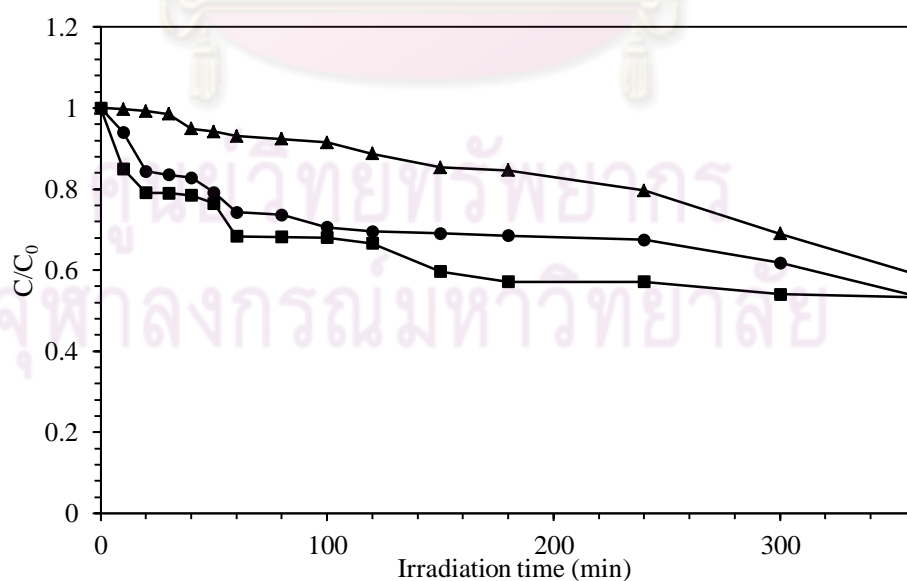


Figure 4.35 Effect of pH of the solution on photodegradation efficiency of diuron on titania.

The pH is adjusted at pH 3 (■), pH 7 (●), and pH 10 (▲).

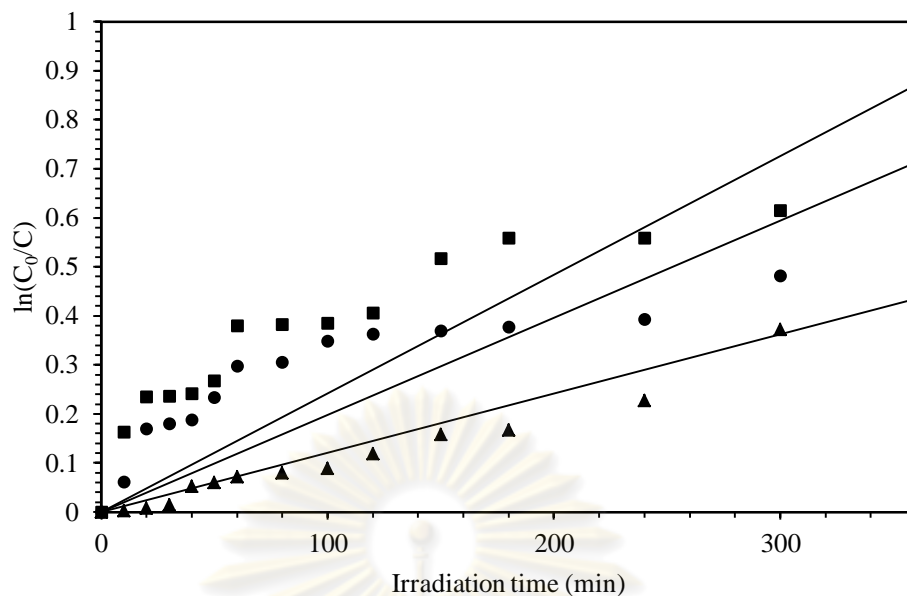


Figure 4.36 First order linear transforms of the photodegradation efficiency of diuron on titania at various pH values. The pH is adjusted at pH 3 (■), pH 7 (●), and pH 10 (▲).

Table 4.10 The apparent rate constant (k_{app}), reaction rate constants (k_r), and the adsorption constant (K) for the photocatalytic degradation of diuron using zinc oxide at various pH of solution.

pH of solution	Pseudo first-order model		Langmuir-Hinshelwood model		
	k_{app} (min^{-1})	R^2	k_r (ppm/min)	K (min^{-1})	R^2
3	0.0024	0.8584	0.9993	0.2450	0.7069
7	0.0020	0.8856	2.4618	0.0008	0.8969
10	0.0012	0.9672	0.9512	0.6677	0.8404

The results indicate that the photodegradation is increased with decreasing pH down to pH 3. At pH 3, 7, and 10, it was found that diuron was degraded by about 46, 46, and 41%, respectively. It can be seen that the pH has a weak effect on the degradation of diuron. However an acidic condition seems to accelerate the degradation kinetics of diuron in the

aqueous solution. Since the reaction mainly occurs at surface of the catalyst therefore, the pH effect should be explained by differences on adsorption with pH [71]. It has been reported that the point of zero charge for titanium dioxide is about 5.6-5.8 [72]. In neutral solution, the surface charge is neutral, whereas at pH lower than 5.6, the surface charge is positive. As a consequence, in acidic solution, molecules are attracted to the surface by their electronegative part [71]. For pH higher than the point zero charge, the surface becomes negative charged. At $\text{pH} < \text{pH}_{\text{pzc}}$ the surface is positive charged according to the following equilibrium:



When titanium dioxide was employed as the catalyst and the solution was adjusted to different pH, various kinds of intermediates were detected by HPLC during the photocatalytic treatment. The results are shown in Figure 4.37-4.39. There are 12, 13, and 16 kinds of intermediates formed from the reaction at pH 3, 7, and 10, respectively. Although quantitative data were not obtained, concentrations of these intermediates are expected to be very low, since the intensities of the HPLC signals for the intermediates are much lower than that of diuron. The concentration of the intermediates also change along the course of the photodegradation.

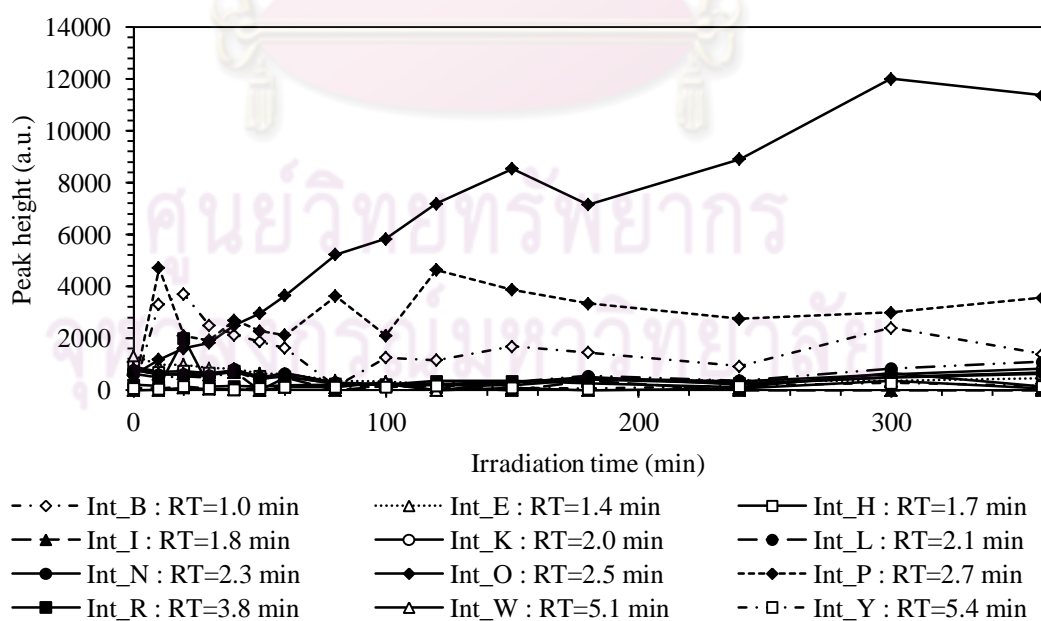


Figure 4.37 HPLC peak height of intermediates generated during photocatalytic degradation on diuron on titanium dioxide and the initial pH of solution 3.

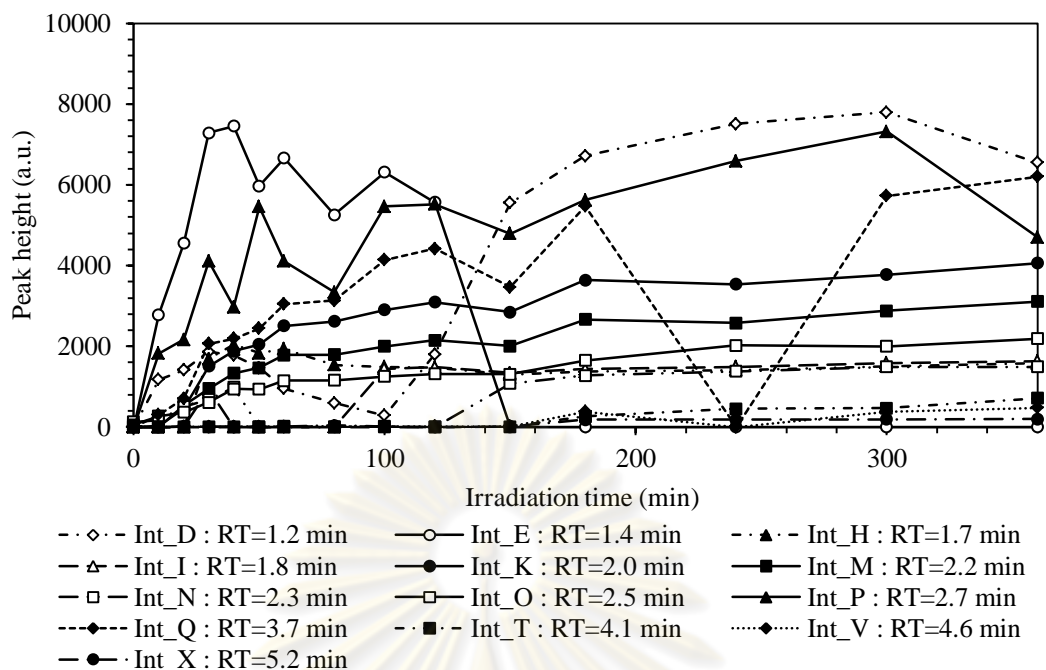


Figure 4.38 HPLC peak height of intermediates generated during photocatalytic degradation on diuron on titanium dioxide and the initial pH of solution 7.

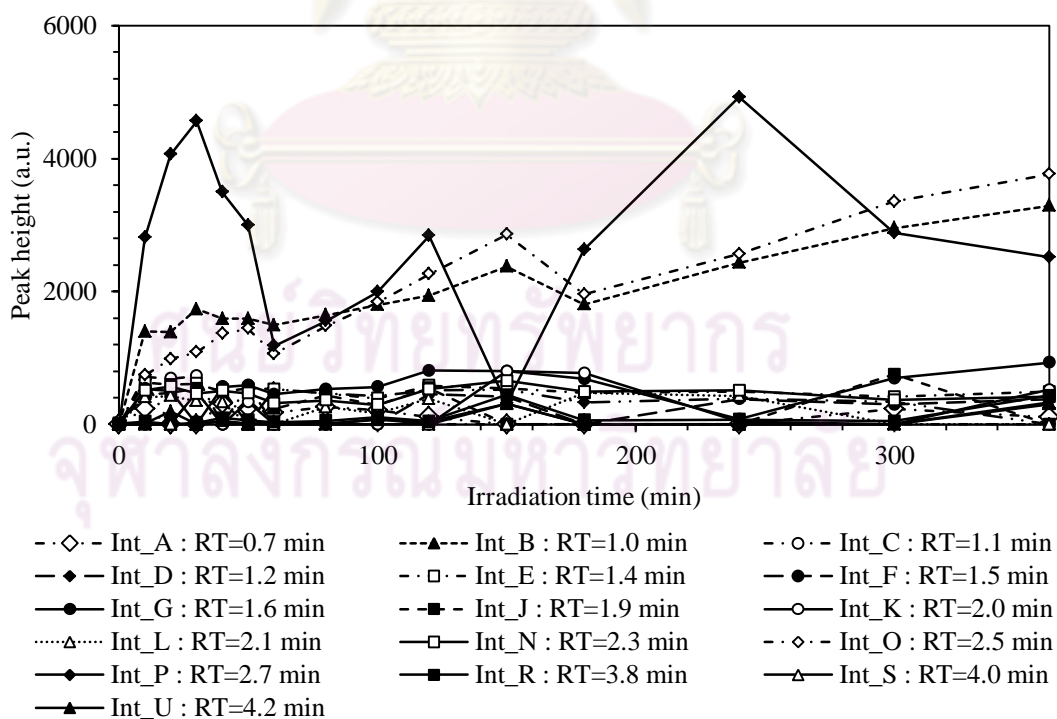


Figure 4.39 HPLC peak height of intermediates generated during photocatalytic degradation on diuron on titanium dioxide and the initial pH of solution 10.

The intermediate products are presented at very low concentration, the data show some fluctuation. Concentration of intermediate increase with irradiation time, and intermediate can be disappear even after 6 hours, some intermediate remain stable even after 6 hours of the reaction.

Comparison of the intermediates formed from the reaction at various pH of solution, reveals common intermediates as well as different intermediates. The attempts were made to identify the intermediate products through analysis using LC-MS. The structures of all intermediates detected are proposed in Table 4.11.

Results obtained when titanium dioxide is used as photocatalyst show that the distribution of products depends on the pH of the solution. In neutral solution, the attack of the hydroxyl radicals is located both on the aromatic ring and on the methyl groups. In acidic solution, it is mainly located on the methyl groups [71].

Table 4.11 Possible intermediates generated from photodegradation of diuron on titanium dioxide at pH of 3, 7, and 10.

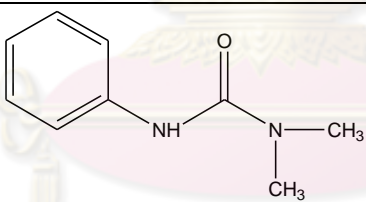
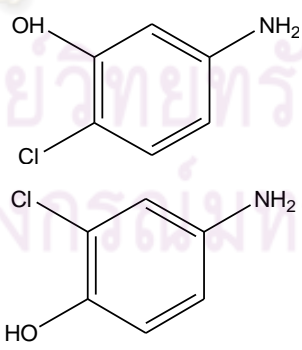
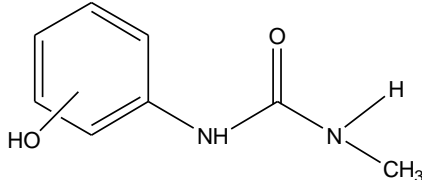
Compound	Structure	pH3	pH7	pH10
1 [60]		◆		
2		◆		◆
3 [44]		◆	◆	◆

Table 4.11 (continued).

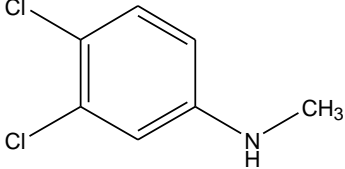
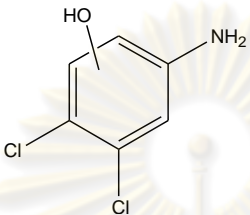
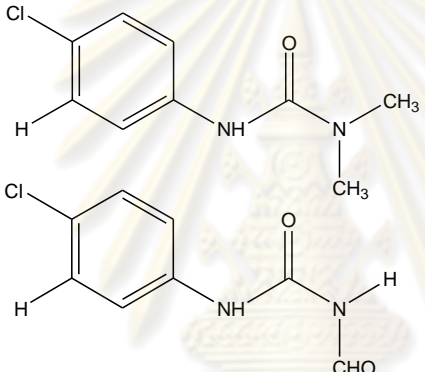
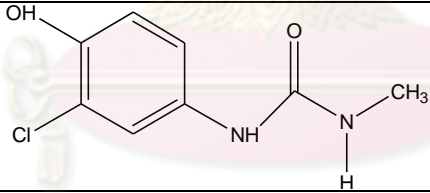
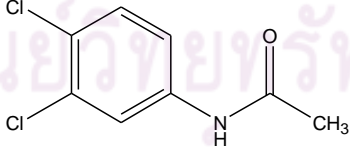
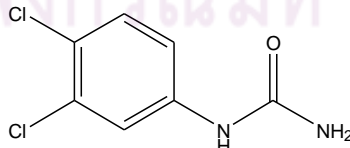
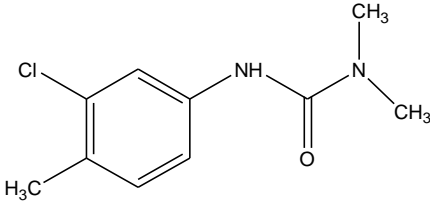
Compound	Structure	pH3	pH7	pH10
4		◆		
5 [62]		◆		
6		◆		
7 [62]		◆	◆	◆
8		◆	◆	
9 [70]		◆		
10 [63]				◆

Table 4.11 (continued).

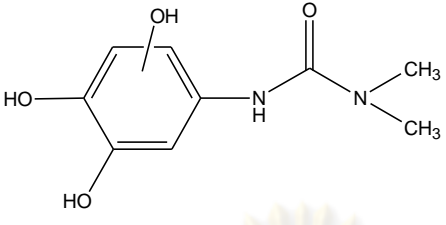
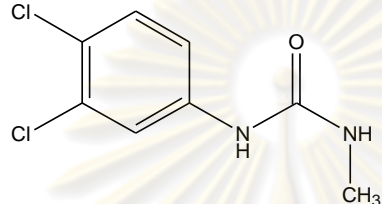
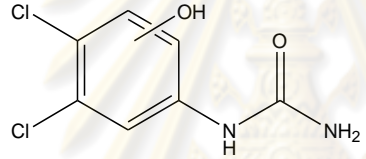
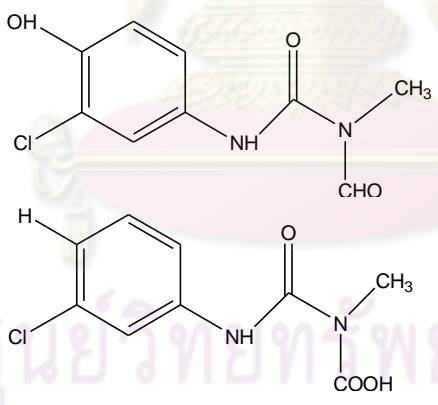
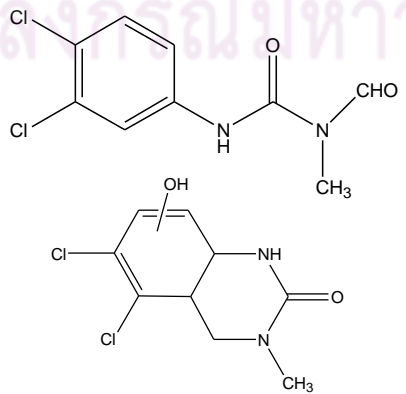
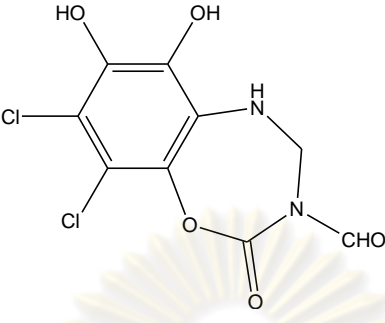
Compound	Structure	pH3	pH7	pH10
11 [66]		◆	◆	
12 [42, 61, 64]		◆	◆	◆
13		◆		◆
14		◆	◆	◆
15.1 [60, 62, 64, 65]		◆	◆	

Table 4.11 (continued).

Compound	Structure	pH3	pH7	pH10
16 [60, 64, 65]			◆	
17 [60, 64]		◆		
18 [42, 62]		◆		

Table 4.11 (continued).

Compound	Structure	pH3	pH7	pH10
19		◆		◆

Different pH of solution has different adsorption properties, which affect the reaction between diuron and the catalyst surface. The possible degradation pathway is proposed in these steps, first, the attack on the aromatic ring by OH^\cdot radical without dechlorination or alkyl chains. The next step involved a series of oxidation process that eliminated alkyl groups and chlorine atom. The last step involved the oxidative opening of aromatic ring, leading to small organic ion and inorganic species.

4.4.2.2 Effect of UV light

Figure 4.40 shows the photocatalytic degradation of diuron using titanium dioxide as catalyst and the UV irradiation, source is either UV-A or UV-C. The results indicate that photodegradation of diuron by UV-C irradiation can reach 90% within 6 h, while the use of UV-A results in only 45% degradation. However, high degradation rate achieved with UV-C is partly due to photolysis of diuron by UV-C. The first orders plots are shown in Figure 4.41 and the apparent rate constant are shown in the Table 4.12. The reaction rate constant and the adsorption rate constant of diuron in the investigation of the effect of UV lamps based on the Langmuir-Hinshelwood model are shown in the Table 4.12.

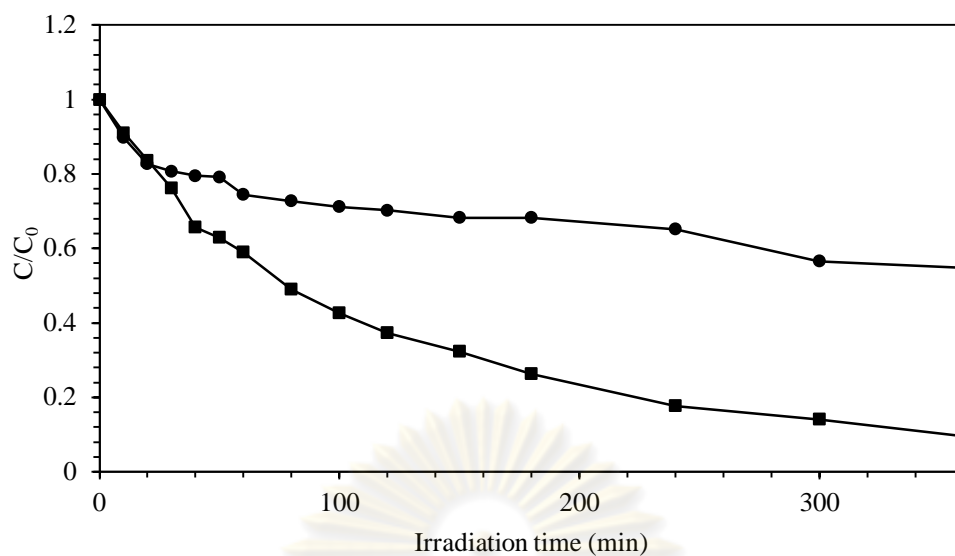


Figure 4.40 The effect of UV-lamp (●) UV-A, (■) UV-C on the degradation of diuron using titania as catalyst.

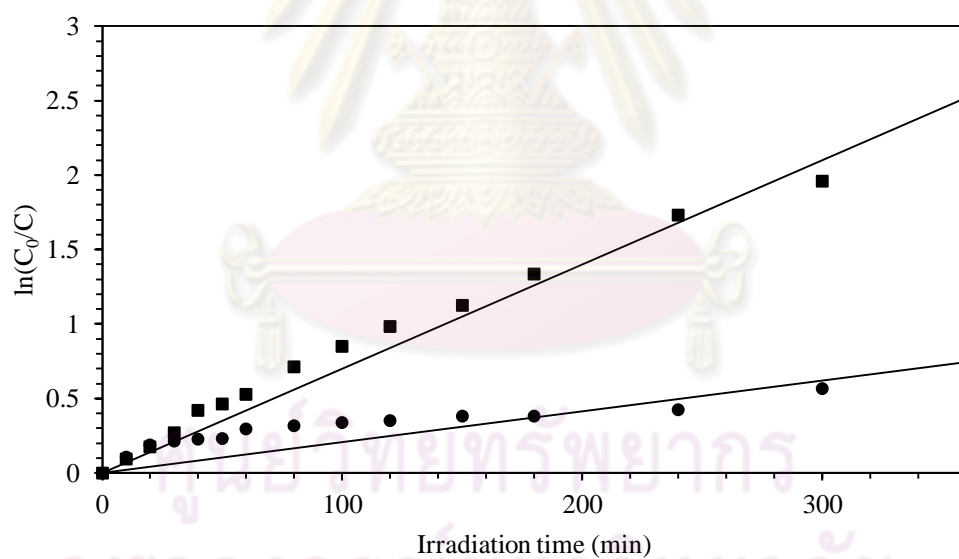


Figure 4.41 First order linear transforms of the photodegradation efficiency of diuron, (●) UV-A, (■) UV-C on the degradation of diuron using titania as catalyst.

Table 4.12 The apparent rate constant (k_{app}), reaction rate constants (k_r), and the adsorption constant (K) for the photocatalytic degradation of diuron using titania at different UV lamp.

Lamp	Pseudo first-order model		Langmuir-Hinshelwood model		
	k_{app} (min ⁻¹)	R ²	k_r (ppm/min)	K (min ⁻¹)	R ²
UV-A	0.0021	0.8847	0.0025	0.1218	0.9979
UV-C	0.0041	0.9579	0.9988	0.0952	0.8866

The results show that the photodegradation of diuron on titania is inconsistent with the Langmuir – Hinshelwood model for both cases, i.e. UV-A and UV-C because KC is close to 1.

Figure 4.42 and 4.43 shows the profile of intermediates generated during photocatalytic degradation of diuron on titanium dioxide using different UV-lamps. It was found that 11 and 9 kinds of intermediates are formed when UV-A and UV-C was used, respectively. The intermediates were detected by HPLC and identified the intermediates by LC-MS as shown in the Table 4.13.

ศูนย์วิทยทรัพยากร
จุฬาลงกรณ์มหาวิทยาลัย

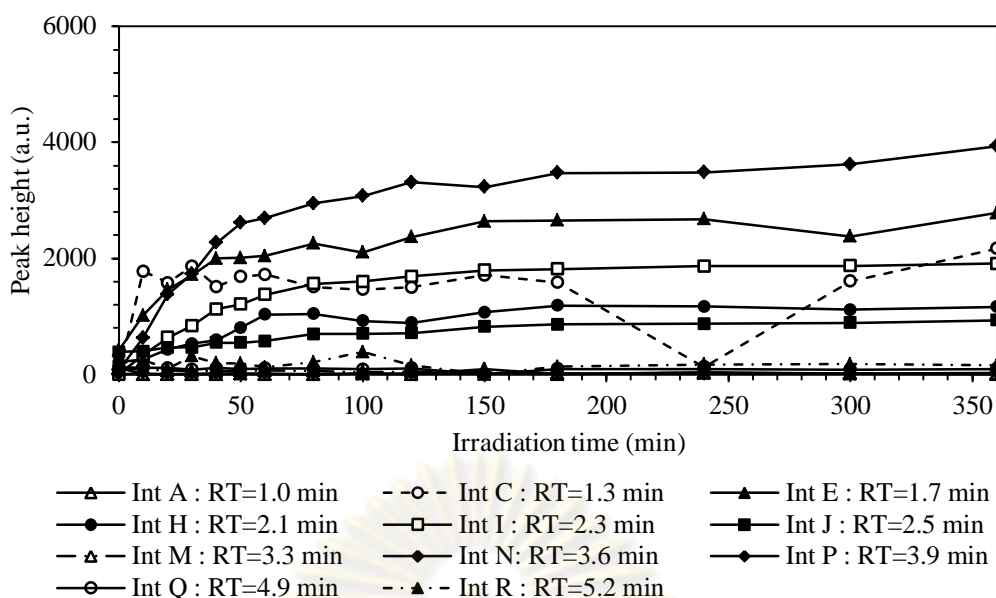


Figure 4.42 HPLC peak height of intermediates generated during photocatalytic degradation on diuron on titanium dioxide using UV-A as light source.

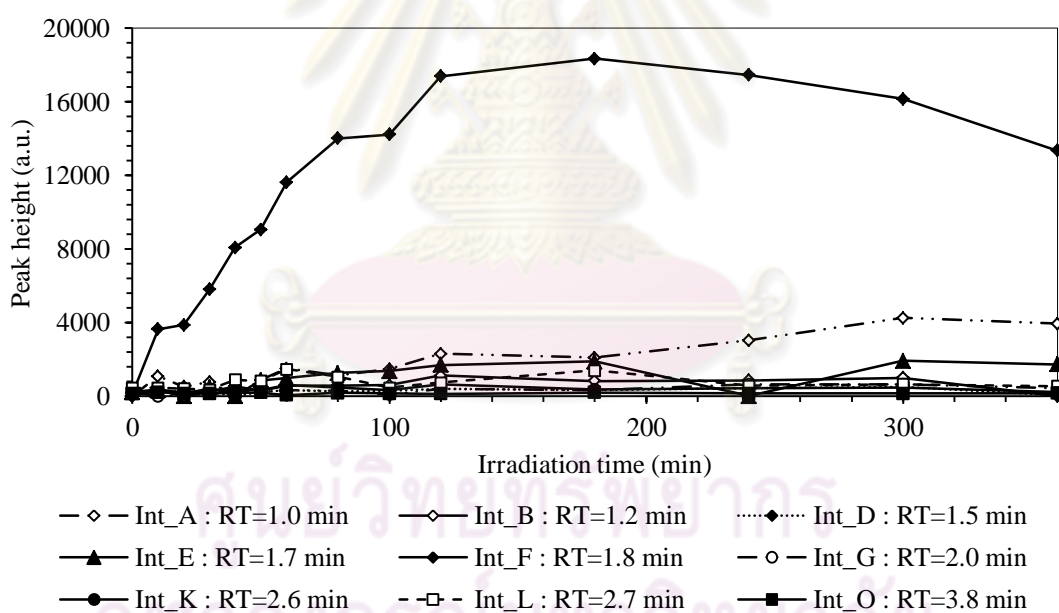


Figure 4.43 HPLC peak height of intermediates generated during photocatalytic degradation on diuron on titanium dioxide using UV-C as light source.

The intermediates are produced and degraded fast during the reaction and some intermediates remain stable even after 6 hours of the reaction. It was found that the concentration of the intermediates also changes along the course of the photodegradation. The structures of the intermediates product were identified by LC-MS as shown in Table 4.13.

Table 4.13 Possible intermediates generated from photodegradation of diuron on titanium dioxide using different UV-lamp.

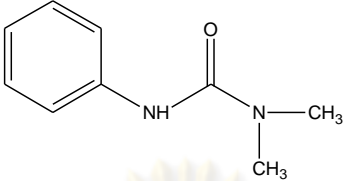
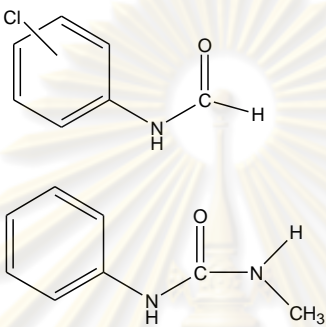
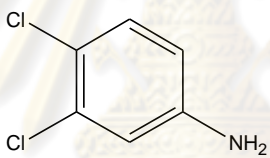
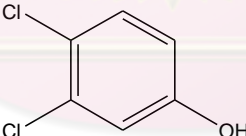
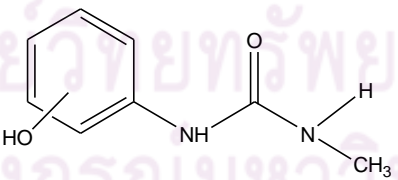
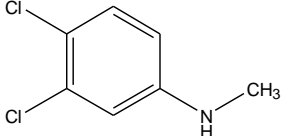
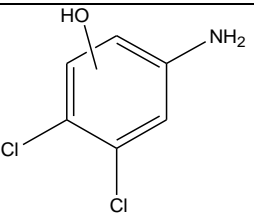
Compound	Proposed structure	UV-A	UV-C
1 [60]			◆
2 [61]		◆	
3 [1, 60, 61, 65]		◆	
4		◆	
5 [44]			◆
6		◆	◆
7 [62]		◆	◆

Table 4.13 (continued).

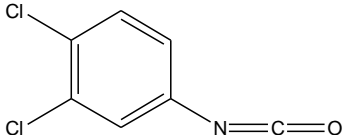
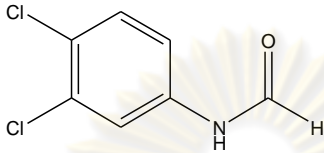
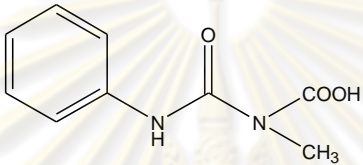
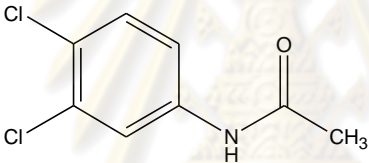
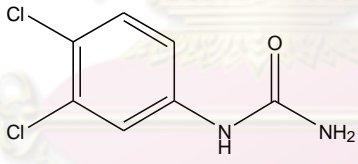
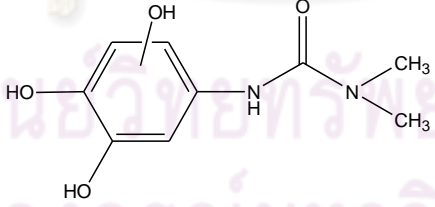
Compound	Proposed structure	UV-A	UV-C
8 [69]		◆	
9 [64]		◆	
10 [66]		◆	
11		◆	
12 [70]		◆	
13 [66]		◆	

Table 4.13 (continued).

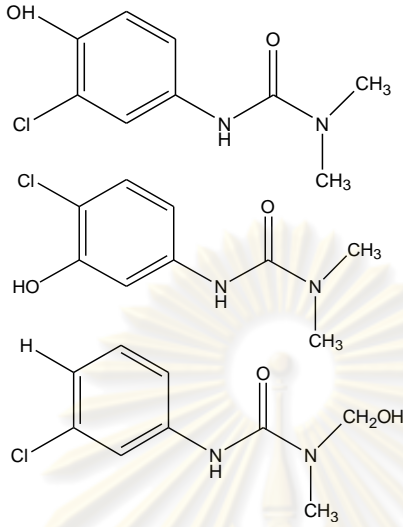
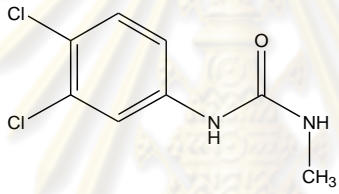
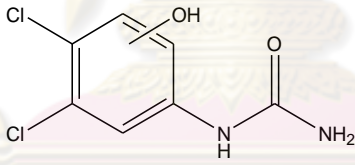
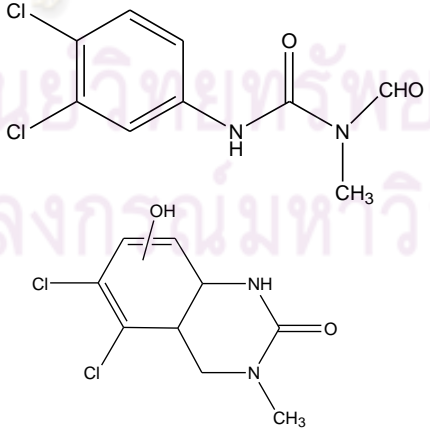
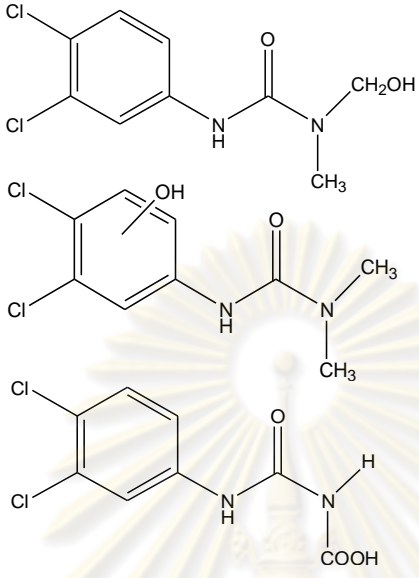
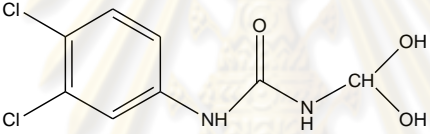
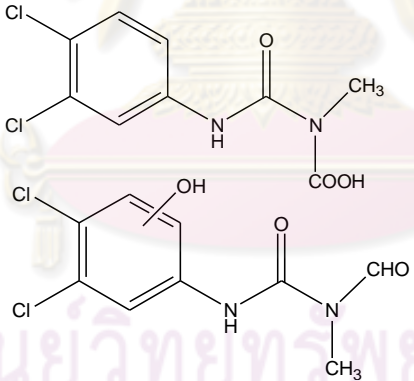
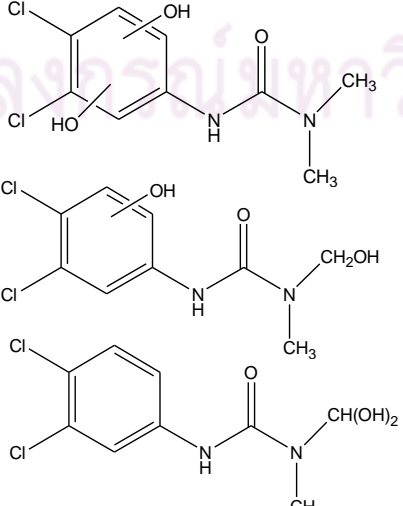
Compound	Proposed structure	UV-A	UV-C
14 [1, 60, 64]		◆	◆
15 [42, 61, 64]		◆	◆
16		◆	◆
17 [60, 62, 64, 65]		◆	◆

Table 4.13 (continued).

Compound	Proposed structure	UV-A	UV-C
18 [60, 64, 65]		◆	
19			◆
20 [60, 64]			◆
21 [42, 62]			◆

UV-light also affects the generation of intermediates Diuron is degraded into smaller compounds during photodegradation process. The degradation rate when using UV-C on titania was faster than using UV-A, the formation of intermediates when using UV-C was also rapid. The possible degradation mechanism of diuron on titania is proposed in Table 4.13 are similar to the mechanism of diuron on zinc oxide.

4.4.3 Effect of type of photocatalysts

Comparison of the intermediates formed from the reaction using different photocatalysts, i.e., titanium dioxide and zinc oxide, reveals common intermediates as well as different intermediates. Attempts were made to identify the intermediate products through analysis using LC-MS. The results confirm that the degradation of diuron generates lots of intermediates. According to the detailed analysis of the obtained mass spectrum, it indicates that the peak detected by HPLC chromatogram (i.e., an intermediate presented in Figure 4.30 and 4.39) is indeed a signal from a collection of intermediates. The structures of all intermediates detected are proposed in Table 4.14. The molecular mass of each product was confirmed by its detection in negative or/and positive mode. The results confirm that diuron is degraded into smaller compounds during photodegradation. While some intermediates are further degraded by the photocatalytic process, the conjugation of intermediates to form larger molecules is also observed.

Table 4.14 Possible intermediates generated from photodegradation of diuron on zinc oxide and titania.

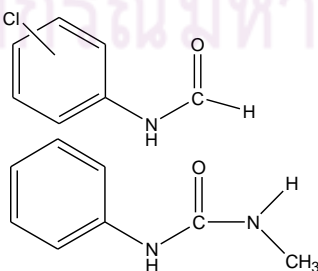
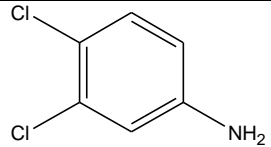
Compound	Proposed structure	ZnO	TiO ₂
1 [42]		◆	◆
2 [1, 60, 61, 65]		◆	◆

Table 4.14 (continued).

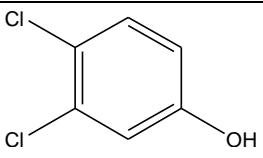
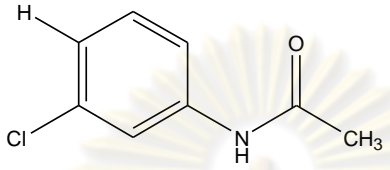
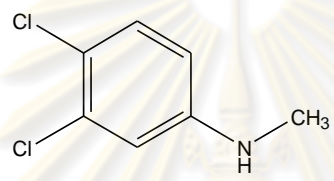
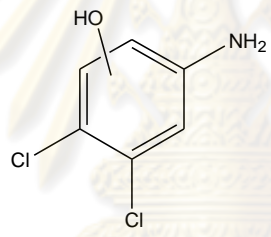
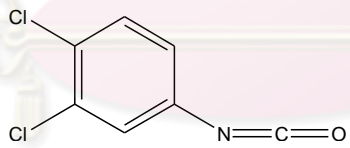
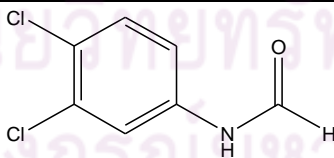
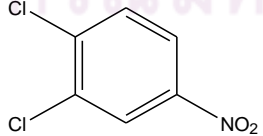
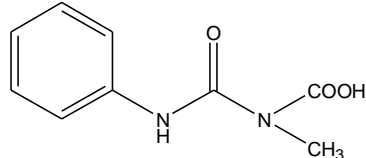
Compound	Proposed structure	ZnO	TiO ₂
3		◆	◆
4		◆	
5			◆
6 [62]			◆
7 [69]			◆
8 [64]			◆
9 [69]		◆	
10 [66]			◆

Table 4.14 (continued).

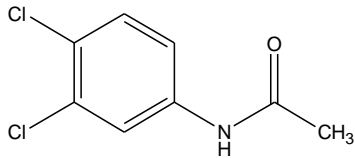
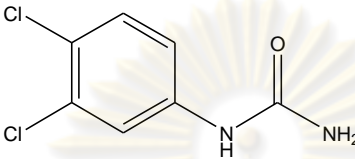
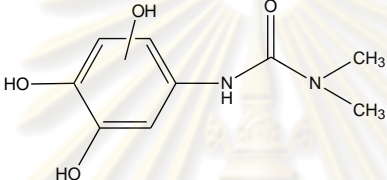
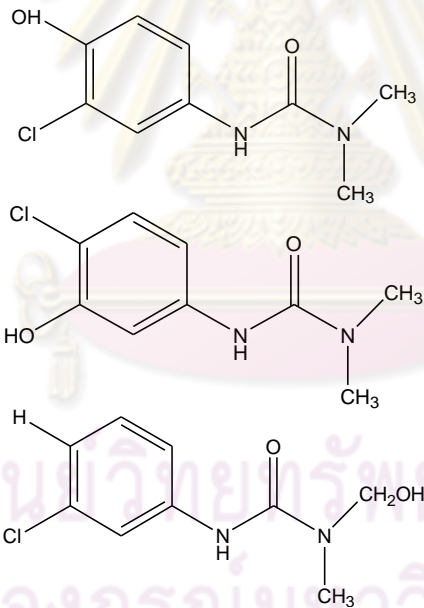
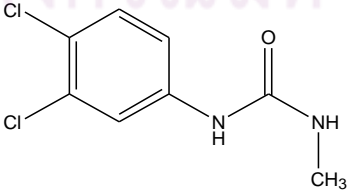
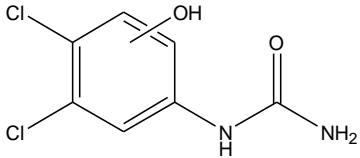
Compound	Proposed structure	ZnO	TiO ₂
11		◆	◆
12 [70]		◆	◆
13 [66]			◆
14 [1, 60, 64]		◆	◆
15 [42, 61, 64]		◆	◆
16		◆	◆

Table 4.14 (continued).

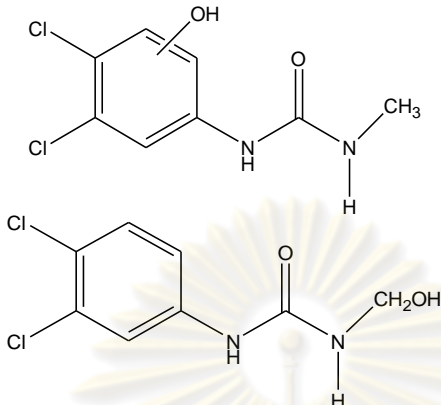
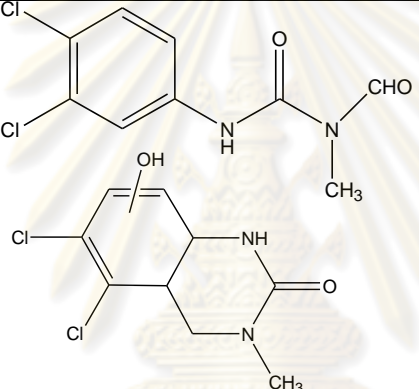
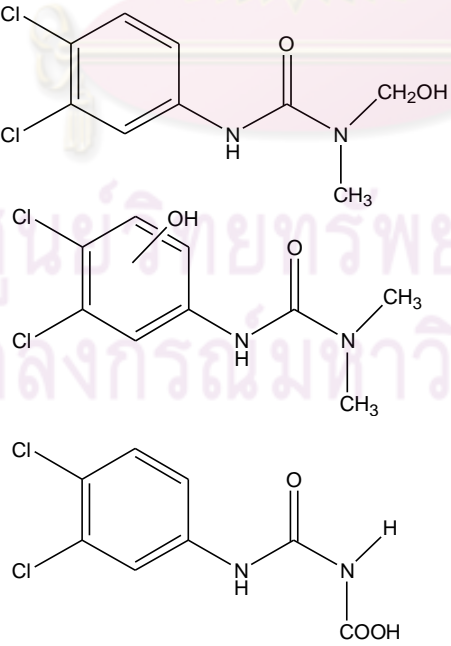
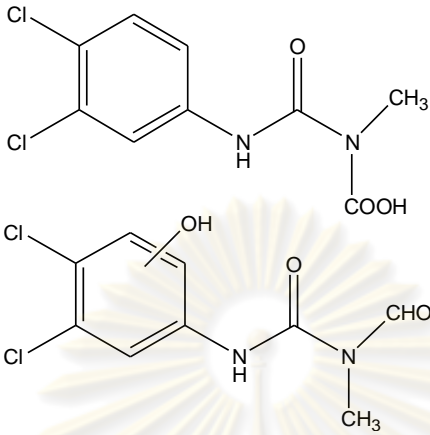
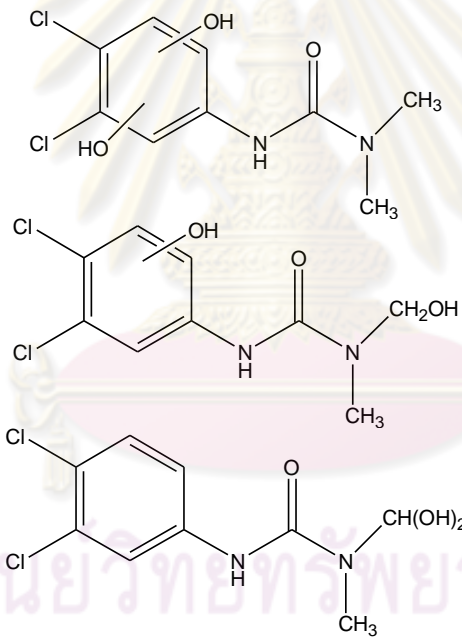
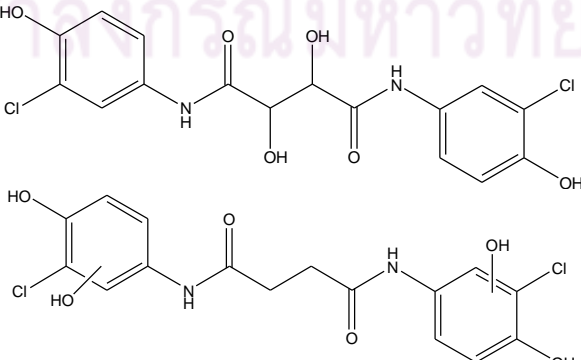
Compound	Proposed structure	ZnO	TiO ₂
17 [70]		◆	
18 [60, 62, 64, 65]		◆	◆
19 [60, 64, 65]		◆	◆

Table 4.14 (continued).

Compound	Proposed structure	ZnO	TiO ₂
20 [60, 64]		◆	
21 [42, 62]		◆	
22		◆	

Different type of catalyst has different surface properties, which affect the interaction between diuron and the catalyst surface. The dissimilarity in the degradation mechanism arises from the difference in interaction between the catalyst surface and the adsorbed diuron. As many of the intermediates listed in the Table 4.7, 4.9, 4.11, and 4.13 are common with those reported in other researches, it confirms that the main degradation pathway of diuron using zinc oxide and titanium dioxide follows the mechanisms previously proposed. They included hydroxylation of the aromatic ring and of the side chain (resulting in compounds 17, 19, 20, and 21), dehalogenation or dechlorination of the aromatic ring (resulting in compounds 1, 4, 14, and 22), demethylation (resulting in compound 12), and condensation (resulting in compound 18).

According to the detailed mass spectra shown in Appendix C, some intermediates product identified from LC-MS were analyzed by LC-MS/MS (MS/MS detector, mass spectrometric detector) which can confirm the structure of the intermediates. In this study, the investigation of intermediates was inconclusive as shown in Appendix D. It can be the result from the fact that the concentration of all unknown intermediates are very low. Therefore, signals from unknown intermediates are very low and does not explicit.



ศูนย์วิทยทรัพยากร
จุฬาลงกรณ์มหาวิทยาลัย

CHAPTER V

CONCLUSIONS

5.1 Conclusions

The conclusions of the present research are the following:

1. Zinc oxide has higher performance in degrading and mineralization of diuron than titanium dioxide.
2. The treatment is not feasible without catalyst in the case of UV-A.
3. The photodegradation reaction of diuron follows a pseudo first order kinetics and the photodegradation of diuron by using zinc oxide is consistent with the Langmuir-Hinshelwood model while the photodegradation of diuron by titania was inconsistent with Langmuir-Hinshelwood model because KC is approximately 1.
4. Intermediates of large molecular weight are detected, suggesting that conjugation of radicals during photodegradation occurs. Many intermediates are formed during the degradation of diuron.
5. When comparing the intermediates produced by two photocatalysts, i.e., zinc oxide and titanium dioxide, some products are similar to one another while some are different. This suggests the involvement of catalyst surface with diuron and hydroxyl radicals during photodegradation.
6. The structure of intermediates generated during the photodegradation process is affected by photocatalyst, pH of solution, and UV irradiation.

5.2 Recommendations

Recommendations for the future work, based on the results of this work, are following.

1. Further identification of the adsorption of diuron on the catalyst surface by using NMR analysis (solid).

2. Investigation of the reaction for long period of irradiation time for photocatalytic degradation of diuron, to achieve 100% conversion and 100% mineralization.
3. Monitor the concentration of the radical such as Cl^{\cdot} , OH^{\cdot} .
4. Identify adsorption isotherm type by sum of error method.
5. Quantity concentration of the intermediates.



ศูนย์วิทยทรัพยากร
จุฬาลงกรณ์มหาวิทยาลัย

REFERENCES

- [1] Katsumata, H., et al. *Photocatalytic degradation of diuron in aqueous solution by platinized TiO₂*. Journal of Hazardous Materials, 2009. 171(1-3): p. 1081-1087.
- [2] Sayeh, R., Coulomb, B., Boudenne, J.L., Belkadi, F., *Elimination of Pollutants Phenyleurea Herbicides by Advanced Oxidation*. Engineering and Applied Sciences, 2007. 2(4): p. 664-670.
- [3] Burrows, H.D., Canle L. M., Santaballa, J. A. and Steenken, S., *Reaction pathways and mechanisms of photodegradation of pesticides*. Journal of Photochemistry and Photobiology B: Biology, 2002. 67(2): p. 71-108.
- [4] Amereh, E. and Afshar, S. *Photodegradation of acetophenone and toluene in water by nano-TiO₂ powder supported on NaX zeolite*. Materials Chemistry and Physics. 120(2-3): p. 356-360.
- [5] Tian, J., Wang, J., Dai, J., Wang, X. and Yin, Y., *N-doped TiO₂/ZnO composite powder and its photocatalytic performance for degradation of methyl orange*. Surface and Coatings Technology, 2009. 204(5): p. 723-730.
- [6] Klongdee, J., Petchkroh, W., Phuempoonsathaporn, K., Praserttham, P., Vangnai, A.S., and Pavarajarn, V., *Activity of nanosized titania synthesized from thermal decomposition of titanium (IV) n-butoxide for the photocatalytic degradation of diuron*. Science and Technology of Advanced Materials, 2005. 6(3-4): p. 290.
- [7] Pal, B. and Sharon, M. *Enhanced photocatalytic activity of highly porous ZnO thin films prepared by sol-gel process*. Materials Chemistry and Physics, 2002. 76(1): p. 82-87.
- [8] Apichatsanee, K., et al. *Investigation of kinetics and intermediates of photodegradation of phenylurea herbicides on nanosized ZnO*, in *Chemical Engineering*. 2008, Chulalongkorn University: Bangkok. p. 103.
- [9] Lee, J., Easteal, A. J., Pal, U. and Bhattacharyya, D., *Evolution of ZnO nanostructures in sol-gel synthesis*. Current Applied Physics, 2009. 9(4): p. 792-796.
- [10] Konstantinou, I.K., *Photocatalytic transformation of pesticides in aqueous titanium dioxide suspensions using artificial and solar light: intermediates and degradation pathways* Applied Catalysis B: Environmental, 2003. 42(4): p. 319-335.
- [11] Floroncio, M.H., et al. *Photodegradation of Diquat and Paraquat in aqueous solutions by titanium dioxide: evolution of degradation reactions and*

- characterisation of intermediates*. Chemosphere, 2004. 55(3): p. 345-355.
- [12] Depero, L.E., Bonzi, P., Zocchi, M., Casale, C. and Gennaro, D.M., *Study of the anatase-rutile transformation in TiO₂ powders obtained by laser-induced synthesis*. Journal of Materials Research 1993 8(10): p. 2709-2715.
- [13] Gouvea, C.A.K., et al., *Semiconductor-assisted photocatalytic degradation of reactive dyes in aqueous solution*. Chemosphere, 2000. 40(4): p. 433-440.
- [14] Marci, G., et al. *Preparation characterization and photocatalytic activity of polycrystalline ZnO/TiO₂ systems. 1. Surface and bulk characterization*. Journal of Physical Chemistry B, 2001. 105: p. 1026-1032.
- [15] Su, C., Hong, B.Y. and Tseng, C.M. *Sol-gel preparation and photocatalysis of titanium dioxide*. Catalysis Today, 2004. 96(3): p. 119-126.
- [16] Payakgul, W., et al., *Effects of reaction medium on the synthesis of TiO₂ nanocrystals by thermal decomposition of titanium (IV) n-butoxide*. Ceramics International, 2005. 31(3): p. 391-397.
- [17] Sue, K., et al., *Rapid hydrothermal synthesis of ZnO nanorods without organics*. Materials Letters, 2004. 58(26): p. 3350-3352.
- [18] Daneshvar, N., et al. *Photocatalytic degradation of the insecticide diazinon in the presence of prepared nanocrystalline ZnO powders under irradiation of UV-C light*. Separation and Purification Technology, 2007. 58(1): p. 91-98.
- [19] Janitabar-Darzi, S. and Mahjoub, A.R. *Investigation of phase transformations and photocatalytic properties of sol-gel prepared nanostructured ZnO/TiO₂ composites*. Journal of Alloys and Compounds, 2009. 486(1-2): p. 805-808.
- [20] Sakka, S., *Applications of sol-gel technology Handbook of sol-gel science and technology : processing, characterization, and applications*. 3.
- [21] Jung, K.Y., Park, S.B, *Anatase-phase titania: preparation by embedding silica and photocatalytic activity for the decomposition of trichloroethylene*. Journal of Photochemistry and Photobiology A: Chemistry, 1999. 127: p. 117-122.
- [22] Cheng, P., Deng, C., Gu, M. and Dai, X., *Effect of urea on the photoactivity of titania powder prepared by sol-gel method*. Materials Chemistry and Physics, 2008. 107(1): p. 77-81.
- [23] Bianchi, C.L., et al., *N-doped TiO₂ from TiCl₃ for photodegradation of air pollutants*. Catalysis Today, 2009. 144(1-2): p. 31-36.
- [24] Bubacz, K., et al., *Studies on nitrogen modified TiO₂ photocatalyst prepared in different conditions*. Materials Research Bulletin. 45(9): p. 1085-1091.
- [25] Arconadaa, N., et al. *Synthesis and photocatalytic properties of dense and porous TiO₂-anatase thin films prepared by sol-gel*. Applied Catalysis B: Environmental, 2009. 86(1-2): p. 1-7.

- [26] Feng, J., Zheng, Z., Luan, J., Zhang, J. and Wang, L., *Degradation of diuron in aqueous solution by ozonation*. Journal of Environmental Science and Health, Part B: Pesticides, Food Contaminants, and Agricultural Wastes, 2008. 43(7): p. 576 – 587.
- [27] Somrani, C., B., et al. *Photocatalytic degradative oxidation of Diuron in organic and semi-aqueous systems over titanium dioxide catalyst*. Journal of Chemistry, 2000. 24(12): p. 999-1002.
- [28] Sies, H., *Strategies of antioxidant defense*. Pharmacological Research, 1995. 31(Supplement 1): p. 161-161.
- [29] Houas, A., et al. *Photocatalytic degradation pathway of methylene blue in water*. Applied Catalysis B: Environmental, 2001. 31(2): p. 145-157.
- [30] Daneshvar, N., et al., *Removal of C.I. Acid Orange 7 from aqueous solution by UV irradiation in the presence of ZnO nanopowder*. Journal of Hazardous Materials, 2007. 143(1-2): p. 95-101.
- [31] Daneshvar, N., Salari, D. and Khataee, A.R. *Photocatalytic degradation of azo dye acid red 14 in water on ZnO as an alternative catalyst to TiO₂*. Journal of Photochemistry and Photobiology A: Chemistry, 2004. 162(2-3): p. 317-322.
- [32] Behnajady, M.A., Modirshahla, N. and Hamzavi, R. *Kinetic study on photocatalytic degradation of C.I. Acid Yellow 23 by ZnO photocatalyst*. Journal of Hazardous Materials, 2006. 133(1-3): p. 226-232.
- [33] Haque, M.M. and Muneer, M. *Heterogeneous photocatalysed degradation of a herbicide derivative, isoproturon in aqueous suspension of titanium dioxide*. Journal of Environmental Management, 2003. 69(2): p. 169-176.
- [34] Liao, D.L., Badour, C.A. and Liao, B.Q. *Preparation of nanosized TiO₂/ZnO composite catalyst and its photocatalytic activity for degradation of methyl orange*. Journal of Photochemistry and Photobiology A: Chemistry, 2008. 194(1): p. 11-19.
- [35] Bianco Prevot, A., et al., *Photocatalytic and photolytic transformation of chloramben in aqueous solutions*. Applied Catalysis B: Environmental, 1999. 22(2): p. 149-158.
- [36] Bamba, D., et al., *Photocatalytic degradation of the diuron pesticide*. Environmental Chemistry Letters, 2008. 6(3): p. 163-167.
- [37] Valente, J.P.S., Padilha, P.M. and Florentino, A.O. *Studies on the adsorption and kinetics of photodegradation of a model compound for heterogeneous photocatalysis onto TiO₂*. Chemosphere, 2006. 64(7): p. 1128-1133.
- [38] Vasanth Kumar, K., Porkodi, K. and Selvaganapathi, A. *Constrain in solving*

- Langmuir-Hinshelwood kinetic expression for the photocatalytic degradation of Auramine O aqueous solutions by ZnO catalyst.* Dyes and Pigments, 2007. 75(1): p. 246-249.
- [39] Kumar, K.V., Porkodi, K. and Rocha, F. *Langmuir-Hinshelwood kinetics - A theoretical study.* Catalysis Communications, 2008. 9(1): p. 82-84.
- [40] Liu, Y., et al., *Adsorption and desorption behavior of herbicide diuron on various Chinese cultivated soils.* Journal of Hazardous Materials. 178(1-3): p. 462-468.
- [41] Salvestrini, S., Di Cerbo, P. and Capasso, S. *Kinetics of the chemical degradation of diuron.* Chemosphere, 2002. 48(1): p. 69-73.
- [42] Oturan, N., et al., *Study of the toxicity of diuron and its metabolites formed in aqueous medium during application of the electrochemical advanced oxidation process "electro-Fenton".* Chemosphere, 2008. 73(9): p. 1550-1556.
- [43] Carrier, M., et al., *Photocatalytic Degradation of Diuron: Experimental Analyses and Simulation of HO₂ Radical Attacks by Density Functional Theory Calculations.* The Journal of Physical Chemistry A, 2009. 113(22): p. 6365-6374.
- [44] Carrier, M., Besson, M., Guillard, C., and Gonze, E., *Removal of herbicide diuron and thermal degradation products under Catalytic Wet Air Oxidation conditions.* Applied Catalysis B: Environmental, 2009. 91(1-2): p. 275-283.
- [45] Oturan, M.A., Edelahe, M. C., Oturan, N., El kacemi, K. and Aaron, J.J., *Kinetics of oxidative degradation/mineralization pathways of the phenylurea herbicides diuron, monuron and fenuron in water during application of the electro-Fenton process.* Applied Catalysis B: Environmental. In Press, Corrected Proof.
- [46] Mittal, A., Kurup, L. and Mittal, J. *Freundlich and Langmuir adsorption isotherms and kinetics for the removal of Tartrazine from aqueous solutions using hen feathers.* Journal of Hazardous Materials, 2007. 146(1-2): p. 243-248.
- [47] Adak, A., Bandyopadhyay, M. and Pal, A. *Removal of crystal violet dye from wastewater by surfactant-modified alumina.* Separation and Purification Technology, 2005. 44(2): p. 139-144.
- [48] Gawade, A.S., Vanjara, A.K. and Sawant, M.R. *Removal of herbicide from water with sodium chloride using surfactant treated alumina for wastewater treatment.* Separation and Purification Technology, 2005. 41(1): p. 65-71.
- [49] Arana, J., et al., *Photocatalytic degradation of phenol and phenolic compounds: Part*

- I. Adsorption and FTIR study*. Journal of Hazardous Materials, 2007. 146(3): p. 520-528.
- [50] Cabilla, G.C., Bonivardi, A.L. and Baltanús, M.A. *FTIR Study of the Adsorption of Methanol on Clean and Ca-Promoted Pd/SiO₂ Catalysts*. Journal of Catalysis, 2001. 201(2): p. 213-220.
- [51] Arana, J., et al., *FTIR study of gas-phase alcohols photocatalytic degradation with TiO₂ and AC-TiO₂*. Applied Catalysis B: Environmental, 2004. 53(4): p. 221-232.
- [52] Armenta, S., et al., *FTIR Approaches for Diuron Determination in Commercial Pesticide Formulations*. Journal of Agricultural and Food Chemistry, 2005. 53(15): p. 5842-5847.
- [53] Sangkhaprom, N., Supaphol, P. and Pavarajarn, V. *Fibrous zinc oxide prepared by combined electrospinning and solvothermal techniques*. Ceramics International. 36(1): p. 357-363.
- [54] Zhang, Y., et al., *Fabrication method of TiO₂-SiO₂ hybrid capsules and their UV-protective property*. Colloids and Surfaces A: Physicochemical and Engineering Aspects. 353(2-3): p. 216-225.
- [55] Burgos, M. and Langlet, M. *The sol-gel transformation of TIPT coatings: a FTIR study*. Thin Solid Films, 1999. 349(1-2): p. 19-23.
- [56] Catalkaya, E.C. and Kargi, F. *Dehalogenation, degradation and mineralization of diuron by peroxone (peroxide/ozone) treatment*. Journal of Environmental Science and Health, Part A: Toxic/Hazardous Substances and Environmental Engineering, 2009. 44(6): p. 630-638.
- [57] Madani, M.E., et al., *Photocatalytic degradation of diuron in aqueous solution in presence of two industrial titania catalysts, either as suspended powders or deposited on flexible industrial photoresistant papers*. Applied Catalysis B: Environmental, 2006. 65(1-2): p. 70-76.
- [58] Naeem, K., Weiqian, P. and Ouyang, F. *Thermodynamic parameters of activation for photodegradation of phenolics*. Chemical Engineering Journal. 156(2): p. 505-509.
- [59] Hincapie, M., et al., *Solar photocatalytic degradation and detoxification of EU priority substances*. Catalysis Today, 2005. 101(3-4): p. 203-210.
- [60] Zielinska, B., et al., *Photocatalytic degradation of Reactive Black 5: A comparison between TiO₂-Tytanpol A11 and TiO₂-Degussa P25 photocatalysts*. Applied Catalysis B: Environmental, 2001. 35(1): p. L1-L7.
- [61] Canle López, M., et al., *Mechanisms of Direct and TiO₂-Photocatalysed UV*

- Degradation of Phenylurea Herbicides*. ChemPhysChem, 2005. 6(10): p. 2064-2074.
- [62] Carrier, M., et al., *Removal of herbicide diuron and thermal degradation products under Catalytic Wet Air Oxidation conditions*. Applied Catalysis B: Environmental, 2009. 91(1-2): p. 275-283.
- [63] Malato, S., et al. *Photocatalytic Treatment of Diuron by Solar Photocatalysis: Evaluation of Main Intermediates and Toxicity*. Environmental Science & Technology, 2003. 37(11): p. 2516-2524.
- [64] Sharma, P. and Suri, C.R. *Biotransformation and biomonitoring of phenylurea herbicide diuron*. Bioresource Technology. 102(3): p. 3119-3125.
- [65] Feng, J., et al., *Degradation of diuron in aqueous solution by ozonation*. Journal of Environmental Science and Health, Part B: Pesticides, Food Contaminants, and Agricultural Wastes, 2008. 43(7): p. 576 - 587.
- [66] Farre, M.J., et al., *Evaluation of the intermediates generated during the degradation of Diuron and Linuron herbicides by the photo-Fenton reaction*. Journal of Photochemistry and Photobiology A: Chemistry, 2007. 189(2-3): p. 364-373.
- [67] Oturan, M.A., et al., *Kinetics of oxidative degradation/mineralization pathways of the phenylurea herbicides diuron, monuron and fenuron in water during application of the electro-Fenton process*. Applied Catalysis B: Environmental. 97(1-2): p. 82-89.
- [68] Song, W., et al., *Free Radical Destruction of -Blockers in Aqueous Solution*. Environmental Science & Technology, 2008. 42(4): p. 1256-1261.
- [69] Proof, E., *International standard ISO 21348*. Environment spatial, 2007. 4.
- [70] Chen, W.-H. and Young, T.M. *Influence of nitrogen source on NDMA formation during chlorination of diuron*. Water Research, 2009. 43(12): p. 3047-3056.
- [71] Oturan, N., et al., *Study of the toxicity of diuron and its metabolites formed in aqueous medium during application of the electrochemical advanced oxidation process "electro-Fenton"*. Chemosphere, 2008. 73(9): p. 1550-1556.
- [72] Richard, C. and Bengana, S. *PH effect in the photocatalytic transformation of a phenyl-urea herbicide*. Chemosphere, 1996. 33(4): p. 635-641.
- [73] Kosmulski, M., *The significance of the difference in the point of zero charge between rutile and anatase*. Advances in Colloid and Interface Science, 2002. 99(3): p. 255-264.
- [74] Ussiri, D.A.N. and Johnson, C.E. *Characterization of organic matter in a northern hardwood forest soil by ¹³C NMR spectroscopy and chemical methods*. Geoderma, 2003. 111(1-2): p. 123-149.

- [75] Dupuy, N., et al., *¹H NMR study of inclusion compounds of phenylurea derivatives in [beta]-cyclodextrin*. *Spectrochimica Acta Part A: Molecular and Biomolecular Spectroscopy*, 2005. 61(6): p. 1051-1057.
- [76] Hassanzadeh, A., et al., *¹H, ¹³C, NH, HH, CH COSY, HH NOESY NMR and UV-vis studies of Solophenyl red 3BL dye azo-hydrazone tautomerism in various solvents*. *Spectrochimica Acta Part A: Molecular and Biomolecular Spectroscopy*, 2006. 63(2): p. 247-254.



ศูนย์วิทยทรัพยากร
จุฬาลงกรณ์มหาวิทยาลัย



APPENDICES

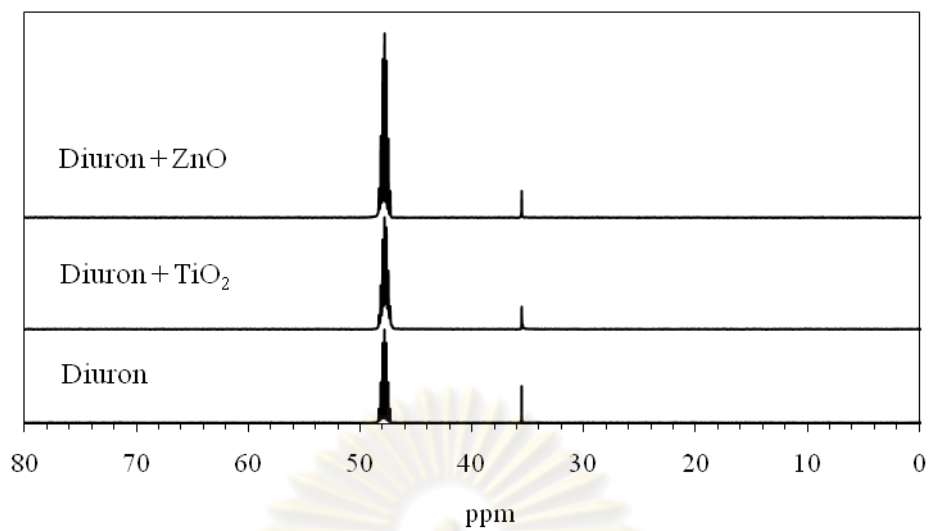
ศูนย์วิทยทรัพยากร
จุฬาลงกรณ์มหาวิทยาลัย

APPENDIX A

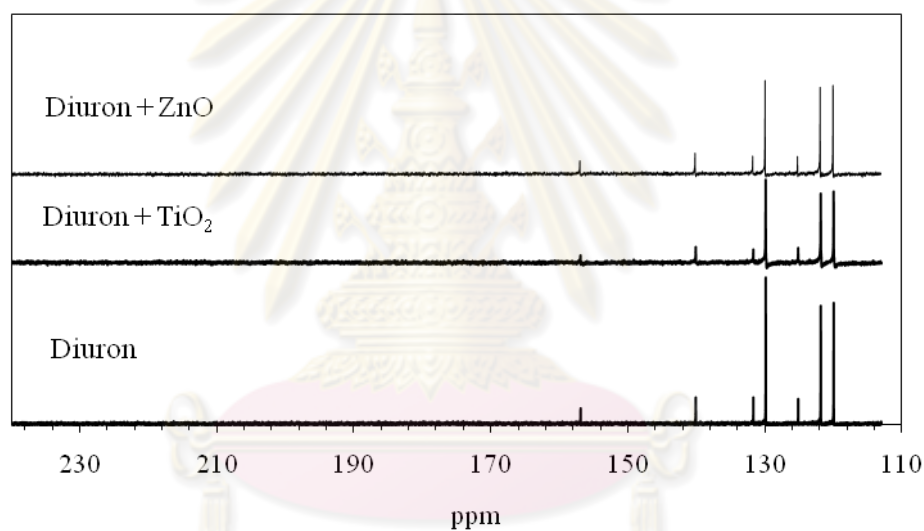
NMR STUDIES

^{13}C NMR analysis was conducted on the diuron solution to determine its chemical structure. Figure A.1 shows ^{13}C NMR spectra obtained from diuron solution in methanol (CD_3OD) and from diuron solution in methanol (CD_3OD) with the presence of TiO_2 and ZnO in the range of chemical shift from (a) 0-80 ppm and (b) 110-240 ppm. In general, all spectra show peaks in the resonance areas of alkyl carbon (0-50 ppm), o-alkyl carbon (50-110 ppm), aromatic carbon (110-160 ppm), and carbonyl carbon (150-220 ppm) [73]. The signal corresponding to carbon from methanol which was used as solvent appears at 48-49 ppm. For diuron, it has 9 atoms of carbon as shown in Figure A.2. The ^{13}C NMR results also indicate 9 atoms of carbon in the molecule. C_1 to C_6 are aromatic carbon corresponding to the chemical shift at 121.187, 141.321, 123.074, 132.915, 126.373, and 131.107 ppm, respectively. The chemical shift of C_7 appears at 158.133 ppm. C_8 and C_9 are alkyl carbon of which the signal appears at 36.732 ppm. The condition of diuron with TiO_2 and ZnO had not chemical shift compared diuron. Due to the NMR analysis, the aqueous suspension had to filter the catalyst from the diuron solution before analyze. It is indicated that, the reaction can not occur without light and catalyst.

Figure A.3 shows ^1H NMR spectra obtained from diuron solution in methanol (CD_3OD) and diuron solution in methanol mixed with TiO_2 and ZnO in the range of chemical shift from (a) 2.5 – 3.5 ppm, (b) 3.5 – 6.5 ppm, and (c) 7.2 -7.8 ppm. In the Figure A.3, the NMR lines in 3.39 – 5.0 ppm are due to CD_3OD as a solvent. The aromatic protons appeared at 7.29, 7.31, and 7.34 ppm [74, 75]. The signal of N,N-dimethyl group was observed at 2.99 ppm as a singlet [74]. The condition of diuron with TiO_2 and ZnO also had not chemical shift compared with diuron due to the NMR analyze as well.



(a)



(b)

Figure A.1 ¹³C NMR spectra from diuron solution in methanol (CD₃OD), diuron solution in methanol (CD₃OD) with TiO₂, and diuron solution in methanol (CD₃OD) with ZnO in the chemical shift from (a) 0-80 ppm and (b) 110-240 ppm.

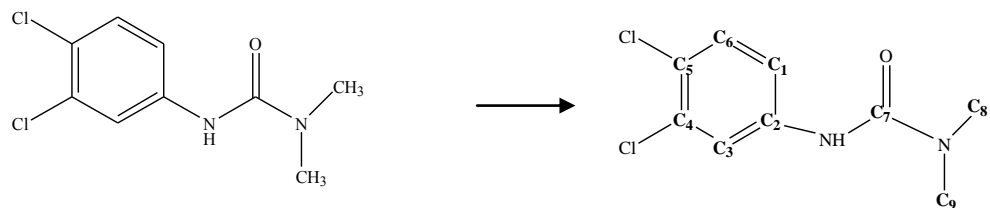


Figure A.2 Chemical structure of diuron.

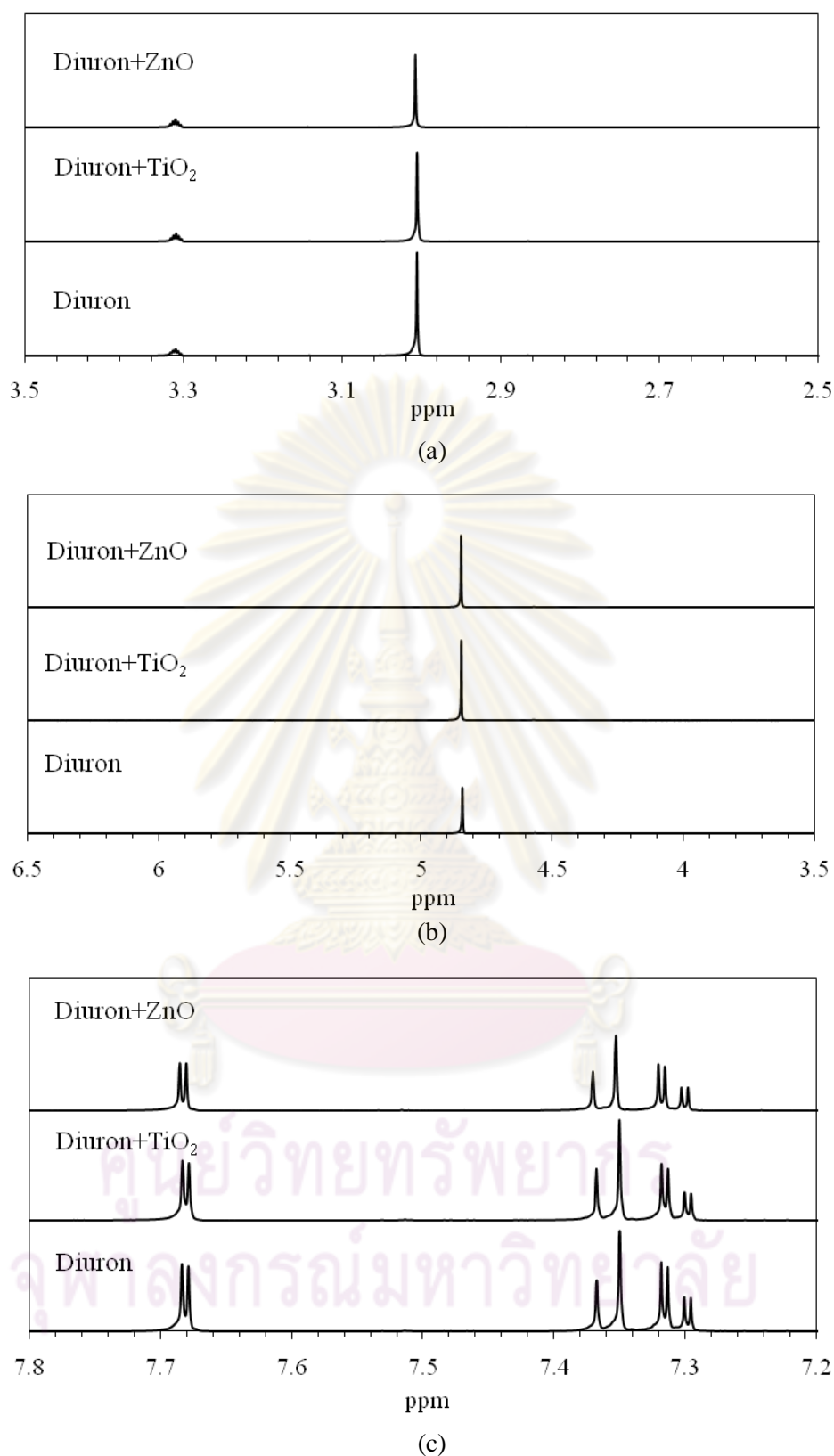


Figure A.3 ^1H NMR spectra from diuron solution in methanol (CD_3OD), diuron solution in methanol (CD_3OD) with TiO_2 , and diuron solution in methanol (CD_3OD) with ZnO in the chemical shift from (a) 2.5-3.5 ppm, (b) 3.5-6.5 ppm, and (c) 7.2-7.8 ppm.

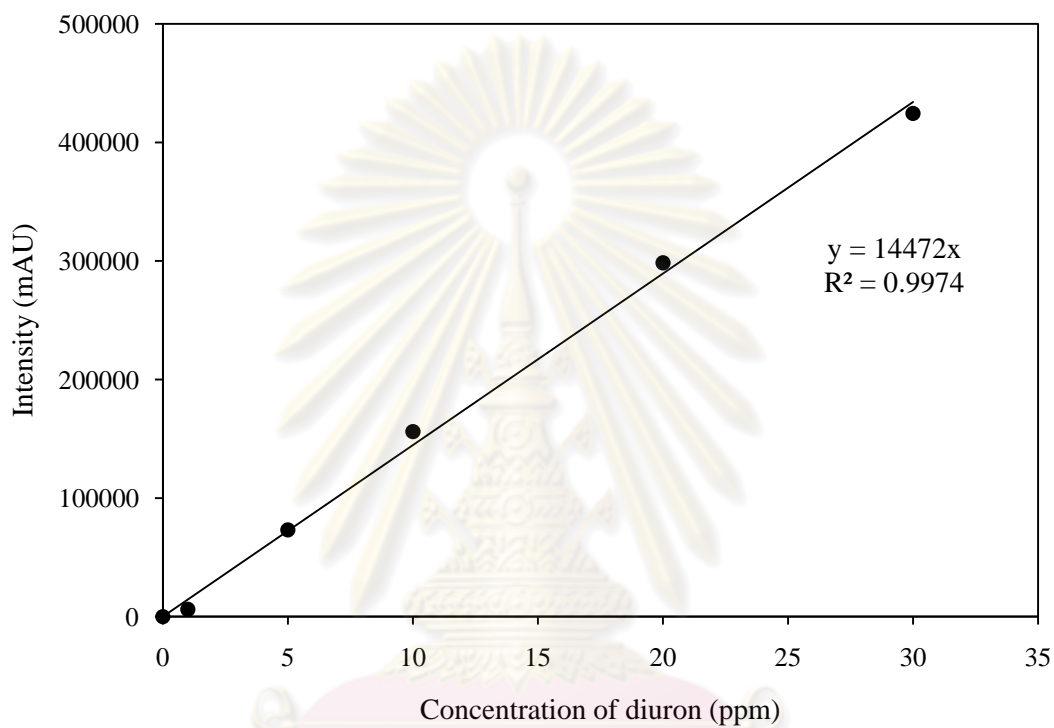
APPENDIX B**DIURON CALIBRATION CURVE**

Figure B.1 The calibration curve of diuron.

ศูนย์วิทยทรัพยากร
จุฬาลงกรณ์มหาวิทยาลัย

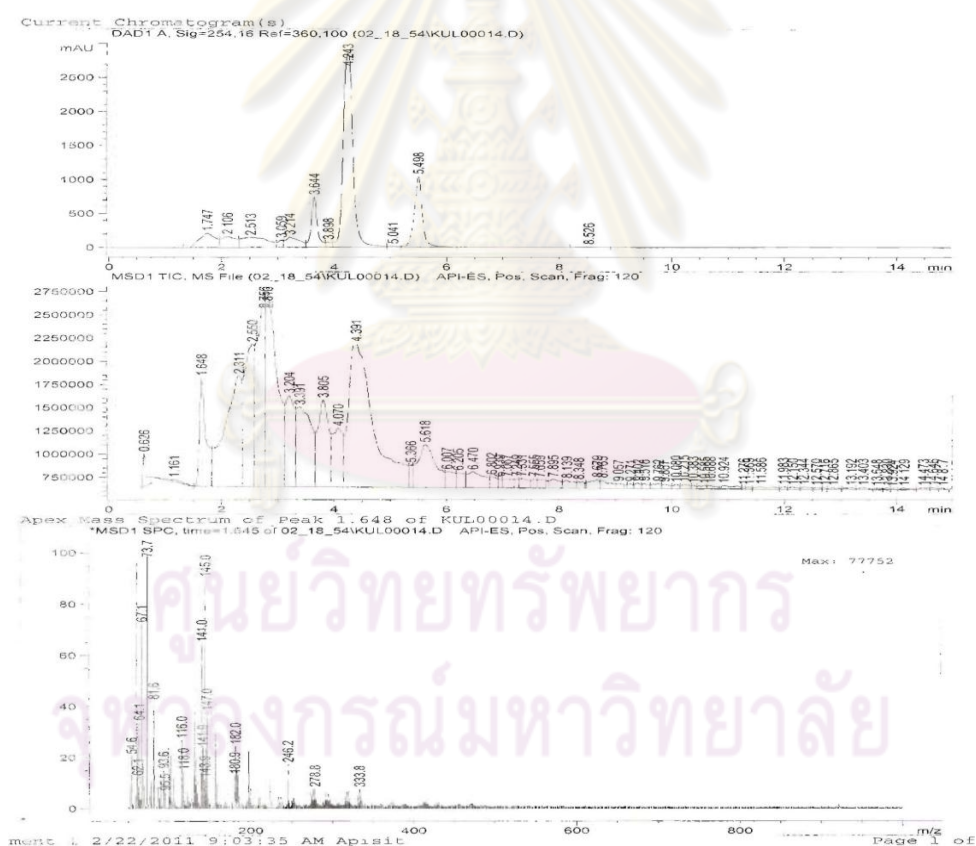
APPENDIX C

LC/MS MASS SPECTRUM

All samples were sent for analysis at Central Laboratory (Thailand) Ltd. Co. During a sample injection, three types of diagrams were obtained: chromatogram from UV detector, chromatogram from mass detector, and mass spectrum. Chromatogram from UV and mass detector spanned the LC runtime. The mass spectrum is obtained at a specific retention time

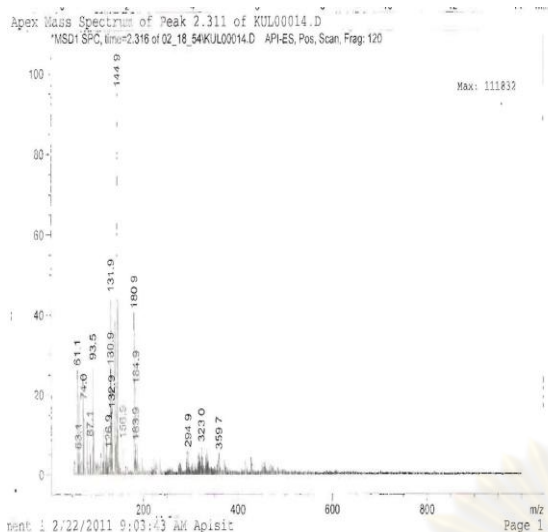
C.1 Mass spectrum of diuron solution from photodegradation by ZnO.

C.1.1 pH 3

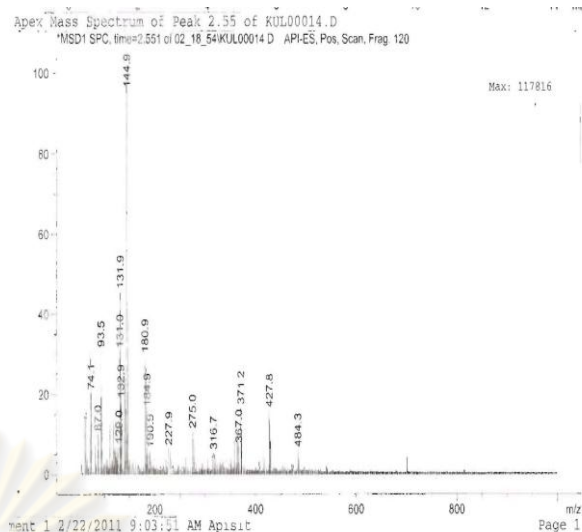


(a)

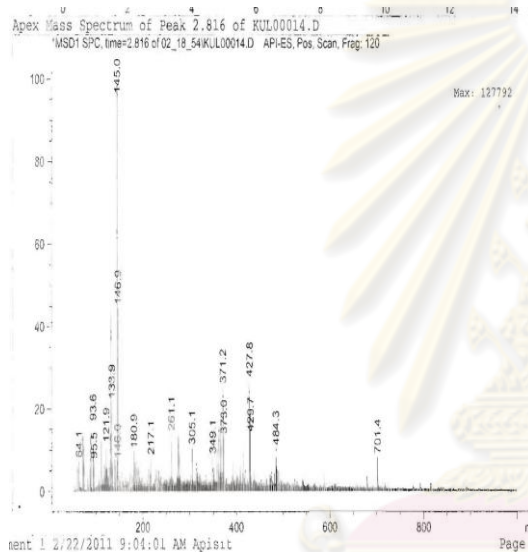
Figure C.1 Chromatogram of diuron solution photodegradation at pH3 obtained from UV detector and mass detector are displayed in (a). Mass spectrums were obtained using fragmentator of 120 V at various retention times as shown in (a)-(p).



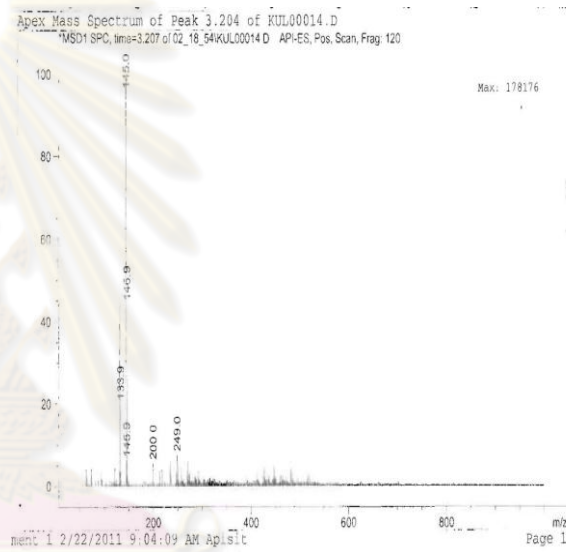
(b)



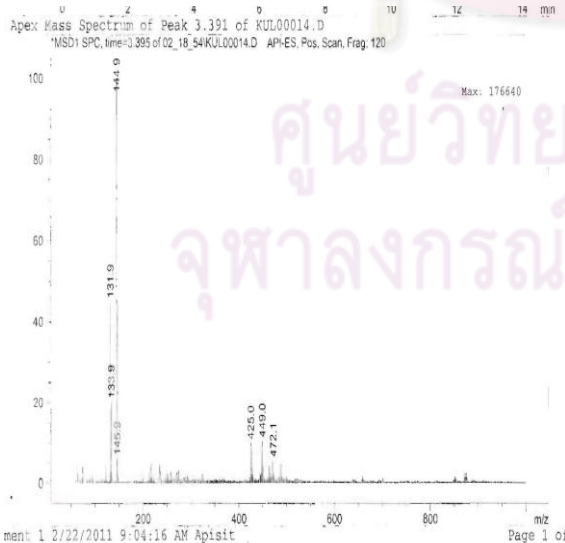
(c)



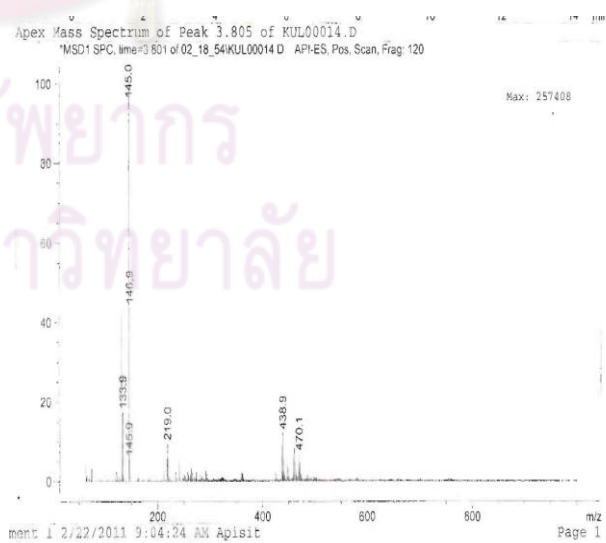
(d)



(e)

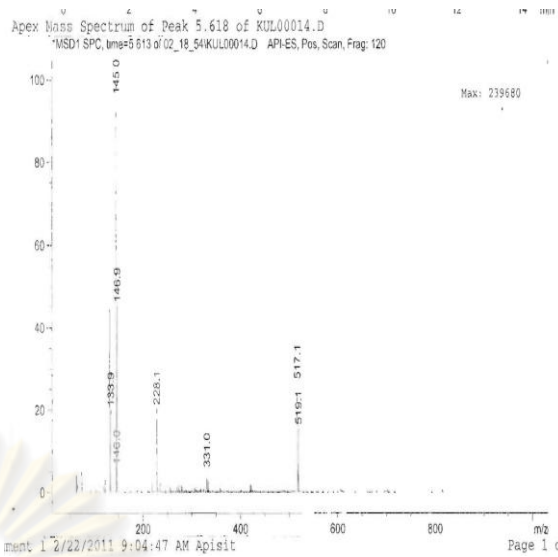
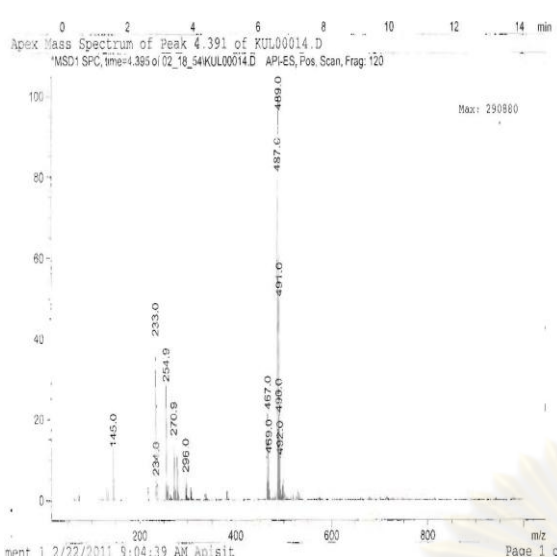


(f)



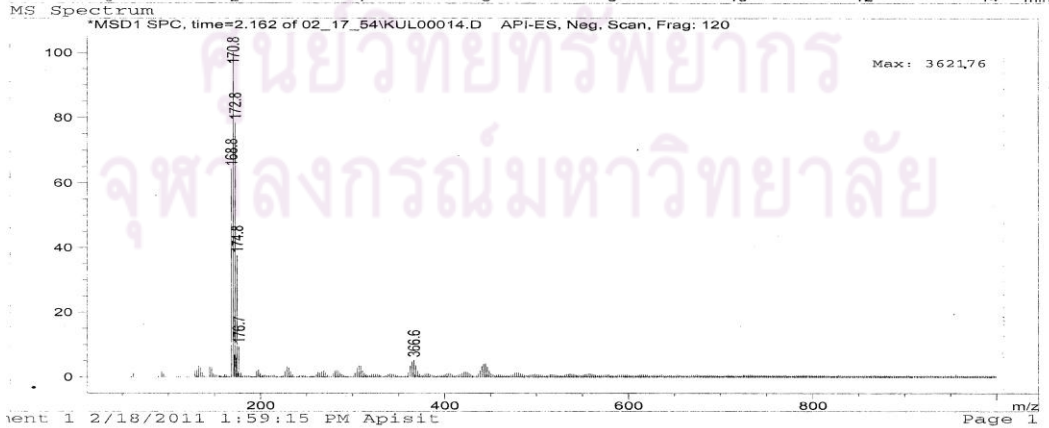
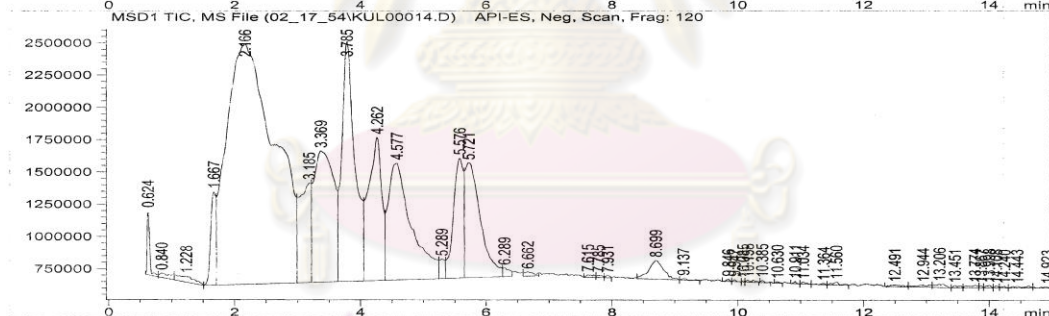
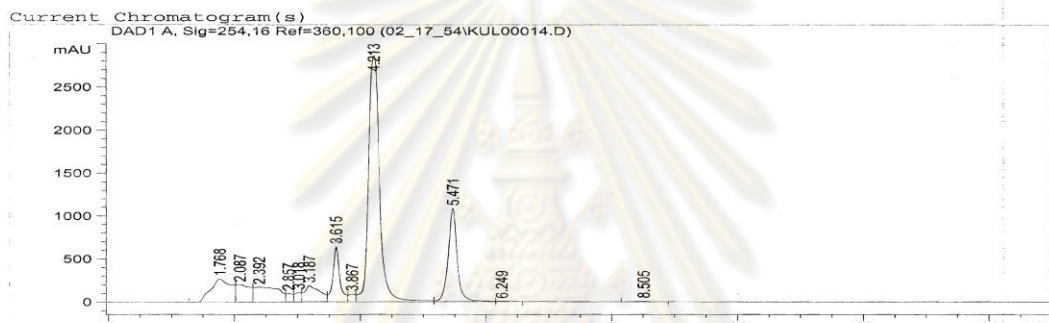
(g)

Figure C.1 (continued).



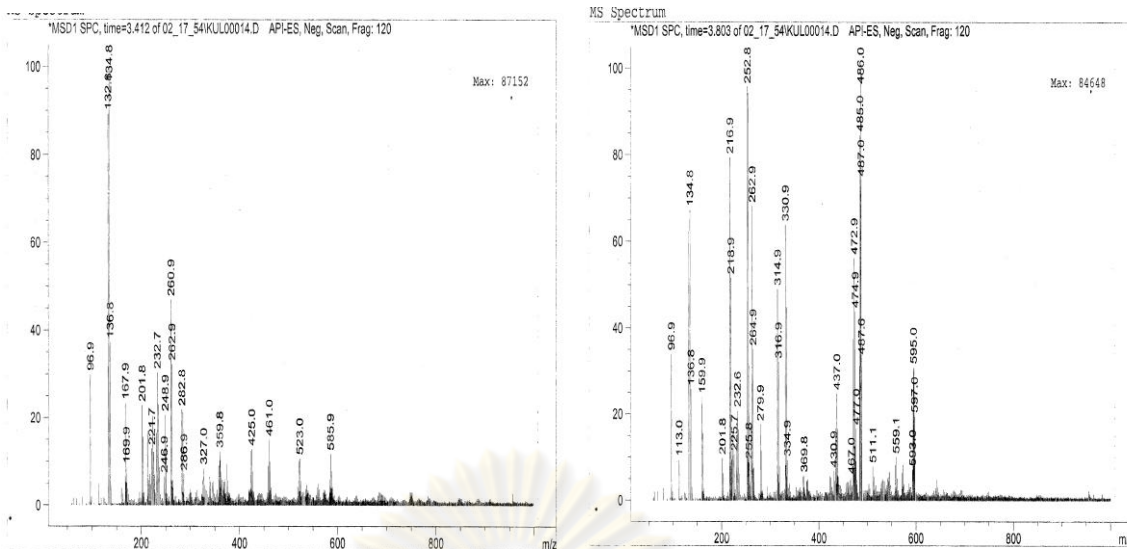
(h)

(i)



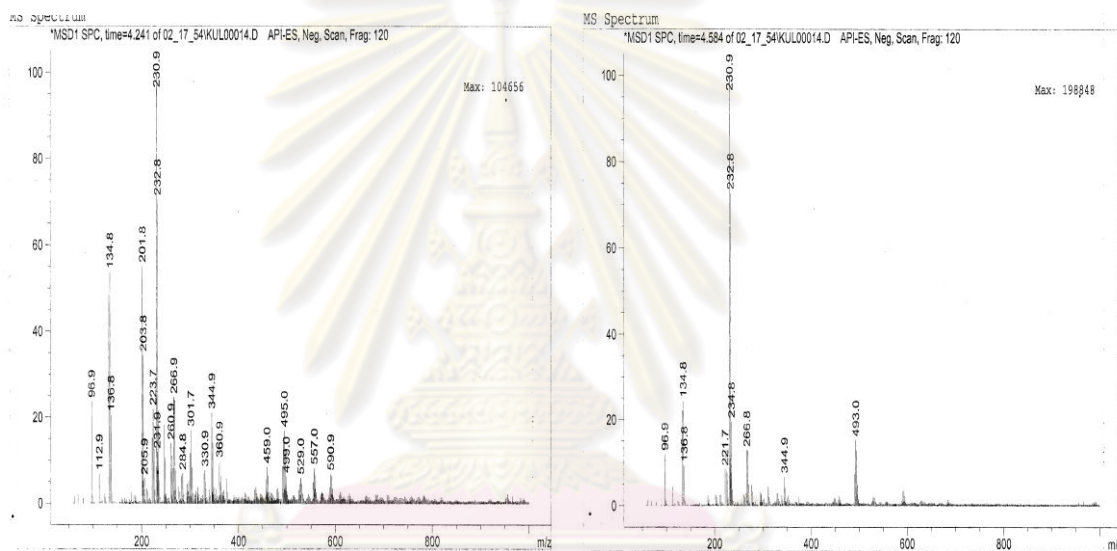
(j)

Figure C.1 (continued).



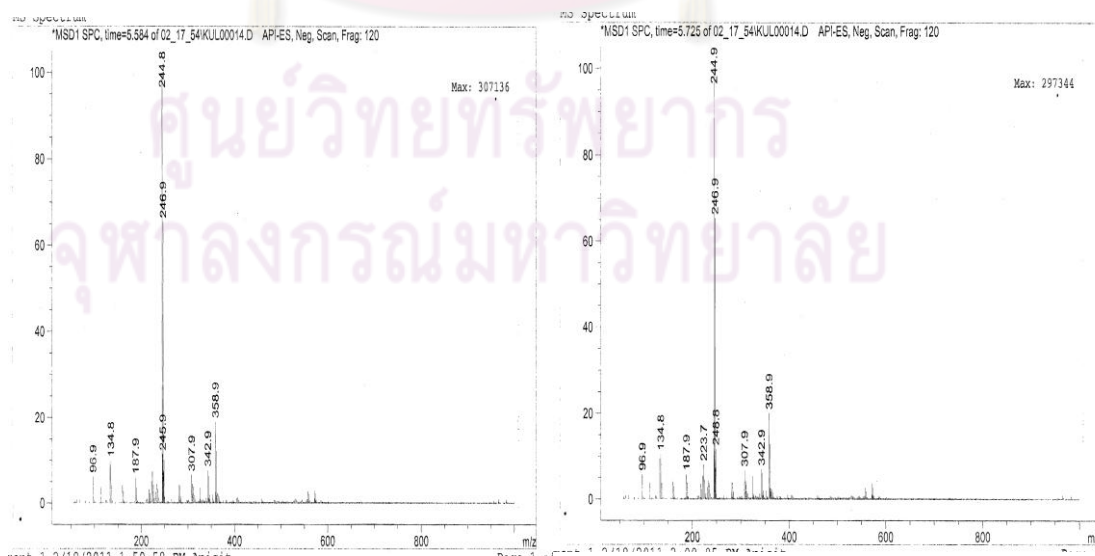
(k)

(l)



(m)

(n)

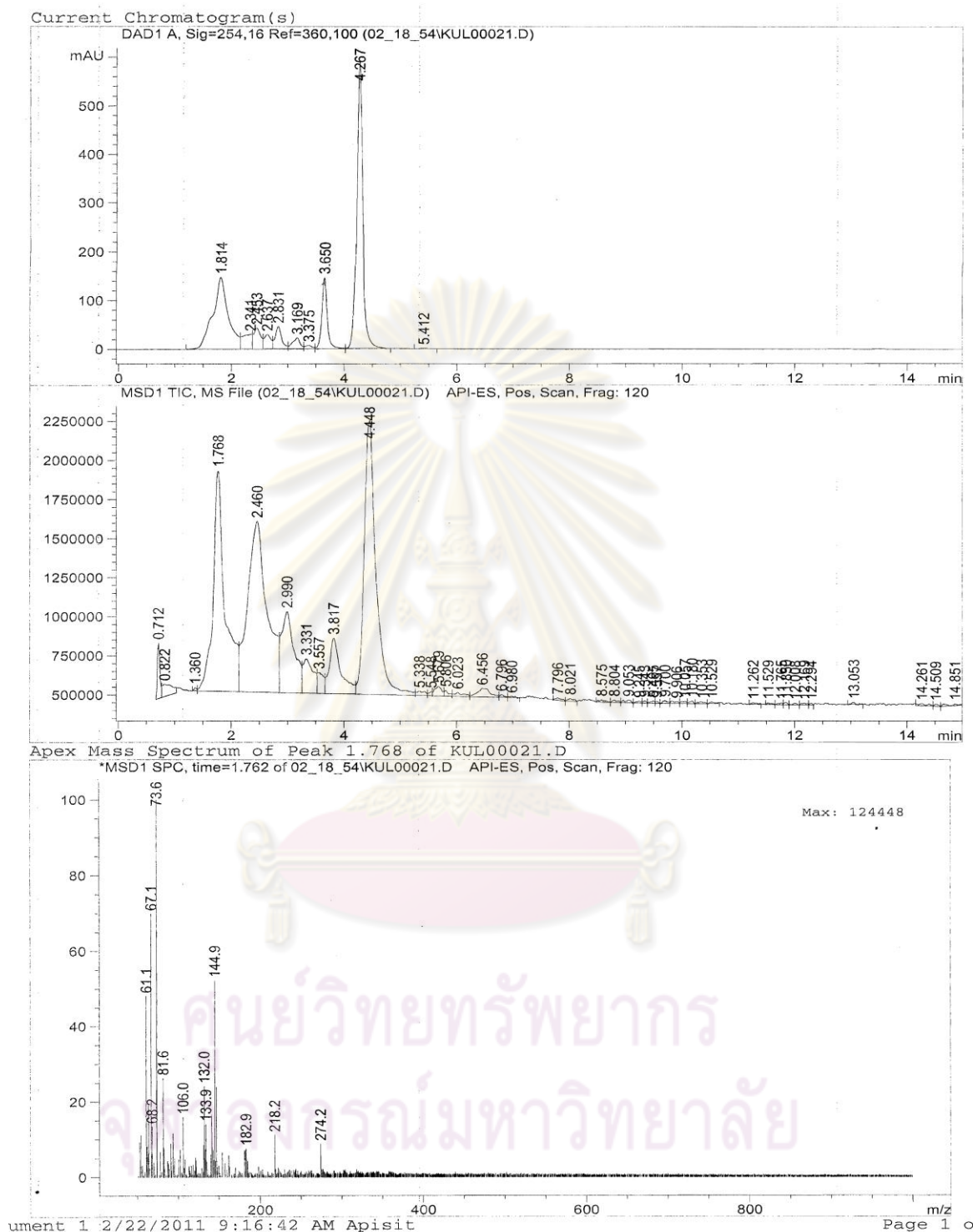


(o)

(p)

Figure C.1 (continued).

C.1.2 pH 7



(a)

Figure C.2 Chromatogram of diuron solution photodegradation at pH7 obtained from UV detector and mass detector are displayed in (a). Mass spectrums were obtained using fragmentator of 120 V at various retention times as shown in (a)-(q).

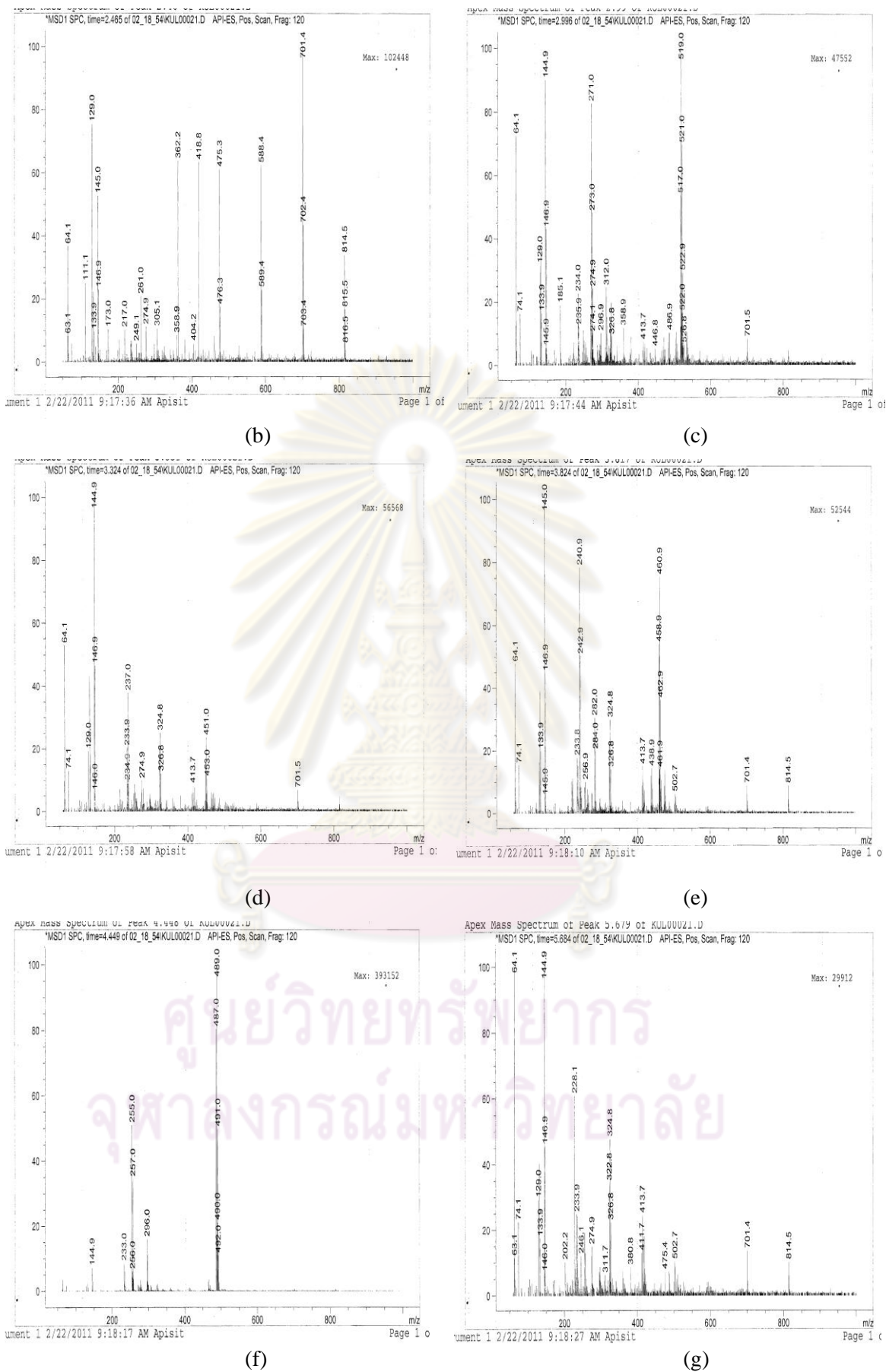
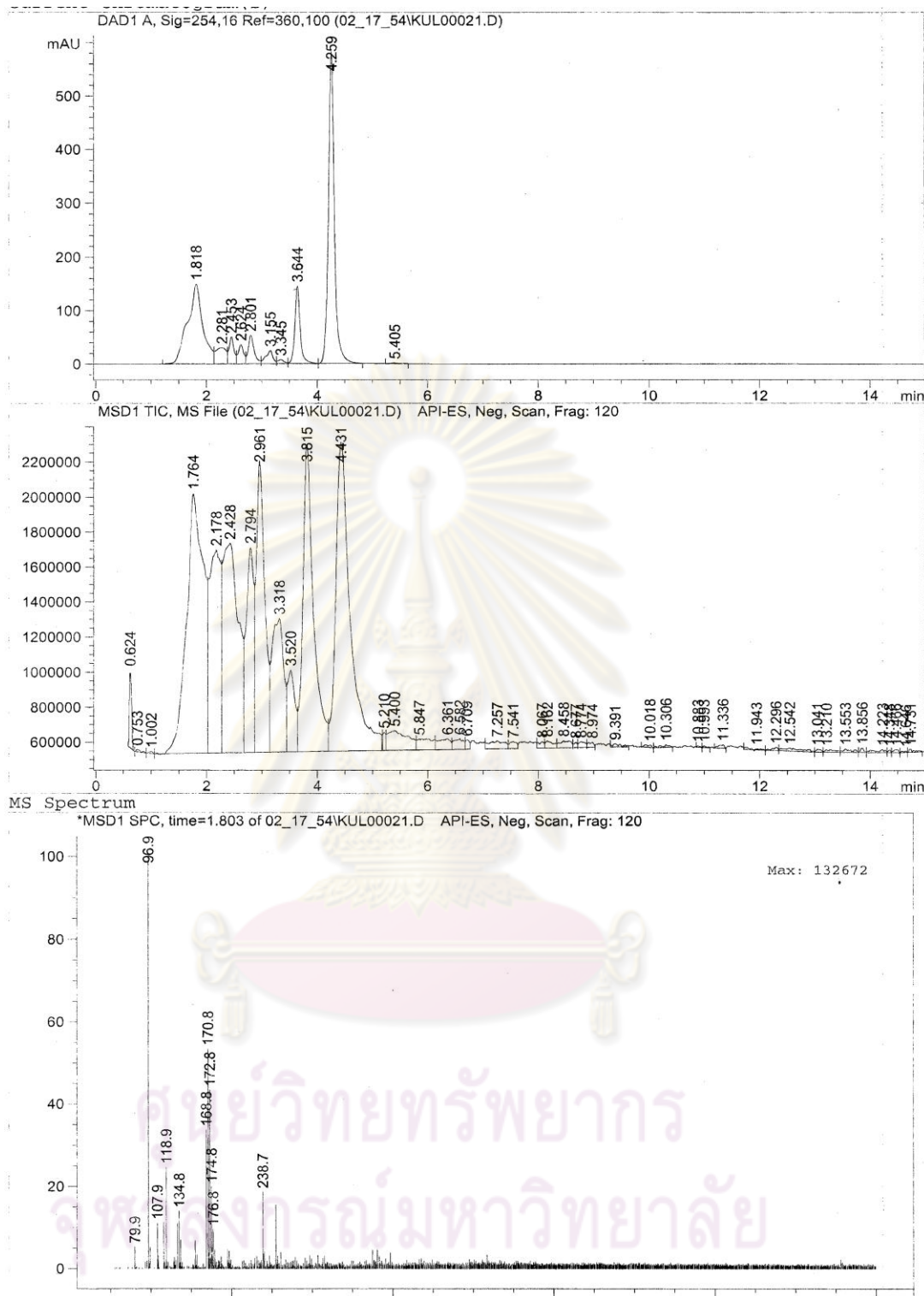
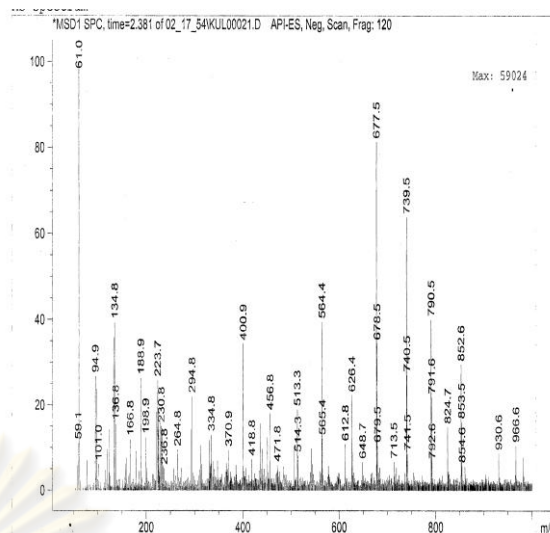
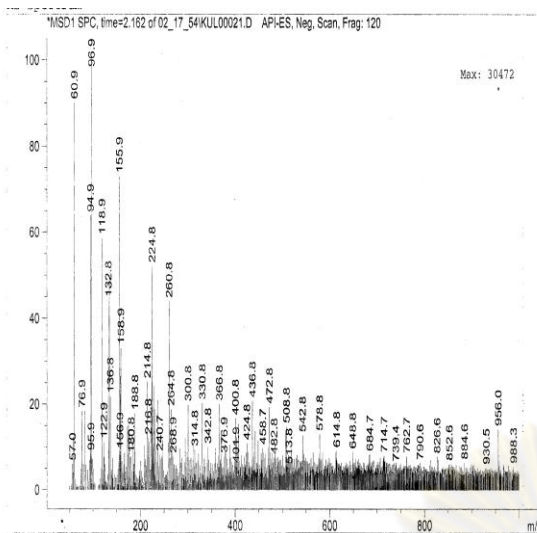


Figure C.2 (continued).



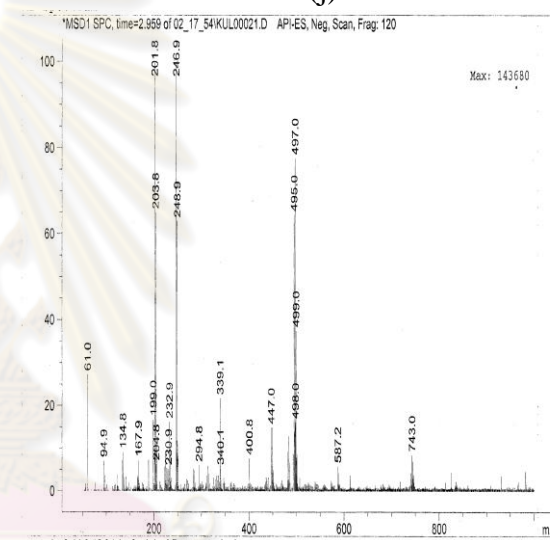
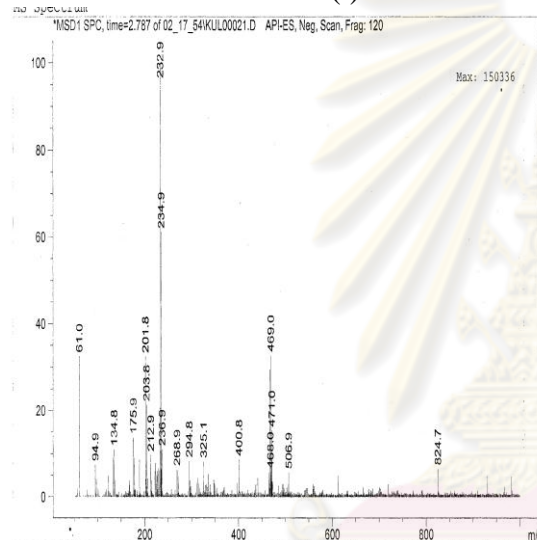
(h)

Figure C.2 (continued).



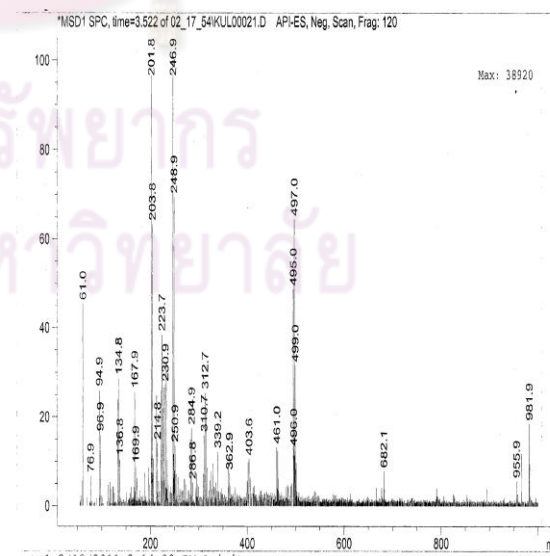
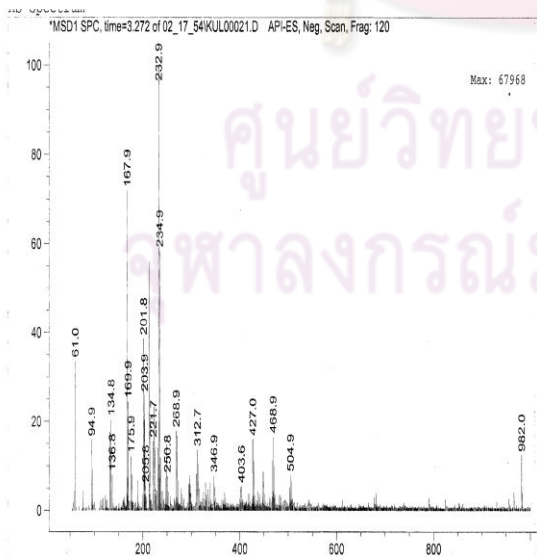
(i)

(j)



(k)

(l)



(m)

(n)

Figure C.2 (continued).

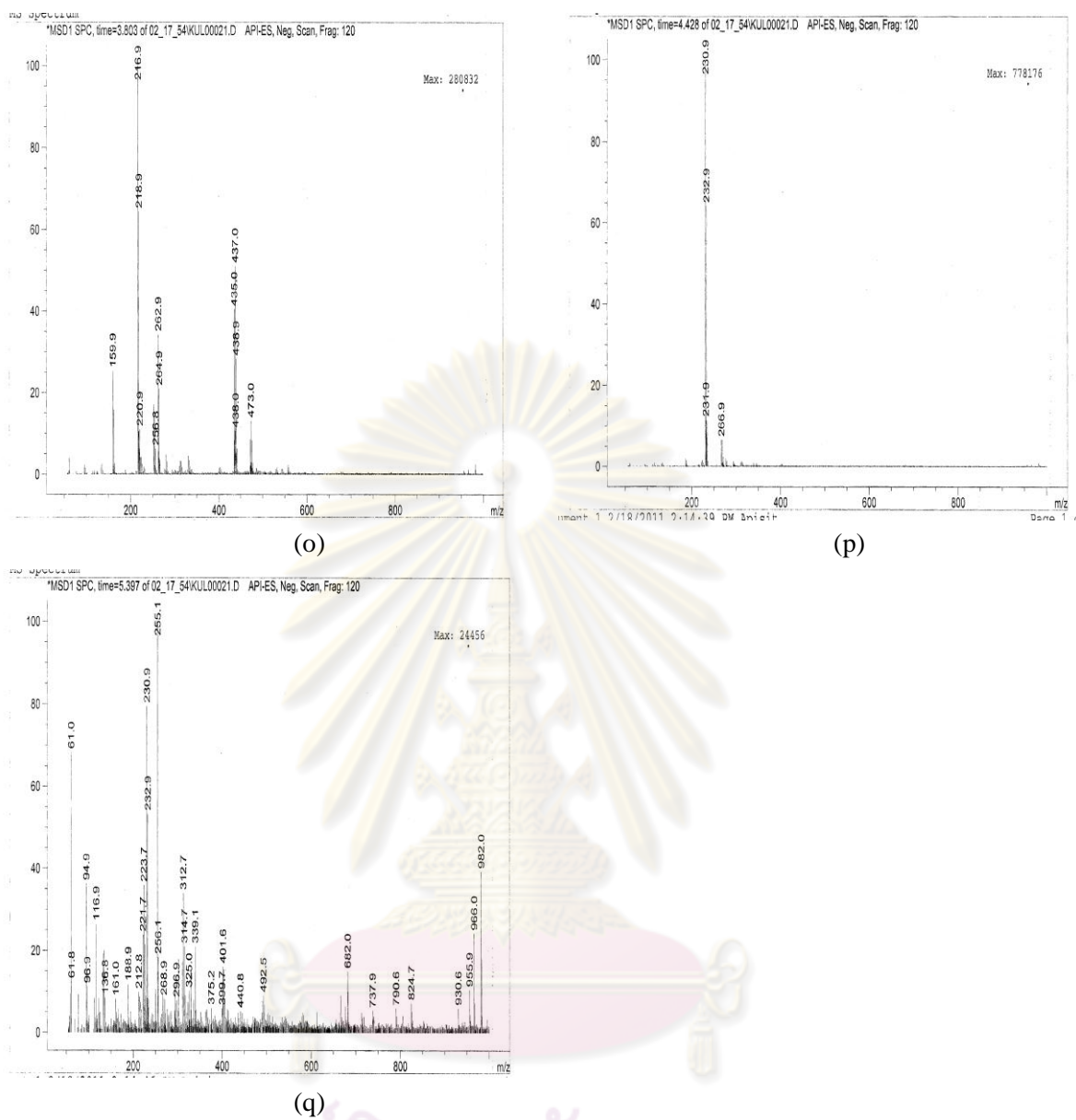


Figure C.2 (continued).

ศูนย์วิทยทรัพยากร
จุฬาลงกรณ์มหาวิทยาลัย

C.1.3 pH10

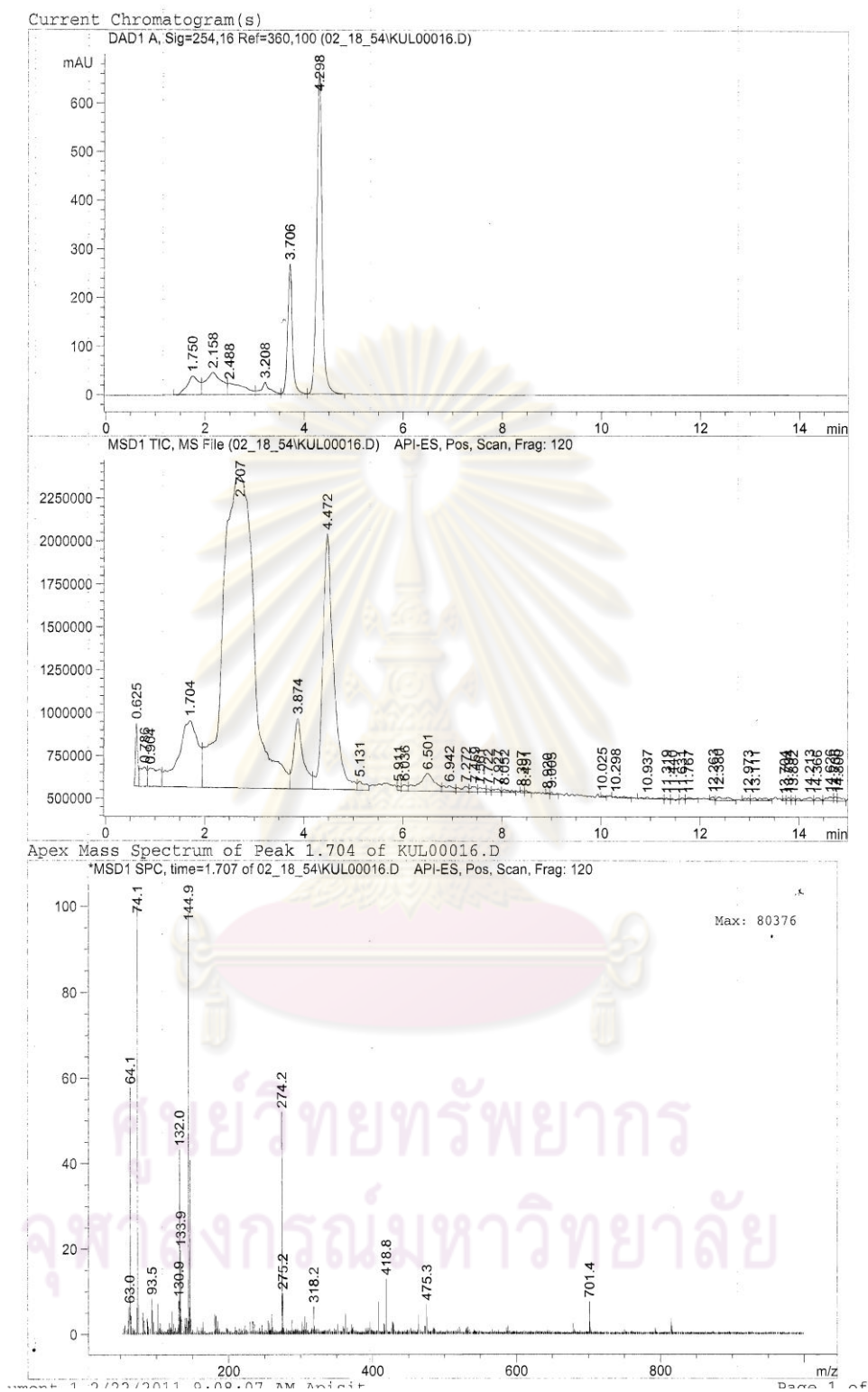


Figure C.3 Chromatogram of diuron solution photodegradation at pH10 obtained from UV detector and mass detector are displayed in (a). Mass spectrums were obtained using fragmentator of 120 V at various retention times as shown in (a)-(n).

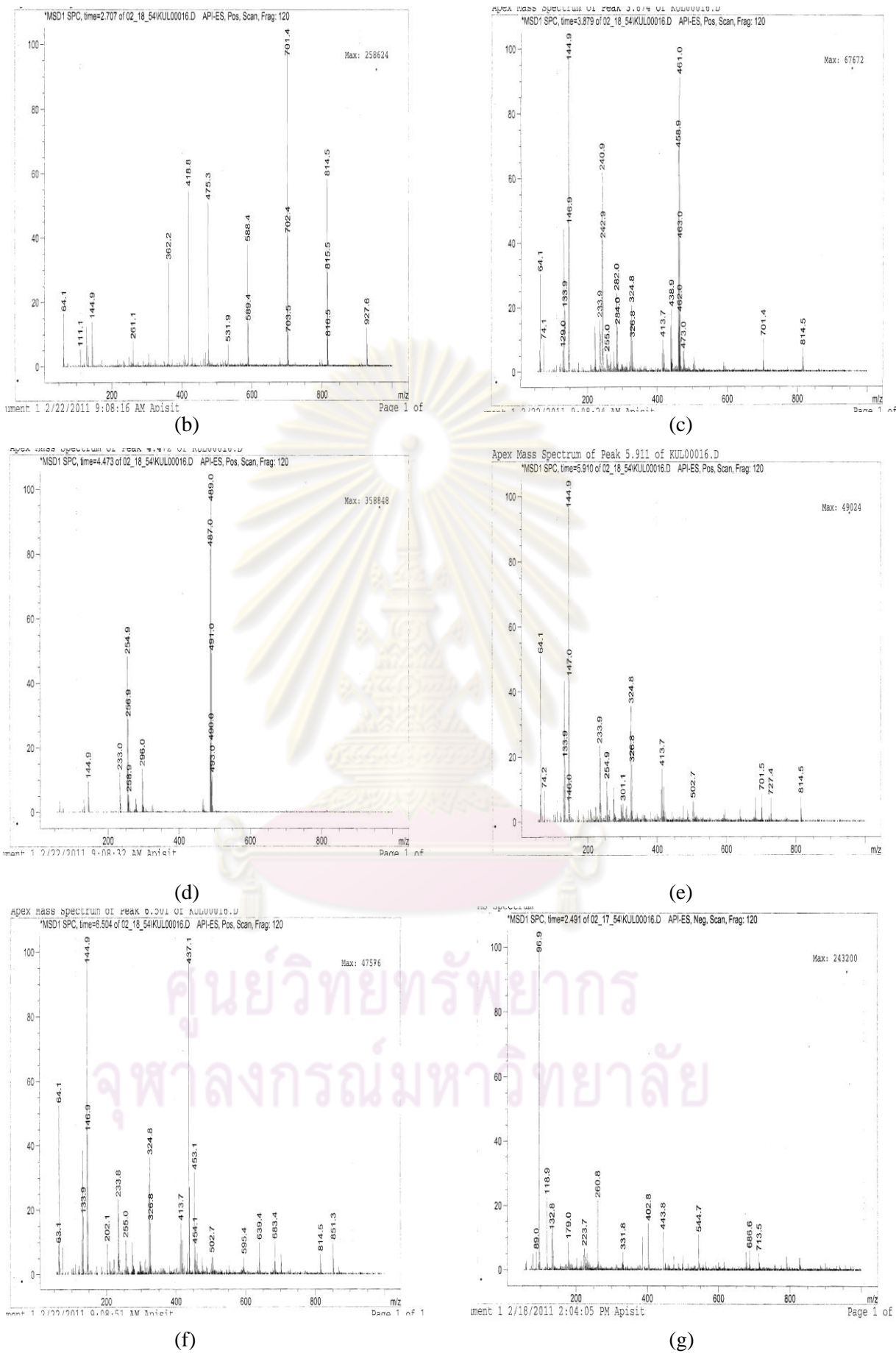
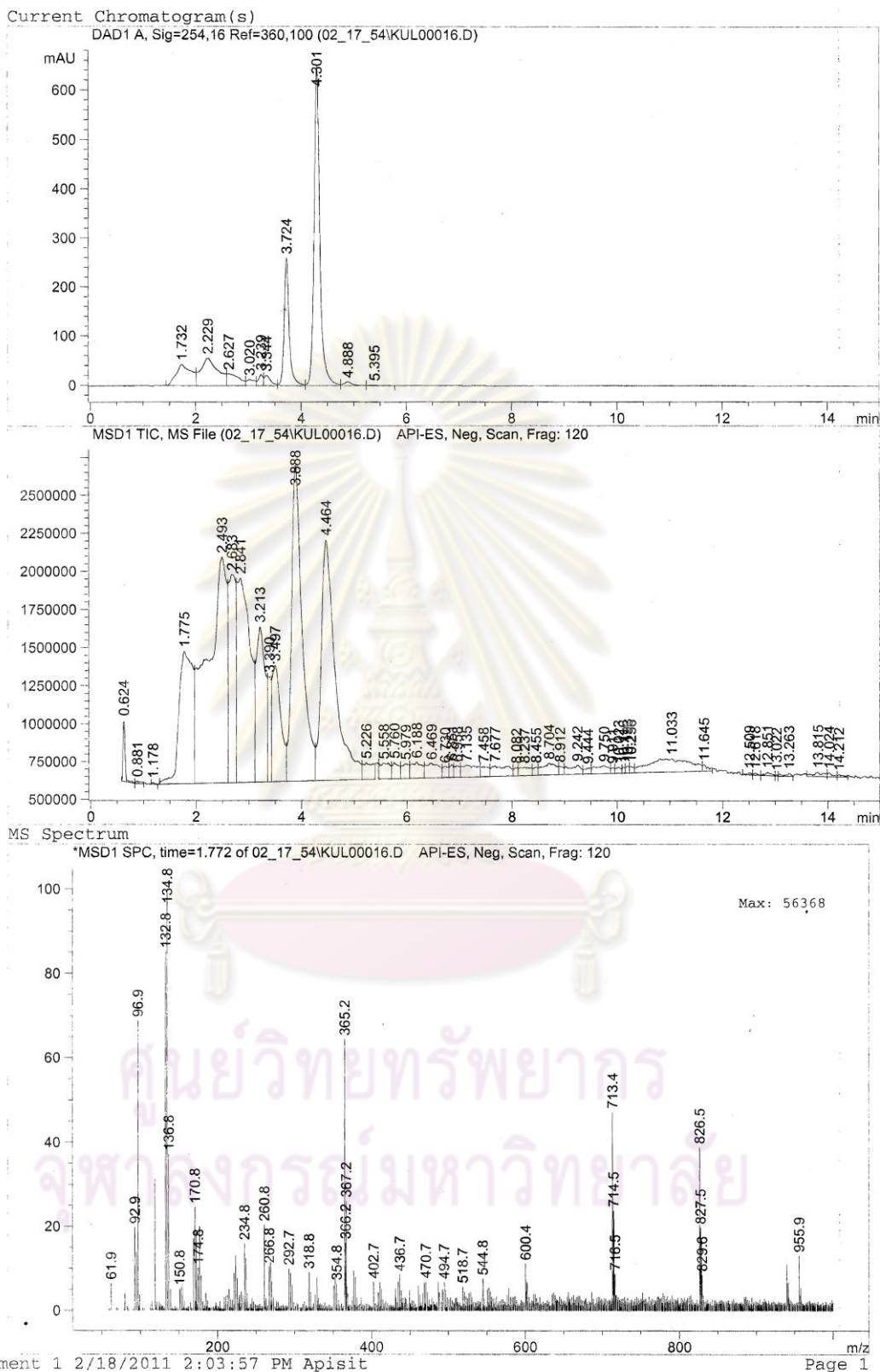
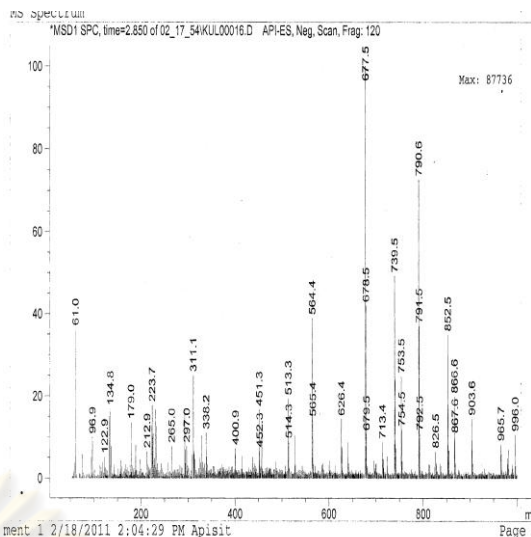
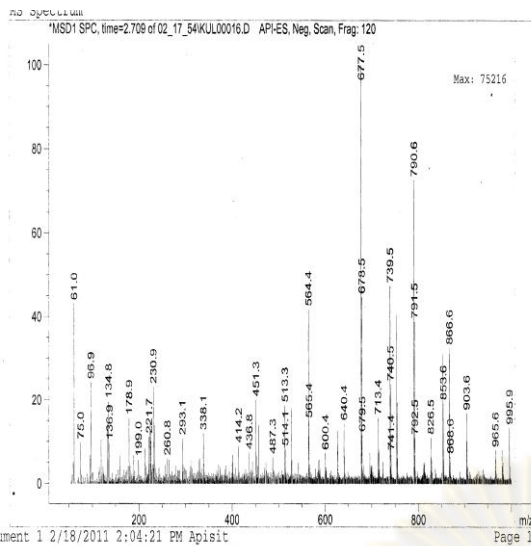


Figure C.3 (continued).



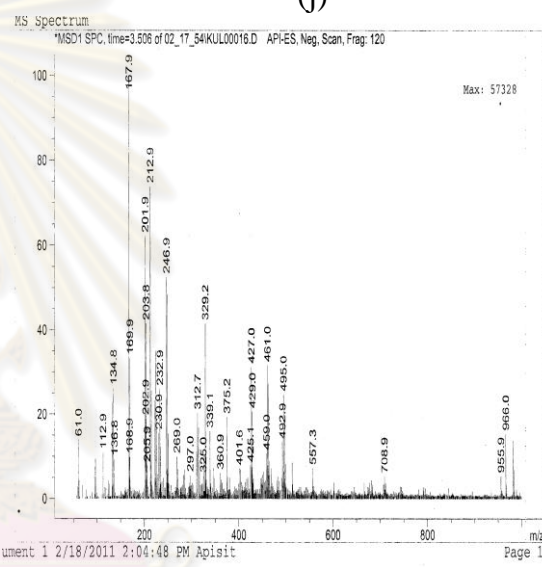
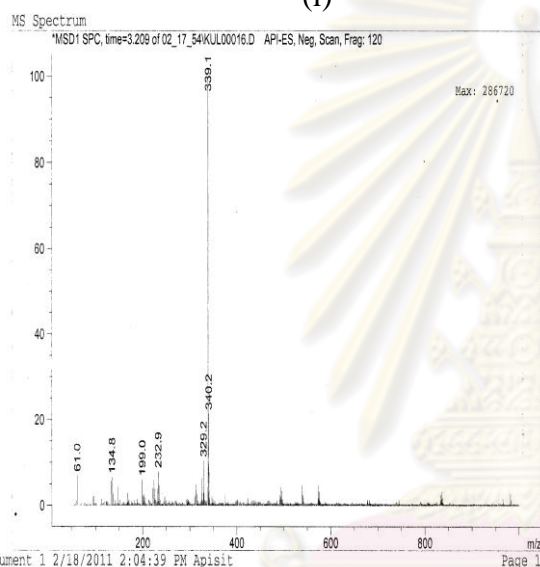
(h)

Figure C.3 (continued).



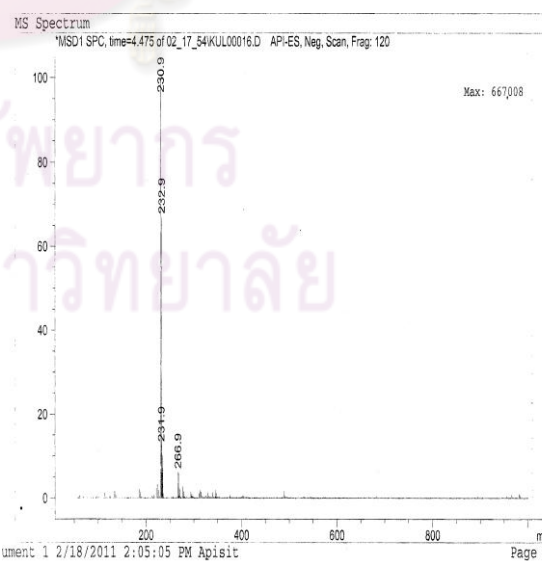
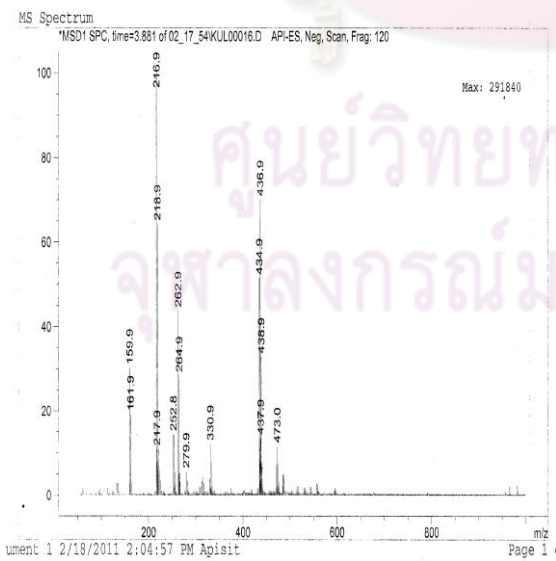
(i)

(j)



(k)

(l)



(m)

(n)

Figure C.3 (continued).

C.1.4 UV-C

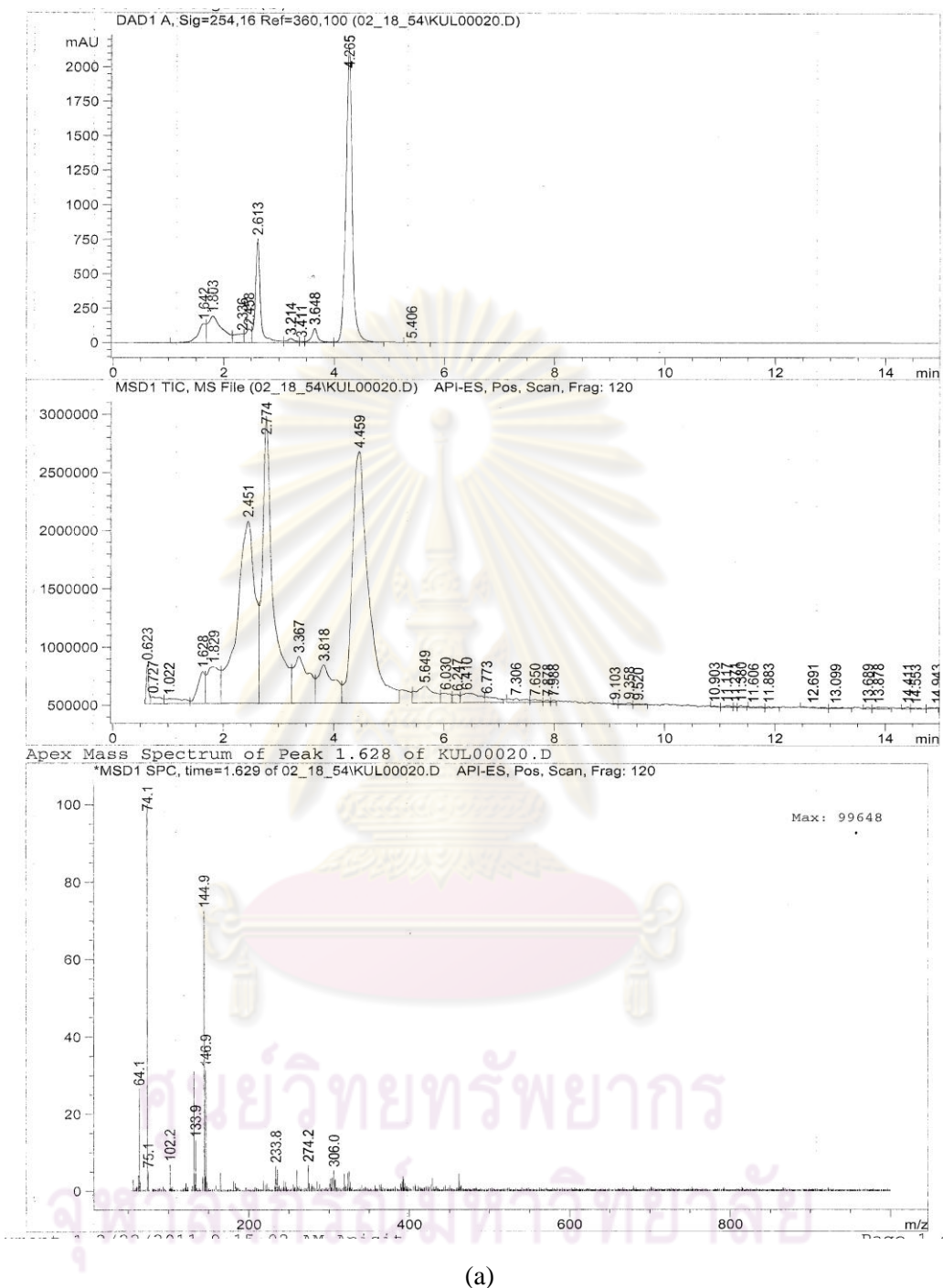
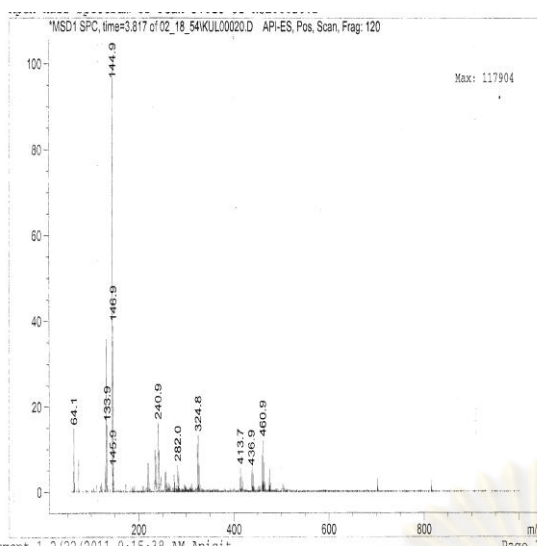
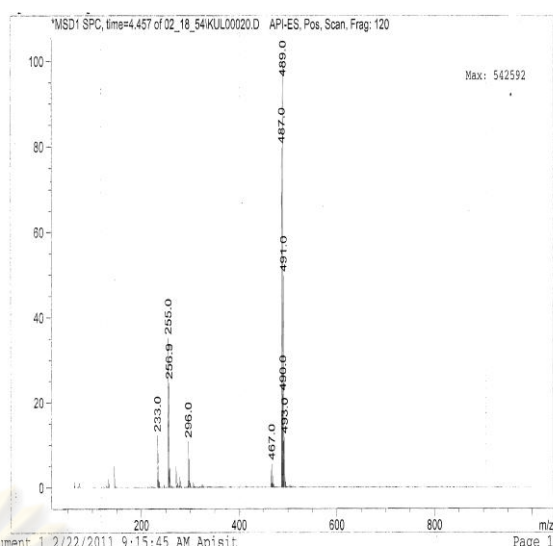


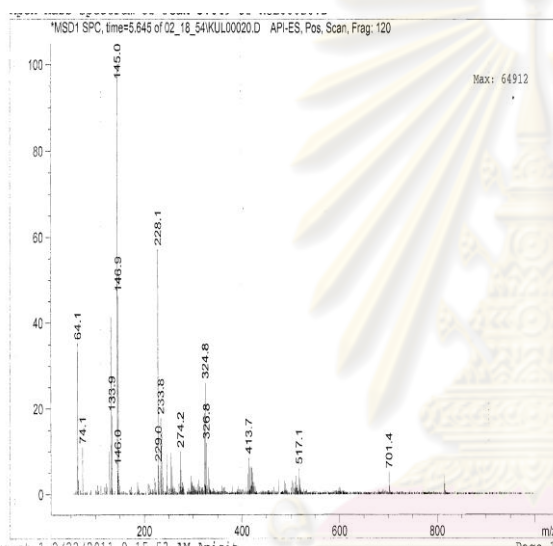
Figure C.4 Chromatogram of diuron solution photodegradation by UV-C obtained from UV detector and mass detector are displayed in (a). Mass spectrums were obtained using fragmentator of 120 V at various retention times as shown in (a)-(n).



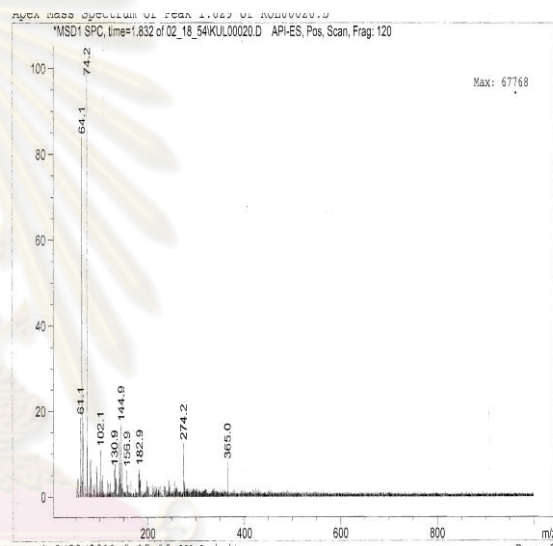
(b)



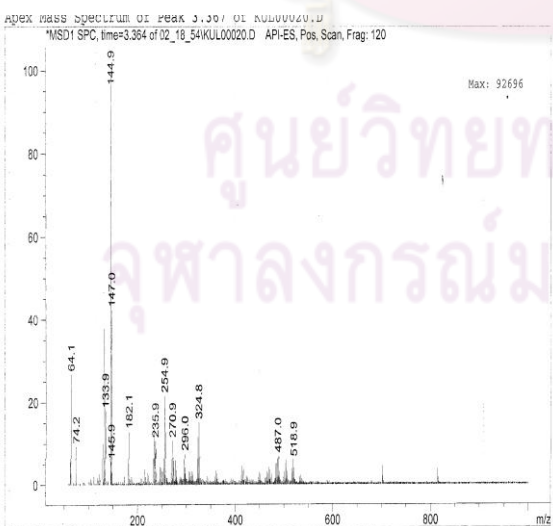
(c)



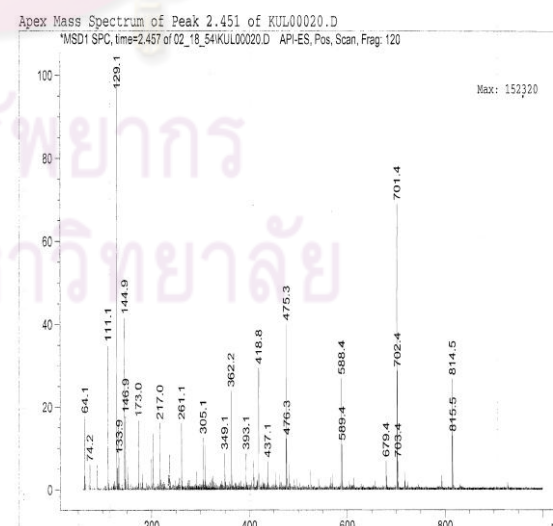
(d)



(e)

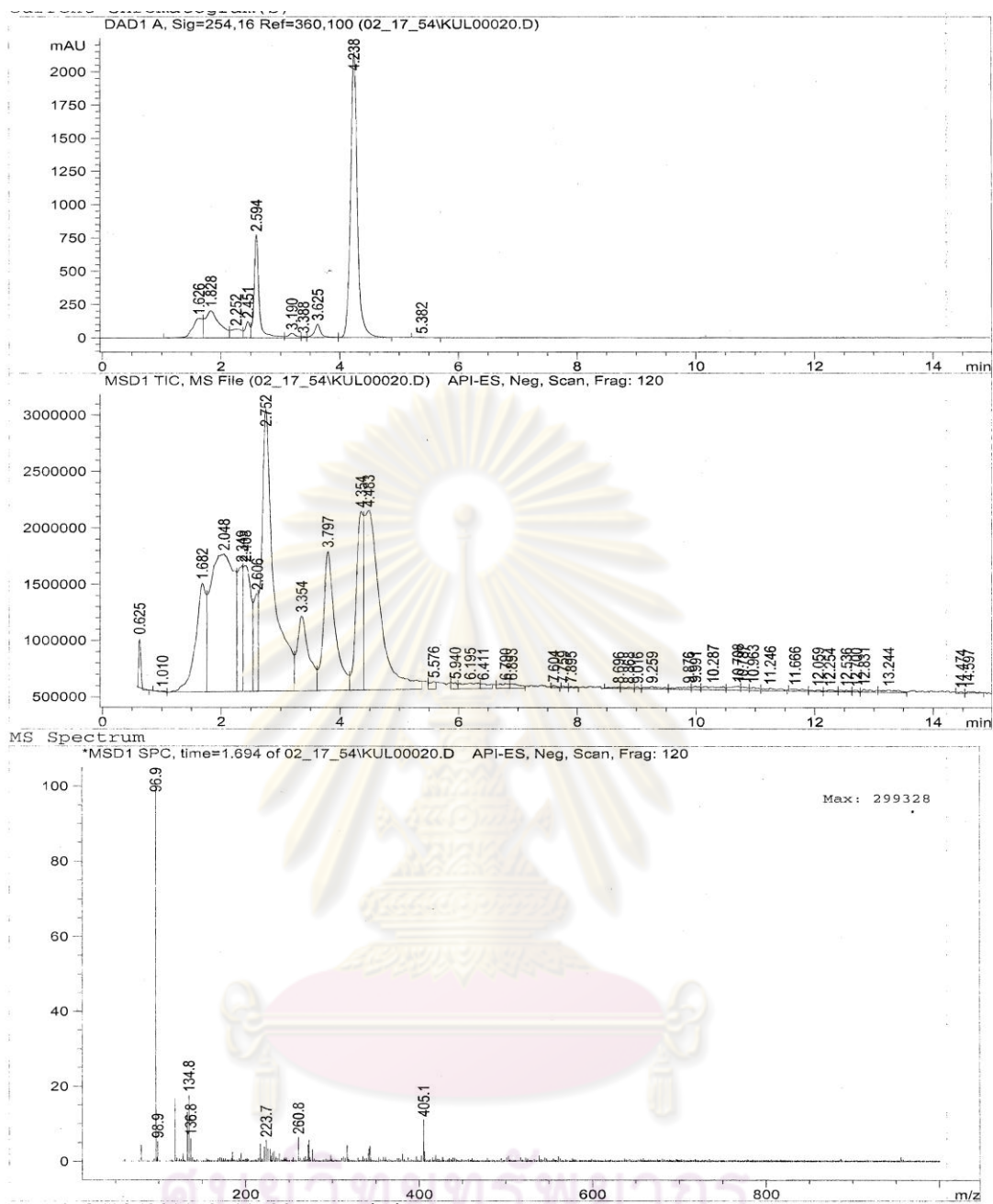


(f)



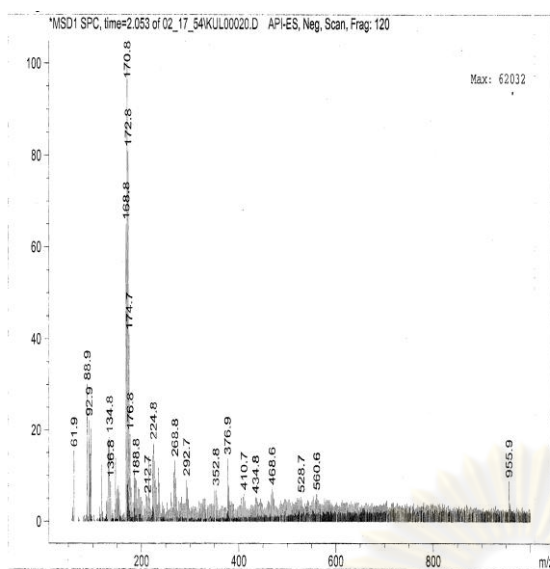
(g)

Figure C.4 (continued).

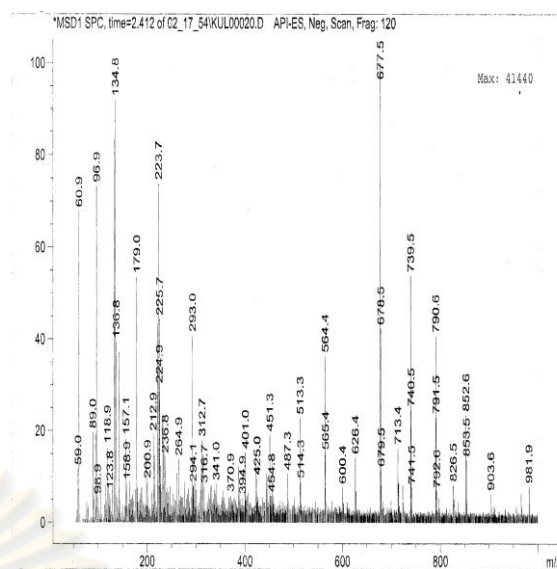


(h)

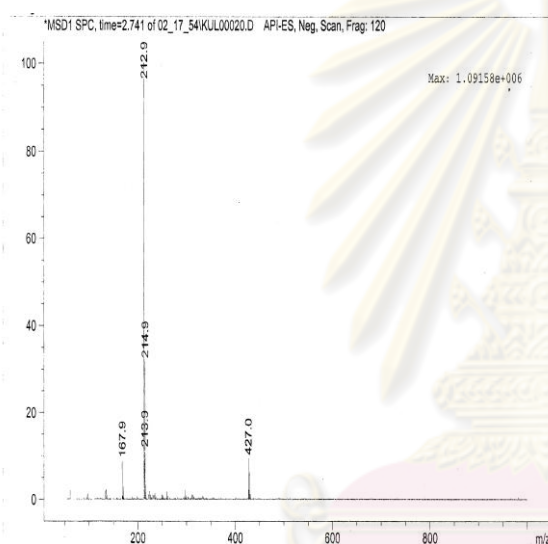
Figure C.4 (continued).



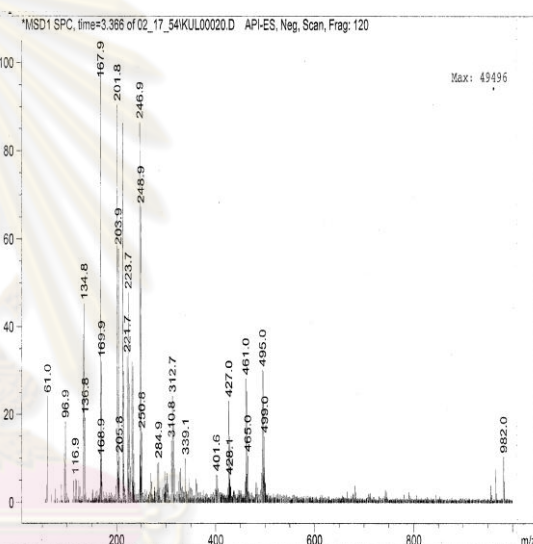
(i)



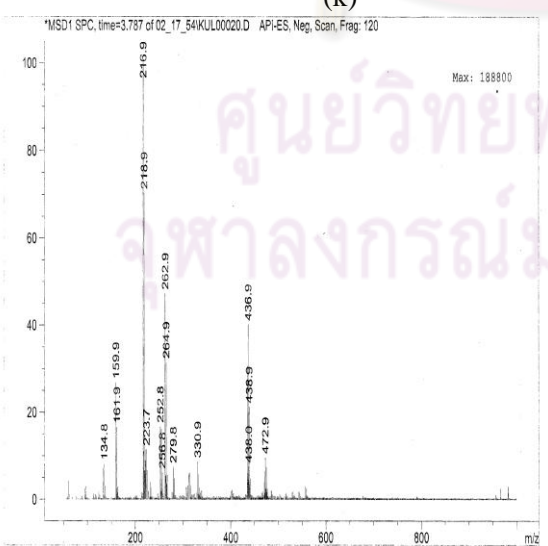
(j)



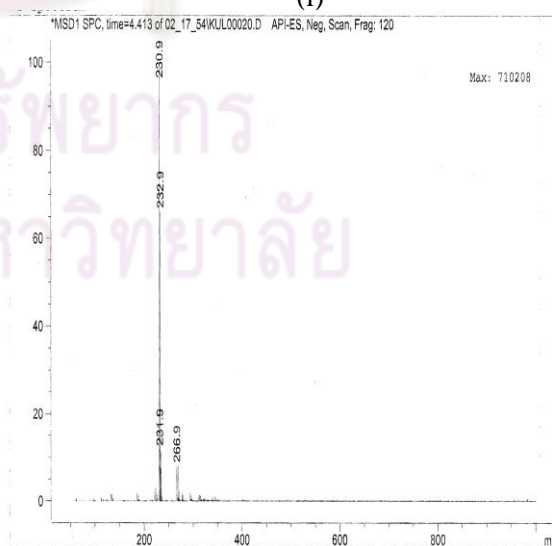
(k)



(l)



(m)



(n)

Figure C.4 (continued).

C.3 Mass spectrum of diuron solution from photodegradation by TiO₂.

C.3.1 pH 3

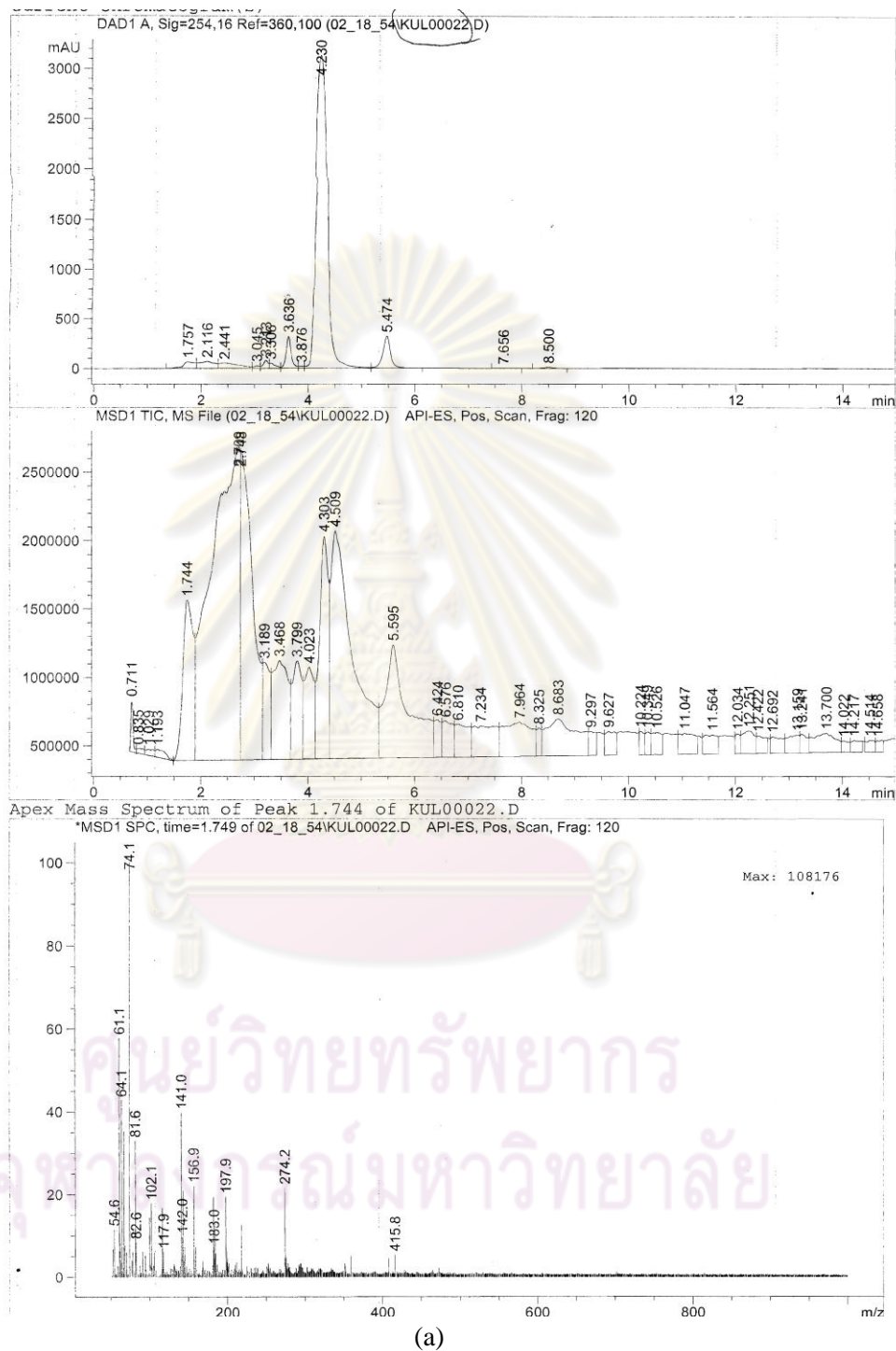


Figure C.5 Chromatogram of diuron solution photodegradation at pH3 obtained from UV detector and mass detector are displayed in (a). Mass spectrums were obtained using fragmentator of 120 V at various retention times as shown in (a)-(p).

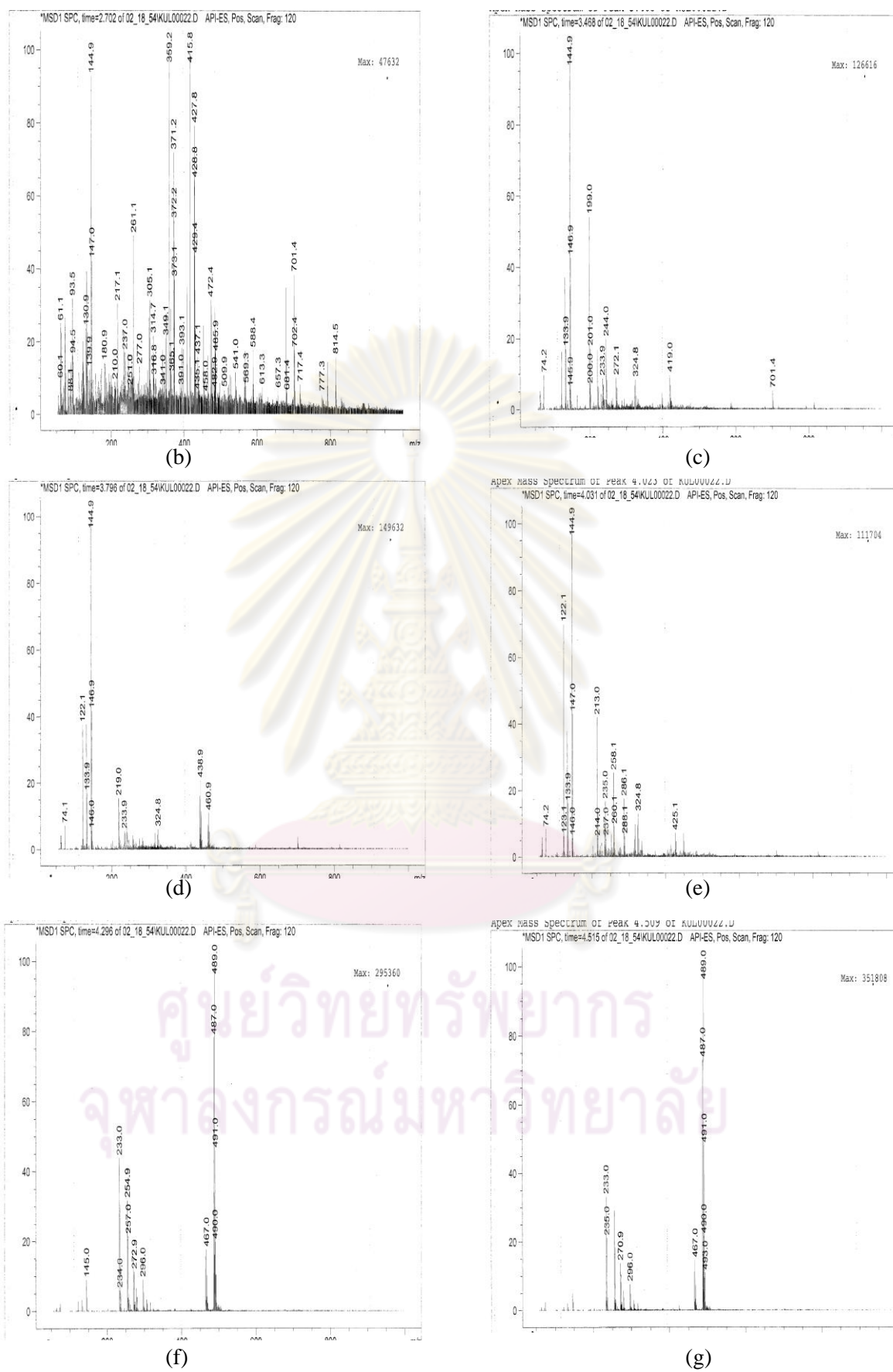
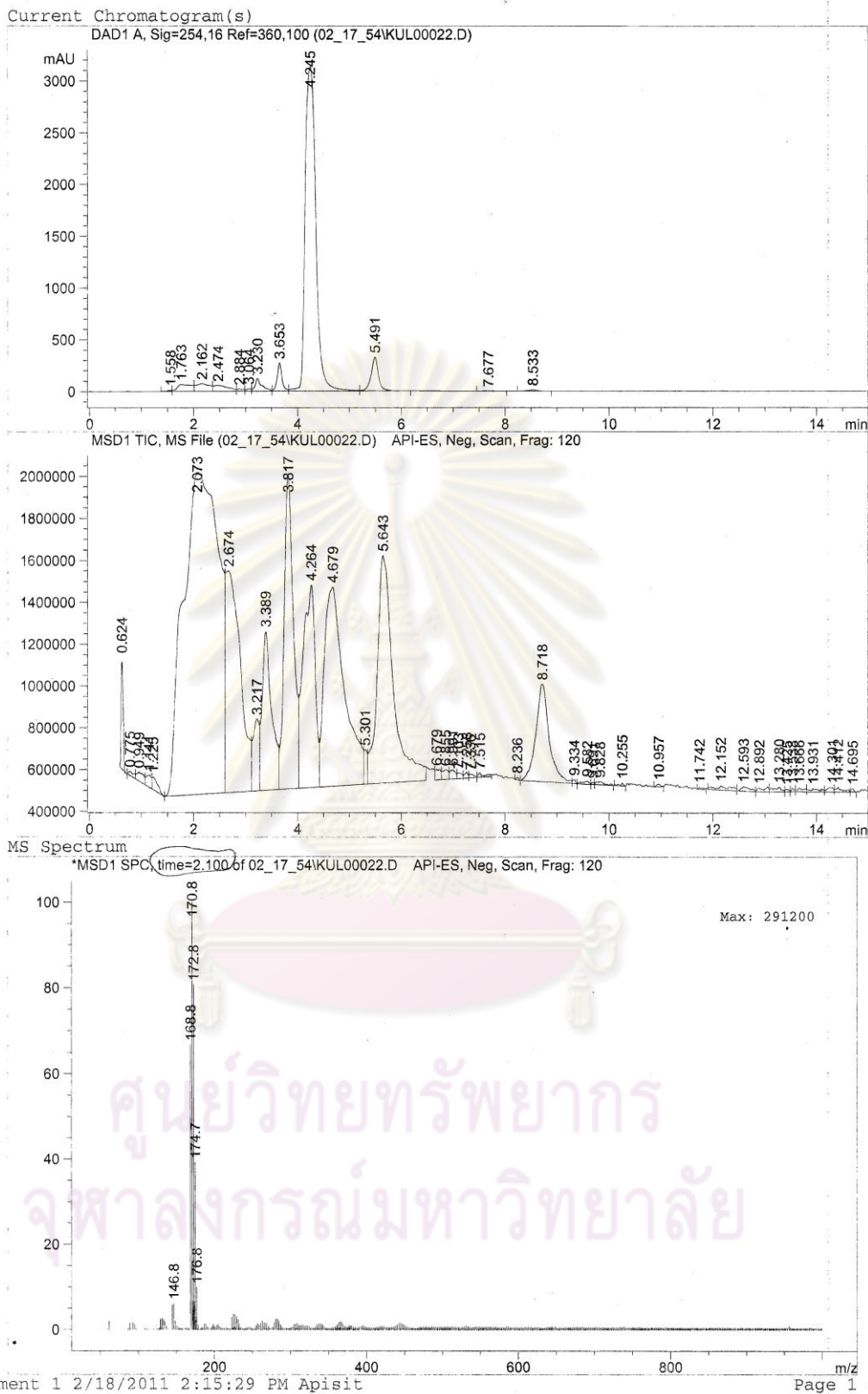


Figure C.5 (continued).



(h)

Figure C.5 (continued).

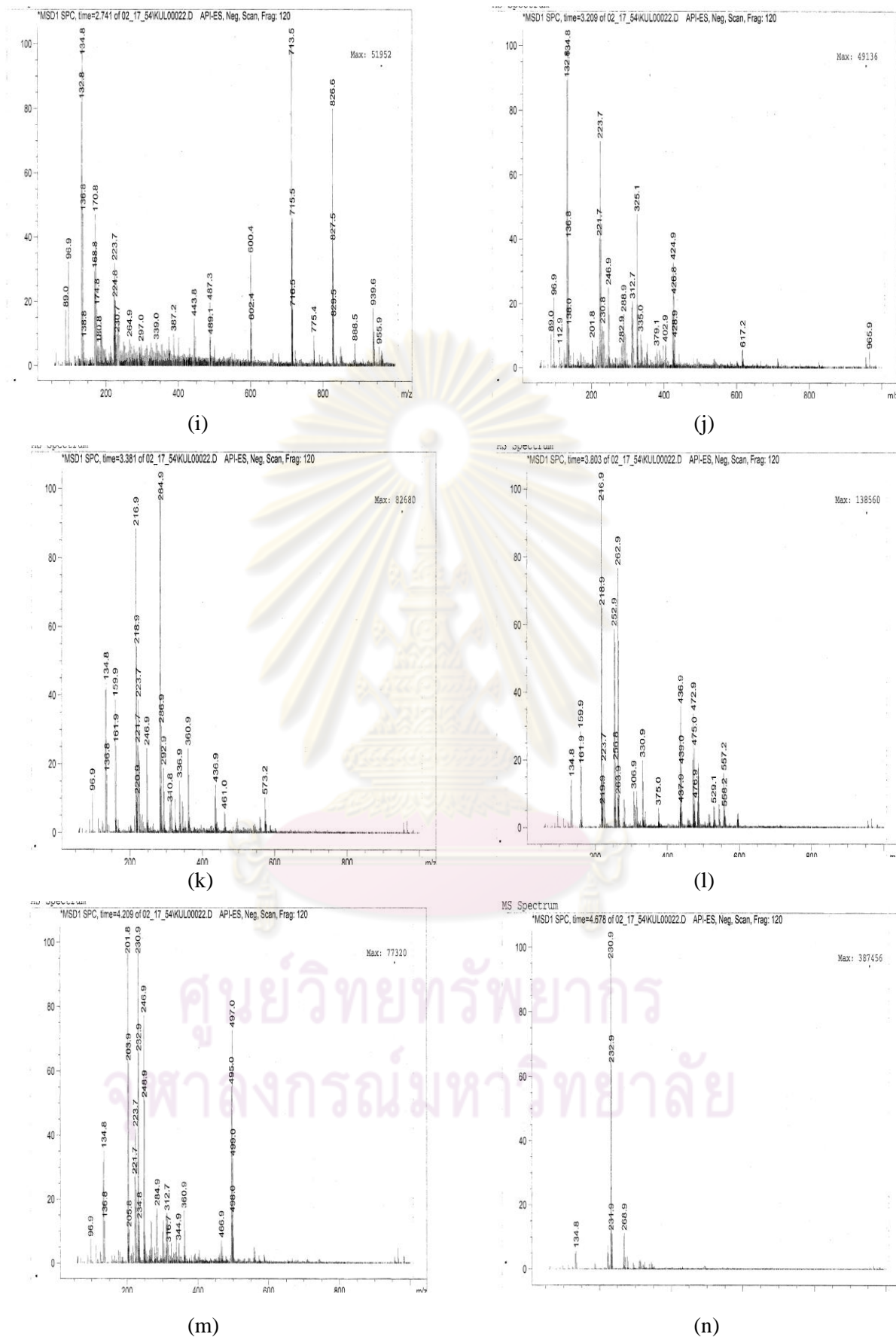


Figure C.5 (continued).

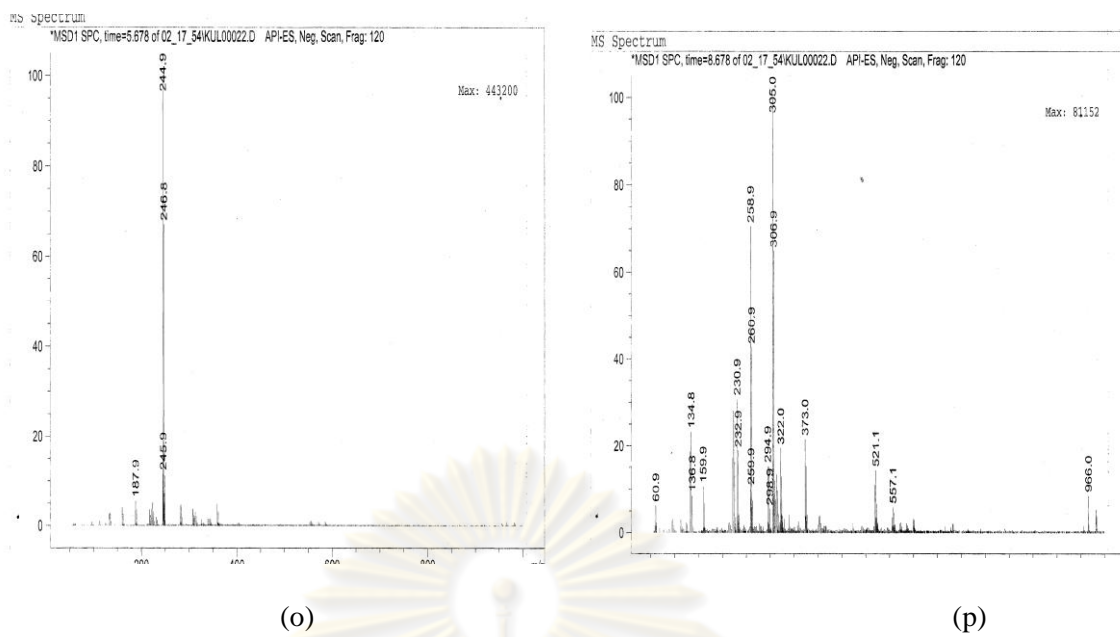
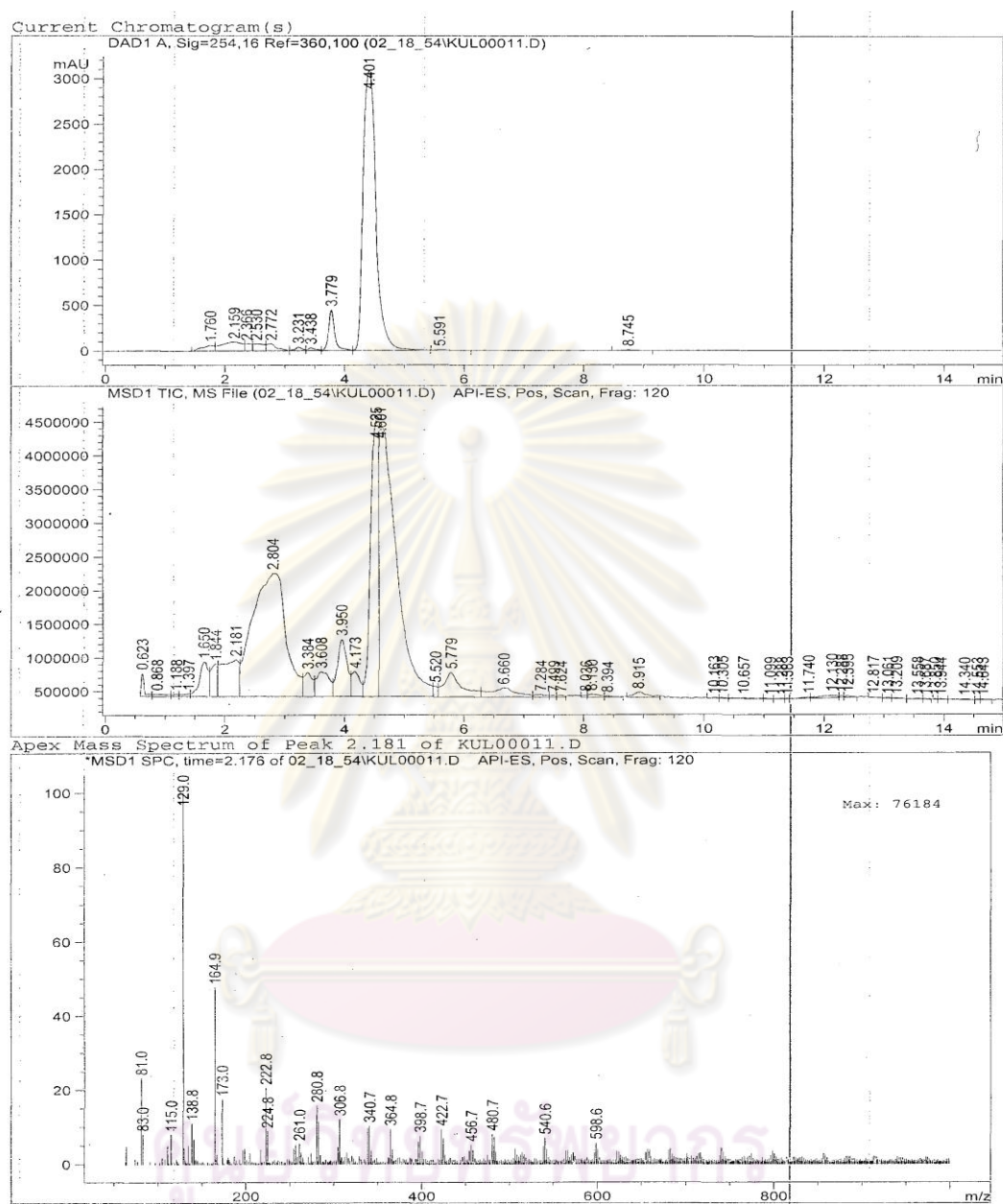


Figure C.5 (continued).

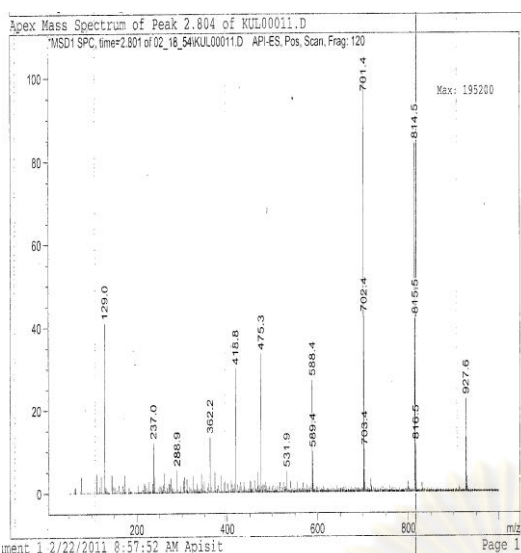
ศูนย์วิทยทรัพยากร
จุฬาลงกรณ์มหาวิทยาลัย

C.3.2 pH 7

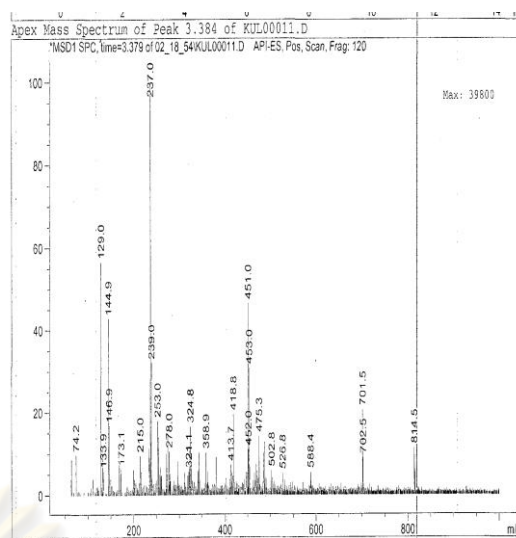


จุฬาลงกรณ์มหาวิทยาลัย (a)

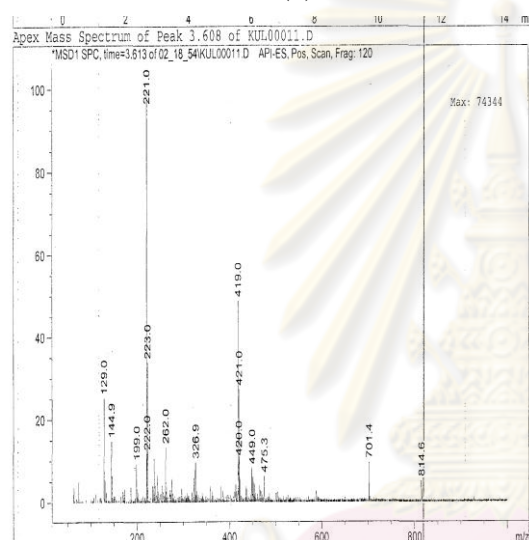
Figure C.6 Chromatogram of diuron solution photodegradation at pH7 obtained from UV detector and mass detector are displayed in (a). Mass spectrums were obtained using fragmentator of 120 V at various retention times as shown in (a)-(r).



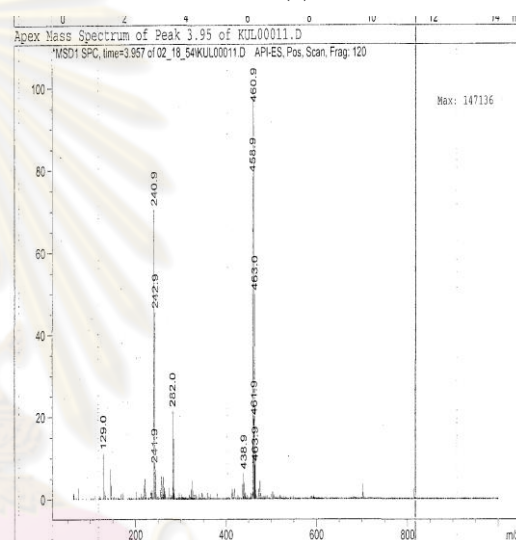
(b)



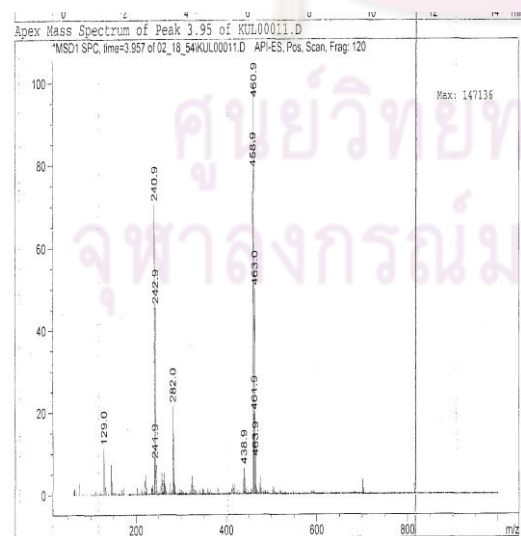
(c)



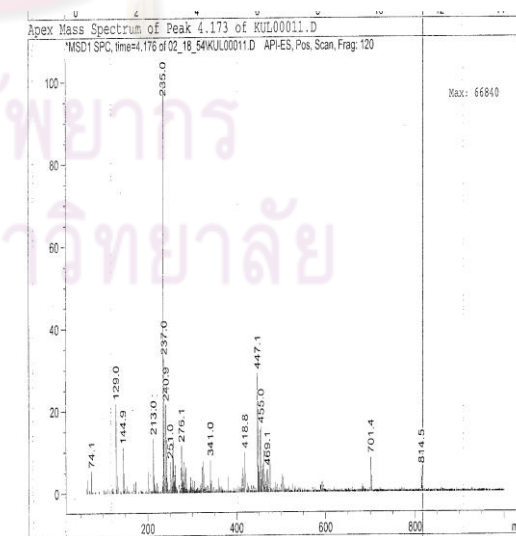
(d)



(e)

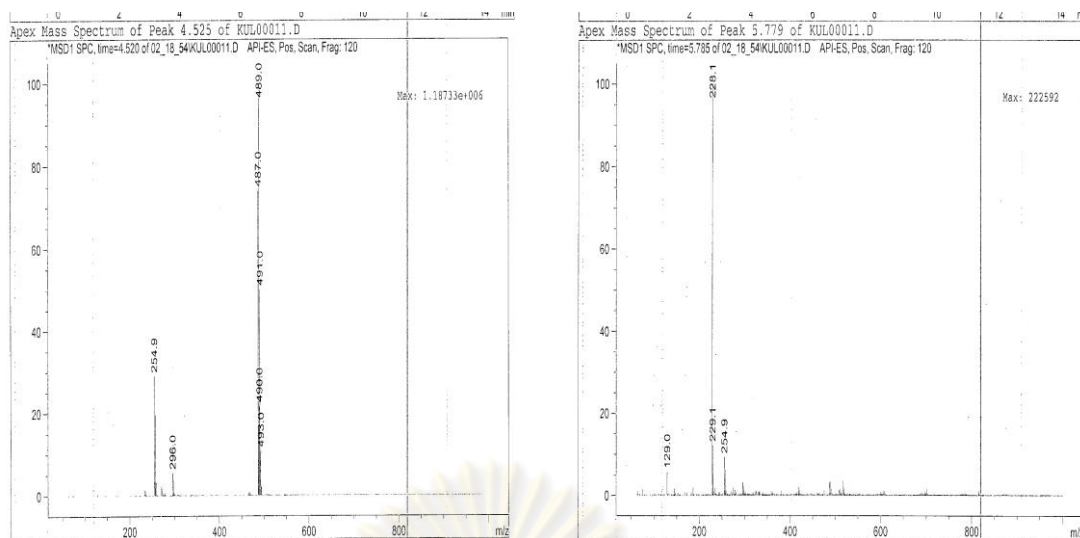


(f)



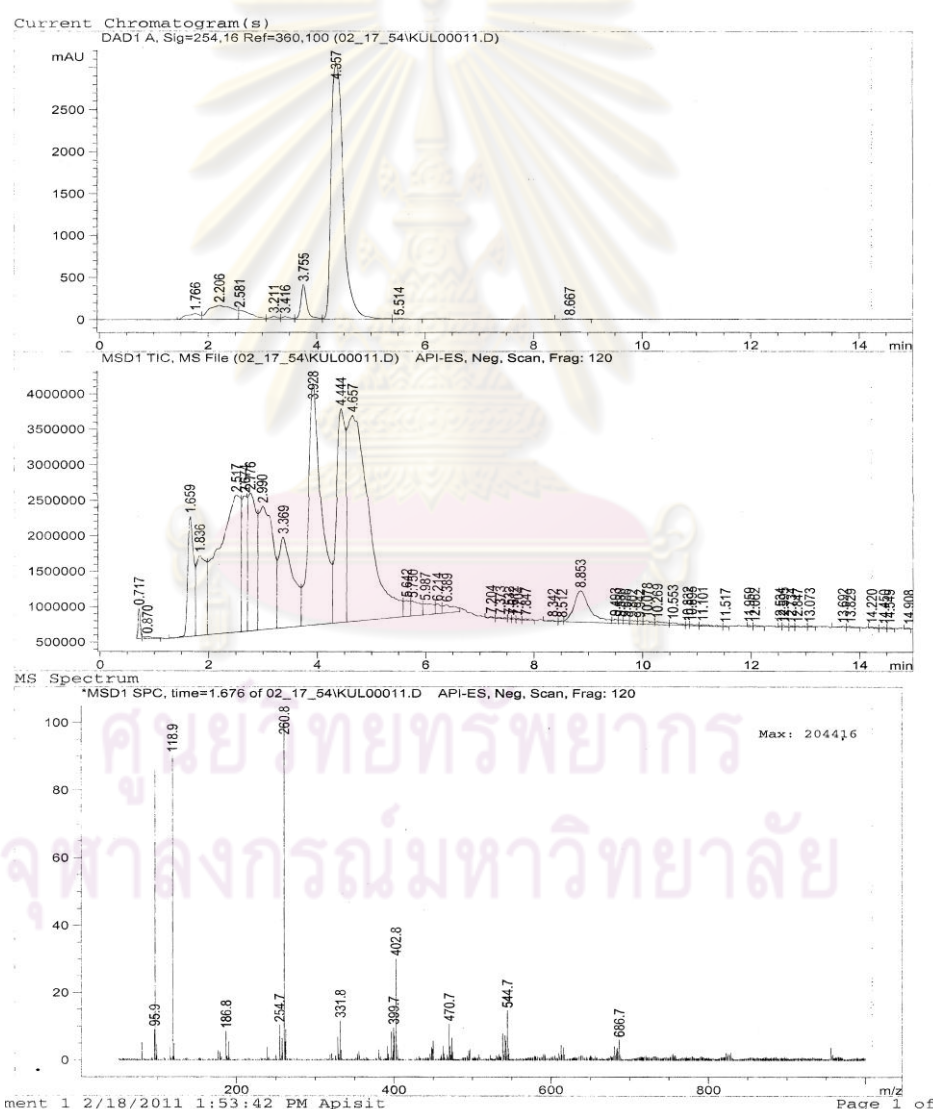
(g)

Figure C.6 (continued).



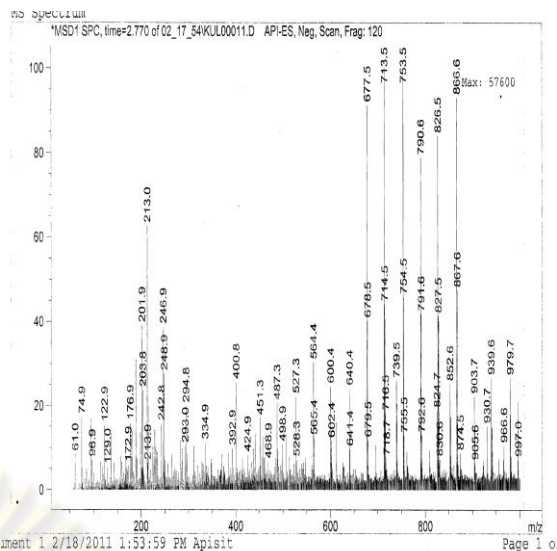
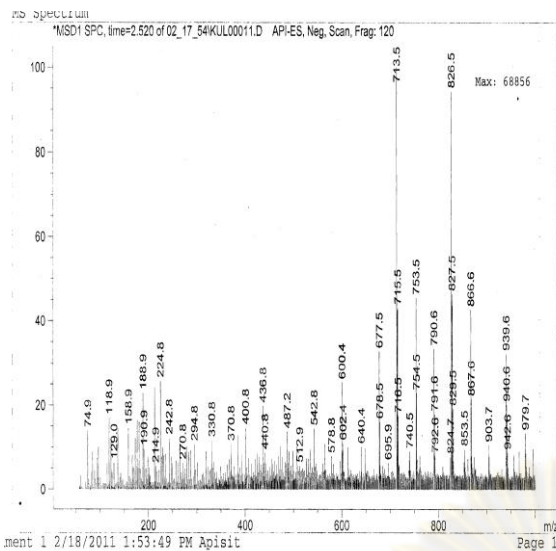
(h)

(i)



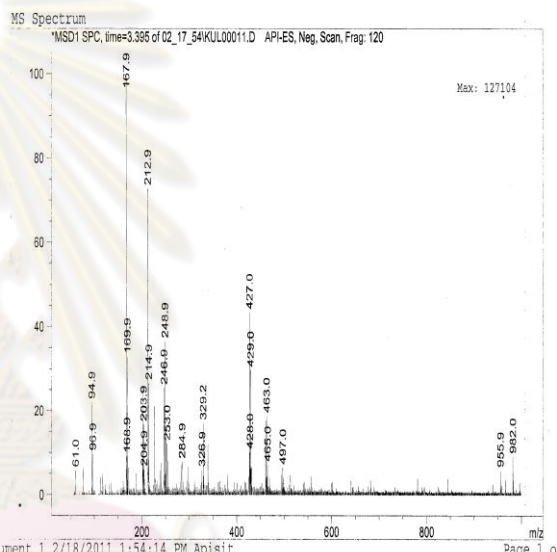
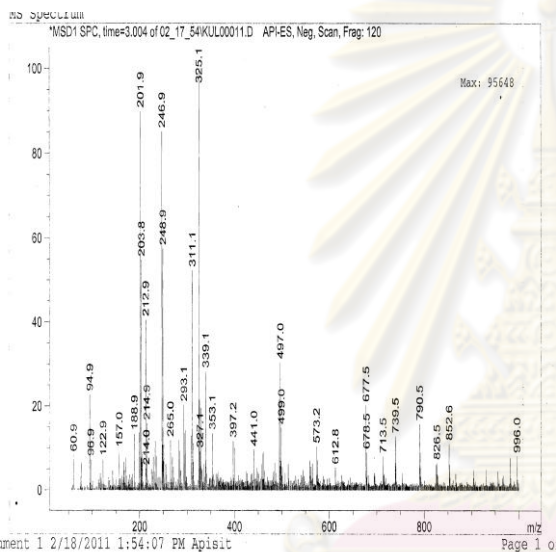
(j)

Figure C.6 (continued).



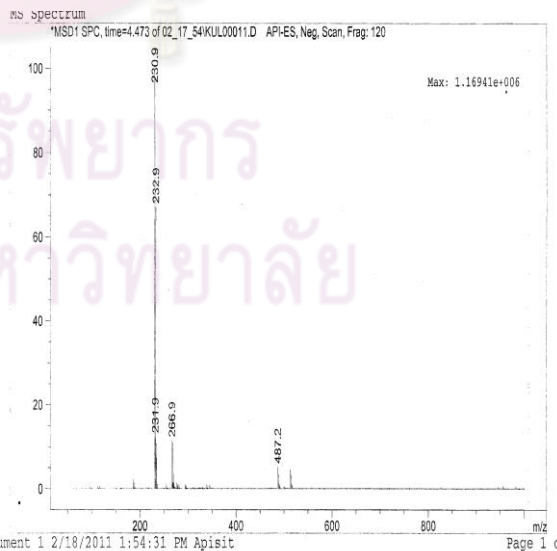
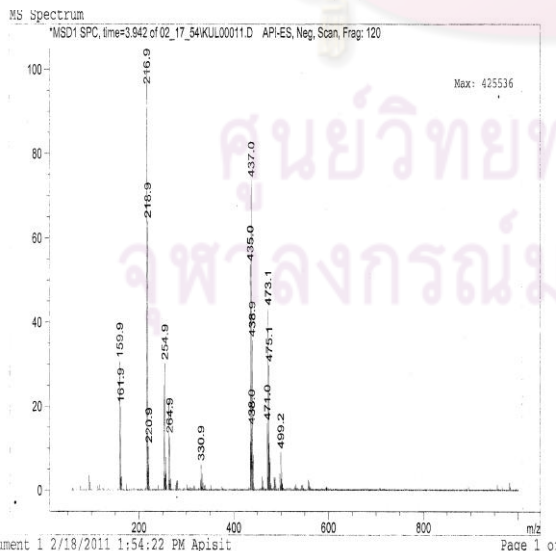
(k)

(l)



(m)

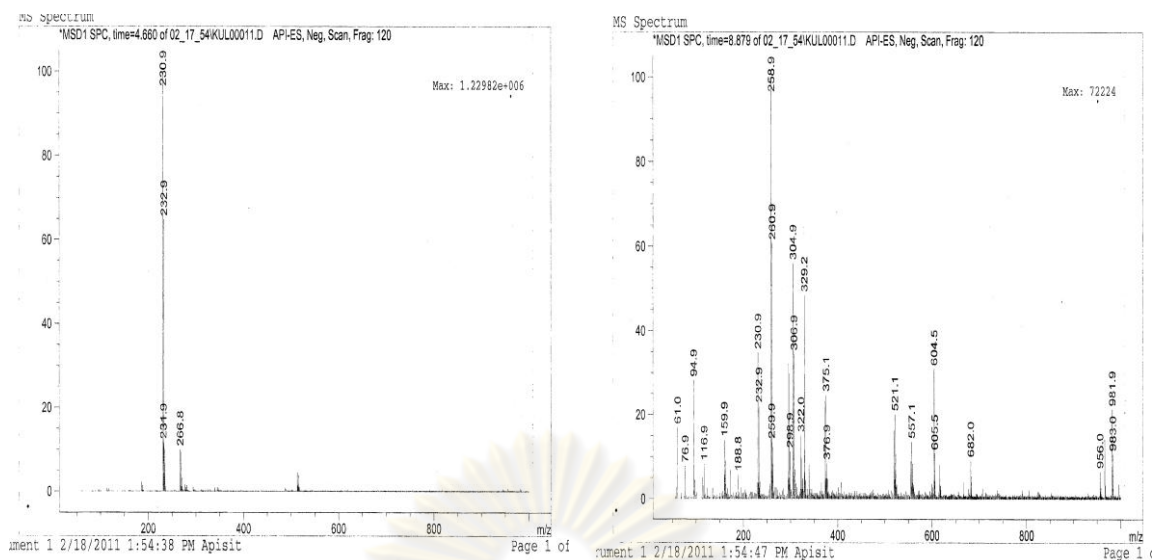
(n)



(o)

(p)

Figure C.6 (continued).



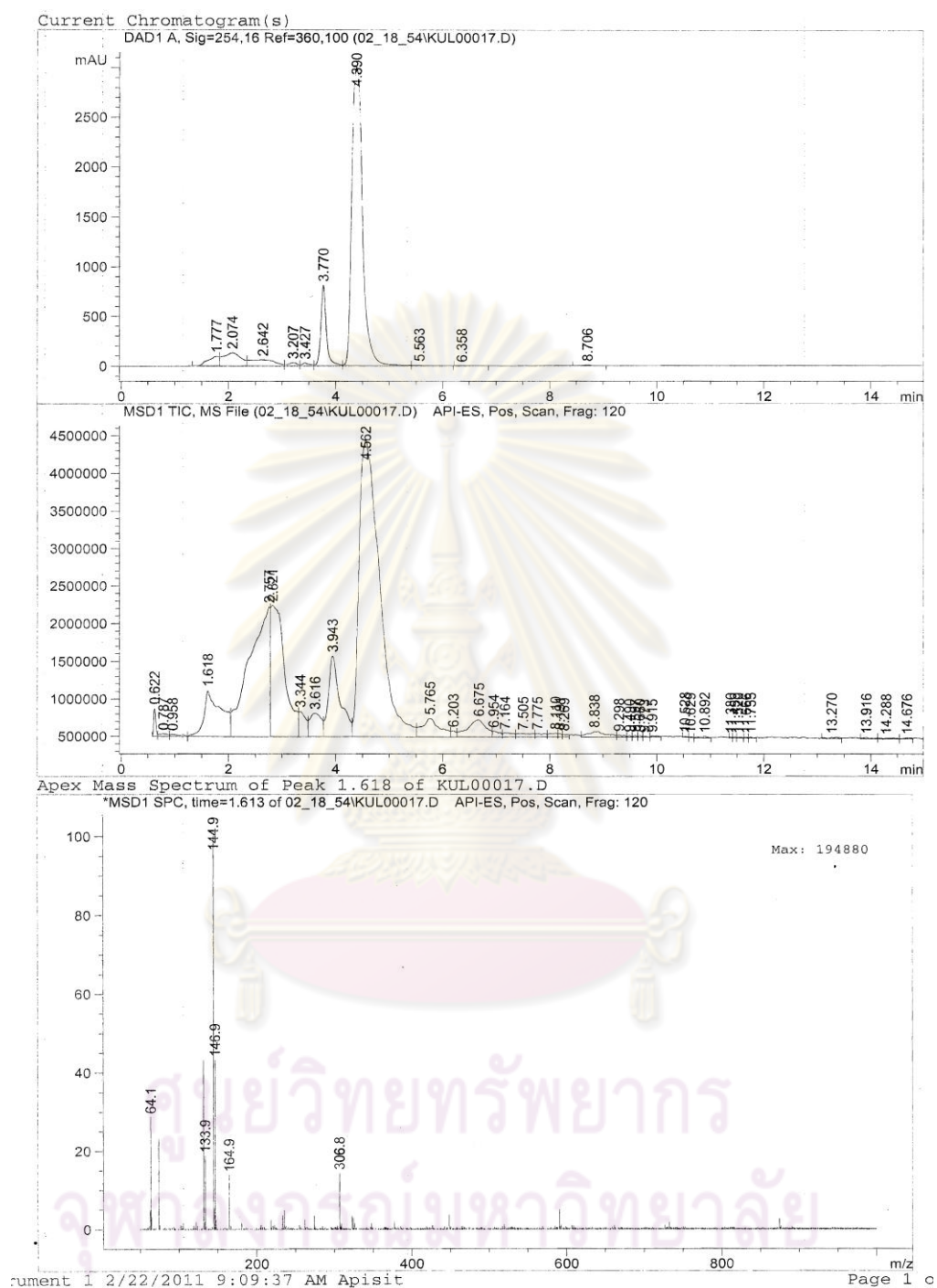
(q)

(r)

Figure C.6 (continued).

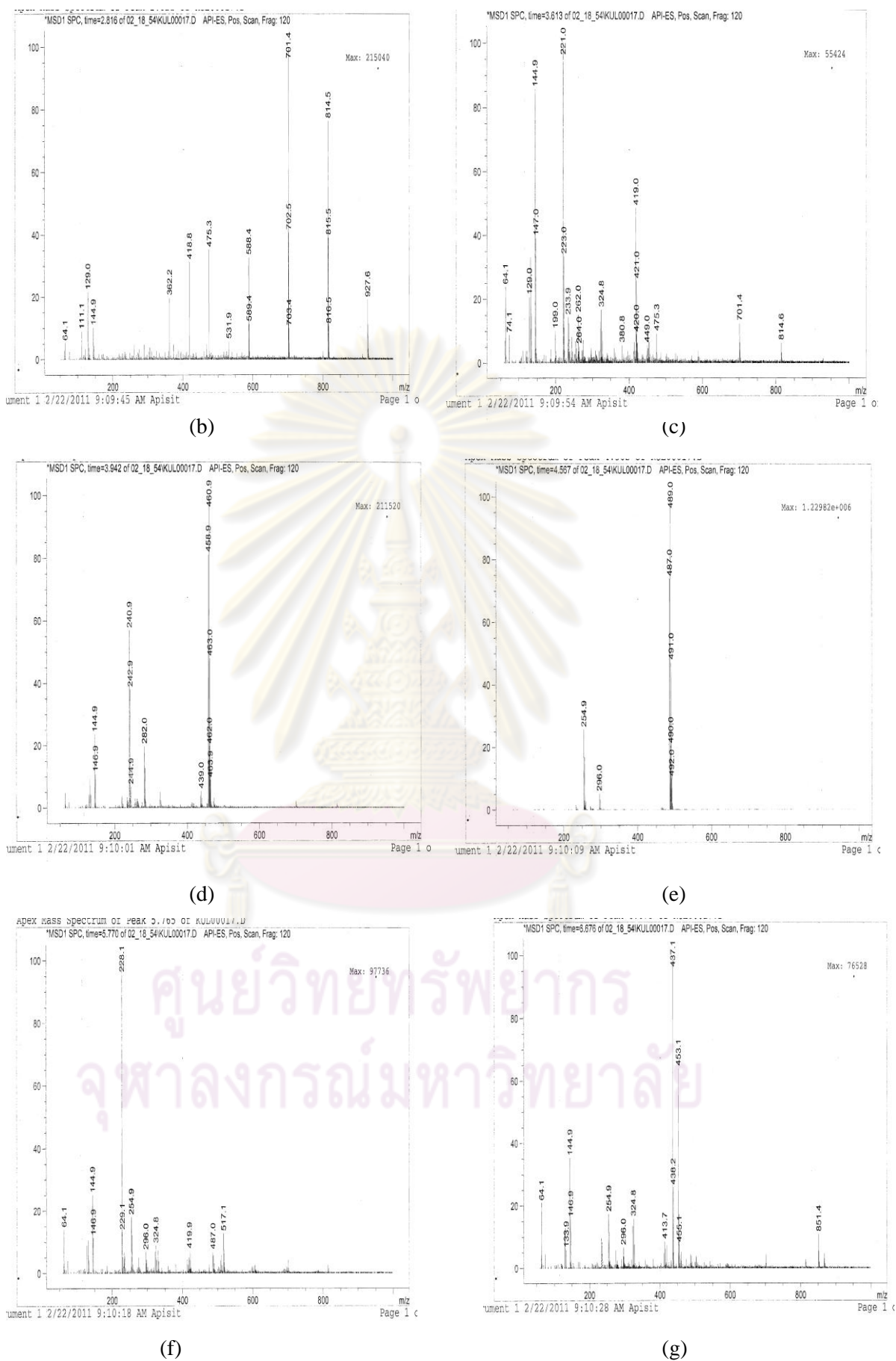
ศูนย์วิทยทรัพยากร
จุฬาลงกรณ์มหาวิทยาลัย

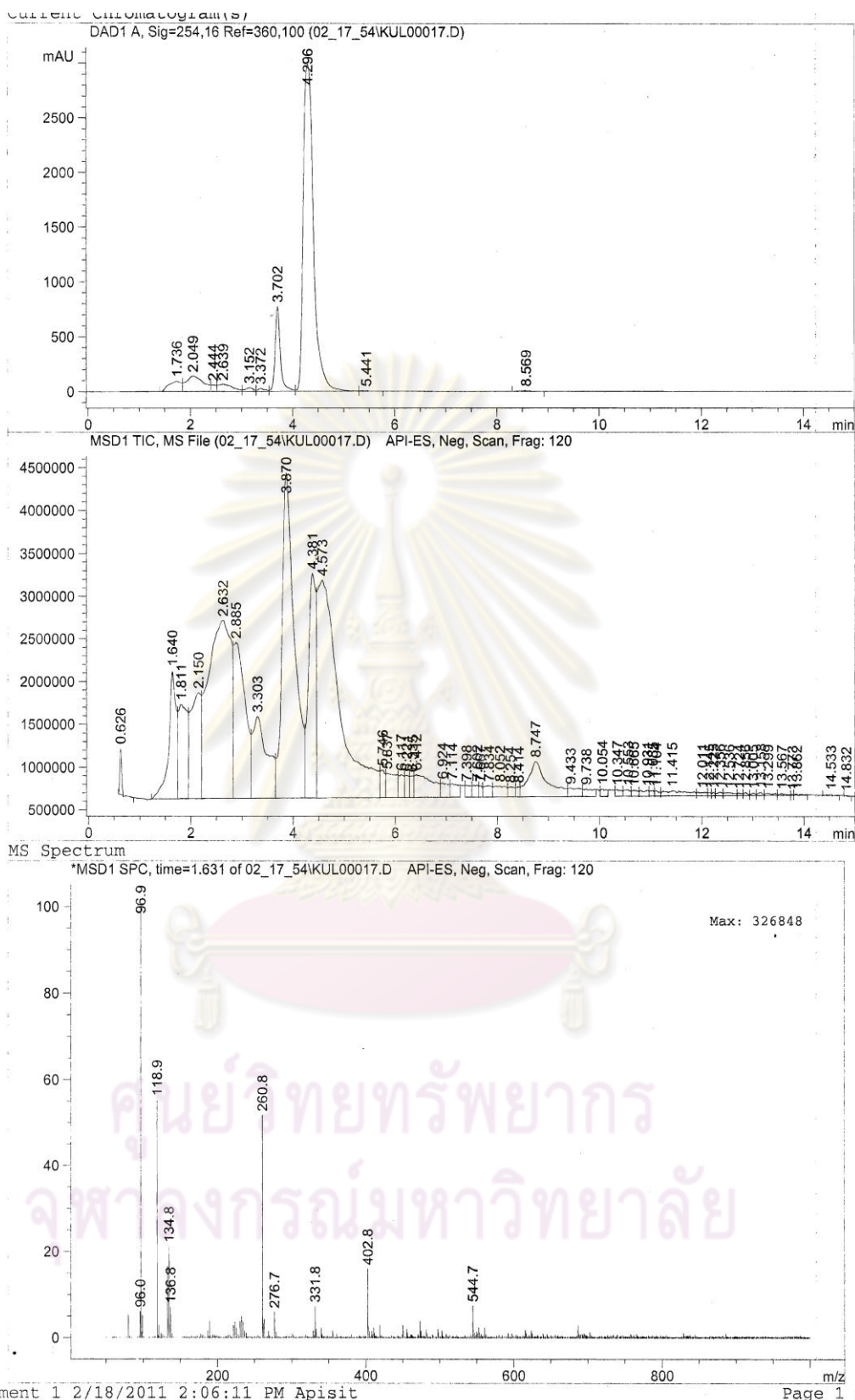
C.3.3 pH10



(a)

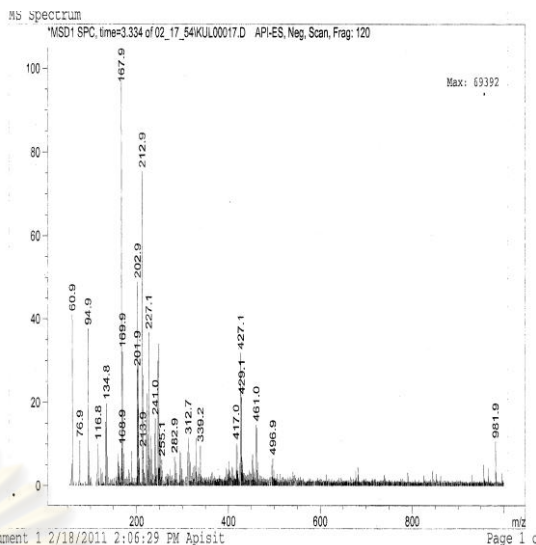
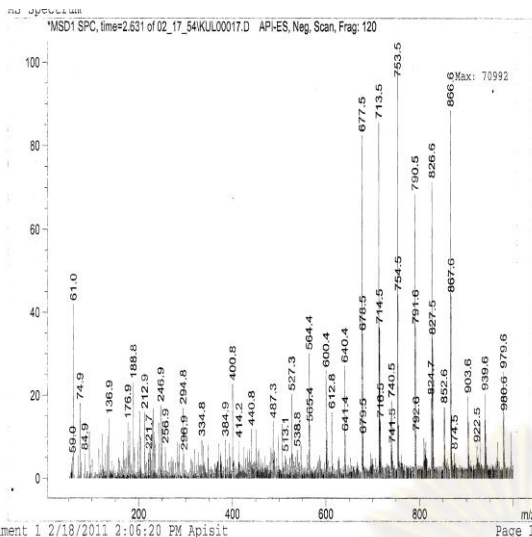
Figure C.7 Chromatogram of diuron solution photodegradation at pH10 obtained from UV detector and mass detector are displayed in (a). Mass spectrums were obtained using fragmentator of 120 V at various retention times as shown in (a)-(n).





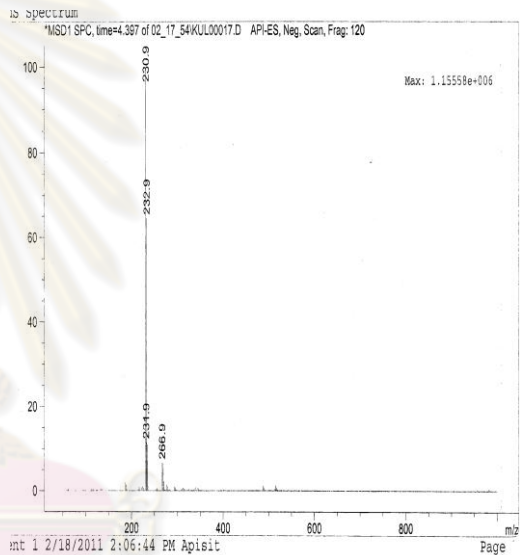
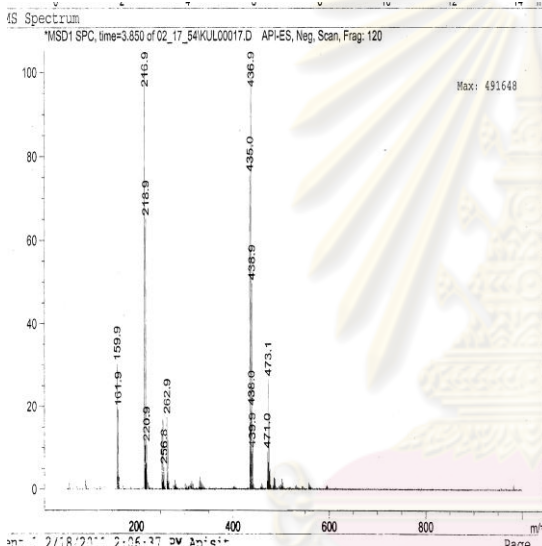
(h)

Figure C.7 (continued).



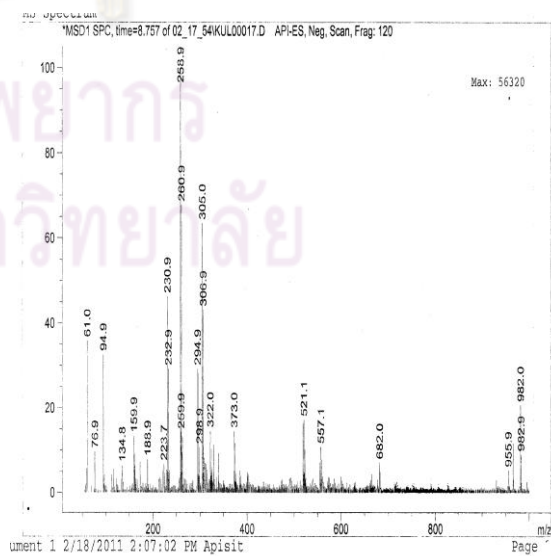
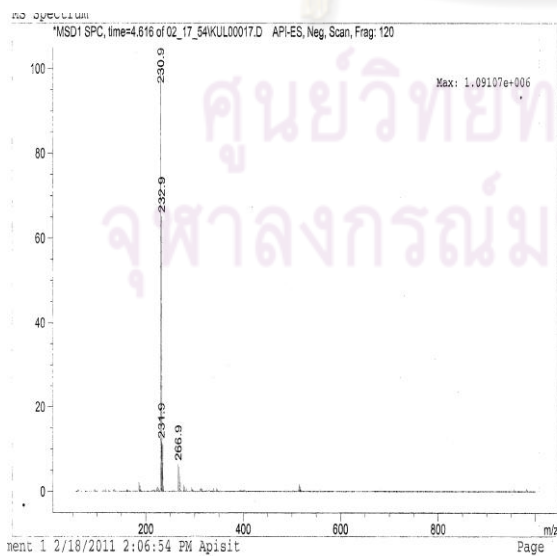
(i)

(j)



(k)

(l)

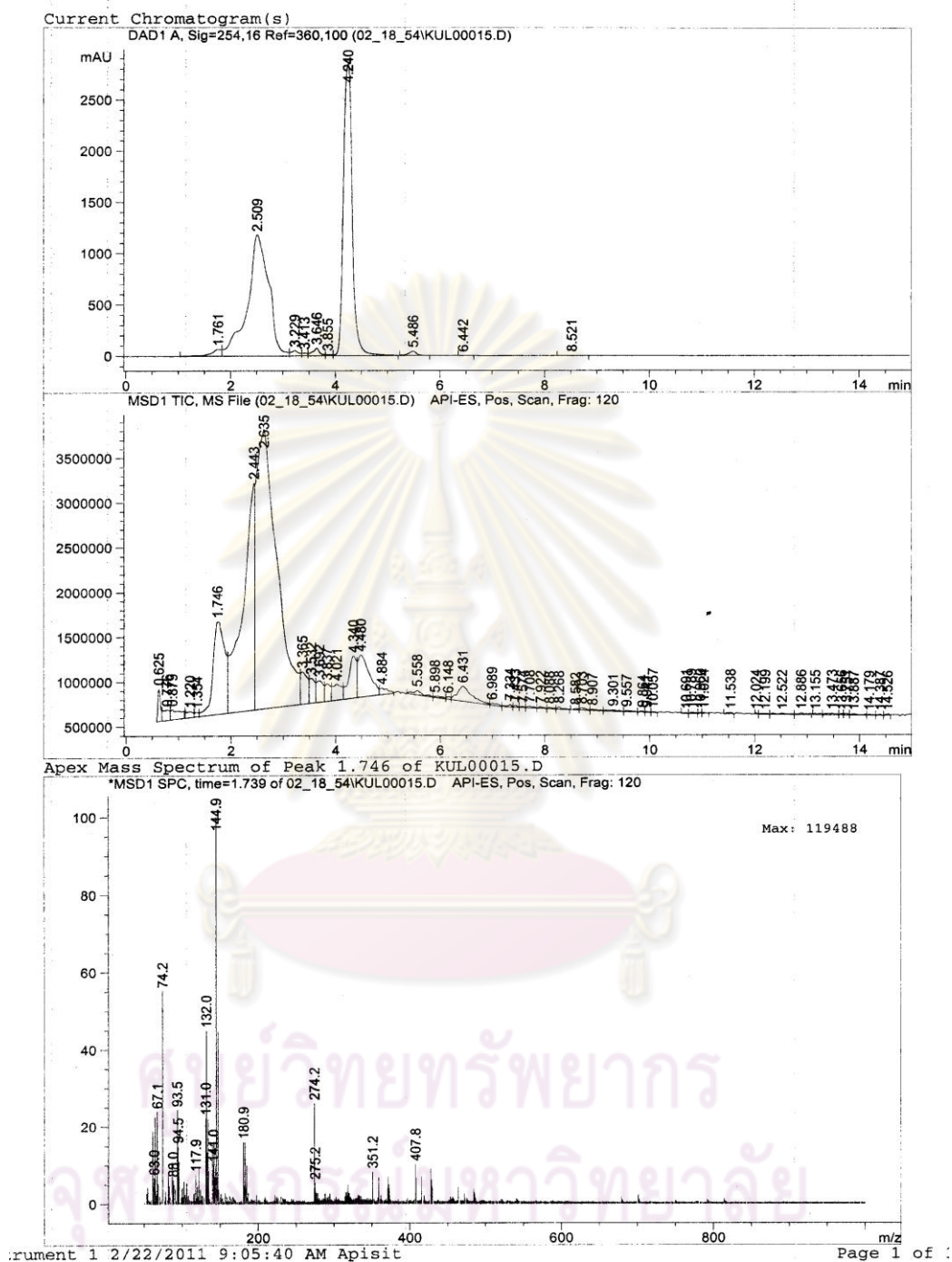


(m)

(n)

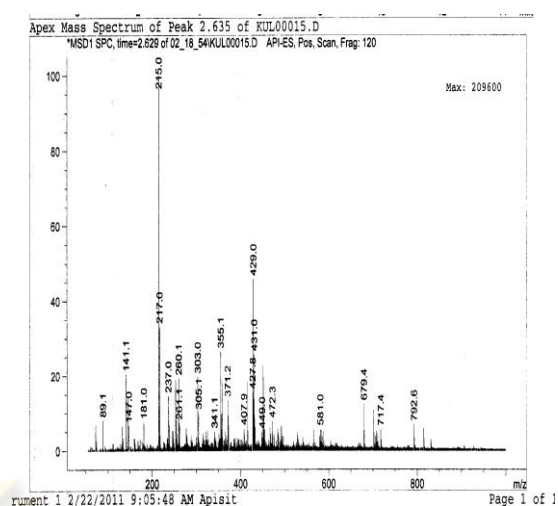
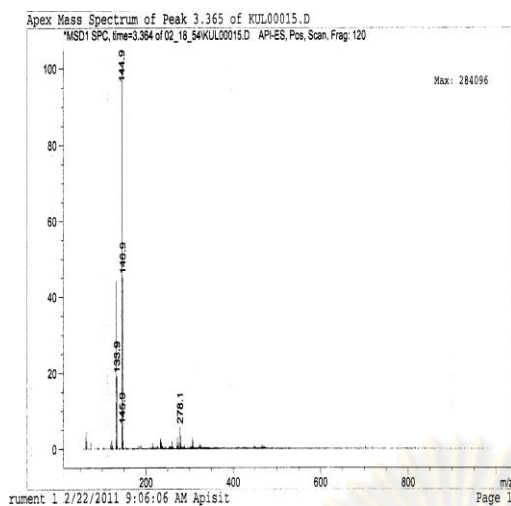
Figure C.7 (continued).

C.3.4 UV-C



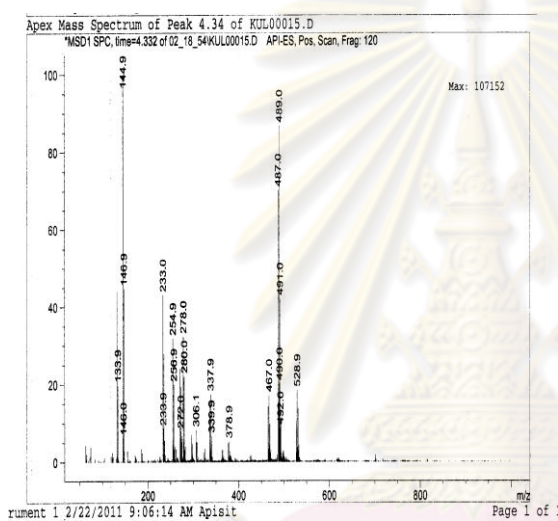
(a)

Figure C.8 Chromatogram of diuron solution photodegradation by UV-C obtained from UV detector and mass detector are displayed in (a). Mass spectrums were obtained using fragmentator of 120 V at various retention times as shown in (a)-(r).

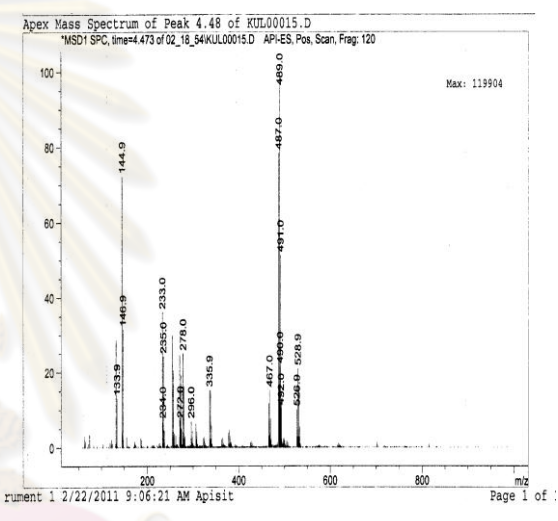


(b)

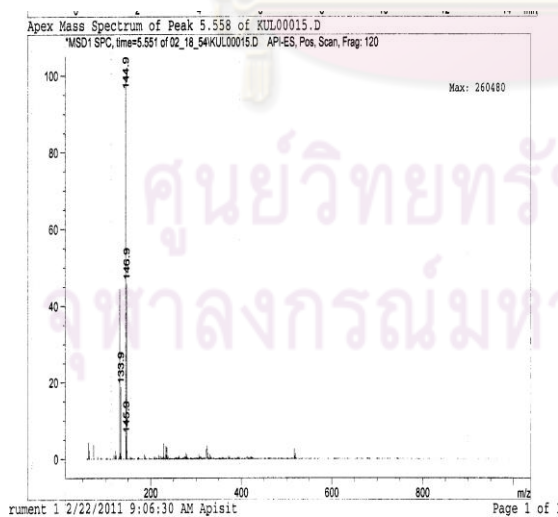
(c)



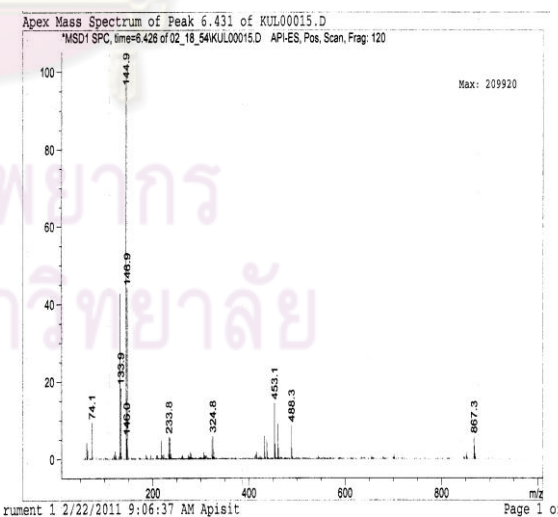
(d)



(e)

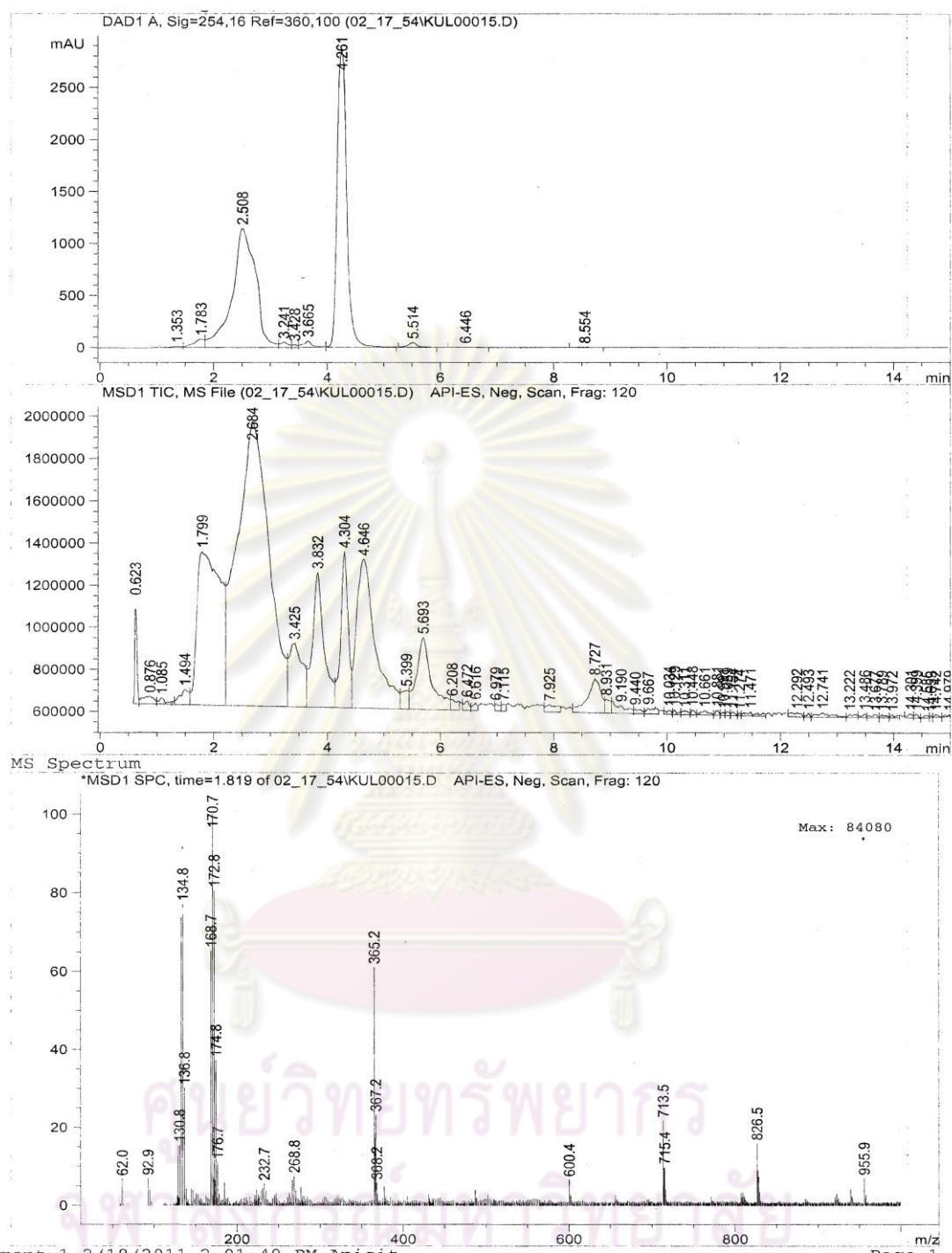


(f)



(g)

Figure C.8 (continued).



(h)

Figure C.8 (continued).

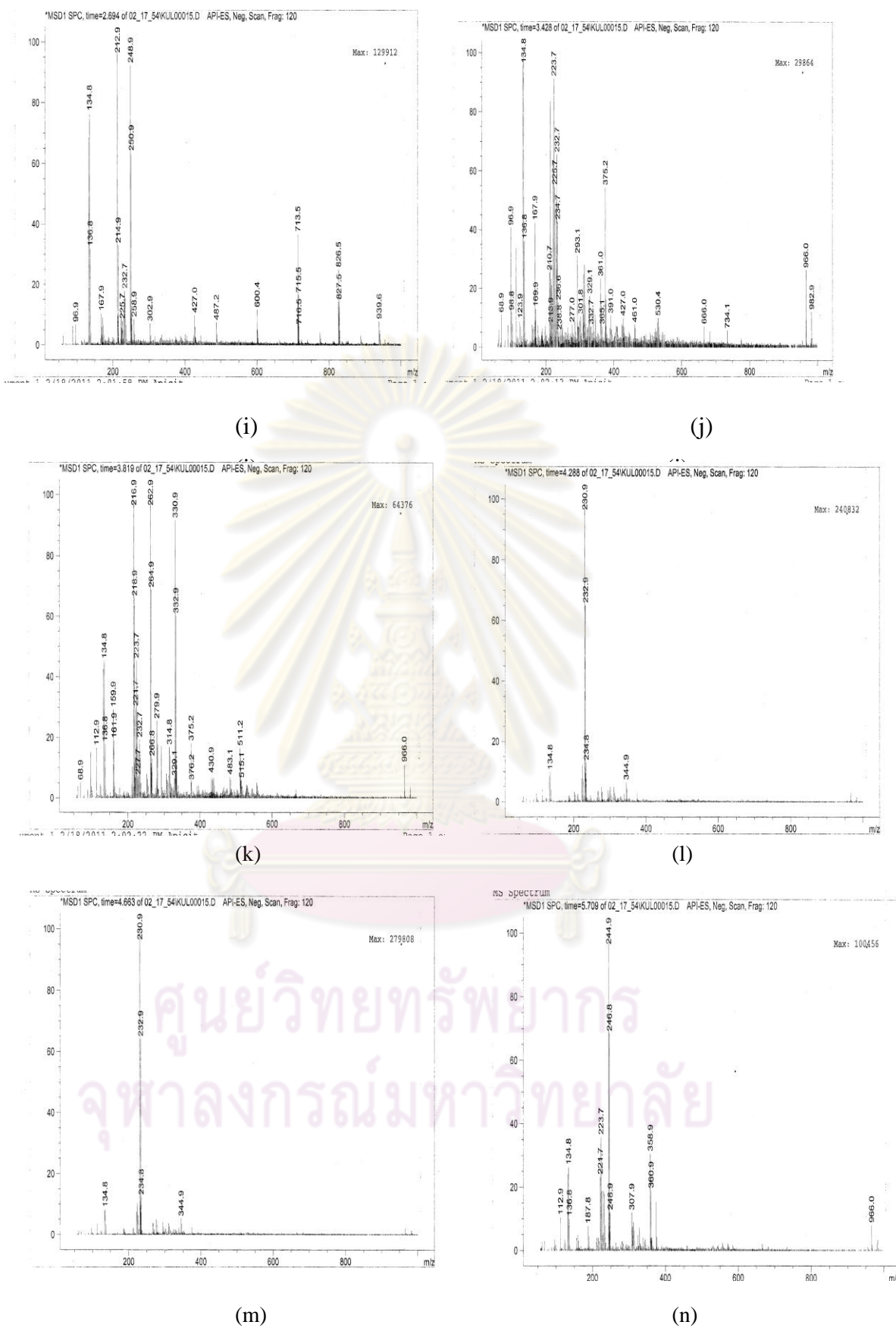
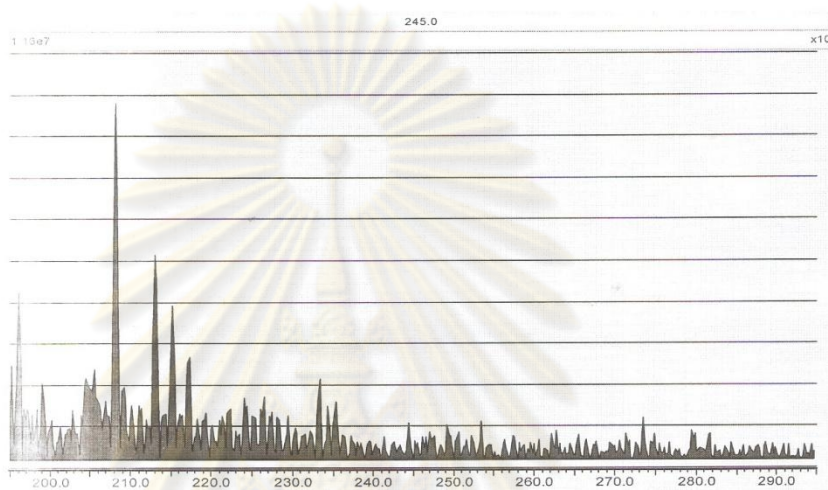


Figure C.8 (continued)

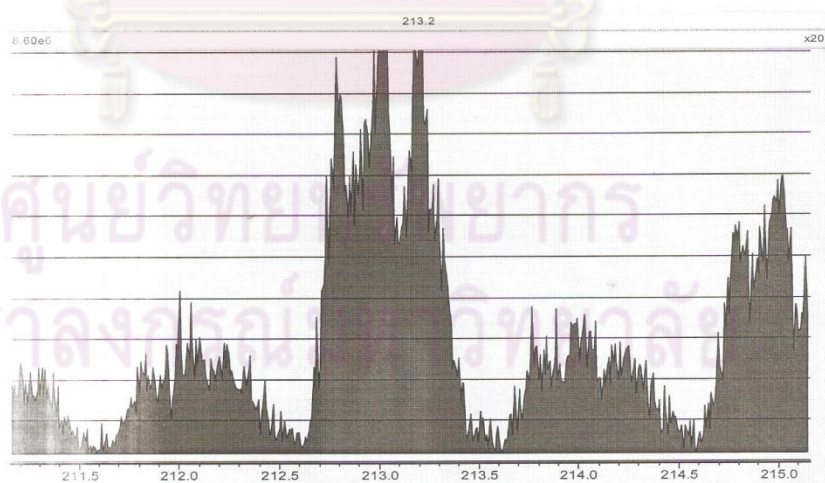
APPENDIX D

LC/MS/MS MASS SPECTRUM

D.1 Set mass spectrum of intermediates for analyzed by MS/MS detector

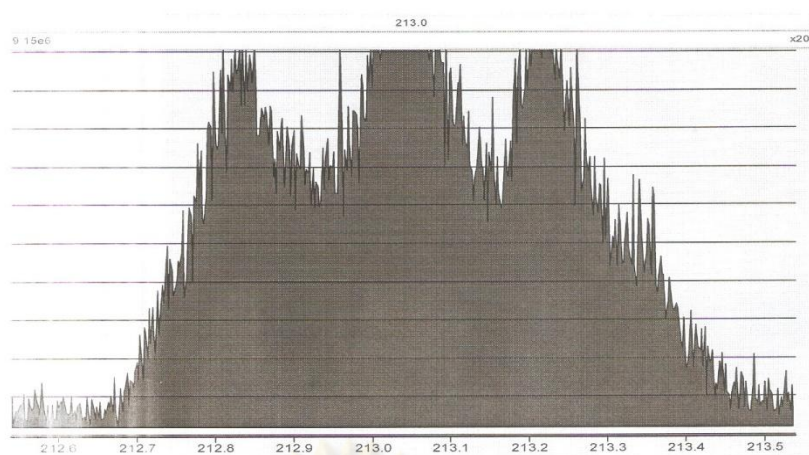


(a)

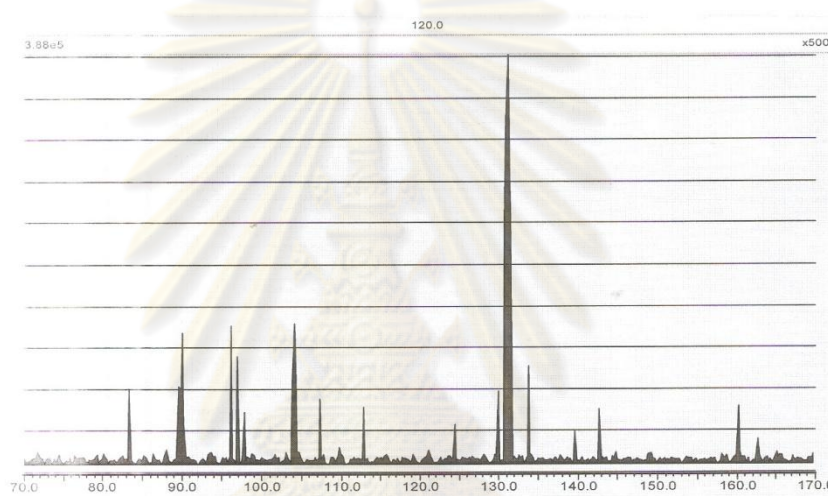


(b)

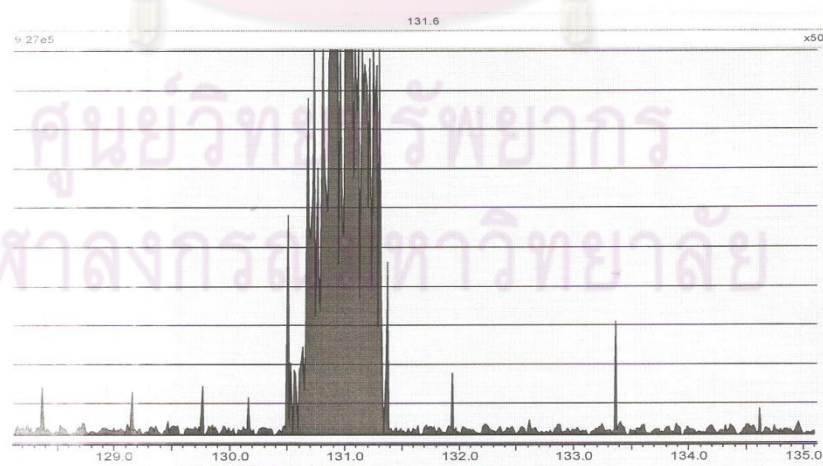
Figure D.1 Chromatogram of diuron solution photodegradation (set mass ~ 213) obtained from LC/MS/MS displayed in (a) (f).



(c)

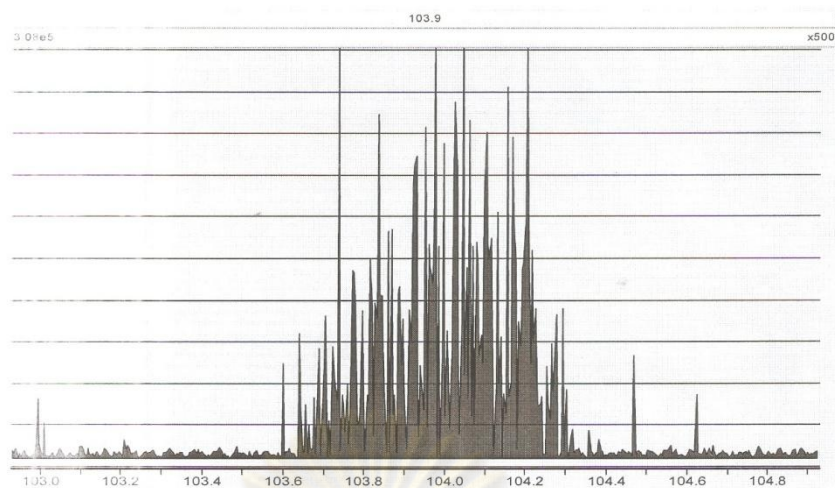


(d)



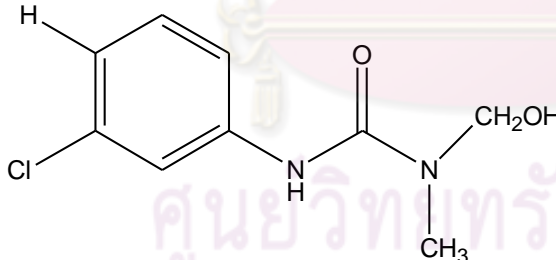
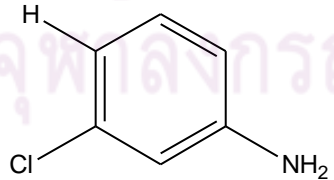
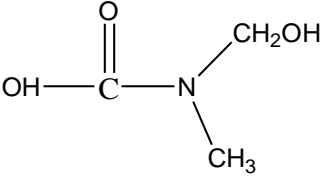
(e)

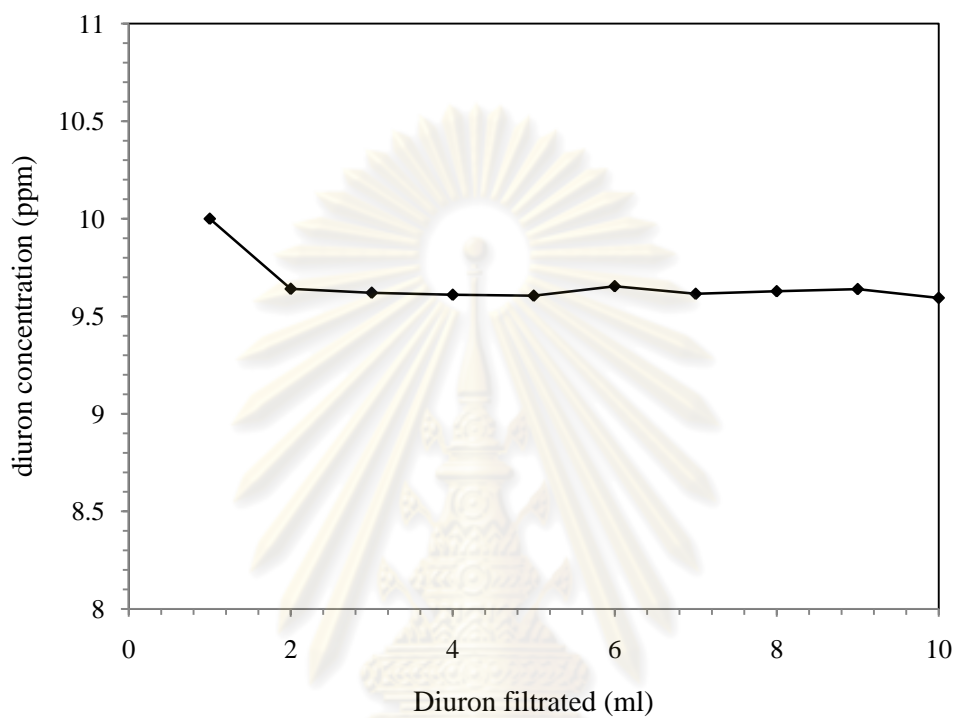
Figure D.1 (continued).



(f)

Figure D.1 (continued)**Table D.1** Mass spectral data for photocatalytic degradation of diuron as analyzed by LC/MS/MS.

Compound structure	m/z
	213 (parent ion)
	131 (daughter ion)
	104 (daughter ion)

APPENDIX E**ADSORPTION OF FILTER TEST****Figure E.1** Adsorption of diuron on filter.

ศูนย์วิทยทรัพยากร
จุฬาลงกรณ์มหาวิทยาลัย



APPENDIX F
TOXICITY OF SOME INTERMEDIATES

ศูนย์วิทยทรัพยากร
จุฬาลงกรณ์มหาวิทยาลัย

F.1 3,4-Dichloroaniline

11. TOXICOLOGICAL INFORMATION

Acute toxicity

LD50 Oral - rat - 545 mg/kg

Skin corrosion/irritation

Skin - rabbit - Severe skin irritation

Serious eye damage/eye irritation

Eyes - rabbit - Severe eye irritation

Respiratory or skin sensitization

May cause allergic skin reaction.

Causes sensitization.

Germ cell mutagenicity

Genotoxicity in vitro - Human - lymphocyte

Sister chromatid exchange

Carcinogenicity

IARC: No component of this product present at levels greater than or equal to 0.1% is identified as probable, possible or confirmed human carcinogen by IARC.

Reproductive toxicity

no data available

Specific target organ toxicity - single exposure

no data available

Specific target organ toxicity - repeated exposure

no data available

12. ECOLOGICAL INFORMATION

Toxicity

Toxicity to fish LC50 - Pimephales promelas (fathead minnow) - 7 - 10 mg/l - 96,0 h

Toxicity to daphnia and other aquatic invertebrates. EC50 - Daphnia magna (Water flea) - 0,05 - 2,20 mg/l - 48 h

Toxicity to algae EC50 - Pseudokirchneriella subcapitata (green algae) - 4,9 mg/l - 72 h
Growth inhibition LOEC - Algae - 1 - 10 mg/l - 28 d

Persistence and degradability

Biodegradability Result: - Not readily biodegradable.

Bioaccumulative potential

Bioaccumulation Poecilia reticulata (guppy) - 48 h
Bioconcentration factor (BCF): 96

Mobility in soil

no data available

PBT and vPvB assessment

no data available

Other adverse effects

Very toxic to aquatic organisms, may cause long-term adverse effects in the aquatic environment.

ศูนย์วิจัยทรัพยากร
จุฬาลงกรณ์มหาวิทยาลัย

F.2 3,4-Dichlorophenol

11. TOXICOLOGICAL INFORMATION

11.1 Information on toxicological effects

Acute toxicity

Skin corrosion/irritation
no data available

Serious eye damage/eye irritation
no data available

Respiratory or skin sensitization
no data available

Germ cell mutagenicity
no data available

Carcinogenicity

IARC: No component of this product present at levels greater than or equal to 0.1% is identified as probable, possible or confirmed human carcinogen by IARC.

Reproductive toxicity
no data available

Specific target organ toxicity - single exposure
no data available

Specific target organ toxicity - repeated exposure
no data available

Aspiration hazard
no data available

Potential health effects

Inhalation

May be harmful if inhaled. Causes respiratory tract irritation.

Ingestion

Harmful if swallowed.

Skin

May be harmful if absorbed through skin. Causes skin irritation.

Eyes

Causes eye burns.

Signs and Symptoms of Exposure

Cough, Shortness of breath, Headache, Nausea, Vomiting, Tremors, Central nervous system depression, prolonged or repeated exposure can cause; Damage to the eyes. To the best of our knowledge, the chemical, physical, and toxicological properties have not been thoroughly investigated.

Additional Information

RTECS: SK8800000

12. ECOLOGICAL INFORMATION

12.1 Toxicity

Toxicity to fish LC50 - *Oryzias latipes* - 1,9 mg/l - 96 h

Toxicity to daphnia and other aquatic invertebrates. EC50 - *Daphnia magna* (Water flea) - 2,77 mg/l - 24 h

Toxicity to algae Growth inhibition EC50 - *Pseudokirchneriella subcapitata* - 3,2 mg/l - 96 h

12.2 Persistence and degradability
no data available

12.3 Bioaccumulative potential
no data available

12.4 Mobility in soil
no data available

12.5 Results of PBT and vPvB assessment
no data available

12.6 Other adverse effects
Toxic to aquatic life.
no data available

F.3 1-Methyl-3-phenylurea

11. TOXICOLOGICAL INFORMATION

11.1 Information on toxicological effects

Acute toxicity

LD50 Oral - rat - 3.440 mg/kg

Skin corrosion/irritation

no data available

Serious eye damage/eye irritation

no data available

Respiratory or skin sensitization

May cause sensitization by skin contact.

Germ cell mutagenicity

Genotoxicity in vivo - mouse - Oral
DNA inhibition

Carcinogenicity

IARC: No component of this product present at levels greater than or equal to 0.1% is identified as probable, possible or confirmed human carcinogen by IARC.

Reproductive toxicity

no data available

Specific target organ toxicity - single exposure

no data available

Specific target organ toxicity - repeated exposure

no data available

Aspiration hazard

no data available

Potential health effects
Inhalation

May be harmful if inhaled. May cause respiratory tract irritation.

Ingestion

May be harmful if swallowed.

Skin

May be harmful if absorbed through skin. May cause skin irritation.

Eyes

Causes eye burns.

Signs and Symptoms of Exposure

To the best of our knowledge, the chemical, physical, and toxicological properties have not been thoroughly investigated.

Additional Information

RTECS: YT8470000

12. ECOLOGICAL INFORMATION

12.1 Toxicity

no data available

12.2 Persistence and degradability

no data available

12.3 Bioaccumulative potential

no data available

12.4 Mobility in soil

no data available

จุฬาลงกรณ์มหาวิทยาลัย
มหาวิทยาลัยทรัพยากร

F.4 3,4-Dichlorophenyl isocyanate

11. TOXICOLOGICAL INFORMATION

11.1 Information on toxicological effects

Acute toxicity

LD50 Oral - rat - 91 mg/kg

LC50 Inhalation - rat - 4 h - 2.700 mg/m³

Remarks: Sense Organs and Special Senses (Nose, Eye, Ear, and Taste):Eye:Lacrimation.
Behavioral:Ataxia. Gastrointestinal:Changes in structure or function of salivary glands.

Skin corrosion/irritation

no data available

Serious eye damage/eye irritation

no data available

Respiratory or skin sensitization

Prolonged or repeated exposure may cause allergic reactions in certain sensitive individuals.

May cause allergic respiratory and skin reactions

Germ cell mutagenicity

no data available

Carcinogenicity

IARC: No component of this product present at levels greater than or equal to 0.1% is identified as probable, possible or confirmed human carcinogen by IARC.

Reproductive toxicity

no data available

Specific target organ toxicity - single exposure

Inhalation - May cause respiratory irritation.

Specific target organ toxicity - repeated exposure

no data available

Aspiration hazard

no data available

Potential health effects

Inhalation

Harmful if inhaled. Causes respiratory tract irritation.

Ingestion

Toxic if swallowed.

Skin

May be harmful if absorbed through skin. Causes skin irritation.

Eyes

Causes serious eye irritation.

Signs and Symptoms of Exposure

burning sensation, Cough, wheezing, laryngitis, Shortness of breath, Headache, Nausea, Vomiting, Repeated exposure may cause asthma. To the best of our knowledge, the chemical, physical, and toxicological properties have not been thoroughly investigated.

Additional Information

RTECS: NQ8760000

12. ECOLOGICAL INFORMATION

12.1 Toxicity

no data available

12.2 Persistence and degradability

no data available

12.3 Bioaccumulative potential

no data available

12.4 Mobility in soil

no data available

12.5 Results of PBT and vPvB assessment

no data available

12.6 Other adverse effects

no data available

F.5 1,2-Dichloro-4-nitrobenzene

11. TOXICOLOGICAL INFORMATION

Acute toxicity

LD50 Oral - rat - 953 mg/kg

Remarks: Nutritional and Gross Metabolic: Weight loss or decreased weight gain.

LC50 Inhalation - rat - 4 h - 10,000 mg/m³

Remarks: Sense Organs and Special Senses (Nose, Eye, Ear, and Taste): Olfaction: Other changes.

Behavioral: Somnolence (general depressed activity). Nutritional and Gross Metabolic: Weight loss or decreased weight gain.

Skin corrosion/irritation

Skin - rabbit - Mild skin irritation - 24 h

Serious eye damage/eye irritation

Eyes - rabbit - Moderate eye irritation - 24 h

Respiratory or skin sensitization

May cause allergic skin reaction.

Germ cell mutagenicity

no data available

Carcinogenicity

IARC: No component of this product present at levels greater than or equal to 0.1% is identified as probable, possible or confirmed human carcinogen by IARC.

Reproductive toxicity

Reproductive toxicity - rat - Oral

Maternal Effects: Other effects.

Specific target organ toxicity - single exposure

no data available

Specific target organ toxicity - repeated exposure

no data available

Aspiration hazard

no data available

Potential health effects

Inhalation

May be harmful if inhaled. May cause respiratory tract irritation.

Ingestion

Harmful if swallowed.

Skin

May be harmful if absorbed through skin. May cause skin irritation.

Eyes

Causes eye irritation.

Signs and Symptoms of Exposure

Absorption into the body leads to the formation of methemoglobin which in sufficient concentration causes cyanosis. Onset may be delayed 2 to 4 hours or longer. To the best of our knowledge, the chemical, physical, and toxicological properties have not been thoroughly investigated.

Additional Information

RTECS: CZ5250000

12. ECOLOGICAL INFORMATION

Toxicity

no data available

Persistence and degradability

Bioaccumulative potential

Bioaccumulation

Oncorhynchus mykiss (rainbow trout) - 36 d

Bioconcentration factor (BCF): 130

Mobility in soil

no data available

PBT and vPvB assessment

no data available

Other adverse effects

no data available

VITA

Miss Wannipa Pradittakan was born on September 22, 1986 in Phang-nga Province, Thailand. She received the Bachelor Degree of Chemical Engineering from Faculty of Engineer, Mahidol University in 2009. She continued her Master's study at Chulalongkorn University in June, 2009.

LIST OF PUBLICATIONS

1. Wannipa Pradittakan, Esara Sadudeewong, Alisa S. Vangnai, and Varong Pavarajarn. "Comparative Study on Mechanism of Photocatalytic Degradation of Diuron on Titanium Dioxide and Zinc Oxide". The 17th Regional Symposium on Chemical Engineering (CRE384), Bangkok, November 22-23, 2010.
2. Wannipa Pradittakan, Esara Sadudeewong, Kamonrat Apichatsanee, Alisa S. Vangnai, and Varong Pavarajarn. "Comparative Study of Photocatalytic Degradation of Diuron on Titanium Dioxide and Zinc Oxide Nanoparticles". The CHEMECA 2011, Sydney, Australia, September 18-21, 2011.

ศูนย์วิทยทรัพยากร
จุฬาลงกรณ์มหาวิทยาลัย